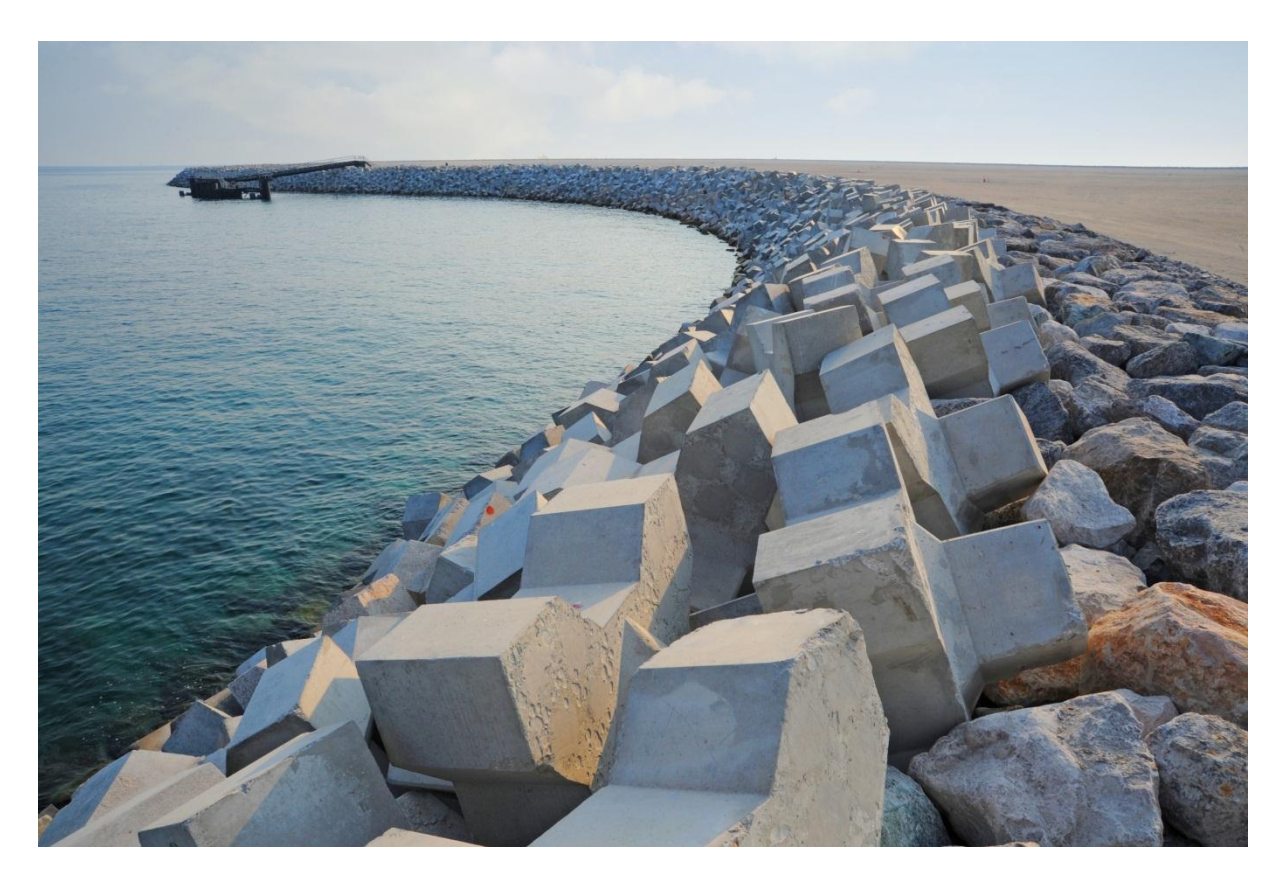
The influence of the under layer on the stability of single layer armour units

Master of Science Thesis



Marc Brouwer

Delft University of Technology 29 November 2013





Front cover image:

Xbloc revetment at DAS Island, Abu Dhabi. Figure courtesy of Delta Marine Consultants.

Master of Science Thesis

The influence of the under layer on the stability of single layer armour units

Author

M.F. Brouwer

Email address: brouwermf@gmail.com
Telephone number: +31(0)616906255

Student number: 1353802

Graduation committee

Prof. dr. ir. W.S.J. Uijttewaal ir. H.J. Verhagen ir. J.P. van den Bos ir. J.S. Reedijk ir. M.P. Muilwijk Delft University of Technology Delft University of Technology Delft University of Technology Delta Marine Consultants Delta Marine Consultants



Delft University of Technology Faculty of Civil Engineering and Geosciences Section Hydraulic Engineering Stevinweg 1 P.O. Box 5048 2600 GA Delft The Netherlands



Delta Marine Consultants H.J. Nederhorststraat 1 P.O. Box 268 2800 AG Gouda The Netherlands

List of trademarks used in this report:

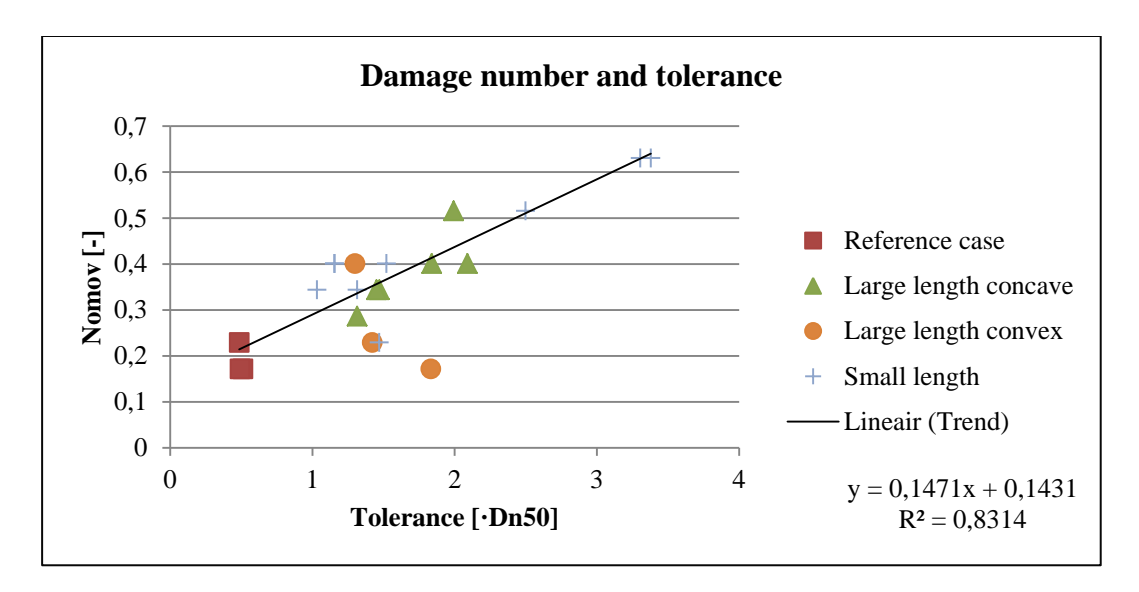
- Accropode is a registered trademark of Sogreah Consultants, France;
- **Delta Marine Consultants** (**DMC**) is a registered trade name of BAM Infraconsult by, The Netherlands;
- **Xbloc** is a registered trademark of Delta Marine Consultants (DMC), The Netherlands;

The use of trademarks in any publication of Delft University of Technology does not imply any endorsement or disapproval of this product by the University.

Summary

This thesis tests the influence of the under layer profile on the stability of the armour layer of concrete interlocking armour units. The analysis is aimed to offer insight into the influence of different under layer profiles on the stability of the armour layer. Furthermore the thesis includes a test of the design guideline of the under layer for Xbloc armour units, which is developed by Delta Marine Consultants (DMC). DMC prescribes that the maximum vertical difference between the constructed and designed profile, i.e. the tolerance, may not exceed 0.5 times the nominal diameter D_{n50} of the under layer rocks. This requirement holds in both the positive and negative perpendicular direction.

Physical model tests have been carried out at the wave flume of DMC in Utrecht, The Netherlands. Different vertical deviations have been tested in combination with variable length scales of the deviations. Furthermore convex and concave shaped profiles are also tested to assess the influence of the direction of the deviation. The under layer profiles are measured with a laser device. A spherical foot staff is simulated numerically in order to represent prototype values of the tolerances. The difference between the laser and simulated sphere is comparable to that of the conventional staff and the sphere and therefore in line with the theoretical difference between a sphere and conventional staff. Tolerance levels are tested in the range between 1.0 and $3.5\,D_{n50}$. The tests show larger damage numbers with increased tolerance. This can be explained by introducing a transition from a steep slope to a milder slope, i.e. the step. Around the step the quality of interlocking is low and consequently this area is very vulnerable to damage. Furthermore deviated profiles have locally milder slopes which result in less interlocking as well. In the figure below the damage during design conditions is plotted versus the tolerances of the individual tests, except for the convex profiles.



Relation between observed damage and tolerances

No clear influence of the length scales of the deviations is observed. Based on three tests with a convex profile it can be concluded that convex shaped profiles are more stable than concave shaped profiles. This can be explained by the absence of the step. Because convex profiles show a different behaviour, they are excluded from the trend line which describes the trend between tolerances and damage. An additional scenario with a narrower grading and larger D_{n50} of under layer material is tested. The results show smaller settlement and larger damage of the armour layer, which are a logical consequence of the increased natural roughness.

It can be concluded that both an increased additional and natural roughness result in more damage of the armour layer. It is therefore recommended not to increase the tolerance requirement for Xbloc armour layers. On the other hand, the experiments show that the lower bound of the tolerance in model situation is close to the prescribed tolerances. It is therefore concluded that sufficient efforts should be made to secure the quality of placement of the under layer. In order to determine the quality of placement of the under layer, a well carried out measurement campaign is recommended.

Keywords

Breakwater, armour layer stability, under layer, tolerance, roughness, measurement method, physical scale model, Xbloc

Acknowledgements

This thesis is the final project in order to obtain a Master of Science degree at Delft University of Technology. It has been carried out in cooperation with Delta Marine Consultants. The topic is the influence of the under layer on the stability of single layer armour units. The core of the research is a set of experiments which have been carried out with a physical scale model.

First of all I would like to thank my graduation committee, which consists of the following members: prof. dr. ir. W.S.J. Uijttewaal, ir. H.J. Verhagen, ir. J.P. van den Bos, ir. J.S. Reedijk and ir. M.P. Muilwijk. During the meetings you provided useful information for the project, which helped me a lot in the process and gave me a step in the right direction. Michiel and Bas are thanked for being my daily supervisors. The discussions we had and the prompt answers to questions are highly appreciated.

Furthermore I would like to thank DMC for giving me the opportunity to work in a nice engineering environment and perform the experimental part of the research in their flume in Utrecht.

Last but not least I would like to thank my parents, friends and my girlfriend Iris for their support.

Marc Brouwer, Delft, November 2013



Table of contents

S	ummar	у	v
A	cknow	ledgements	vii
L	ist of fi	gures	xi
L	ist of ta	ables	xiii
L	ist of sy	ymbols	xiv
1	Intr	oduction	1
	1.1	General aspects of coastal structures	1
	1.2	Problem description	2
	1.3	Research objective and hypothesis	3
	1.4	Research approach	3
	1.5	Outline of this report	4
2	The	eoretical background	5
	2.1	Parameters of interest	5
	2.2	Hydraulic stability of the armour layer	7
	2.3	Aspects of the under layer	13
3	Phy	vsical scale model	23
	3.1	Scaling	23
	3.2	Set-up of the experiments	26
	3.3	Wave aspects	28
	3.4	Test program	30
	3.5	Parameters to be measured	32
4	Obs	servations	35
	4.1	General observations	35
	4.2	Observations of damage	39
5	Tes	t results	43
	5.1	Wave measurements	43
	5.2	Measurements of under layer profiles	45
	5.3	Damage of the armour layer	52
	5.4	Discussion	66
6	Cor	nclusions and recommendations	75
	6.1	Conclusions	75
	6.2	Recommendations	76
R	eferenc	ces	78
Δ	nnendi	ces	80



List of figures

Figure 1-1 Multi-layer rubble mound breakwater. Figure from Coastal engineering manual, 20	006 1
FIGURE 1-2 IMPRESSION OF THE XBLOC. FIGURE FROM TEN OEVER, 2006	
FIGURE 2-1 DEFINITION OF A WAVE IN A TIME RECORD OF A SURFACE ELEVATION. FIGURE FROM HOLTHUIJSE	N,
2007	
FIGURE 2-2 SIEVE CURVES FOR HEAVY ROCK GRADINGS. FIGURE FROM CIRIA, 2007.	
FIGURE 2-3 ANGLE OF REPOSE AS A FUNCTION OF THE PARTICLE SIZE. FIGURE FROM FROEHLICH, 2011	
Figure 2-4 types of breakers and corresponding values of $\pmb{\xi}$ [Schiereck, 2001]	
FIGURE 2-5 FORCES ON ARMOUR UNITS DUE TO OSCILLATING FLOW [BURCHARTH, 1993]	
FIGURE 2-6 CONTACT FORCES ON INTERLOCKING CONCRETE ARMOUR UNITS [BURCHARTH, 1993]	9
FIGURE 2-7 INFLUENCE OF THE SLOPE ANGLE ON INTERLOCKING AND STABILITY. FIGURE FROM BURCHARTH,	
FIGURE 2-8 TYPICAL FAILURE MECHANISMS OF THE ARMOUR LAYER OF A BREAKWATER [BURCHARTH, 1993].	
FIGURE 2-9 GEOMETRY OF THE XBLOC. FIGURE FROM WWW.XBLOC.COM	
FIGURE 2-10 INFLUENCE OF PLACEMENT DENSITY ON STABILITY [BAKKER ET AL., 2005]	
FIGURE 2-11 UNDER LAYER CONSTRUCTION IN PROTOTYPE. FIGURE FROM WWW.SEAPORTSERVICES.COM	
FIGURE 2-12 PLACEMENT OF THE UNDER LAYER IN MODEL SITUATION	
FIGURE 2-13 DEFINITION OF THE NEGATIVE AND POSITIVE TOLERANCES	
FIGURE 2-14 DIFFERENCE BETWEEN PERPENDICULAR AND VERTICAL TOLERANCE	
FIGURE 2-15 RELATION BETWEEN EXTRACTION FORCE AND TOLERANCE. FIGURE FROM MONSTER AND PHILIP	
2010	17
FIGURE 2-16 NATURAL ROUGHNESS OF A RELATIVELY FLAT STRUCTURE. FIGURE FROM CUR PUBLICATION	1.5
'CONSTRUCTION ACCURACIES' (IN PREPARATION)	
FIGURE 2-17 ADDITIONAL ROUGHNESS AS A RESULT OF INACCURACIES DURING CONSTRUCTION. FIGURE FROM	
CUR PUBLICATION 'CONSTRUCTION ACCURACIES' (IN PREPARATION)	
FIGURE 2-18 DIMENSIONS OF ROUGHNESS OF THE UNDER LAYER	
FIGURE 2-19 SURVEY WITH THE SPHERICAL FOOT STAFF. FIGURE FROM MEULEPAS <i>ET AL.</i> , 1999	
FIGURE 2-20 MEASUREMENT LEVELS OF DIFFERENT SURVEY METHODS. FIGURE FROM CIRIA, 2007	
FIGURE 2-21 SINGLE AND MULTI-BEAM ECHOUSOUNDER SYSTEMS AND THEIR FOOTPRINTS. FIGURE FROM CIR	
2007	
FIGURE 3-1 DMC WAVE FLUME IN WHICH THE EXPERIMENTS HAVE BEEN CARRIED OUT	
FIGURE 3-3 CROSS SECTION OF THE BREAKWATER OF THE PHYSICAL MODEL TESTS. DIMENSIONS IN MM	
FIGURE 3-4 WAVE GENERATOR IN THE FLUME OF DMC.	
FIGURE 3-5 SCHEMATIZATION OF LARGE AND SMALL LENGTHS OF THE DEVIATIONS	
FIGURE 3-0 WOODEN FRAME WITH LASER DEVICE WHICH IS USED TO MEASURE THE PROFILE OF THE UNDER LA	
FIGURE 3-7 SPHERICAL FOOT STAFF MEASUREMENT OF THE UNDER LAYER IN MODEL SITUATION	
FIGURE 4-1 MECHANISM OF ROCKING OF A SINGLE ARMOUR UNIT	
FIGURE 4-2 MECHANISM OF EXTRACTION OF AN ARMOUR UNIT	
FIGURE 4-3 MECHANISMS OF SETTLEMENT OF ARMOUR UNITS	
FIGURE 4-4 LIFTING OF MULTIPLE ARMOUR UNITS	
FIGURE 4-5 BREAKWATER CROSS SECTION AND THE STEP. FIGURE FROM ARCHETTI AND LAMBERTI, 1996	
FIGURE 4-6 PLACEMENT TIMES OF THE ARMOUR UNITS	
FIGURE 4-7 OBSERVATION OF DEGREE OF DAMAGE NEAR THE STEP	
FIGURE 5-1 UNDER LAYER PROFILE WITH AND WITHOUT SPIKES	
FIGURE 5-2 LASER AND SPHERICAL FOOT STAFF MEASUREMENT AT THE SAME LOCATION	
FIGURE 5-3 SIMULATION AND MEASUREMENT CARRIED OUT WITH THE SPHERICAL FOOT STAFF. LEFT: SINGLE	+0
MEASUREMENT AND RIGHT: AVERAGE OF THE THREE MEASUREMENTS	47
FIGURE 5-4 LASER MEASUREMENT AND SIMULATED SPHERICAL FOOT STAFF MEASUREMENT. LEFT: SINGLE	17
MEASUREMENT AND RIGHT: AVERAGE OF THE THREE MEASUREMENTS	48

FIGURE 5-5 DETERMINATION OF THE LENGTH SCALE OF DEVATIONS	51
FIGURE 5-6 DAMAGE OF TEST SCENARIO B VERSUS DAMAGE OF REFERENCE CASE	53
FIGURE 5-7 DAMAGE OF TEST SCENARIO E VERSUS DAMAGE OF REFERENCE CASE	53
FIGURE 5-8 DAMAGE OF TEST SCENARIO G VERSUS DAMAGE OF REFERENCE CASE	53
FIGURE 5-9 DAMAGE OF TEST SCENARIO C VERSUS DAMAGE OF REFERENCE CASE	54
FIGURE 5-10 DAMAGE OF TEST SCENARIO D VERSUS DAMAGE OF REFERENCE CASE	54
FIGURE 5-11 DAMAGE OF TEST SCENARIO F VERSUS DAMAGE OF REFERENCE CASE	55
FIGURE 5-12 BOXPLOT OF DAMAGE NUMBERS OF THE DIFFERENT SCENARIOS DURING DESIGN CONDITIONS	55
FIGURE 5-13 DAMAGE NUMBERS DURING DESIGN CONDITIONS PLOTTED VERSUS TOLERANCES FOR INDIVIDUA	AL
TESTS	56
FIGURE 5-14 DAMAGE NUMBER VERSUS TOLERANCE FOR THE 80% CONDITION	57
FIGURE 5-15 DAMAGE NUMBER VERSUS TOLERANCE FOR THE 60% CONDITION	58
FIGURE 5-16 PLACEMENT GRID OF ARMOUR UNITS	59
FIGURE 5-17 RPD'S OF THE INDIVIDUAL TESTS FOR THE TWO METHODS	60
FIGURE 5-18 SETTLEMENTS DURING THE REFERENCE CASE TESTS	62
FIGURE 5-19 SCAN OF ARMOUR AND UNDER LAYER BEFORE AND AFTER TEST G-2	63
Figure 5-20 Damage level \boldsymbol{S} and the development of an S-curve with erosion area \boldsymbol{A} . Figure from)M
Verhagen et al., 2012	64
$Figure \ 5-21 \ Relation \ Between \ extraction \ force \ and \ tolerance. \ Figure \ from \ Monster \ and \ Philippe \ from \ Philippe \ from \ force \ from \ force \ from \ force \ from \ force \ force \ from \ force \ from \ force \ from \ force \ force \ from \ force \ fo$,
2010	66
Figure 5-22 Results of the extraction force tests and the found relation between damage and the found relation between damage and $\frac{1}{2}$)
TOLERANCES	66
FIGURE 5-23 FORCES ON ARMOUR UNIT DURING HYDRAULIC AND EXTRACTION FORCE TESTS	67
$FIGURE\ 5-24\ Stability\ of\ different\ parts\ of\ a\ Breakwater\ as\ a\ function\ of\ the\ relative\ freeboards$	RD.
Figure from van den Bosch et al., 2012	69
$FIGURE\ 5-25\ OCCURRENCE\ OF\ ROCKING\ ON\ CREST\ AND\ SLOPE.\ FIGURE\ FROM\ VAN\ DEN\ BOSCH\ {\it Et\ AL.},\ 2012\$	69
$FIGURE\ 5-26\ Physical\ difference\ between\ low-crested\ breakwaters\ and\ breakwaters\ with\ a\ label{eq:figure}$	
TOLERANCE	70
FIGURE 5-27 DAMAGE OF TEST SCENARIO WITH DIFFERENT UNDER LAYER GRADING VERSUS DAMAGE OF	
REFERENCE CASE	71
Figure 5-28 Influence angle of wave incidence on stability of the armour layer. Figure from	
Bakker <i>et al.</i> , 2005.	73
FIGURE 6-1 DAMAGE NUMBERS DURING DESIGN CONDITIONS PLOTTED VERSUS VERTICAL TOLERANCES FOR	
INDIVIDUAL TESTS	76

List of tables

List of symbols

A list of frequently used symbols is given in this section. Furthermore frequently used indices and abbreviations are added.

Roman symbols

Symbol	Description	Unit
В	Width of a layer	[m]
D	Height of armour unit	[m]
D_n	Nominal diameter	[m]
D_{n50}	Nominal diameter of rock	[m]
f	Frequency	$[s^{-1}]$
Fr	Froude number	[-]
g	Acceleration due to gravity	$[m/s^2]$
$H_{1/3}$	Average highest one third wave height	[m]
H_{m0}	Significant wave height derived from frequency signal	[m]
H_{S}	Significant wave height derived from time signal	[m]
h	Water depth	[m]
h_t	Water depth above the toe	[m]
K_D	Stability coefficient	[-]
L_0	Deep water wave length	[m]
L_{x}	Horizontal length of the section	[m]
L_{y}	Upslope length of the section	[m]
l	Length	[m]
N_{od}	Relative number of extracted units	[-]
N_{omov}	Relative total number of moving units	[-]
N_{or}	Relative number of rocking units	[-]
N_{S}	Stability number	[-]
N_{x}	Number of units in horizontal direction	[-]
N_{y}	Number of units in upslope direction	[-]
n_x	Scale of parameter x	[-]
PD	Placement density	$[m^{-2}]$
Re	Reynolds number	[-]
S	Additional steepness under layer profile	[-]
T	Wave period	[s]
t	Average vertical tolerance in terms of nominal diameter	[m]
и	Flow velocity	[m/s]
V	Volume	$[m^3]$
W_{50}	Mean mass of rock	[kg]
x_m	Value of 'x' in model	[-]
x_p	Value of 'x' in prototype	[-]

Greek symbols

Symbol	Description	Unit
α	Slope angle	[°]
α	Energy scale wave spectrum	[-]
γ	Peak-enhancement factor wave spectrum	[-]
Δ	Relative density	[-]
$ ho_{\scriptscriptstyle S}$	Density of rock	[kg/m ³]
σ	Peak-width parameter wave spectrum	[-]
ν	Kinematic viscosity of water	$[m^2/s]$
ξ	Surf similarity parameter	[-]
arphi	Phase angle	[°]

Frequently used indices

Index	Description
p	Prototype
m	Model
n	Nominal

Frequently used abbreviations

Abbreviation	Description
DMC	Delta Marine Consultants
LW	Low Water
RPD	Relative Placement density
SWL	Sea Water Level



1 Introduction

In this thesis the influence of the under layer on the stability of single layer armour units is investigated. In this chapter an introduction to the topic is given. Furthermore the problem is identified and a research approach is discussed. Furthermore a hypothesis is set up and the outline of this report is added.

1.1 General aspects of coastal structures

1.1.1 Functions of coastal structures

Coastal structures are used throughout the world. These structures are mainly applied to protect port areas from wave action. They reduce the wave impact on the lee side of the structure by reflection of the waves back into the sea and by dissipation of the wave energy. These type of structures are called breakwaters. However, they might also be used to protect beaches from erosion or to protect residential areas from waves due to storms. In these cases they are generally referred to as groins and revetments. A general distinction between monolithic and rubble mound structures can be made. Monolithic structures protect certain areas from wave action mainly by reflecting the wave energy, usually by means of a caisson. Rubble mound structures mostly dissipate the energy from the waves by turbulent flow in the structure. This report is about rubble mound coastal structures and focuses on breakwaters.

1.1.2 Design aspects of breakwaters

Initially rubble mound breakwaters were designed only with natural rock, later other construction materials were used as well. In Figure 1-1 a typical cross section of a rubble mound breakwater is presented. These types of breakwaters are widely applied around the world. From Figure 1-1 it becomes clear that rubble mound breakwaters consist of multiple layers. The **armour layer** is the outer layer of the breakwater. Because this layer is most exposed to wave attack, it is constructed with the largest stones. The main function is absorbing the wave energy. Under the armour layer is the **under layer**. This layer is constructed with smaller rocks to prevent outwash of core material and to ensure stability. The inner part of the breakwater consists of the **core**, which is usually quarry run. Usually also a **toe** is applied. This part of the breakwater can be seen as the foundation of the armour layer.

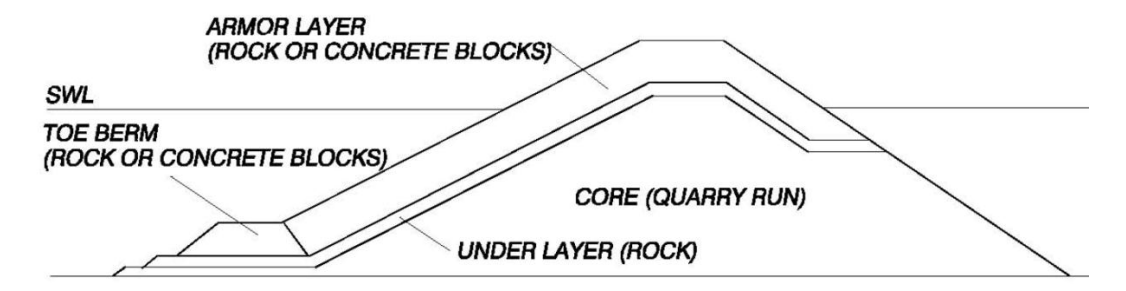


Figure 1-1 Multi-layer rubble mound breakwater. Figure from COASTAL ENGINEERING MANUAL, 2006

The rubble mound breakwaters, as presented in the Figure 1-1, require large rocks from quarries to construct the armour layer. A general prerequisite is that these large rocks are available. In some cases these rocks are unavailable or the quarry is located far away from the location of the breakwater. For

these reasons it can be attractive to use concrete armour units, which have been developed in the past decades.

1.1.3 Development of Xbloc armour unit

The Xbloc is an armour unit which is developed by Delta Marine Consultants (DMC). It has been designed for exposed conditions, single layer placement, with a simple shape, with balanced hydraulic and structural stability and for fast and easy placement [Reedijk *et al.*, 2005]. The Xbloc can be described as an X-shaped body with 2 cubes attached in the centre. An impression of the Xbloc is presented in Figure 1-2.

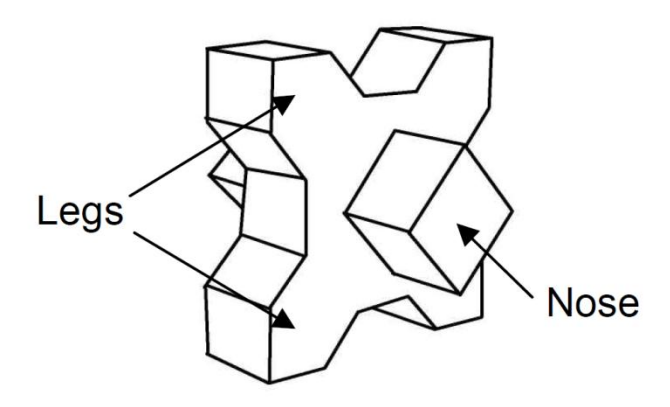


Figure 1-2 Impression of the Xbloc. Figure from TEN OEVER, 2006

The Xbloc has been applied several times in the armour layer of breakwaters and has proved to be suitable for exposed conditions. The units are placed on a predefined grid with random orientation. The units interlock with each other, and this allows to reach a stable armour layer. The Xbloc is economical due to the fact that the units are applied in a single layer with a high porosity; hence the demand of concrete is limited. Another advantage is that the Xbloc does not have a non-interlocking side. Therefore it will find a stable position in the armour layer automatically [REEDIJK *et al.*, 2005].

In this report the focus is on concrete interlocking armour units in general and Xbloc armour units in particular.

1.2 Problem description

The way how the interlocking armour units are placed is a vital factor for the quality of the interlocking of the armour layer and is therefore thus important for the stability of this type of armour units [MUTTRAY *et al.*, 2005]. The armour units are placed on top of the under layer, which is constructed with natural rock. Because the quality of placement is important, DMC has defined certain requirements for the under layer. One of the requirements is that the as built profile of the under layer may not deviate too much from the designed profile of the under layer. In fact, the built profile of the under layer may not deviate more than half the nominal diameter D_{n50} of the under layer material, in both positive and negative vertical direction. This is also called the **tolerance** of the under layer profile, which has a prescribed value of +/-0.5 D_{n50} . According to DMC this requirement holds in the direction perpendicular to the slope. This requirement is based on experience from the past with concrete interlocking armour units, but no scientific basis is present. It is therefore unknown whether the requirement of the under layer profile (equivalent to the tolerance of the under layer profile) is correct. This thesis will fill this gap.

The stability of interlocking armour units is in most cases tested in a wave flume by means of a physical scale model. For these tests the under layer profile is not measured because it is expected that the constructed under layer profile meets the requirements. Therefore the tolerances of the under layer in model situation are unknown, which is going to be investigated in the current thesis report.

1.3 Research objective and hypothesis

In this section the research objective and hypothesis are identified. The research objective is the final goal of this thesis and the hypothesis is meant to help with the assessment of the results.

1.3.1 Research objective

The influence of the under layer profile on the stability of armour layers with concrete interlocking armour units is an important research subject from both an academic as well as a practical point of view. Knowledge on this influence will give a better insight in the behaviour and stability mechanism(s) of concrete interlocking armour units in prototype conditions. This will improve the degree of understanding regarding the theoretical performance of concrete interlocking armour units, and is therefore of academic importance. At the same time this knowledge is essential for consultants and contractors because these parties could build their design rules or work methods on sound tests and improve them when felt necessary. The research objective is defined as follows:

The primary goal of this thesis is to investigate and quantify the influence of deviations in the under layer profile on the stability of the armour layer, including a comparison between different measurement methods of the under layer profile. Then recommendations can be made to parties involved in the construction process.

1.3.2 Hypothesis

In addition to the research objective a hypothesis is defined. Earlier research showed that the profile of the under layer has a significant influence on the interlocking of the armour units [MONSTER AND PHILIPSEN, 2010]. This influence has only been tested by means of extraction force tests and has not been tested hydraulically. During these extraction force tests only the influence of the vertical deviations was investigated. The influence of the length scale of these deviations was not considered. The hypothesis is defined as follows:

The tolerance levels of the under layer for breakwaters, which are constructed with interlocking armour units, may not exceed $0.5D_{n50}$ in perpendicular direction. The stability of the armour layer decreases for larger tolerance levels and this effect is larger for short length scales of deviations in the under layer profile.

1.4 Research approach

The research includes a literature study on the stability of interlocking armour and the under layer tolerances. This literature study only serves as a theoretical background, because no literature was found testing the influence of the under layer profile on the hydraulic stability of the armour layer. This theoretical background helps to understand and interpret the results which are obtained during the physical model tests. A physical scale model is the most appropriate tool to investigate problems like these. By testing the physical scale model in a flume, the behaviour of the prototype can be observed

and understood. After the testing phase a data analysis is carried out in order to assess the behaviour quantitatively.

1.5 Outline of this report

The structure of the report is roughly the same as the chronological order of the entire project. In Chapter 1 an introduction is given and the problem is identified. In Chapter 2 the most important aspects of the literature study are discussed. Literature on breakwaters in general, on Xbloc and interlocking armour in particular and earlier research related to this thesis are discussed. In Chapter 3 the physical scale model is discussed. First some aspects of scale models are treated before the test program and measurements of parameters is discussed. In Chapter 4 a qualitative overview of the observations are given. The mechanisms of the observed damage are discussed and explained. In Chapter 5 the test results are presented and discussed. Under layer profiles and damage levels are treated separately before the influence of these parameters is linked. Furthermore earlier research is compared to the results of the tests and possible shortcomings of the set-up are given. The thesis ends with the conclusions and recommendations, which are presented in Chapter 6.

2 Theoretical background

The relevant aspects of the literature study are presented in this chapter and the most important findings are discussed. This chapter serves as a theoretical background for the remaining part of the report.

2.1 Parameters of interest

The most important parameters are identified in this section. A distinction is made between hydraulic and structural parameters. It is meant to give a short overview of important basic aspects related to breakwaters, which are relevant for this thesis.

2.1.1 Hydraulic parameters

The most important parameters related to waves are discussed in this section.

Waves in general

The formal description of a **wave** can be expressed by considering a time record of a sea surface elevation. In such a record, a wave is the profile of the surface elevation between two successive downward crossings of the elevation [HOLTHUIJSEN, 2007]. Figure 2-1 clarifies the formal definition of waves by presenting this through an example of a time record of a surface elevation.

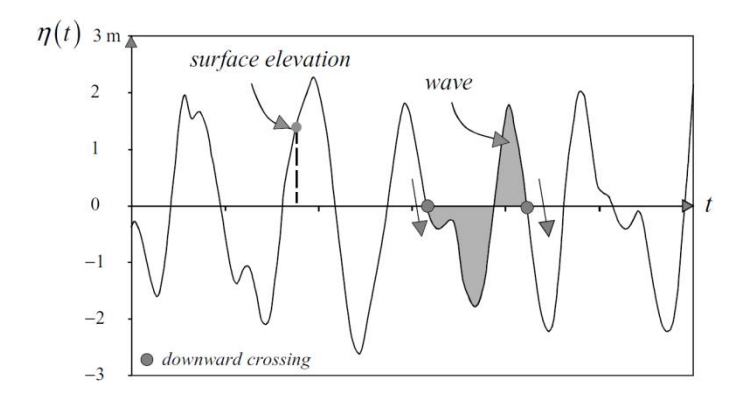


Figure 2-1 Definition of a wave in a time record of a surface elevation. Figure from HOLTHUISEN, 2007

Only wind-generated waves are considered in this report, because they are the most important types when dealing with stability aspects of breakwaters. A general distinction is made between **sea** and **swell** waves. Sea is generated by local winds, it's irregular and short crested. When these waves leave the generation area, they become regular and long crested. These type of waves are called swell.

Wave height

The wave height H is usually defined as the vertical distance between the highest and the lowest surface elevation. This is true for a single wave. In general not all waves are the same, this is visible in Figure 2-1. Therefore the **significant wave height** H_s is used to describe the wave height. Virtually all relations and formulae related to breakwaters make use of the significant wave height at the toe of the breakwater. The significant wave height is defined as the average height of the highest third part of the waves and therefore also sometimes denoted as $H_{1/3}$.

Wave period

The wave period T is the time that elapses between the start and the end of the wave. Usually the peak period T_p is used in breakwater design. The peak period is fairly close to the significant wave period, which is the mean period of the highest one third of waves. For swell waves the peak period is

approximately equal to the significant wave period. For sea waves the peak period is approximately 5 per cent larger than the significant wave period.

Wave length

The wave length L is the horizontal distance between two troughs. The wave length becomes smaller when the wave propagates from deep into shallow water. Usually only the **deep water wave length** L_0 is considered. The deep water wave length can be calculated with:

$$L_0 = \frac{g \cdot T^2}{2\pi} \tag{2.1}$$

2.1.2 Structural parameters

Some important structural parameters which are relevant for this thesis are discussed here.

Nominal diameter

The **nominal diameter** of rock can be determined by weighing all the stones and determining the mean value of the mass of the stones. This is usually done if the rocks are too large to sieve. Then one can calculate the nominal diameter with the equation given below. This parameter is generally used to indicate the size of the rock particles.

$$D_{n50} = \left(\frac{W_{50}}{\rho_s}\right)^{\frac{1}{3}}$$
 2.2

In which:

W_{50}	Mean mass of the rocks	[kg]
$\rho_{\rm s}$	Density of rock	[kg/m ³]

The nominal diameter of rock can also be determined with sieves, which is usually done if the rocks are relatively small. With sieves the mean diameter D_{50} can be determined. One obtains the nominal diameter D_{n50} by multiplying the D_{50} with a shape factor. Because rocks are generally similar in shape, a shape factor of 0.84 is generally applied [CIRIA, 2007].

Rock size and mass

The rocks which are used for constructing any layer except from the armour layer of the breakwater consists of rocks in a certain grading. These rocks originate from a quarry and vary in particle size and mass. The particle mass distribution is most conveniently presented in a percentage lighter by mass cumulative curve, where W_{50} expresses the block mass for which 50% of the total sample mass is of lighter blocks (i.e. the median mass) and W_{85} and W_{15} are similarly defined. The overall steepness of the curve indicates the grading width, and is usually expressed in terms of W_{85} / W_{15} or D_{85} / D_{15} [SCHIERECK, 2001]. Figure 2-2 shows an example of a sieve curve.

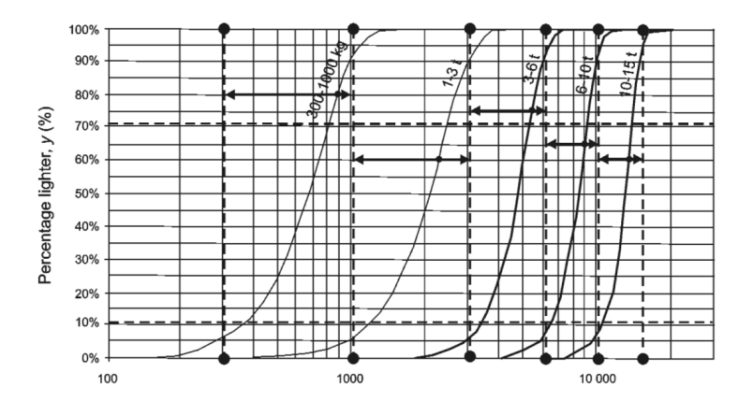


Figure 2-2 Sieve curves for heavy rock gradings. Figure from CIRIA, 2007.

Angle of repose

The maximum slope at which a certain material, dropped down through a natural process, remains stable, is called the **angle of repose** [RAO, 2000]. The angle of repose of granular material is not dependent on the height of the slope, but does depend on the size of the particles, the shape of the material and the width of the grading. Field tests performed by FROEHLICH, 2011 show that the angle of repose depends primarily on the angularity of the material. A higher degree of angularity leads to a higher angle of repose. To a much lesser extend the particle diameter and width of the grading affect the angle of repose. The tests show that a wider grading leads to a small increase in angle of repose. In Figure 2-3 the observed angle of repose is plotted as a function of the particle diameter.

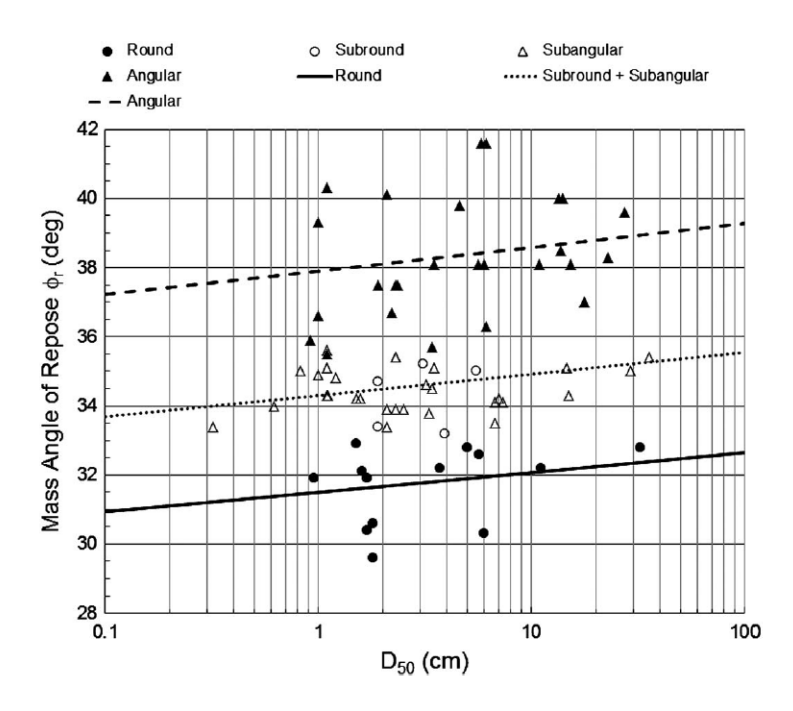


Figure 2-3 Angle of repose as a function of the particle size. Figure from FROEHLICH, 2011

2.2 Hydraulic stability of the armour layer

The hydraulic stability of the armour layer is a major subject in the literature study. In this section insight is given in different types of waves, the forces due to waves on armour units and stability mechanisms of armour units. In the end stability calculations are discussed for breakwaters in general and specific for Xbloc armour units.

2.2.1 Breaking of waves on a structure

The breaking of waves is a result of instability. It occurs because the wave becomes too steep or the water depth is insufficient. Not all waves break in the same way. The **wave steepness** is important in wave breaking. The wave steepness is defined as the wave height divided by the wave length. When it comes to waves on a slope, the steepness of the structure is of importance as well. Iribarren [SCHIERECK, 2001] defined the **surf similarity parameter**, which indicates the ratio of slope steepness and wave steepness:

$$\xi = \frac{\tan \alpha}{\sqrt{\frac{H}{L_0}}}$$
 2.3

In which α is the angle of the slope of the structure and $\sqrt{\frac{H}{L_0}}$ is the square root of the ratio wave height and deep water wave length. This ratio is a measure of the wave steepness. For different values of ξ the breaking waves show a different character. In Figure 2-4 the breaker types are presented for different values of ξ .

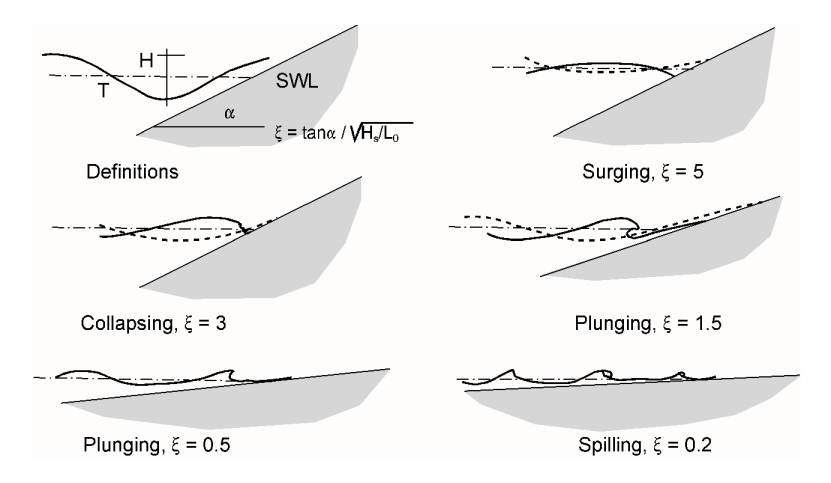


Figure 2-4 types of breakers and corresponding values of ξ [Schiereck, 2001]

The transition between breaking and non-breaking waves lies around a value of $\xi \approx 2.5$ to 3. For higher values of ξ the wave shows a surging behaviour. The collapsing breaker is between breaking and non-breaking. A plunging breaker shows a strongly asymmetric crest. The crest curls over and impinges on the slope like a water jet. If the slope is less steep, the wave shows a spilling behaviour.

2.2.2 Wave forces on the armour layer

The oscillating motion of the waves that hit the breakwater exert forces on the armour layer of the breakwater.

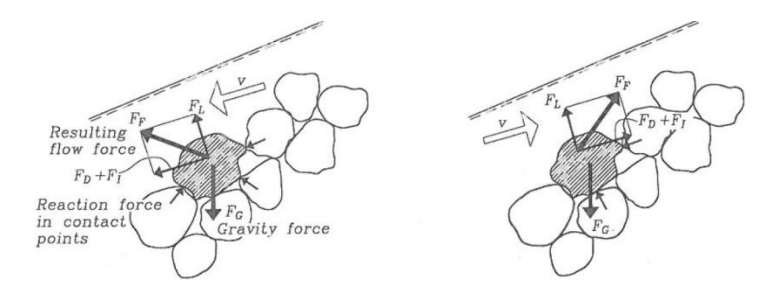


Figure 2-5 Forces on armour units due to oscillating flow [BURCHARTH, 1993]

In Figure 2-5 the forces due to the wave motion are presented. The arrow below 'v' indicates the direction of the flow. The resulting flow force F_F is the sum of the forces due to lift (F_L) , drag (F_D) and inertia (F_I) . It can be interpreted as a resulting force that tries to move the armour unit. The gravitational force F_g is the stabilizing force. Unfortunately the magnitudes of these forces are unknown and cannot be determined accurately. Although the schematization gives a qualitative overview of the forces on an armour layer during wave attack, it is not possible to calculate the stability of the armour layer with this schematization. It's common practice to use a different approach when calculating the stability of armour layers, which is discussed in section 2.2.5.

2.2.3 Stability mechanisms of the armour layer

There are three different mechanisms that can provide stability of the armour layer:

- The **weight** of the armour units
- The **friction** between armour units and/or under layer
- The **interlocking** between armour units

For breakwaters with an armour layer which consists of natural rock, the stability is determined by the weight of the rocks in the armour layer. The same applies for cubic shaped concrete units. Hollow cube armour units need friction in order to be stable. The friction between those blocks determines the stability. Interlocking is an important mechanism for concrete armour units such as the Xbloc. The armour units exert contact forces to the units next to them. The figure below presents the concept of contact forces between interlocking armour units.

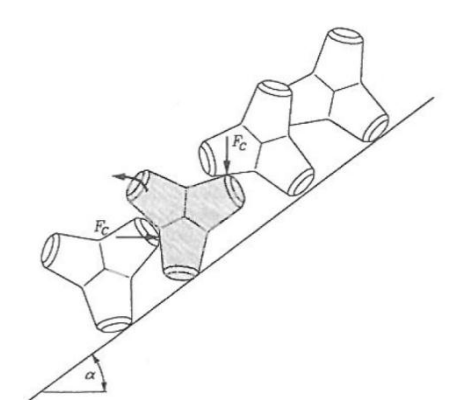


Figure 2-6 Contact forces on interlocking concrete armour units [BURCHARTH, 1993]

It becomes clear that the shape of the armour units has a large influence on the stability mechanism of the armour layer. The contribution of the different stability mechanisms is also influenced by the angle of the slope. Price did some tests with Dolos armour units and found that the interlocking capacity increased for a larger slope angle [BURCHARTH, 1993].

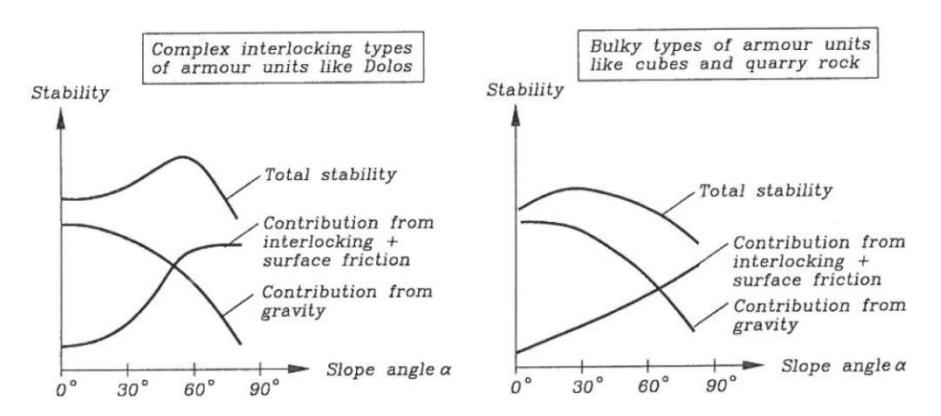


Figure 2-7 Influence of the slope angle on interlocking and stability. Figure from BURCHARTH, 1993

2.2.4 Failure mechanisms of the armour layer

A definition of **failure** is: a condition in which the structure loses its specified functionality [VERHAGEN *et al.*, 2012]. The main function of the armour layer is, as described in section 1.1.2, the absorption of wave energy. Hence one could say that failure of the armour layer can be interpreted as the inability to absorb wave energy. Some typical failure mechanisms of the armour layer of the breakwater are presented in Figure 2-8.

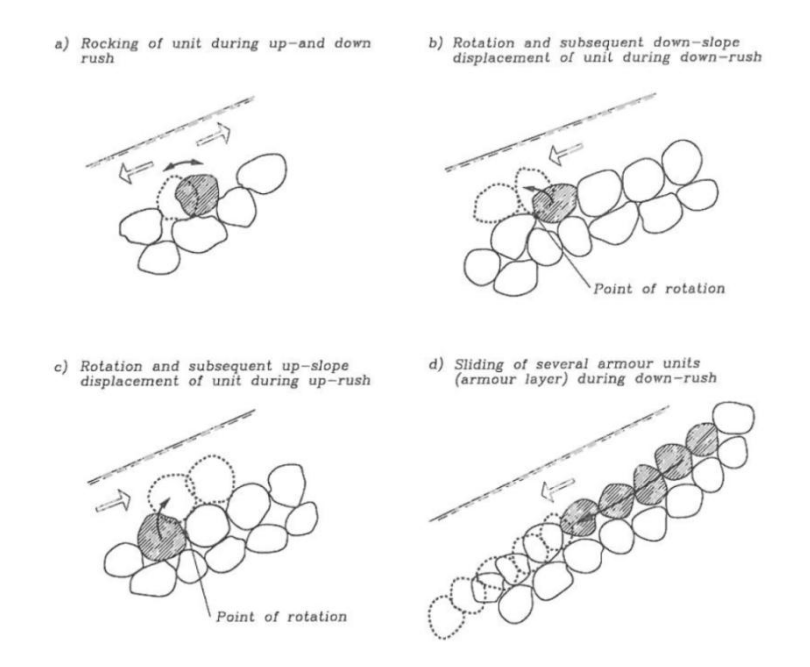


Figure 2-8 Typical failure mechanisms of the armour layer of a breakwater [Burcharth, 1993]

Rocking is the rotational movement of an armour unit due to wave loading. As the wave loading varies in size and direction rapidly due to the oscillating character of the wave itself, the armour unit will return to its original position due to the stabilizing effect of the gravitational force. If the wave loading becomes higher, **extraction** might occur. In this situation the units are also moved due to the wave loading, but the stabilizing effect of the gravitational force is not large enough to make sure the unit returns to its original position. Hence the unit is displaced. A more severe failure mechanism is the **sliding** of several armour units along the slope during down-rush.

2.2.5 Hydraulic stability formulae

Because the water movement due to breaking waves on a slope is very complex, it is (still) not possible to determine the forces on armour units accurately. Therefore empirical formulae have been designed in order to calculate the stability of armour layers.

Stability number

An important parameter is the **stability number**, which is defined as in the equation below. For many concrete armour units the design criterion is that this stability number should be a certain value.

$$N_{s} = \frac{H_{s}}{\Delta \cdot D_{n}}$$
 2.4

Hudson formula

Many tests were performed by Hudson in 1953 [SCHIERECK, 2001] on the stability of rock. He proposed the following formula for the required weight of the armour stone:

$$W = \frac{\rho_{s} \cdot H_{s}^{3}}{K_{D} \cdot \Delta^{3} \cdot \cot \alpha}$$
 2.5

It can be written in another form as:

$$\frac{H_s}{\Delta \cdot D_n} = \sqrt[3]{K_D \cdot \cot \alpha}$$
 2.6

In which:

$ ho_{\scriptscriptstyle S}$	Density of armour material	[kg/m ³]
Δ	Relative density of armour material	[-]
D_n	Nominal diameter of stone	[m]
K_D	Stability coefficient	[-]
α	Slope angle	[°]

This formula is very simple and used worldwide. However, the validity is limited. Furthermore the stability coefficient K_D is the factor in which all the unknown effects are included, it is the 'dustbin factor' of the formula. The stability coefficient is in the order of 3 for natural rock and in the order of 10 for concrete interlocking units. The stability coefficient includes some accepted damage, but the definition of damage is not very clear [SCHIERECK, 2001]. Some important aspects are neglected or they are implicitly taken into account by means of the K_D factor. However, this is not very clear. It should be mentioned that van der Meer proposed a design formula which takes more variables into account. This formula is only for armour layers with natural rock and therefore not discussed further. One is referred to e.g. SCHIERECK, 2001 for more details.

2.2.6 Design aspects of armour layers with Xbloc

This section elaborates the design of Xbloc armour layers. For the general aspects of Xbloc one is referred to section 1.1.3.

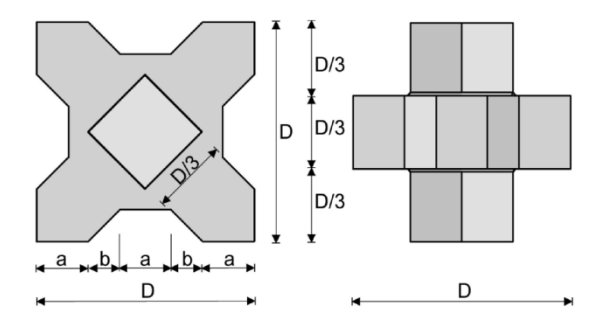


Figure 2-9 Geometry of the Xbloc. Figure from www.xbloc.com

Calculation of the block size

The required volume of the units can be calculated with the following formula:

$$V = \left(\frac{H_s}{2.77 \cdot \Delta}\right)^3 \tag{2.7}$$

The height of the Xbloc units can be determined with:

$$D = \sqrt[3]{3 \cdot V}$$
 2.8

The factor 2.77 in equation 2.7 represents the stability number. This value corresponds to a K_D value of 16 in the Hudson formula for a 3:4 slope, which is a normal steepness for slopes with concrete armour units. However, it should be noted that the Hudson formula is not valid for this slope.

Placement

Because interlocking armour units derive their stability from neighbouring units, placement is important. The preferred Xbloc placement orientation is with one of the legs of the X pointing downward. It turns out that this placement method leads to the highest stability. The units are placed on a predefined grid with a random orientation. An important aspect is the density of placement. Physical model tests which were performed in 2002 show that the density of placement of Xbloc units influences the stability. It was found that a higher placement density results in a higher stability number [BAKKER *et al.*, 2005]. Figure 2-10 presents the results of these tests. From the figure it becomes clear that placement with a density of more than 1.18 units/D² lead to a better hydraulic stability. Lower placement densities show a constant stability.

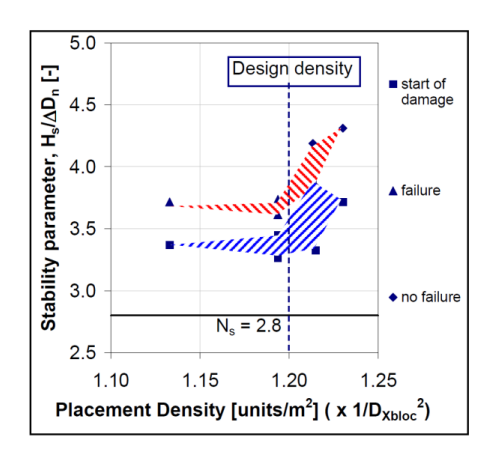


Figure 2-10 Influence of placement density on stability [BAKKER et al., 2005]

The placement density can be determined with:

$$PD = \frac{(N_x - 1)(N_y - 1)}{L_x \cdot L_y}$$
 2.9

In which:

PD	Placement density	$[m^{-2}]$
N_{x}	Number of units in horizontal direction	[-]
N_y	Number of units in upslope direction	[-]
L_{x}	Horizontal length of the section	[m]
L_y	Upslope length of the section	[m]

The target value of the placement density for Xbloc armour layers is 1.20 units/D^2 , where D denotes the diameter of the Xbloc. The actual value of the placement density should be in the range of 98 to 105 per cent of the target value.

Slope angle

In section 2.2.3 it was discussed that for interlocking armour units a steeper slope results in better interlocking and a higher stability. Therefore the design slope of Xbloc breakwaters is between 2:3 and 3:4 (vertical: horizontal) which is relatively steep for a rubble mound breakwater. If the steepness of the slope is less than 2:3 then the weight of the armour units has to be increased.

Wave steepness

Physical model tests were performed to investigate the influence of the wave steepness on the stability. It turned out that higher wave steepness leads to a higher stability number, but also to a larger scatter in the results [BAKKER *et al.*, 2005]. The wave steepness is not taken into account in the design.

Zero damage

Because the Xblocs are applied in a single layer, zero damage is prescribed. Damage of the armour layer could result in outwash of under layer and core material. This could lead to the development of failure

Phenomena that affect the required unit size

In some cases the stability factor of 2.77 is not sufficient for the armour units to be stable. Local conditions or phenomena may result in a larger required armour unit. Some phenomena result in higher wave loads on the structure and/or a decreased stability of the armour layer. In appendix I the correction factors prescribed by DMC for different phenomena are given.

2.3 Aspects of the under layer

In this section insight in the under layer of breakwaters is given. Design guidelines are discussed before the under layer in model and prototype are compared. Earlier research on the under layer profile for Xbloc breakwaters is discussed and the different methods of measuring the under layer are treated.

2.3.1 Design of the under layer

The under layer is in general constructed with a thickness of two times the median nominal diameter of the under layer rock size D_{n50} . DMC prescribes that the weight of the rocks in the under layer should be 1/15 to 1/7 of the weight of the weight of the armour units. Furthermore standard rock

gradings should be applied in under layers of breakwaters which are constructed with Xbloc armour units. DMC prescribes that a certain range of Xbloc sizes should be applied on a standard rock grading of the under layer; e.g. DMC prescribes an under layer of 300 to 1000kg for Xbloc units with a diameter of 1.65 to 2.99m. This implies that different sizes of Xbloc units are applied on the same size of rocks in the under layer.

2.3.2 The under layer in prototype and model

Prototype situation

The under layer in prototype consist of heavy rocks; in general gradings of 300 to 1000 kg or more. Therefore the rocks are placed individually, for example with a hydraulic excavator which is presented in Figure 2-11.



Figure 2-11 Under layer construction in prototype. Figure from www.seaportservices.com

The under layer in prototype can deviate from the designed under layer. Wave attack during construction or simply insufficient quality of construction can be causes of these deviations. In prototype the under layer consists of a heavy rock grading and is constructed with large equipment [MONSTER AND PHILIPSEN, 2010]. These factors make it difficult to construct the under layer according to the design. A survey campaign is usually carried out to check if the under layer is placed according to the design.

Model situation

The under layer in model situation is placed in bulk: multiple rocks are placed at once. The cross section of the breakwater is usually drawn on the side windows of the flume. As a result, the constructor knows where to place the rocks. The layer is smoothened with a spatula in order to place the layer as drawn on the windows, see also Figure 2-12. The under layer profile is usually not measured because it can be compared with the designed profile, which is drawn on the side windows.



Figure 2-12 Placement of the under layer in model situation

2.3.3 Tolerances of the under layer

The term **tolerance** relates to the extent of deviation from the ideal that can be accepted or tolerated [CIRIA, 2007]. In Figure 2-13 a constructed profile and a designed profile is presented. The dotted red and green lines represent the positive and negative tolerances. The maximum deviations from the designed profile are indicated by means of arrow 1 and 2. These maximum deviations are equal to the tolerances.

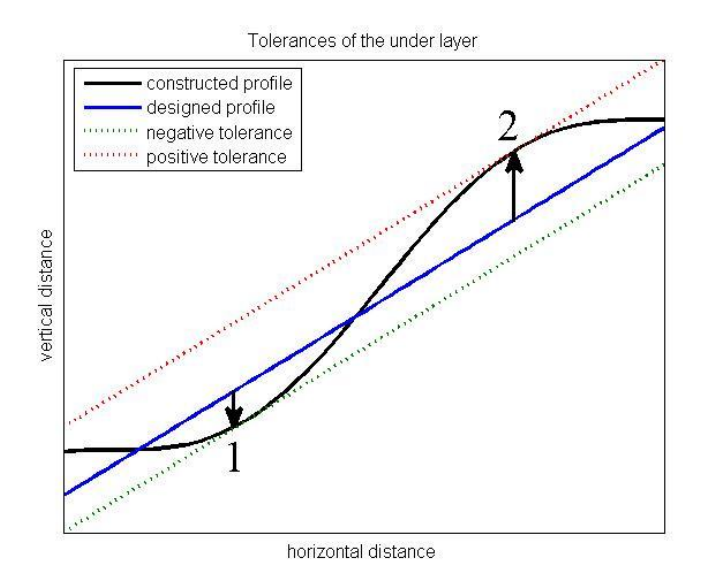


Figure 2-13 Definition of the negative and positive tolerances

Magnitude of tolerances

The criteria for a certain tolerance can be based on the possibilities of construction, the requirements, the necessity and the affordability. The setting of tolerances requires a careful balance of the mentioned criteria. In Table 2-1 the practical, achievable vertical tolerances for rock with a mean mass larger than 300kg placed with land based equipment are presented. These values apply for under layers constructed with equipment such as hydraulic excavators or crawler cranes in case of individual placement, or dump trucks in case of bulk placement.

Table 2-1 Practical, achievable vertical placing tolerances with land based equipment. C	JIRIA, 2007
--	-------------

Depth of placing	Placed in Bulk	Placed individually	
relative to LW		Individual	Design profile to
		measurements	actual mean profile
Above LW = dry	+0.4 m to -0.2 m	$+/-0.3D_{n50}$	$+0.35$ to $-0.25D_{n50}$
0 to -5m	+0.8 m to -0.3 m	+/- 0.5 <i>D</i> _{n50}	$+0.60$ to $-0.40D_{n50}$
-5 to -15m	+1.2 m to -0.4 m	Unknown	Unknown
Below -15m	+1.5 m to -0.5 m	Unknown	Unknown

The tolerances depend on the type of grading, according to HAUER, 2000. Remarkable is that larger positive tolerances than negative tolerances are expected according to Table 2-1. This is a logical consequence of measurements with the spherical foot staff method. This is discussed in section 2.3.5. Although the tolerances for individually placed rock are not given for depths larger than 5m, it is expected that they increase with increasing depth because this applies to bulk placed rock. In Table 2-2 the proposed values for the tolerances are presented. They values are applicable to heavy gradings, which are generally applied in under layers in breakwaters.

Table 2-2 Vertical tolerances according to HAUER, 2000

Land base	Waterborne equipment	
Above water	Under water	Under water
+/- 0.5 <i>D</i> _{<i>n</i>50}	+/- 0.6 <i>D</i> _{n50}	+/- 0.8 <i>D</i> _{n50}

It should be mentioned that the values presented in Table 2-2 are the sum of construction and measurement tolerances.

Magnitude of tolerances for Xbloc breakwaters

DMC prescribes that the tolerance in perpendicular direction may not exceed the value of $0.5\ D_{n50}$. In general the profile is measured vertically. For breakwaters with slopes between 2:3 and 3:4 this implies a vertical tolerance between 0.60 and $0.63\ D_{n50}$ in both positive and negative direction for the mentioned slopes. In Figure 2-14 the difference between vertical and perpendicular tolerance is made more clear for a 2:3 slope.

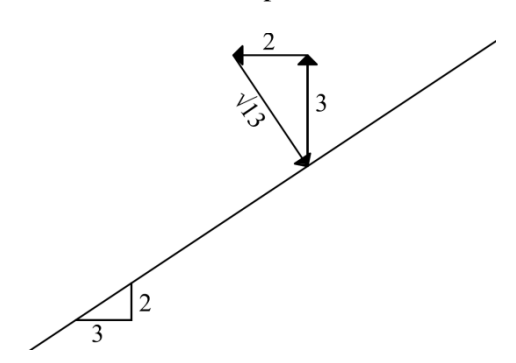


Figure 2-14 Difference between perpendicular and vertical tolerance

For a 2:3 slope, a perpendicular tolerance of 0.5 D_{n50} corresponds to a vertical tolerance of 0.6 D_{n50} . Please note that the concept of tolerance implies a tolerance in vertical direction, unless stated otherwise.

Tolerances and stability of the armour layer

The influence of the tolerance of the under layer on the interlocking of the armour layer was investigated by means of extraction force tests [Monster and Phillipsen, 2010]. These types of tests give an indication of the interlocking of the armour units, but they do not give information about the hydraulic stability of the units during wave attack. The tests showed a constant interlocking for a perpendicular tolerance up to $+\frac{3}{4}D_{n50}$ to $-\frac{1}{2}D_{n50}$. In Figure 2-15 the relation between extraction force and tolerance according to Monster and Philipsen is given.

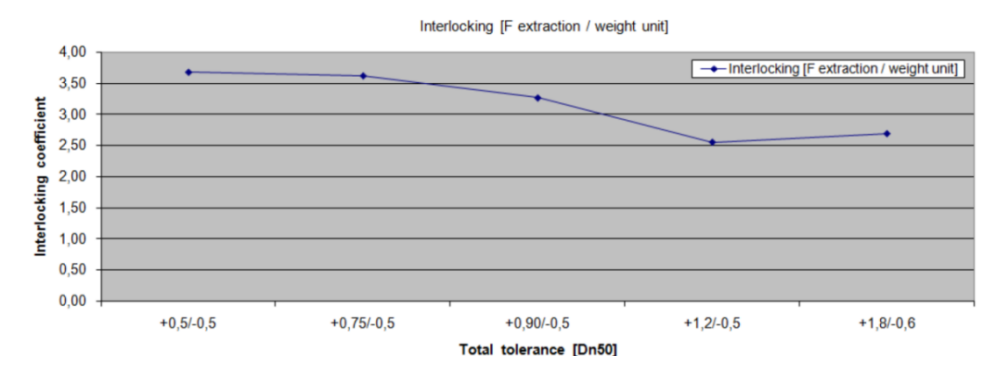


Figure 2-15 Relation between extraction force and tolerance. Figure from Monster and Philipsen, 2010

If the under layer does not meet the prescribed tolerances, the under layer has a higher roughness due to the deviations from the designed profile. This results in differences in packing density and interlocking along the slope of the armour layer. It is very likely that the hydraulic stability will vary along the slope as a result of this.

2.3.4 Roughness of the under layer

The roughness of the under layer is an indication of the course of the profile. Both the natural and additional roughness are discussed here.

Natural roughness

The natural roughness is always present, even in a completely flat bed or bank structure. Complete flatness is hereby defined as the situation in which all the top levels of the rocks are situated in the same plane. The real top level still consists of the tops of the rock particles which are higher than the holes between these particles. This is made more clear in Figure 2-16.

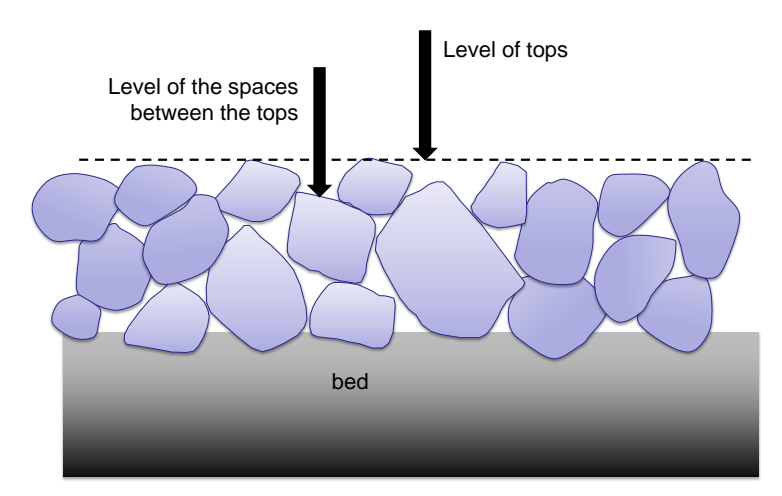


Figure 2-16 Natural roughness of a relatively flat structure. Figure from CUR publication 'Construction accuracies' (in preparation)

The length scale of the natural roughness is in the order of the nominal diameter of the rock material.

Additional roughness

The additional roughness occurs due to inaccuracies during the construction phase. They occur (amongst other factors) due to placement methods, environmental conditions during construction and skill of the work crew.

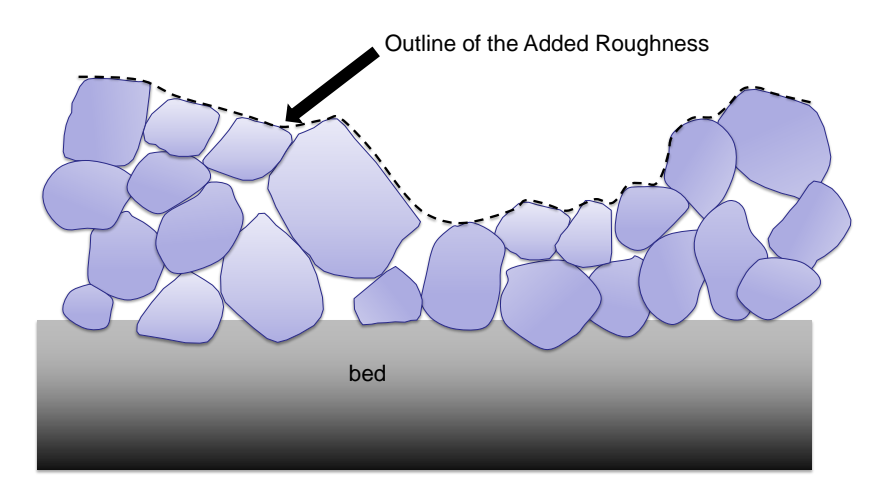


Figure 2-17 Additional roughness as a result of inaccuracies during construction. Figure from CUR publication 'Construction accuracies' (in preparation)

This type of roughness is subject to design criteria such as maximum allowable vertical tolerances. A larger additional roughness corresponds to a larger vertical tolerance. Depending on the construction process, different length scales of roughness can occur. The effect of the under layer profile which is investigated in this thesis refers in general to the effect of the additional roughness, unless stated otherwise. Research performed by DE LANGE, 2010 show that a larger roughness of the under layer lead to a lower stability of the armour layer. The magnitude of the roughness of those tests is unfortunately not specified.

Characteristic parameters of roughness

In Figure 2-18 the two characteristic dimensions of the roughness of the under layer are shown. A fictional constructed profile is plotted versus a designed profile in order to show the deviation in vertical and horizontal direction. Not only the deviation perpendicular to the designed profile is of importance, but also the length scale of the deviation influences the roughness. The deviation in vertical direction is denoted with 'a' and the length scale of the deviation along the slope with 'l'. Another characteristic parameter is the position of the deviation along the slope.

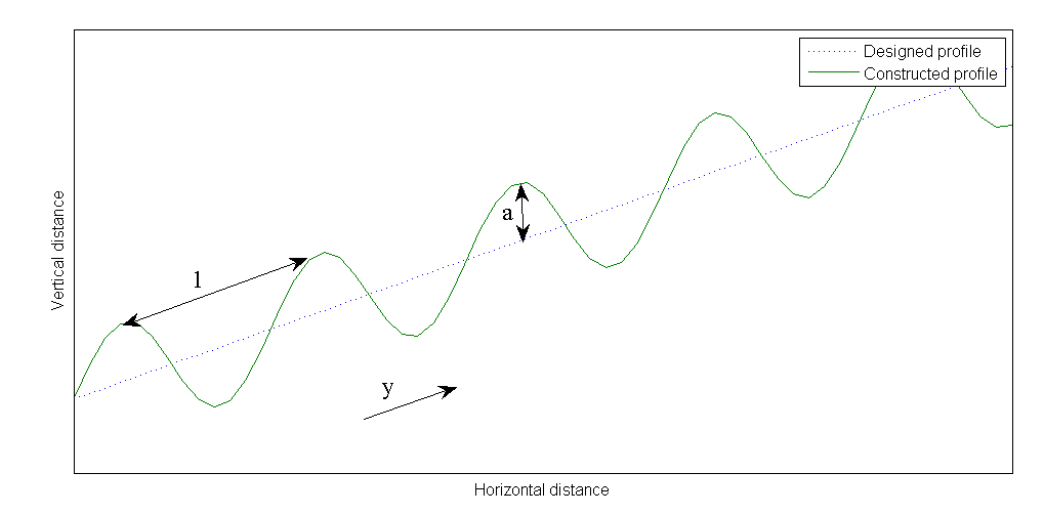


Figure 2-18 Dimensions of roughness of the under layer

2.3.5 Survey techniques and accuracies

Different methods are available to measure under layer profiles. The most important methods and the difference in results are discussed.

Above water

The survey method with the **spherical foot staff** is recommended by CIRIA, 2007. It consists of a probe with a spherical end with a recommended diameter of $0.5\ D_{n50}$. Measurements should be carried out at intervals of $0.75\ D_{n50}$ across the measurement profile. It should be noted that if the sphere has a larger diameter than the diameter of the holes in the structure, these holes cannot be measured [BOSMA, 2001]. Therefore the size of the sphere has a large influence on the outcome of the survey campaign. In Figure 2-19 the staff with the spherical foot is presented.



Figure 2-19 Survey with the spherical foot staff. Figure from MEULEPAS et al., 1999.

Other methods available for survey are the highest point method and the conventional staff method. Each method results in a different level which is measured, this is made more clear in Figure 2-20.

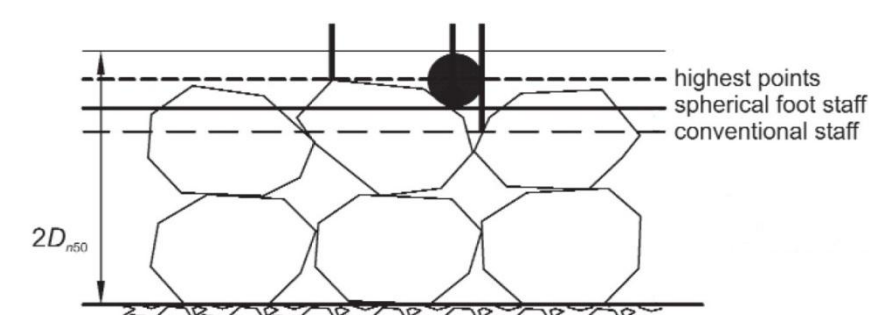


Figure 2-20 Measurement levels of different survey methods. Figure from CIRIA, 2007.

In practice the spherical foot staff method is commonly used to measure the profile of the under layer. This spherical foot staff is the preferred method, but other methods are used as well.

Under water

Parts of the structure that are under water are usually measured with an echosounder. Echosounders measure the water depth by determining the difference in time between the moment of sending the sound signal and the moment of receiving the signal after reflection from the bed. A distinction can be made between single and multi-beam echosounders. **Single-beam** systems make use of one sound beam so that only the section right underneath the survey vessel is being measured. The circular section which is being measured is called the footprint. **Multi-beam** systems make used of more than one sound beam. This allows a line of points to be measured in one measurement sequence. When rough or hard surfaces are being measured (e.g. heavy gradings), acoustic disruptions occur, disrupting the processing of the sound beams. This can lead to systematic errors [CIRIA, 2007]. The principle of single and multi-beam echosounders and their footprint is presented in Figure 2-21.

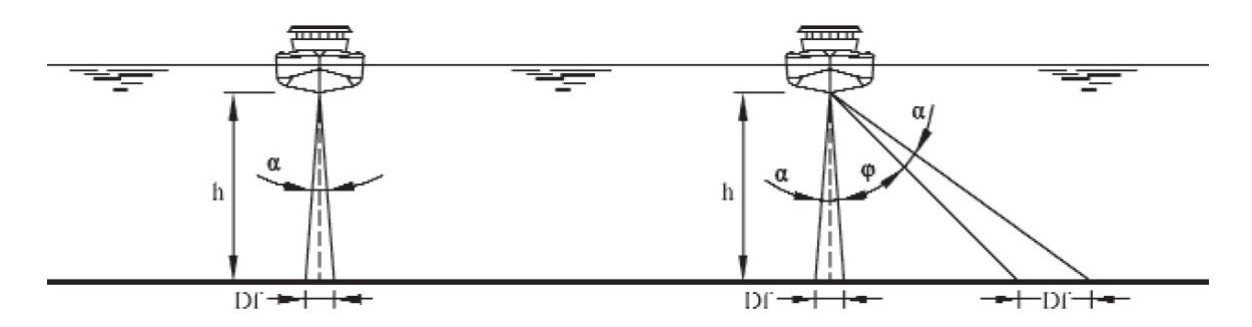


Figure 2-21 Single and multi-beam echousounder systems and their footprints. Figure from CIRIA, 2007.

Differences in results of the methods

In order to assess the difference in outcomes of measurements with different systems, an experiment was performed in the dry dock of Verolme in the Port of Rotterdam. Two layers of armour stones were placed with a different grading; 10-60kg and 40-200kg. For more details one is referred to MEULEPAS *et al.*, 1999. The layer thickness which was used is $2.5 D_{n50}$.

Table 2-3 Differences in measurement of the average layer thickness compared with results obtained from spherical foot staff measurements. From HAUER, 2000

Grading	Measurement system		
	Single-beam	Multi-beam	Conventional staff
10 - 60 kg	-3%	-21%	-14%
40 – 200 kg	-5%	-11%	-8%

From Table 2-3 it becomes clear that the spherical foot staff measures a higher profile than other methods. The single-beam echosounder gives comparable results. The fact that this method gives slightly lower levels can be explained by the size of the footprint which was not large enough to exclude the holes in the structure. If one wants to measure only the top levels of the stones, the footprint should be at least 3 to 5 times the nominal stone diameter. The conventional staff method gives a lower layer thickness and lower profile than the spherical foot staff. The values of minus 8% and minus 14% correspond to differences of 20% to 40% of the D_{n50} . The multi-beam method shows even lower levels than the conventional staff method. This is remarkable because the conventional staff is able to measure all the holes and hence the multi-beam method cannot measure lower levels. Therefore the low levels of the multi-beam method can only be explained by the acoustic disruptions causing errors [HAUER, 2000]. A different method is the survey with the bucket of a hydraulic excavator. This method is not further discussed because no literature is available on this method. BOSMA, 2001 performed research into different survey techniques as well. He investigated the difference between the conventional staff and the spherical foot system. He found that the difference in profile height is a function of the nominal stone diameter and can be written as:

$$z_{difference} = 0.204 \cdot D_{n50} + 0.18 \tag{2.10}$$

In this case the dimension is [cm]. Apparently he found a difference of approximately 20% of the nominal diameter in profile height. A new version (which is not published yet) of the book '*Maak-en meetnauwkeurigheden*' describes a difference in measured profile height of 21% of the nominal diameter between the spherical foot staff method and a conventional staff method.

2.3.6 Conclusions

For under layers with Xbloc armour layers standard classes of natural rock gradings are used for different sizes of the armour units. This implies that different sizes of Xbloc units are applied on the same size of rocks in the under layer. The maximum deviation of the under layer in constructed profile from the designed profile is $0.5D_{n50}$ in both positive and negative perpendicular direction. i.e. the tolerances of the under layer for Xbloc breakwaters is $+/-0.5D_{n50}$ in perpendicular direction. Earlier research by means of extraction force tests showed that the tolerances of the under layer cannot be adapted further than $+\frac{3}{4}D_{n50}$ and $-\frac{1}{2}D_{n50}$ (in perpendicular direction). The measured profile height is dependent on the measurement method. The standard method is the spherical foot staff method, which measures a relatively high profile compared to other methods such as the conventional staff. This difference in measured profile height is a consequence of the shape of the sphere.

3 Physical scale model

The experimental part of this thesis is conducted in the flume of DMC in Utrecht, The Netherlands. A physical scale model is used to investigate the influence of the under layer profile on the stability of the armour layer.

3.1 Scaling

When a prototype is scaled to a physical model one has to know which criteria have to be met and how accurate the physical model actually is. In this section a brief overview of scale models, the requirements and shortcomings is given.

3.1.1 General aspects of physical models

The basis of all physical modelling is the idea that the model behaves in a manner similar to the prototype it is intended to emulate. Thus, a properly validated physical model can be used to predict the prototype under a specified set of conditions [Hughes, 1993].

Scale

Physical models are usually applied as a scale model. In this context, **scale** means the relation of the value of a certain parameter in prototype and model. According to this definition the following formula holds for the scale of parameter 'x':

$$n_x = \frac{x_p}{x_m} \tag{3.1}$$

In which:

 x_p value of 'x' in prototype x_m value of 'x' in model

Motivation for physical models

Especially in Coastal Engineering practice physical models are valuable due to the fact that the physical processes involved are not yet completely described by design equations or formulae. Advantages of physical models are the fact that they are cost effective in large coastal projects such as breakwater construction. The processes that occur during testing are visible for the observer which makes interpretation of the results more easy. Furthermore a lot of relevant data can be generated due to the reduced size of the model. Disadvantages of physical models are laboratory effects and scale effects. An example of a laboratory effect is the influence of the boundaries of the model on the physical processes. Scale effects occur due to the difference in size between prototype and model. i.e. it is usually impossible to simulate all variables in correct relation to each other [HUGHES, 1993].

Similarity and similitude

An important concept in physical modelling is **similitude**. Similitude is achieved when all major factors influencing reactions are in proportion between model and prototype, while those factors that are not in proportion throughout the modelled domain are so small as to be insignificant to the process. Criteria of similitude are imposed by means of physical relations between parameters. They are mathematical conditions that must be met by certain ratios between prototype and model, and they cannot be adjusted without adjusting the underlying assumptions. These criteria are also called **scale laws**, which is the topic of the next section. A different concept is **similarity**. Conditions of similarity are chosen in order to make the model produce satisfactory results. These conditions usually comprise

one or more criteria of similitude and some other conditions determined by observation or intuition [Hughes, 1993].

3.1.2 Scale requirements

HUGHES, 1993 defined requirements which have to be met in scale models of coastal structures. He stated that the most important forces are inertia and gravity and these forces must be scaled correctly. Furthermore the flow near a coastal structure is always turbulent in prototype. Therefore the flow must be turbulent in the model as well. A third requirement is that the geometry of the model should be scaled correctly from prototype to model. These requirements are discussed below.

Froude scaling law

The Froude number is defined as:

$$Fr \equiv \sqrt{\frac{inertial\ force}{gravity\ force}} = \frac{u}{\sqrt{gl}}$$

In which l is a certain length [m] (in most cases the water depth) and u the flow velocity [m/s]. An important requirement in physical modelling of coastal structures is that the ratio between the inertial force and gravity force is the same in prototype and model. i.e. the Froude number must be the same. This requirement results in:

$$\left[\frac{u}{\sqrt{gl}}\right]_{n} = \left[\frac{u}{\sqrt{gl}}\right]_{m} \tag{3.3}$$

In which 'p' denotes prototype and 'm' denotes model. Rearranging equation 3.3 to an expression in terms of scales yields:

$$\frac{n_u}{\sqrt{n_g \cdot n_l}} = n_{Fr} = 1 \tag{3.4}$$

As gravity cannot be scaled, it follows that:

$$n_{u} = \sqrt{n_{l}}$$
 3.5

Reynolds scaling law

As mentioned the flow in the model must be turbulent. A widely used parameter used to indicate turbulence is the Reynolds number, which is defined as:

$$Re \equiv \frac{inertial\ force}{viscous\ force} = \frac{u \cdot l}{v}$$

In which ν is the viscosity of water. The Reynolds number is used to distinguish between laminar and turbulent flow. In order to achieve similitude, Reynolds number in prototype and model must be the same. The criterion for similitude is:

$$\frac{n_u \cdot n_l}{n_u} = n_{Re} = 1 \tag{3.7}$$

This criterion is impossible to meet, due to the fact that the viscosity of water ν is the same in prototype and model. However, this is not a problem in physical models of coastal structures. Near

and on coastal structures the flow is turbulent in prototype, hence the ratio inertial force and viscous force is large. As long as this ratio is still large in the model, the flow is still turbulent and behaves roughly the same.

Geometric similarity

The model must be **geometrically undistorted** in order to represent the prototype in an accurate way. This implies that the horizontal and vertical scales are the same, and they represent the true geometric reproduction of the prototype. According to Warnock, 1950 'geometric similarity exist between two objects or systems if the ratio of all corresponding linear dimensions are equal. This relationship is independent of motion of any kind and involves only similarity in form' [HUGHES, 1993].

3.1.3 Scale effects

In general it is impossible to achieve complete similitude as not all processes can be modelled according to the scale laws. As a result, **scale effects** occur. Scale effects occur due to intrinsic properties of water that cannot be adjusted (e.g. viscosity, air content, surface tension), interaction with compliant structures and other causes [TIRINDELLI AND LAMBERTI, 2004].

Viscous flow effects

As discussed in section 3.1.2 it is important that the flow in the model is turbulent. At the typical scales of physical models of coastal structures, in a model this is usually the case for the flow in the armour layer. However, the flow in the under layer and core of the breakwater might be laminar in the model. As a result viscous scale effects occur due to a reduced permeability of core layers and this may lead to higher downrush pressures from inside the structure. It is therefore required that the flow in the armour layer in model situation is turbulent. The armour layer Reynolds number is used to indicate the type of flow in the armour layer:

$$Re_{armour} = \frac{\sqrt{g \cdot H_S} \cdot l_a}{v}$$
 3.8

In which H_s is the significant wave height and l_a is the length of the armour unit. It was found that a minimum value of Re_{armour} in the order of 10^4 results in negligible scale effects.

Friction effects

In physical models the contact friction between the armour units may differ from prototype. This is due to the fact that in the model the roughness of the armour units can be relatively rougher than in prototype [HUGHES, 1993]. Painting the armour units makes them smoother. As the armour units are painted, with the purpose to be able to distinguish the units from each other, no scale effects of importance are expected.

Aeration effects

Hall, 1990 [HUGHES, 1993] performed experimental research on the entrainment and movement of air bubbles due to the water movement near breakwaters. He found that in small scale models the air bubbles are relatively large compared to the prototype. This results in more energy dissipation along the slope in model than in prototype. This phenomenon has influence on the wave run-up. In this thesis the focus is on the stability of the armour layer. It is therefore assumed that aeration scale effects are negligible.

3.2 Set-up of the experiments

The hydraulic tests have been carried out at the wave flume of DMC in Utrecht, The Netherlands. The flume has a length of 25m, a width of 0.60m and a height of 1.0m. The water level can vary between 0.40 and 0.70m for physical model tests.

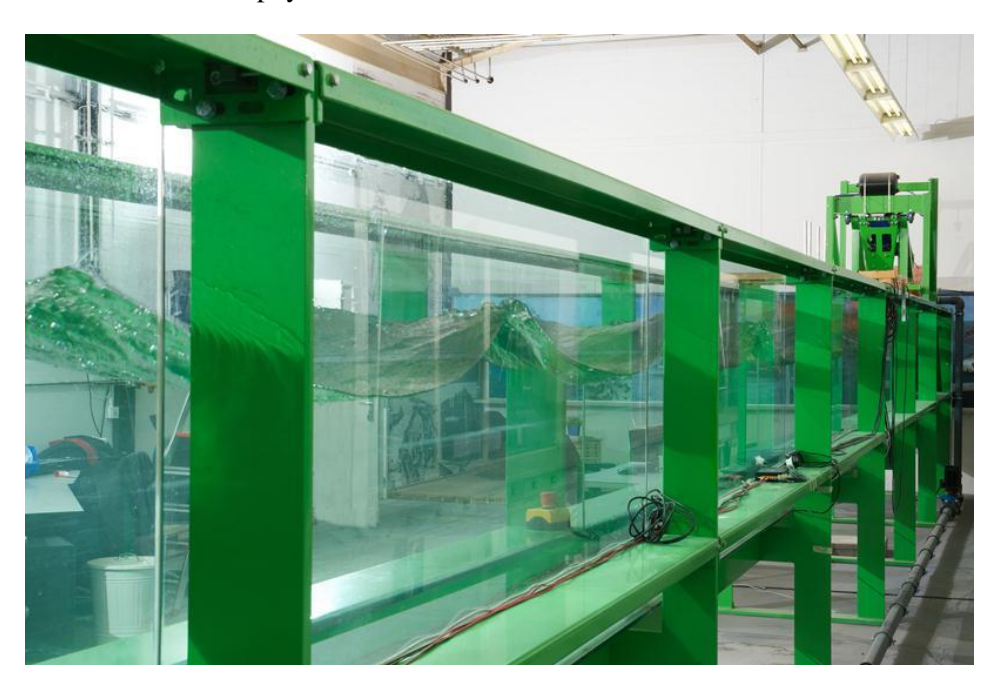


Figure 3-1 DMC wave flume in which the experiments have been carried out.

3.2.1 Flume layout

In Figure 3-2 a schematic side view of the wave flume is shown.

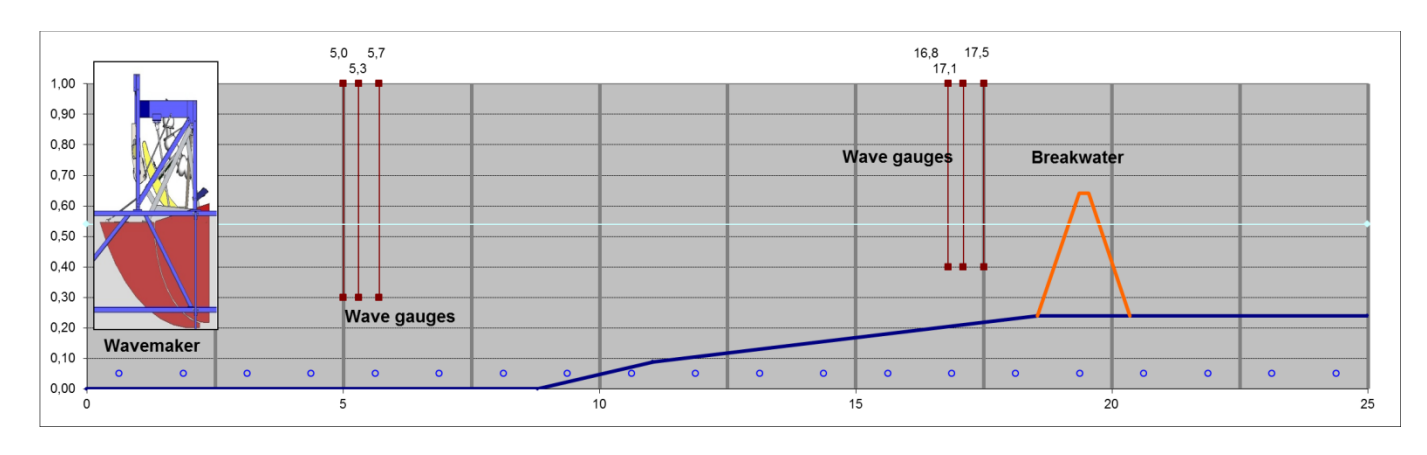


Figure 3-2 Schematic side view of the flume

Near the wave maker the water depth is 54cm. In order to simulate a sloping foreshore, which is found in prototype, a foreshore with slopes of 1:25 and 1:50 is applied. Due to practical reasons two different slopes are applied in the foreshore. In total there are six wave gauges installed to measure the waves. Three of them are placed at a small distance from the wave maker and three are located close to the breakwater.

3.2.2 Breakwater design

The tested breakwater has a design with dimensions which are generally applied in practice. An existing prototype situation is reproduced on scale in the wave flume. The geometric scale is 41.3. In Figure 3-3 the cross section of the model is presented.

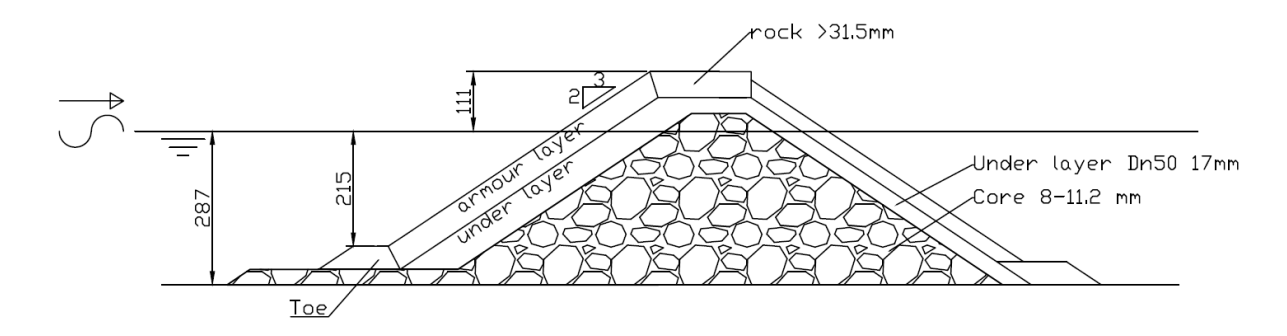


Figure 3-3 Cross section of the breakwater of the physical model tests. Dimensions in mm.

Armour layer

The armour layer consists of Xbloc armour units with a mass of 95.2 gram. These units have a height of 49.6 mm. The units which are used in the test are weighed individually; the results are given in appendix B. The armour units are scaled in such a way that the stability number N_s is the same in model and prototype:

$$\left[\frac{H_s}{\Delta D_n}\right]_{model} = \left[\frac{H_s}{\Delta D_n}\right]_{prototype}$$
3.9

In prototype the significant wave height $H_s = 4.9$ m. Applying equation 3.9 yields a significant wave height in model situation of 11.83cm. These values imply a geometric scale of 41.3. In section 2.2.6 the design calculation of Xbloc armour units was discussed. The general value of the stability number for Xbloc armour units is 2.77. In this case the stability number is 2.53. The reason behind this lower value of the stability number is the height of the crest, which is relatively low. The freeboard is approximately one significant wave height and the size of the armour units is adjusted for this. In appendix G details are given on the grid on which the armour units are placed.

Under layer

The under layer is scaled geometrically. The scale of the under layer and other parts which consists of natural rock is not the same as the geometrical scale of 41.3. This is because of the difference in relative density due to the density difference between fresh water in model situation and salt water in prototype situation. As a result the scale of the layers with natural rock, such as the under layer, is 43.0. In prototype the under layer consists of 300-1000kg rock. This grading is reproduced in the scale model. In the model under layer two standard gradings are used: 11 to 16.2mm and 16.2 to 22.4mm. These two gradings are mixed in a volume ratio of 1:2 in order to obtain the required nominal diameter of $D_{n50} = 14.5$ mm. Furthermore the thickness of the under layer is four times the nominal diameter. This thickness is larger than the prescribed thickness of $2D_{n50}$ because deviations of more than $2D_{n50}$ are constructed in the under layer. More details on the under layer are given in appendix C.

Core

The core cannot be scaled geometrically. This is due to the fact that otherwise significant viscous scale effects would occur. These effects can influence several physical processes, resulting in an inaccurate representation of the prototype by the model. Therefore the core is scaled in such a way that

the characteristic pore velocity is scaled according to the Froude scaling principle, which is described in section 3.1.2. The method proposed by BURCHARTH *et al*, 1999 is used to scale the core material. A nominal diameter of the core material of 9.6mm is applied in the model. More details on the scaling of the core are given in appendix A.

Toe

The toe of the breakwater is the foundation of the armour layer. In this project the focus is on the stability of the armour layer. Movement or failure of the toe has influence on the armour layer and is therefore unwanted. The toe has a safe design in order to prevent influence of (in)stability of the toe on the armour layer. A stability calculation has been done and it turns out a mass of 980 kg in prototype is required. Therefore it is chosen to scale the 1-3 ton grading to model dimensions and use these stones as toe material. More details on the calculation and the rock grading are given in appendix D.

Crest and rear side of the structure

On the crest rocks are located with a mean mass of 54 gram. The grading is presented in appendix E. Epoxy tiles have been used on the rear slope due to practical reasons. On the rear side also a toe is constructed to support these tiles. This toe consist of the same material as the crest.

3.2.3 Scales applied in the model

As mentioned earlier the geometric scale of the model is 41.3. This implies that the dimensions in the model are 41.3 times smaller than in prototype. The density of the armour units in the model is smaller than in prototype. This is done because fresh water is used in the flume and in this way the relative density is the same in model and prototype. The density of natural rock cannot be adjusted and therefore the geometric scale of the natural rocks are a bit larger than the geometric scale of the other parts of the scale model. In Table 3-1 the scales of the most important parameters is given:

Parameter	Symbol	Scale
Density	$n_{ ho}$	1
Length	n_l	41.3
Length (natural rock)	$n_{l,natural\ rock}$	43.0
Time	n_t	$\sqrt{41.3} = 6.4$
Gravity	n_g	1
Mass of natural rock	n_{mass}	$43^3 = 7.9 \cdot 10^5$

Table 3-1 Scales used in the model

3.3 Wave aspects

3.3.1 Wave generator

The wave flume of DMC is equipped with an Edinburgh Designs piston wave generator (see Figure 3-4). This wave generator can generate both regular and irregular waves. It corrects the paddle motion to absorb reflected waves. As a result, the produced wave field is approximately equal to the predicted wave field.



Figure 3-4 Wave generator in the flume of DMC

3.3.2 Energy density spectrum

The model tests are performed with irregular waves. Irregular waves represent natural conditions. These irregular waves are described with an energy density spectrum. In this case a JONSWAP spectrum is used, which is used widely to describe wind-generated waves. This spectrum describes young sea states, which are the most common sea states near coastal structures such as breakwaters. The JONSWAP energy spectrum is formulated as:

$$E_{JONSWAP}(f) = \alpha g^2 (2\pi)^{-4} f^{-5} \cdot \exp\left[-\frac{5}{4} \left(\frac{f}{f_{peak}}\right)^{-4}\right] \cdot \gamma^{\left[\frac{1}{2} \left(\frac{f}{f_{peak}-1}}\right)^2\right]$$
 3.10

In which:

$E_{JONSWAP}$	Energy density	$[m^2 \cdot s]$
f	Frequency	$[s^{-1}]$
α	Energy scale	[-]
f_{peak}	Peak frequency	$[s^{-1}]$
γ	Peak-enhancement factor	[-]
σ	Peak-width parameter	[-]

Furthermore $\sigma = \sigma_a$ for $f \le f_{peak}$ and $\sigma = \sigma_b$ for $f > f_{peak}$

For a standard JONSWAP spectrum, which is applied in this case, the following holds:

 $\sigma_a = 0.07$ $\sigma_b = 0.09$ $\gamma = 3.3$ $\alpha = 0.0081$

3.3.3 Wave characteristics

The waves which are generated are the same for all the tested scenarios. The wave height is increased with each run of the test. At the start the waves have a height of 60% of the design value of the significant wave height. At the next run this value is 80%, followed by 100% and the last run is an overload condition of 120% of the design wave height. This stepwise increase in wave loading is done in order to simulate milder wave attack than the design storm, which is expected to occur in prototype situation as well. As a result the armour units can settle a little bit and form a stable armour layer.

Wave parameters

The design value of the significant wave height is 4.9m in prototype. The corresponding peak period is 10s. Dividing the prototype value of the wave height by the scale yields a design wave height in the model of 11.83cm. As mentioned the wave height is increased stepwise from 60 to 120% of this value. During all the runs the wave steepness in deep water is constant. Every run consists of 1000 waves. In Table 3-2 the characteristic parameters of the waves are presented.

Table 3-2 Imposed	wave conditions
-------------------	-----------------

Condition	H _s [mm]	$T_p[s]$	$\frac{H_s}{L_0}$ [-]	Test duration [min]
60%	70.98	1.276	0.031	21
80%	94.64	1.389	0.031	23
100%	118.3	1.554	0.031	26
120%	141.9	1.702	0.031	28
(overload)				

Breaker types

Because the deep water wave steepness $\frac{H_S}{L_0}$ is held constant, the surf similarity parameter ξ is also constant for the different runs. The value of ξ is 3.8, which corresponds to surging waves. This implies that (mostly) non breaking waves are expected to be observed.

3.4 Test program

3.4.1 Constructability of the under layer

Tests of the constructability of deviations of under layers have been performed. This is done in order to see if it is actually possible to construct specific deviations in the under layer profile. Because the angle of repose is close to slope angle of 3V:4H it is not possible to construct deviations of more than one D_{n50} from the designed profile. This is due to the fact that at the location of the deviations the slope is locally steeper than the designed slope. The limiting parameter is the angle of repose, which simply does not allow the 3:4 slope (36.9°) to become steeper. This is according to the theory, see section 2.1.2. Trend lines are plotted of the measured profiles; they show that the intended 3:4 slope is only achieved in an exceptional case. The average steepness of these slopes is 0.72 instead of 0.75. This corresponds to a difference of 1.1° . Because it is very hard to construct the 3:4 profile, even without the deviations, it is chosen to apply a 2:3 slope.

3.4.2 Test scenarios

After the constructability tests were performed, a test program has been set up for the hydraulic stability tests. In Table 3-3 the tested scenarios are presented. Every scenario is tested three times. It should be mentioned that the values of tolerances in the table are the intended values of tolerances. The exact values of the tolerances in the model are discussed in section 5.2.4.

Table 3-3 Different test scenarios

Deviation under layer	Test name
None	A
$3.0 D_{n50}$ over short distance	В
$2.0 D_{n50}$ over long distance	С
(concave)	
$2.0 D_{n50}$ over long distance	D
(convex)	
$1.5 D_{n50}$ over short distance	Е
$1.5 D_{n50}$ over long distance	F
$1.0D_{n50}$ over short distance	G

First a reference case is tested with no deviation in the under layer. This means constructing the under layer profile as close to the designed profile as possible. After these tests the under layer profile is adjusted and deviations are constructed. This implies that roughness is added to the under layer, i.e. the additional roughness is increased. These deviations are constructed over a long and short distance along the slope. Short distance is meant here as the shortest possible alongslope distance at which it is possible to construct the vertical deviation. Long distance is meant here as the longest distance alongslope at which it is possible to construct the vertical deviation. This is schematically presented in Figure 3-5. The lines represent profiles as seen from a virtual cross section.

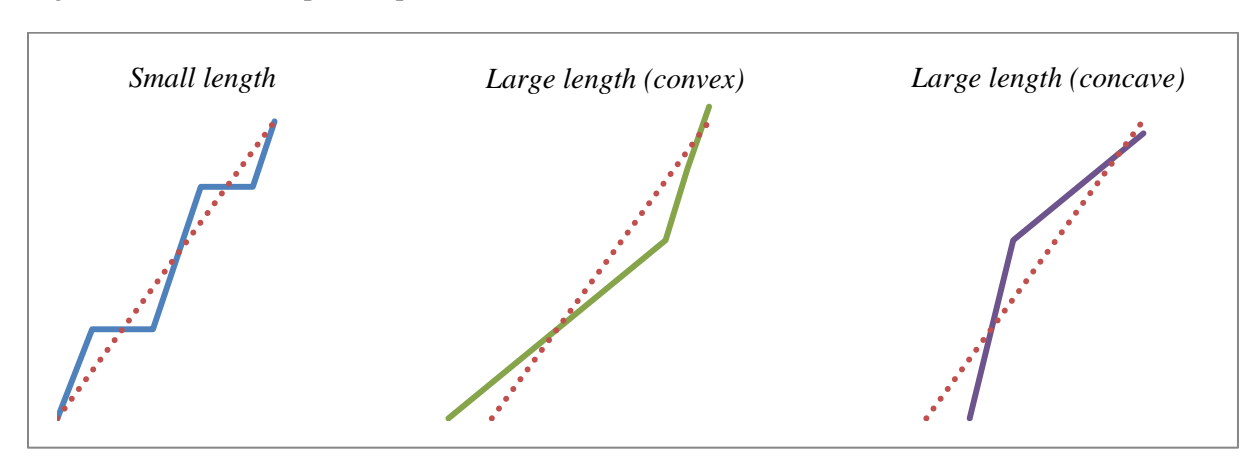


Figure 3-5 Schematization of large and small lengths of the deviations.

The red dotted line represents the profile of the reference case. The solid lines represent the deviated profiles which are constructed. The small length deviation is constructed with locally steep slopes followed by horizontal slopes. In case of large length the slope is locally milder or steeper than the 2:3 slope. Both convex and concave profiles are tested.

3.5 Parameters to be measured

3.5.1 Definition of damage

DMC prescribes zero damage of the armour layer for design with Xbloc. Three modes of damage of the armour layer can be distinguished, namely **settlements**, **rocking** and **extraction** of the armour units.

Settlements

Settlement is defined as a small extraction of a unit to a location with better interlocking. Settlements are likely to occur at the very beginning of the test. After these initial settlements the units generally find a stable position in the armour layer. Therefore these type of small settlements should not be counted as damage. Significant settlements are settlements of more than 0.5D (half the diameter of the armour unit). Significant settlements can cause loss of interlocking and should therefore be prevented.

Rocking

An armour unit is rocking in case it is visibly moving during more than 2 % of the waves. Visible movement is a rotational movement of more than 5° of the armour unit. According to DMC an armour unit which is rocking has an unacceptable risk of fracturing in prototype. Rocking of more than 2% of the armour units decreases the interlocking of the armour units and can therefore cause extraction of the armour units [ZWANENBURG, 2012]. Therefore a maximum of 2% of the armour units are allowed to move during more than 2% of the waves.

Extraction

Extraction of an armour unit was defined by DE ROVER, 2006 as a total removal of a unit from the armour layer leading to no contribution of this unit to the protection of the first under layer. Extraction of armour units are considered damage and are therefore not allowed to occur during the design wave condition nor the overload condition.

Damage number

In order to express the observed extraction and/or rocking of the armour units, the following formula is used:

$$N_{omov} = N_{od} + N_{or} 3.11$$

In which:

N_{omov}	Relative total number of moving units	[-]
N_{od}	Relative number of extracted units	[-]
N_{or}	Relative number of rocking units	[-]

 N_{omov} is a measure for the damage that occurs during a test. It expresses the number of moved units within a strip of a breakwater with a width of the nominal diameter of the armour unit. The numerical value of N_{omov} can be calculated with:

$$N_{omov} = \frac{n_{extracted}}{B/D_n} + \frac{n_{rocking}}{B/D_n}$$
3.12

In which:

$n_{extracted}$	Total number of extracted units	[-]
$n_{rocking}$	Total number of rocking units	[-]

B Width of the layer [m] D_n Nominal diameter of armour unit [m]

 N_{omov} is used to express the damage and is therefore called the **damage number**.

3.5.2 Wave measurements

The wave heights are measured with two sets of wave gauges, each consisting of three gauges. The first set of gauges is located approximately one wave length from the paddle and the other set is located close to the structure. The distance between the gauges is indicated in Figure 3-2. These gauges measure the water level during the tests. The wave gauge consist of two wire resistance probes that are simple and reliable. The measurement method of the wave gauges is based on electricity conduction through water. The conductivity of water changes with temperature and therefore calibration of the wave gauges is of great importance. The wave gauges are calibrated every time when the flume is refilled and at the start of every day. The incoming and reflected wave can be determined with the computer program WAVELAB which uses the method described by MANSARD AND FUNKE, 1980. One is referred to their report for details on this method. Before the model of the breakwater is constructed in the flume, the generated waves are checked and calibrated. More details on the calibration of the waves are given in appendix G.

3.5.3 Settlements and RPD

The Xbloc armour units are placed on a prescribed grid, which is presented in appendix F. The coordinates are marked on paper strips which are used to check the coordinates during placement. This is a first order estimation to see if the units are placed on the right position. Photographs of the armour layer are taken before test and after the 100% condition run. With the help of a Matlab script the positions of the armour units can be determined based on these photographs. In order to calibrate the positions which are determined with the Matlab script, a sheet of A4 paper which is located on the armour layer is photographed. Furthermore the distances between armour units are measured with a ruler in order to compare the results with measured values. With the data of the positions of the armour units the placement density of the armour layer and the settlements of individual armour units can be determined. According to VAN ZWICHT, 2009 this is the most accurate method to determine the placement density

3.5.4 Profile of the under layer

Laser scanner

The profile of the under layer is measured with a laser scanner which is capable of measuring a vertical distance. The laser scanner is mounted on a wooden frame which allows horizontal movement in perpendicular and lateral direction. The scanner can be moved along the frame with the help of a wire and a pulley. This is made more clear in Figure 3-6.



Figure 3-6 Wooden frame with laser device which is used to measure the profile of the under layer

The laser device has an (adjustable) measuring rate of 312.5 to 2500 Hz. The diameter of the laser spot is 1.5mm. This corresponds to a spot of approximately 6 cm in prototype. The wire runs over a wheel which gives a pulse at approximately every millimetre. Therefore it is possible to determine the vertical distance with small horizontal step. The result is a more or less continuous signal. The laser device gives a signal in Volt, which can be converted to a distance after calibrating the device. The profile is measured at three locations. One is located in the middle of the flume and the two other locations are 18.6cm to the right and left of the middle. In this way three rows of measurements of the under layer are performed.

Spherical foot staff

In order to simulate a prototype survey, also a spherical foot survey is carried out. A fixed frame is used to ensure correct positioning of the staff. The staff is located in the frame and can move in vertical position within the frame. This is made more clear in Figure 3-7.

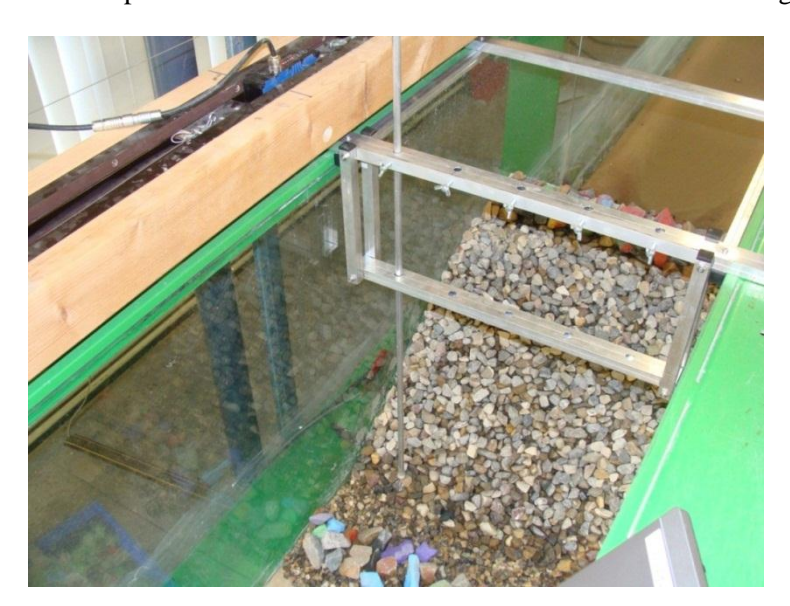


Figure 3-7 Spherical foot staff measurement of the under layer in model situation

3.5.5 Observation of rocking and extractions

Rocking and extractions are determined by means of visual inspection. The tests are recorded on video in order to be able to see the behaviour of the structure again after the tests.

4 Observations

In this chapter the observations from the model tests are treated. First some general observations are discussed before the different modes of damage are treated. This chapter has the purpose to give a qualitative impression of the results of the model tests. In chapter 5 the test results are discussed and a more quantitative overview is given.

4.1 General observations

4.1.1 Modes of damage

In this section some general observations are presented. The focus is on the three modes of damage; rocking, extraction and settlements. They were defined in section 3.5.1. During the tests, however, a fourth mode of damage was observed. In some cases lifting of multiple armour units was observed as well. This phenomenon is elaborated in this section as well.

Rocking

Rocking has been observed during uprush. The upward directed flow causes an upward directed rotational movement of the armour unit. During downrush the armour unit is moved back to its original position. During uprush the sum of the lift and drag force acts in more or less the same direction of the flow. This is indicated in Figure 4-1. The sum of lift and drag is denoted as F_{uprush} . Rocking occurs if rotational movement is possible due to an insufficient degree of interlocking. It has been observed that rocking predominantly occurs around the water surface. In this area the packing density is decreased due to settlements of the armour units lower on the slope.

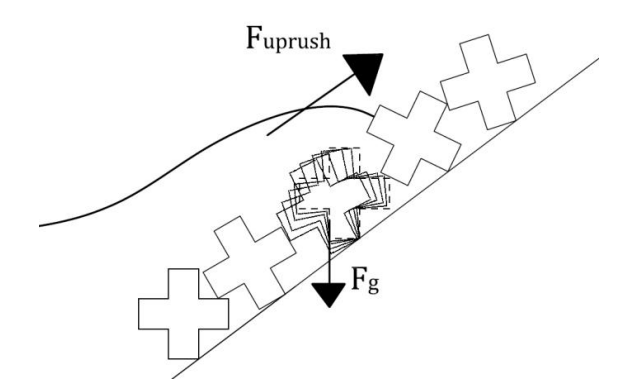


Figure 4-1 Mechanism of rocking of a single armour unit

Extractions

Extraction of an armour unit from the armour layer has only been observed during uprush. During the tests it has been observed that the displaced armour units were rocking (heavily) before being displaced from the armour layer. Drag and lift forces in combination with the outward directed flow from the core ($F_{outflow}$) of the breakwater can cause extractions. First the unit is lifted from the under layer because the sum of lift, drag and pressure from the core is larger than the resistance due to the weight of the armour unit and the contact forces from the neighbouring units. When the unit is loose from the armour layer, the armour unit is transported in upslope direction during uprush due to lift and drag forces of the flow. A few extractions have been observed during the tests; in all cases a few large waves hit the structure before the extraction took place. High run-up and low run-down levels caused

rocking of the armour unit and in most cases the unit was lifted from the under layer before the actual extraction occurred.

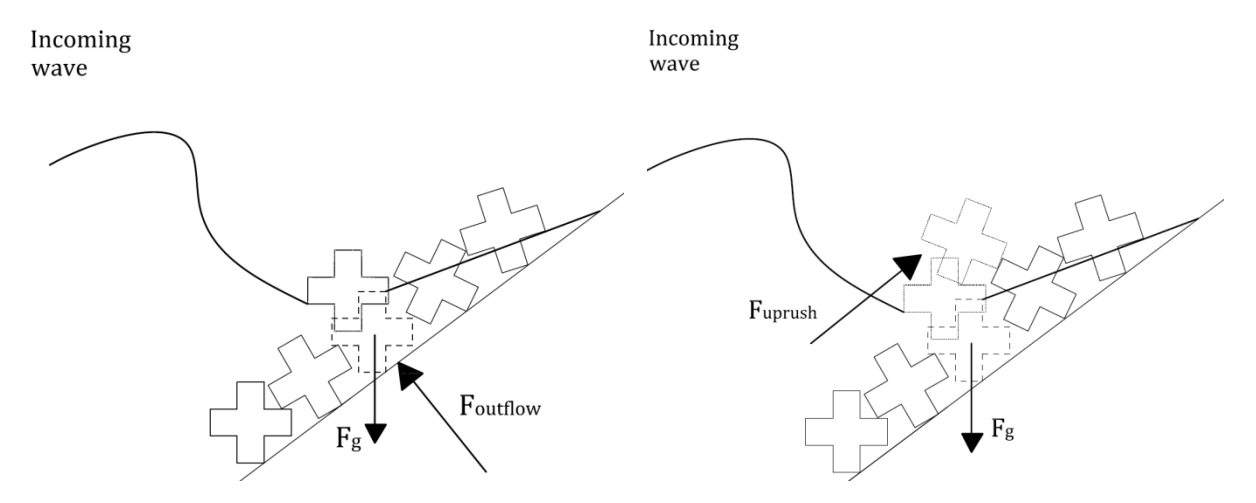


Figure 4-2 Mechanism of extraction of an armour unit

Settlements

Different types of settlement have been observed. Initial settlements occurred after a few waves hit the structure at the beginning of a test. Due to these small settlements the armour units find a more stable position. Therefore initial settlements are not considered to be damage. Due to a combination of outward directed flow from the core $(F_{outflow})$ and a downward directed force $(F_{downrush})$ during downrush settlements can occur. The friction between under and armour layer is decreased during downrush due to outward directed flow and pressure from the core. The drag force during downrush can push the unit in downward direction which can result in settlements. During the tests only small sudden settlements have been observed. In some cases the actual settlements were only visible by comparing the photographs before and after the tests. No sliding or sudden settlement of a large number of armour units has been observed.

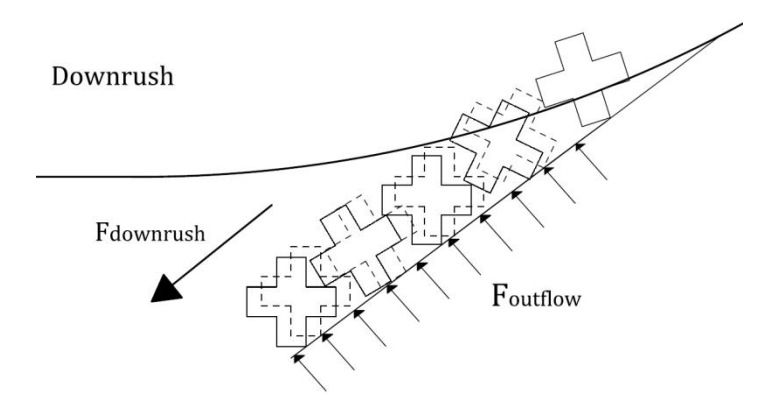


Figure 4-3 Mechanisms of settlement of armour units

Lifting of armour units

In a few exceptional cases lifting of multiple armour units from the under layer has been observed. The mechanism that drives lifting of multiple armour units is the same for extractions of armour units. Outward directed flow from the core and drag force due to uprush generate the lifting. But because the armour units interlock well enough, extraction of an armour unit cannot occur. In some cases a certain section of the armour layer was not only lifted, but also moved upwards and/or downwards during uprush or downrush.

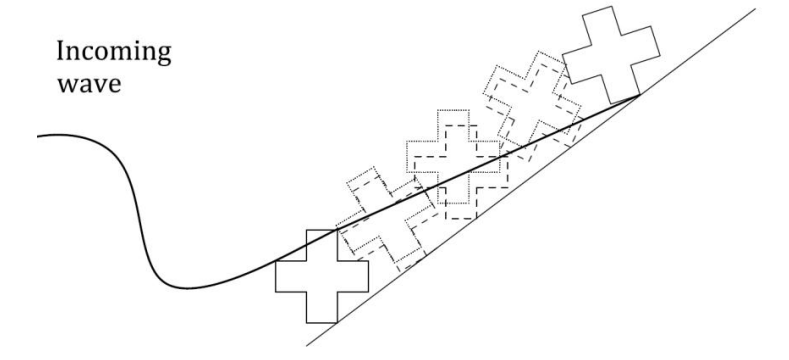


Figure 4-4 Lifting of multiple armour units

4.1.2 Under layer

Different under layer profiles are tested. After every test the under layer was partly removed and a new profile was constructed. A spatula is used to profile the under layer. The deviations over a small length scale are constructed with locally steep slopes; they are constructed with the steepest possible slopes alternated by (nearly) horizontal slopes. It turned out that a local steepness of approximately 45° could be achieved. This implies that the slope is roughly 10° steeper than the 2:3 slope. If one tries to make the slope steeper than this, stones will roll off or the slope will (partly) shear off. The deviations over large length scales consist of a part of the slope which is steeper than the 2:3 slope and a section which is less steep. The steepness of the slopes depend on the vertical deviation in this case. An important definition is the **step**, which exists because of different slope angles on the same slope. This is illustrated in Figure 4-5.

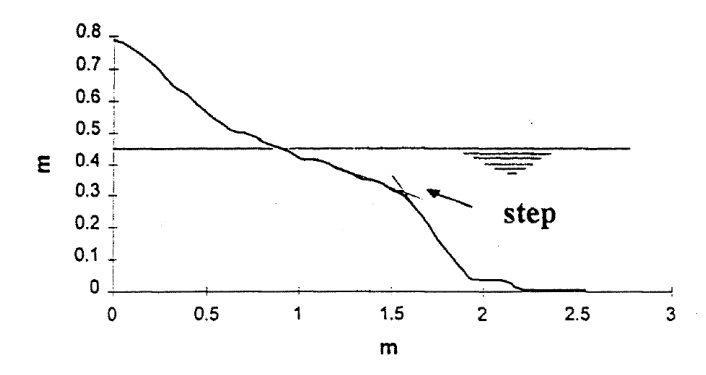


Figure 4-5 Breakwater cross section and the step. Figure from Archetti and Lamberti, 1996

The step is defined as the intercept of tangents to the profile in the lowest part of the berm and below it [ARCHETTI AND LAMBERTI, 1996]. In case of deviations over large length scales there are no berms in the profile. In these cases the expression 'step' refers to the location of the transition of a steeper slope to a milder slope or vice versa.

4.1.3 Placement of the armour layer

Observations during placement

During placement of the tests with deviated profiles it was found that there is less freedom to place the armour units, compared to the reference case. The increased roughness hinders the placement of the armour units. Due to the increased roughness under layer stones protrude. As a result it's less easy to place the armour units in a stable position. Furthermore placement is more difficult at the very steep

and horizontal slopes. At the very steep sections there is less space to manoeuvre the armour units before placement, compared to milder slopes. At the horizontal sections of the slope it was observed that placement is difficult as well. This is due to the fact that the armour unit should have contact with two armour units on the row below, two armour units on the row above and with the under layer. For the units located on the first row on the horizontal part, next to the step, it's difficult to place them according to these rules. There is a large difference in slope angle resulting in a larger distance between the armour units located on the steep slope and horizontal slope than prescribed. This results in some cases in visibly less interlocking of the armour units.

Placement speed

For every test the time required to construct the armour layer is measured. It was found that the under layer profile has no influence on the time required to construct the armour layer. In some cases the prescribed placement density is not met and some parts of the armour layer have to be reconstructed. The placement times are corrected for this by dividing the time by total number of units which are placed. In Figure 4-6 the placement times are presented, in terms of required time to place one armour unit.

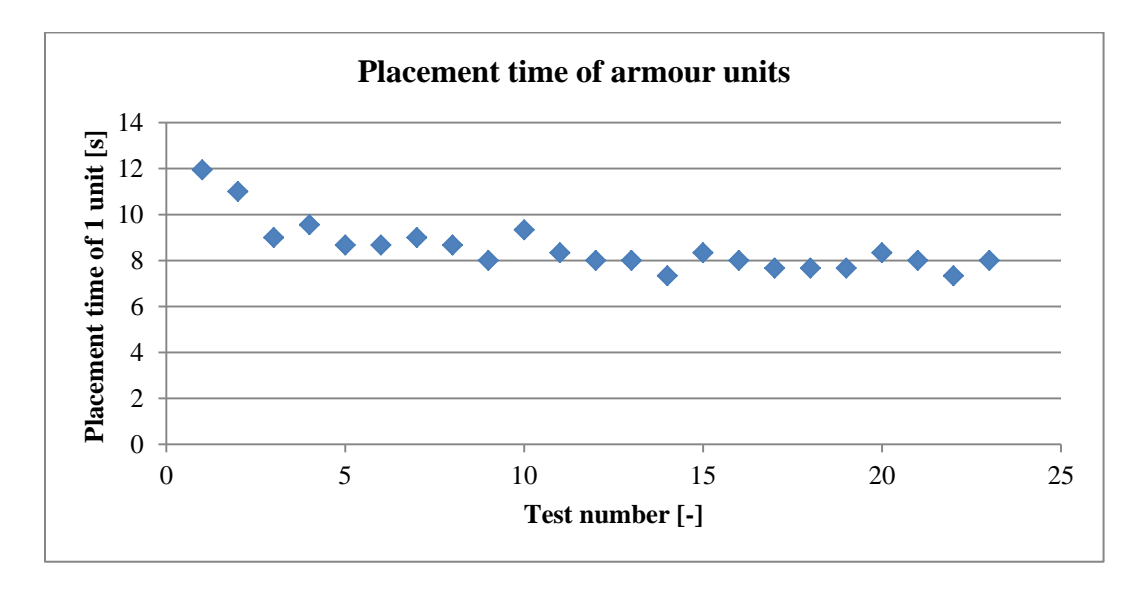


Figure 4-6 Placement times of the armour units

Because the test numbers are presented in chronological order, it can be concluded that after a few tests the placement time is more or less constant. Test 7 and further are tests with deviated under layer profiles. Apparently the under layer profile has no clear influence on the time required to place the armour layer. Although it has been observed that it's less easy to place the armour units on a deviated under layer, this effect does not influence the placement times.

Observations after placement

When one compares the placement of the amour layer with the photos which are taken before the tests, it can be observed that for quite a number of tests the quality of the placement is lower than in the reference case. Some armour units do not interlock properly, which is in general a logical consequence of the presence of the vertical deviations in the profile of the under layer. Furthermore the deviations in profile cannot be seen from the photos, while they are clearly visible when one observes the physical scale model from an angle. This indicates that photos of the armour layer do not provide enough inside into the quality of placement of the armour layer, in case of large deviations of the under layer.

4.1.4 Wave structure interaction

In section 3.3.3 a value of the breaker parameter ξ of 3.8 is calculated. This value corresponds to surging waves, which do not break. During the 60% condition only surging waves have been observed, with occasionally a breaking wave with a small layer of visible turbulent water motion. During the 80% condition the same type of waves have been observed. Differences are that the waves are higher and longer and more turbulent breakers have been observed. During the 100% condition a few collapsing breakers have been observed during the higher waves of the test runs. During the 120% condition more collapsing breakers have been observed. More turbulent water motion is observed at higher waves.

4.2 Observations of damage

In this section an overview is given of the observed damage of the armour layer. Before the different test scenarios with different under layer profiles are described, the reference case is treated. A distinction is made between under layer profiles with a small and a large length scales of deviations. The exact values of length scales and vertical deviations are discussed in chapter 5.

4.2.1 Reference case

First a reference case is tested to determine the stability of the armour layer in ideal conditions. The tests with deviated profiles are compared with this case in order to assess the possible differences.

Rocking

Rocking was observed during wave heights equal to or larger than 80% of the design wave height. During the 60% condition runs no rocking was observed. During the 80% tests 1 or 2 units showed rocking and during 100% 3 or 4 units. The reference case is considered to be stable because not more than 2% of the units show rocking during the 100% condition. During the 120% condition more rocking units have been observed, but there is also a larger scatter in the number of rocking units. In one case 7 units showed rocking, but 2 units in the upper row were rocking. This probably could have been prevented by positioning the stones on the crest in such a way that the armour units would have interlocked better. Rocking has been observed in the area of $-\frac{1}{2}H_{s,design}$ and $+1H_{s,design}$.

Settlements

All tests show initial settlements, visible settlements occurred during wave attack of a single wave. In general the first eight rows on the slope show negligible settlements. Settlements occur predominantly in the upper part of the slope. The highest units on the slopes show minor settlements. In general the settlements remain bounded to roughly 60% of the height of the armour unit. During one test a few units showed larger settlements. During this test the placement density in some parts of the upper section of the slope is less than in the other tests, which can be an explanation for the larger settlements.

Extractions

No extractions have been observed.

Lifting of armour units

No lifting of armour units has been observed.

4.2.2 Deviations over a small length scale

Deviations from the designed profile in vertical direction are constructed over a small length scale. Below the observations during test scenario B, E and G are treated.

Rocking

Rocking has been observed during all wave heights, except during the 60% condition at one test with the smallest vertical deviation. Rocking starts in all cases at the step which is located just below the water surface. At higher wave conditions also rocking units at the lower located step(s) have been observed. In general the area in which rocking units have been observed expands to further upslope with increasing wave heights. The number of rocking units increases with the vertical deviation. Furthermore the number of rocking units is larger in virtually every test run than in the reference case.

Settlements

During all tests initial settlements have been observed. During test scenario E also second and third series of visible settlements have been observed. In general more and larger settlements have been observed than in the reference case. The largest settlements have been observed during test scenario E. Apparently more series of settlements lead to larger settlements. During test scenario B comparable settlements to the reference case have been observed. During tests with scenario G significant larger settlements than in the reference case have been observed.

Extractions

A few extractions of amour units from the armour layer have been observed. During test case B one unit was displaced during the overload condition and two units, which were located next to each other, were displaced during the 80% condition. During one test of scenario E an armour unit was displaced during the overload condition. Remarkable is that the unit rolled upslope due to uprush and during downrush the unit returned to its original position and stayed there for the rest of the test. During one test of scenario G an armour unit was displaced. This occurred during the 100% condition. All the observed extractions have one thing in common; the units are located near the step.

Lifting of armour units

During tests of scenario B lifting of the armour units has been observed during the highest wave attack on the structure. It was observed that the rows of armour units which are located just below, on and above the step were lifted from the armour layer and moved a little up and down along the slope due to up- and downrush.

4.2.3 Deviations over a large length scale

Deviations from the designed profile in vertical direction are constructed over a large length scale. Below the observations of test scenario C, D and F are discussed.

Rocking

Rocking has been observed during all wave heights. For the concave under layer profile rocking during the 60% condition has been observed mostly at units which are located near the step. For this profile more rocking has been observed at higher wave conditions further upslope. In this region the slope is milder than 2:3 and therefore the interlocking is less. For the convex profile rocking starts significantly lower on the slope. For this profile the slope is milder than 2:3 on the lower side of the slope and therefore the interlocking is less in this area. In general the number of observed rocking units is larger than in the reference case. The tests with concave under layer profiles show significant more rocking than the reference case. The scatter in observed rocking units is larger than in the

reference case as well. During tests with the convex profile less rocking units have been observed compared to the concave profile, but the scatter in results is large.

Settlements

During all tests initial settlements have been observed. During a few tests also a second settlement has been observed after a few waves hit the structure. During test scenario C less settlements have been observed than in the reference case. This can be explained by the milder steepness of the upper half of the slope. On a mild slope the effect of gravity pushing units in downward direction is smaller than on a steeper slope. Remarkable is that during tests of scenario F more and larger settlements occur. The tests with the convex profile showed more settlements than the reference case, which can be explained by the steeper upper part of the slope.

Extraction

One extraction of an armour unit has been observed, during test scenario F. An inspection of the placement shows that the unit was not properly placed and therefore interlocking was significantly less.

Lifting of armour units

No lifting of armour units has been observed.

4.2.4 Influence of the step on the observed damage

From the observations it becomes clear that the step has a large influence on the stability of the armour layer. MONSTER AND PHILIPSEN, 2010 mention that in this area differences in packing density occur and therefore a lower force is required to extract an armour unit from the armour layer.

Damage in the area of the step

A more detailed look at the rocking of the units and the location of these units with respect to the step shows that the area which is located just on and below the step is the most vulnerable to damage. The rows of armour units directly below and above this area are also vulnerable. Research on low crested breakwaters with interlocking armour units showed the same trend [VAN DEN BOSCH *et al.*, 2012]. In Figure 4-7 this is made more clear. The red area indicates the area with the largest damage, orange indicates smaller but still considerable damage and green indicates virtually the same damage as observed during the reference case test.

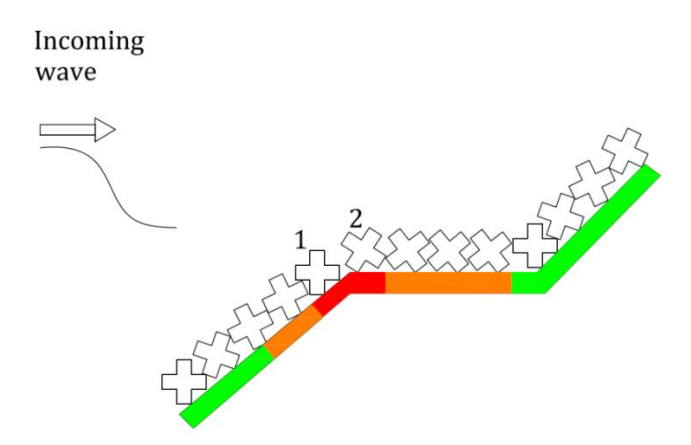


Figure 4-7 Observation of degree of damage near the step

The armour units just below the step can settle while the units just above the step cannot settle due to the much milder slope. As a result a gap, and consequently a loss in packing density, is created between the units located just above and below the step, which are indicated with armour unit '1' and '2' in Figure 4-7. The red area is the area where most damage has been observed. The horizontal part has a lower degree of interlocking because the contact forces between the armour units are smaller due to the very mild slope. The area located just below armour unit '1' is also quite vulnerable. This is because the contact forces from the units above are small due to the fact that only one or two units generate support from above.

Location of the step

In the scenarios with vertical deviations over a short length scale there are two or three steps present in the profile. Rocking generally starts at the step which is located the closest to the water surface. At higher wave conditions damage occurs at the lower located step(s) as well. However, the step which is located the closest to the water surface is the most vulnerable.

4.2.5 Conclusions

From the observations it becomes clear that the introduction of a larger tolerance results in more rocking of armour units, larger settlements and in some cases even extractions of armour units. Due to the larger tolerances a step is created in the under layer profile. The area around the step is the most vulnerable to rocking and extraction of armour units. In this area there is a lower packing density and lower degree of interlocking, which explains the vulnerability to damage. At the step which is located the closest to the water surface the most damage has been observed, in case of more than one step present in the slope. In Table 4-1 a qualitative overview of the observations of the model tests is given. All test scenarios are compared with the reference case. '+' denotes a higher observed level, '-' denotes a lower observed level and 'o' denotes a similar observed level compared to the reference case.

Table 4-1 Overview of observed damage of the armour layer, compared with the reference case.

Scenario	Description	Rocking	Extraction	Settlements
В	$3.0 D_{n50}$ over short distance	++	++	0
С	$2.0 D_{n50}$ over long distance (concave)	+	0	-
D	$2.0 D_{n50}$ over long distance (convex)	+	0	+
Е	1.5 D_{n50} over short distance	+	+	++
F	1.5 D_{n50} over long distance	+	+	++
G	$1.0D_{n50}$ over short distance	+	+	+

5 Test results

In this chapter the test results are elaborated. Before the damage of the armour layer is discussed, first some information on the wave and under layer profile measurements is given.

5.1 Wave measurements

5.1.1 Characteristic wave parameters

The waves are measured during the tests, as described in section 3.5.2. In this section the results are presented.

Results

In Table 5-1 the imposed wave conditions are shown.

Table 5-1 Imposed wave conditions

Condition	Significant wave height [mm]	Wave peak period [s]
60%	70.1	1.276
80%	94.6	1.389
100%	118.3	1.554
120% (overload)	141.9	1.702

With the computer program WAVELAB the characteristic wave parameters are determined by means of a reflection analysis. In Table 5-2 the wave conditions near the structure which are determined with a reflection analysis with WAVELAB are presented. H_s is based on the output from the time domain analysis and H_{m0} is based on the output from the frequency domain analysis. One is referred to appendix H for detailed wave data.

Table 5-2 Wave conditions 1m in front of the structure

Condition	H_s [mm]		H_{m0} [mm]		$T_p[s]$	
	Mean	Standard deviation	Mean	Standard deviation	Mean	Standard deviation
60%	69.7	0.33	71.5	0.38	1.260	0.02
80%	93.8	0.62	95.8	0.61	1.394	0.01
100%	115.7	0.66	118.2	0.69	1.543	0.04
120% (overload)	137.7	0.88	142.1	0.80	1.753	0

The values presented in Table 5-2 are not the exact values at the toe of the structure. The waves are calibrated with the gauges located at the toe of the structure and at the location of the gauges during the tests (1m in front of the toe). It was found that the significant wave heights near the structure are up to 2% larger than 1m in front of it, see appendix H. This is of minor importance because the difference between these two locations is rather small. Furthermore the small standard deviations in wave heights, which are presented in Table 5-2, show that the wave conditions are almost constant between the different tests. It should be mentioned that the outcomes of WAVELAB are sensitive to differences in the bin size which is used. Differences in the order of a few per cent can occur for different bin sizes. This aspect is neglected and not considered a problem, because the wave conditions are quite constant between the tests.

Accuracy

As mentioned in section 3.5.2 the wave gauges have to be calibrated frequently because the principle of the measurements is the conductivity of water, and the conductivity is sensitive to changes in temperature. After calibration the measurement error is in the order of 0.1% [VERDEGAAL, 2013]. A different error occurs due to the determination of the water surface in the flume. The height of the water surface is marked on the side wall of the flume and the filling of the flume is stopped manually when the water surface is visually determined to be at the marked position. As a result the water depth is expected to show a maximum variation of a few millimetres between the tests. This variation influences the generated waves and the loading on the structure. Furthermore an error occurs due to the processing method of WAVELAB, which is described on the previous page.

5.1.2 Maximum wave heights

The maximum wave height (H_{max}) during a test can be determined with the reflection analysis of WAVELAB. However, WAVELAB produced unrealistic values of H_{max} . WAVELAB calculated larger maximum wave heights at lower significant wave heights. An analysis of the measured wave heights at the different wave gauges showed that the calculated value of H_{max} was even larger than the measured waves at the gauges. This is physically not possible because the measured waves at a gauge contain both the incoming and reflected wave. The maximum incoming wave, H_{max} , cannot be larger than the sum of the incoming and reflected wave. The phase angle between the incoming and reflected waves at the location of the wave gauges can be calculated with the equation below [MUTTRAY, 2000].

$$\Delta_{\varphi} = -\frac{8\pi \cot \alpha}{T} \cdot \sqrt{\frac{h}{g}} + 2 \cdot x \cdot \frac{2\pi}{L}$$
5.1

In which:

T	Wave period	[s]
α	Slope angle	[°]
h	Water depth at the toe	[m]
x	Horizontal distance between toe and wave gauges	[m]
L	Wave length	[m]

This phase angle is calculated for the different wave conditions and has a value between 170° and 190° for the 80% and 100% conditions. A phase angle of 180° implies that the difference between the incoming and reflected wave is at a maximum. Apparently this phase angle, which is close to the maximum difference, causes an error when calculating the maximum wave heights. Therefore the maximum wave heights of the calibration session are considered to give the most accurate information on the maximum wave heights. These are given in Table 5-3.

Table 5-3 Maximum wave heights for the test conditions

Test condition	H_{max} at the toe of structure [mm]
60%	131.3
80%	143.8
100%	160.4
120%	172

5.2 Measurements of under layer profiles

In this section the measured under layer profiles are discussed. First the results of the laser scanner are treated. The spherical foot staff measurements and simulation of this method are elaborated as well. Not all the under layer profiles are presented in this section. One is referred to appendix J for the plots of the different profiles.

5.2.1 Results laser scanner

The under layer profile is measured with a laser scanning device, as described in section 3.5.4.

Results

Unfortunately the laser device generates some spikes. These spikes are removed from the dataset with a Matlab script, which is given in appendix O. In Figure 5-1 the result is shown.

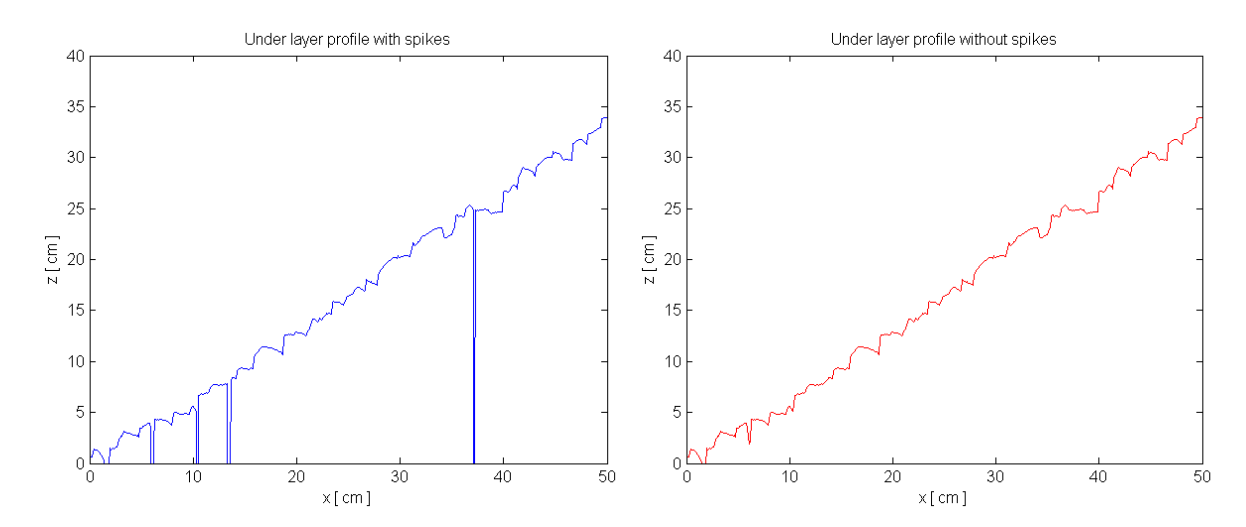


Figure 5-1 Under layer profile with and without spikes

Figure 5-1 shows the result of one measurement. Before every test the under layer profile is measured on three locations. The average profile of the three measurements is used in further processing. Although the majority of the spikes are removed there are still some small deep holes in a few datasets. This is not considered to be a problem because a spherical foot is simulated and this measurement system does not measure small holes.

Accuracy

The laser device gives an output in the range of 2 to 10 Volt and has a range of 20 to 95 cm. The data are given in three decimals. In order to convert the signal in Volt to a distance, the laser device is calibrated. Two distances which are near the borders of the range are measured with the device and with a ruler in order to convert the signal in Volt to a distance. Therefore the calculated distances have the same order of accuracy as the measurement of the ruler. It is expected that the maximum error due to this calibration procedure is approximately 1 to 2 mm. Due to non-linearity of the laser device a maximum error of 0.75mm can occur. Other possible effects from the laser scanner are neglected. In appendix N the specifications of the laser device are given. A measurement error occurs due to the movement of the wooden frame of the laser. Two wooden beams are placed at a fixed position on top of the flume in order to stabilize the wooden frame. The correct position of the wooden frame is indicated with place marks on the wooden frame and the beams. It is therefore likely that the position of the wooden frame deviates with a few millimetres between the different tests. This error is minimized by averaging over the three measured profiles every test. Furthermore the laser device seems to generate some unrealistic low measurements. Removing the spikes is possible to some

extent, but in some cases the result still shows some holes which are not realistic. This effect is minimized by averaging over the three measured profiles every test.

5.2.2 Spherical foot staff measurements

Spherical foot staff measurements are carried out on the under layer of the model. The under layer is measured with the laser scanner before this survey is carried out, in order to compare the results.

Results

The spherical foot staff measurements are compared with the laser measurements. In general the spherical foot staff measures a higher profile than the laser. This is according to the theory as described in section 2.3.5. The survey is carried out with a horizontal interval of $\frac{3}{4}D_{n50}$. Two types of spheres are used. One with a diameter of $1D_{n50}$ and one with a diameter of $\frac{1}{2}D_{n50}$, which is the recommended diameter of the sphere. The sphere with a diameter of $1D_{n50}$ measures a higher profile because the sphere is too large to measure the holes in the profile. The $\frac{1}{2}D_{n50}$ sphere can only penetrate the larger holes of the under layer. The measurements are carried out two times. One time a reference case profile is measured and one time a deviated profile is measured. In Figure 5-2 a plot is given of a laser measurement and a spherical foot measurement at one location. One is referred to appendix K for the complete set of results.

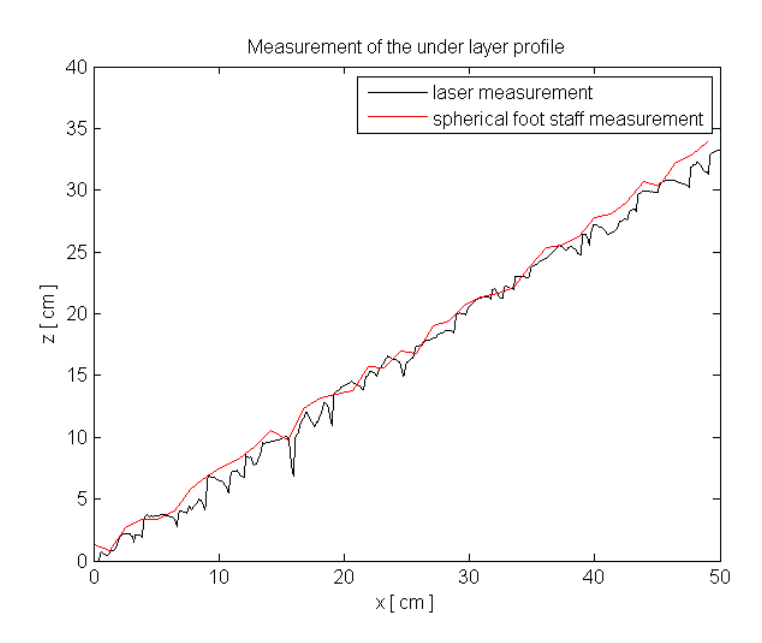


Figure 5-2 Laser and spherical foot staff measurement at the same location

All measurements show the same trend, namely that the spherical foot does not measure holes with a small horizontal distance and in general the measured profile is higher.

Accuracy

The spherical foot staff measurements are carried out with the help of a fixed frame. This method is described in section 3.5.4. The vertical and horizontal distances are measured with a ruler. It is expected that the measured values are accurate up to 2 mm. Although the frame is fixed, small movement of the staff is still possible. Therefore it's possible that the staff is not always exact in vertical position. Furthermore an error occurs due to small deformations of the under layer during the

measurements. Because the staff weighs more than the under layer stones, it was observed that during the positioning of the staff some stones moved.

5.2.3 Simulation spherical foot staff

In order to simulate a prototype measurement of the under layer, the spherical foot staff measurement method is numerically simulated with the help of a Matlab script. This script is used to convert the laser measurements to spherical foot measurements. With the help of this simulation the measured vertical deviations and tolerances can be expressed in prototype values, because in prototype standard measuring device is the spherical foot staff.

Results

The Matlab script is given in appendix O. Input parameters are the interval between the measurement locations and the diameter of the sphere. In Figure 5-3 a simulated spherical foot measurement is plotted in the same graph as the outcome of a measurement that is actually performed with a spherical foot staff in the flume. The left part of Figure 5-3 is the result of one location and the right part the result of the average of the three locations.

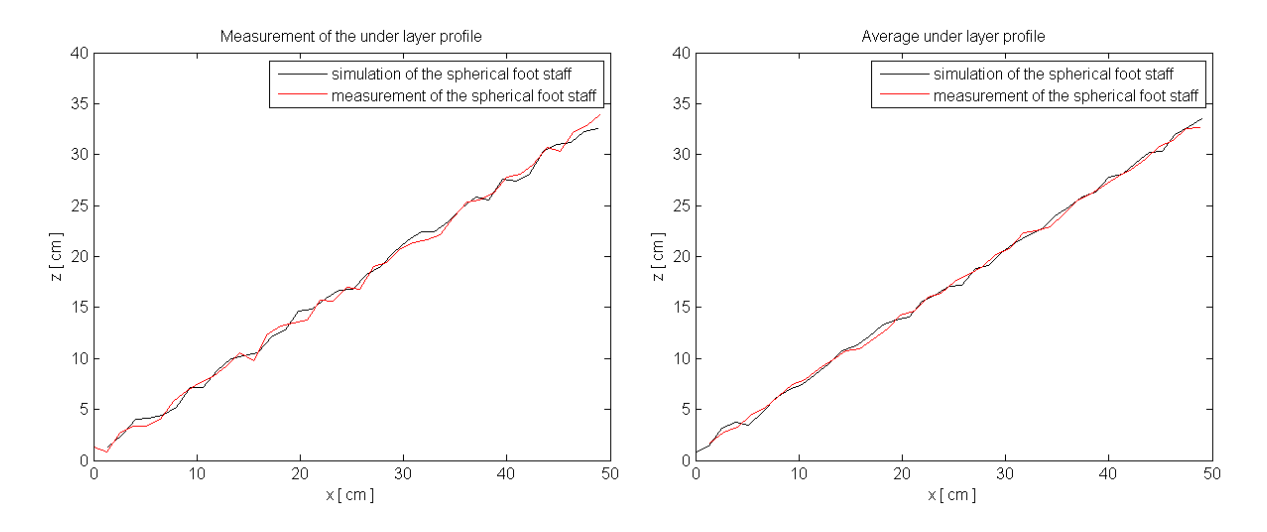


Figure 5-3 Simulation and measurement carried out with the spherical foot staff. Left: single measurement and right: average of the three measurements.

From the left part of Figure 5-3 it becomes clear that the results are similar but small differences occur. This could be due to small deformations of the under layer during the measurements. Furthermore the sphere is three dimensional in reality and the simulated sphere is two dimensional. This introduces an error, because the effect of the sphere in y-direction is neglected. From the right figure is becomes clear that the difference between the simulation and measurements is a lot smaller for the average profile of the three locations.

Difference between measurements and simulation of spherical foot staff

From Figure 5-3 it becomes clear that the measurements and simulations give comparable results. In Table 5-4 the maximum deviations in positive and negative vertical direction for the two methods are given.

Table 5-4 Maximum vertical deviations in positive and negative direction for the measurement and simulation of spherical foot staff

Reference	Measurement	Simulation
profile	[cm]	[cm]
Max positive	1.41	1.04
Min positive	-0.01	-0.47
Average	0.72	0.76

Deviated	Measurement	Simulation
profile	[cm]	[cm]
Max positive	2.47	2.54
Min positive	-0.25	-1.25
Average	1.37	1.89

From Table 5-4 it becomes clear that the average deviation of the reference profile is roughly the same. For the deviated profile this is different. It is very well possible that the laser device measured on a slightly different location in lateral direction and measured a hole, while the spherical foot staff did not. By averaging over the three profiles this effect is minimized. Because the average tolerances are used for data processing the simulation method is considered accurate enough.

Difference between simulated sphere and laser
In Figure 5-4 laser measurements and simulated sphere data is presented:

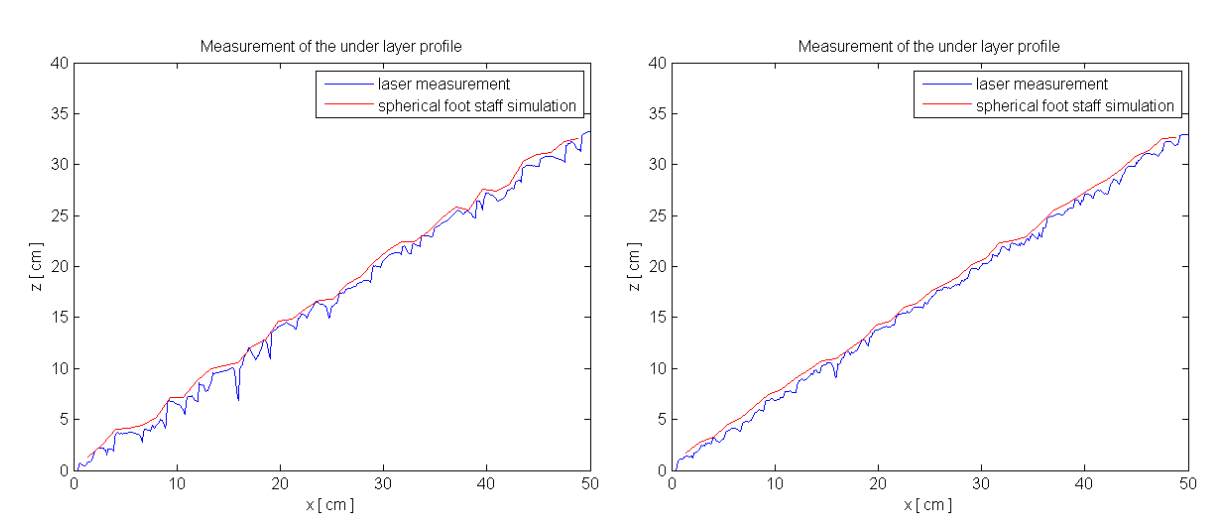


Figure 5-4 Laser measurement and simulated spherical foot staff measurement. Left: single measurement and right: average of the three measurements.

From Figure 5-4 it becomes clear that the sphere measures a higher profile than the laser device, which is in line with the theory. The difference in profile height between the laser measurements and simulated spherical foot measurements are determined. The complete set of results is given in appendix L. For every test the mean difference in profile between these two methods is determined. It appears that the mean difference in profile height between these two methods, based on all the measured profiles, is 0.495cm which is 34% of the nominal diameter D_{n50} . BOSMA, 2001 found the following expression for the difference in profile height in [cm]:

$$z_{difference} = 0.204 \cdot D_{n50} + 0.18$$
 5.2

If one applies this equation, a difference of 0.476 cm is obtained. It should be noted that Bosma performed his tests with a range of stone diameters (1 to 8 cm) and in this case D_{n50} =1.45cm. Although the stone sizes are different, the differences in measured profile height are comparable. HAUER, 2000 measured differences in the range of 20 to 40% of D_{n50} between these two methods. The obtained value of 34% of D_{n50} indicates that the results are in the same range.

Validation of the simulated spherical foot staff

The results of the spherical foot survey carried out in the flume are fairly similar to the simulated spherical foot measurements and according to the theory. Furthermore the difference between the laser and simulated spherical foot measurements is also in the same order of magnitude as earlier measurements and research outcomes. Therefore the simulated spherical foot measurements are considered to represent the real situation and usable for further processing.

Sensitivity analysis

The sensitivity of a few input parameters of the simulated sphere is discussed in this section. For test A-3 and B-2 (which is a reference case test and a test with one of the largest tolerances) a sensitivity analysis is carried out. The influences of averaging over three profiles, diameter of the sphere, interval of measurement points of the sphere and the influence of the starting point of the measurement is varied. The diameter of the sphere is varied between 0.25 and $0.75D_{n50}$, the interval is varied between 0.38 and $1.5D_{n50}$. This implies half and double the prescribed value of the parameters. In appendix M the complete set of results is given.

Table 5-5 Sensitivity of the parameters of the spherical foot simulation

Parameter	Maximum difference $[\cdot D_{n50}]$	Minimum difference $[\cdot D_{n50}]$
Interval	+0.09	-0.14
Diameter	0	-0.14
Start position	+0.10	-0.17

From the analysis it becomes clear that the start position of the simulation has the largest influence. This shows that the location of the measurements with the sphere are of great importance for determining the tolerances. The values presented in Table 5-5 show the same trend between the two tests. The values in the table show the importance of using the same sphere at fixed intervals, as recommended by the Rock Manual [CIRIA, 2007]. The effect of averaging over three profiles is a decrease in tolerance by 0.15 to $0.20D_{n50}$ in the case of test A-3. For test B-2 this decrease goes up to $1.6\ D_{n50}$. The effect of averaging over the three measured profiles is analysed for multiple tests and the differences in tolerances are between 20 and 40% of the D_{n50} . Apparently there are significant variations in profiles in lateral directions. In general it is hard to construct the profiles without deviations in lateral direction because the spatula does not cover the entire width of the flume. Furthermore the under layer profiles are constructed with locally very steep slopes. As a result some stones roll off which explains the deviations in lateral direction.

5.2.4 Magnitude of the tolerances of the test cases

Because the magnitude of the tolerances is determined in prototype with a spherical foot staff survey, the spherical foot simulation is used to determine the tolerances of the under layer profiles of the tests. In this way a comparison can be made between the profiles in mode and prototype situation. The tolerances are determined by calculating the maximum difference between the designed profile and the profile of the simulated spherical foot measurement. The positive tolerance is the maximum deviation in positive vertical direction and the negative tolerance is the maximum deviation in negative vertical direction. Both are expressed in terms of the nominal stone diameter D_{n50} . The results are presented in Table 5-6.

Table 5-6 Tolerances of the tests

Test	Positive tolerance $[\cdot D_{n50}]$	Negative tolerance $[\cdot D_{n50}]$
A-1	0.73	0.29
A-2	0.89	0.09
A-3	0.70	0.27
B-1	2.67	2.33
B-2	3.63	3.12
B-3	3.57	3.04
C-1	2.45	1.23
C-2	2.42	1.57
C-3	2.47	1.71
D-1	1.31	1.29
D-2	1.46	1.37

Test	Positive tolerance $[\cdot D_{n50}]$	Negative tolerance $[\cdot D_{n50}]$
D-3	1.76	1.90
E-1	2.22	0.82
E-2	1.52	0.78
E-3	1.47	1.16
F-1	1.51	1.12
F-2	1.83	1.12
F-3	1.80	1.09
G-1	1.79	1.14
G-2	1.31	0.99
G-3	1.39	0.67

In Table 5-7 the average values for every test scenario are given:

Table 5-7 Average tolerances of the test scenarios

Test scenario	Positive tolerance $[\cdot D_{n50}]$	Negative tolerance $[\cdot D_{n50}]$	Average tolerance $[\cdot D_{n50}]$
A	0.78	0.22	0.50
В	3.29	2.83	3.06
C	2.45	1.50	1.98
D	1.51	1.52	1.52
Е	1.74	0.92	1.33
F	1.71	1.11	1.41
G	1.50	0.93	1.21

Findings

From Table 5-6 and 5-7 a few things can be concluded. It turns out that the positive tolerance is in nearly every case larger than the negative tolerance. This is according to the theory of the Rock Manual [CIRIA, 2007]. Practical values of tolerances are given in Table 2-1. Unfortunately some movement of the wooden frame of the laser is possible. As a result the positive and negative tolerances show some considerable deviations in some cases. Therefore the average tolerance is used for further processing. The deviations can also be explained from the fact that for all tests the under layer was removed and reconstructed. Therefore it's a logical consequence that tolerances deviate from test to test. It is remarkable that the tolerances of the reference case are $0.5\ D_{n50}$. Apparently this is the lower bound of the tolerances in the model. This value does meet the prescribed norm of $0.5\ D_{n50}$ in perpendicular direction, because this prescription implies a tolerance of $0.6\ D_{n50}$ in vertical direction.

5.2.5 Magnitude of the length scales of the deviations

A distinction is made between large and small length scales of the deviations in the under layer profile. The length scale was defined in section 2.3.4 as the length between one local maximum in profile to another maximum. The length scales are determined by calculating the average horizontal distance between the two maxima and the two minima. This distance is corrected for the slope angle of 2:3. In Figure 5-5 this is made more clear.

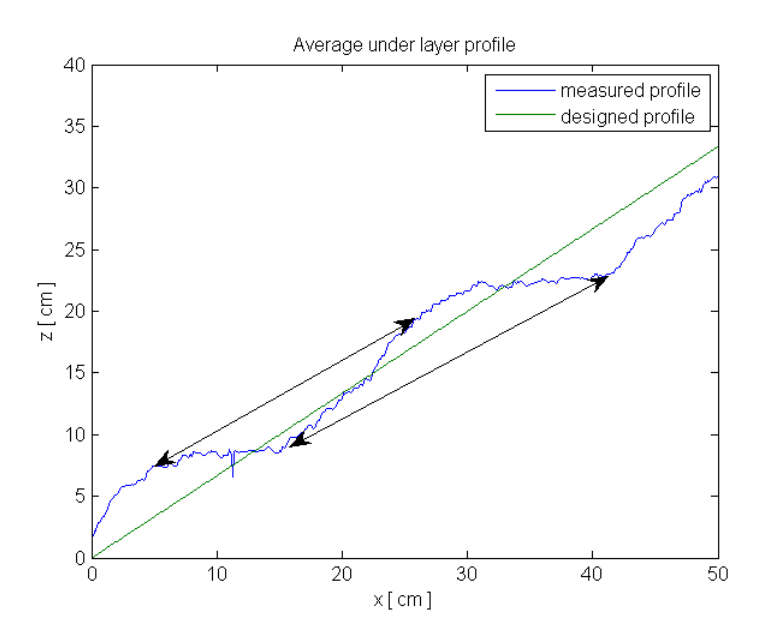


Figure 5-5 Determination of the length scale of devations

In Table 5-8 the length scales for the test scenarios are given. The tests with large length scales have a length scale which is equal to the length of the slope, which is 60.2 cm. If one takes the sum of the average values of the tolerances for the test scenarios, as described in the previous section, and divides this by the length scale, a certain *additional steepness* 's' can be calculated:

$$s = \frac{postive \ tolerance + negative \ tolerance}{length \ scale \ of \ the \ deviation}$$
5.3

Table 5-8 Length scales of the deviations for the test scenarios

Test scenario	Length scale	Length scale	Length scale	Additional steepness
	[cm]	$[\cdot D_{n50}]$	$[\cdot D_{Xbloc}]$	[-]
В	26.4	18.2	3.7	0.34
С	60.2	41.5	8.4	0.09
D	60.2	41.5	8.4	0.07
Е	18.5	15.3	3.1	0.17
F	60.2	41.5	8.4	0.07
G	13.3	11.0	2.2	0.22

From Table 5-8 it becomes clear that the length scale is relative. The concept of small length scales implies lengths in the order of 2 to 4 armour units. Large length scales are lengths of

5.2.6 Natural roughness

The natural roughness, which is discussed in section 2.3.4, is the roughness which is always present due to the shape of rocks. The tests of the reference case and other reference profiles which were

constructed in order to test the constructability, are compared with each other in order to determine the lower boundary of the possible tolerances. For all these reference profiles the tolerances are determined based on the spherical foot staff simulation. Because the profiles of the 3:4 constructability tests turned out to be milder than 3:4, the difference between the simulated spherical foot staff and the trend line of the measured profile is defined as the tolerance in this case. The average value of the determined tolerances is $0.5\ D_{n50}$, based on 9 measured cases. This means that all the reference profiles have an average maximum deviation of $0.5\ D_{n50}$ in both the positive and negative direction. Hence the lower bound of the tolerances is $0.5\ D_{n50}$, which is smaller, but close to the prescribed tolerance of DMC. This makes clear that the tolerances, as prescribed by DMC, can only be achieved if the under layer is placed with a very high quality. It is therefore recommended to pay careful attention to the placement of the under layer in prototype.

5.2.7 Conclusions

The under layer profile is measured with a laser device. In prototype the standard device to measure the under layer and to determine the tolerances is a spherical foot staff. This type of measurement is performed in the flume and is simulated numerically in order to determine the tolerances. The found difference between the laser measurements and spherical foot staff simulation is in line with earlier research on differences between point measurement and measurements with a sphere. The length scales of the different test scenarios are determined and have the following values: for small length scales a value in the order of 2 to 4 armour units and 8 to 9 armour units for large length scales. The tolerances of the individual tests are determined with the simulated sphere. It is found that in general a larger positive tolerance is determined than a negative one. Unfortunately the exact values of the tolerances are not accurate enough and therefore the average tolerance is used for further processing. It is found that the natural roughness has a vertical deviation of $0.5 \, D_{n50}$. This implies that the lower bound of the tolerances is $0.5 \, D_{n50}$, which is close to the prescribed tolerances of DMC. Therefore it can be concluded that careful attention has to be paid to construction of the under layer.

5.3 Damage of the armour layer

In this section the damage of the different test scenarios is discussed. First the different test scenarios are compared with each other. After this the individual tolerances per test and damage numbers are compared with each other.

5.3.1 Damage numbers

In this section the damage numbers for the different test scenarios are plotted versus the stability numbers, which are a measure for the wave loading on the structure. One is referred to section 3.5.1 and 2.2.5 for more information on these parameters. The damage number is defined as:

$$N_{omov} = \frac{n_{displaced}}{B/D_n} + \frac{n_{rocking}}{B/D_n}$$
 5.4

And the stability number is defined as:

$$N_{S} = \frac{H_{S}}{\Delta \cdot D_{n}}$$
 5.5

Deviations over a small length scale

In the figures below the damage number is plotted versus the stability number.

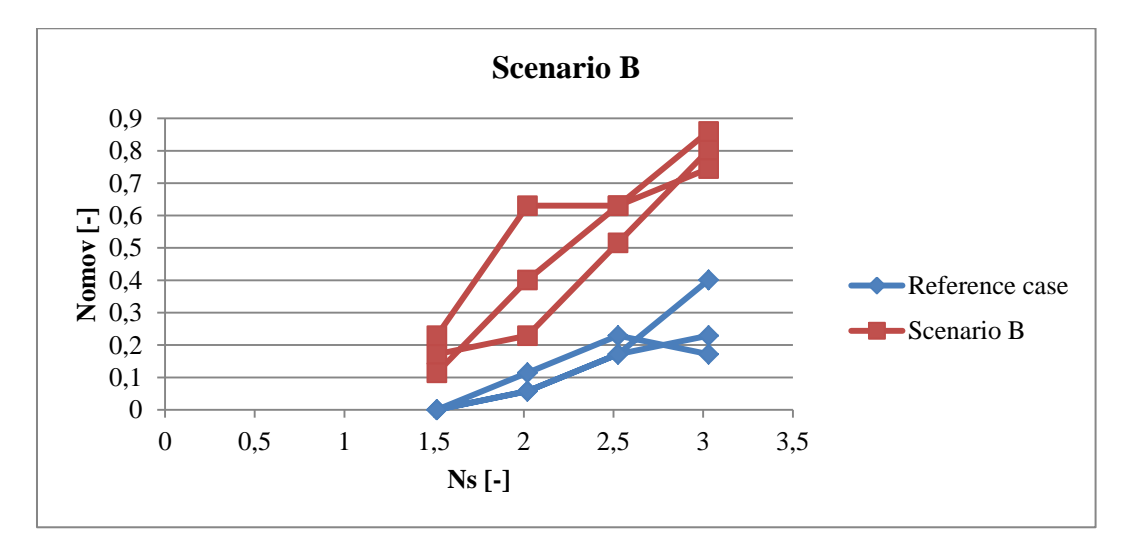


Figure 5-6 Damage of test scenario B versus damage of reference case

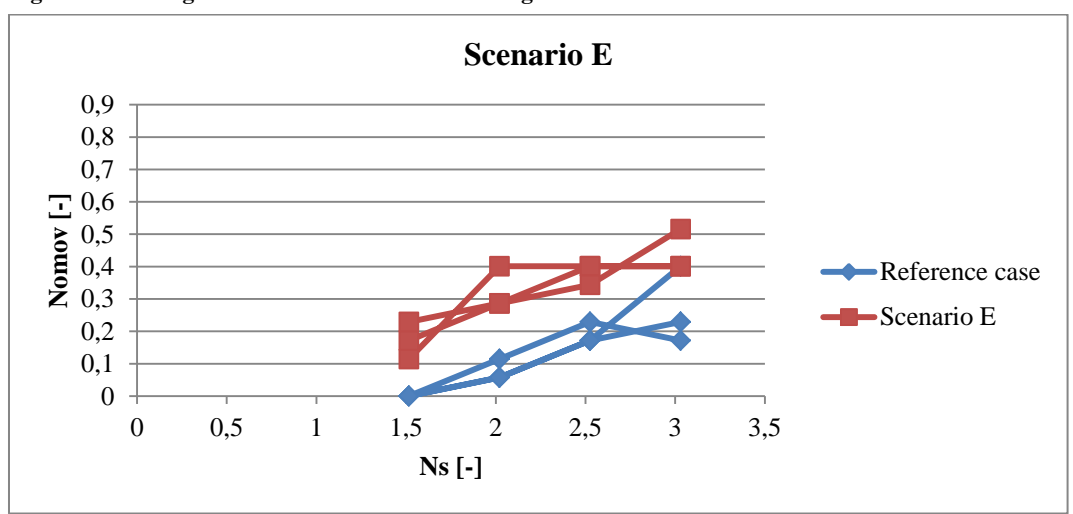


Figure 5-7 Damage of test scenario E versus damage of reference case

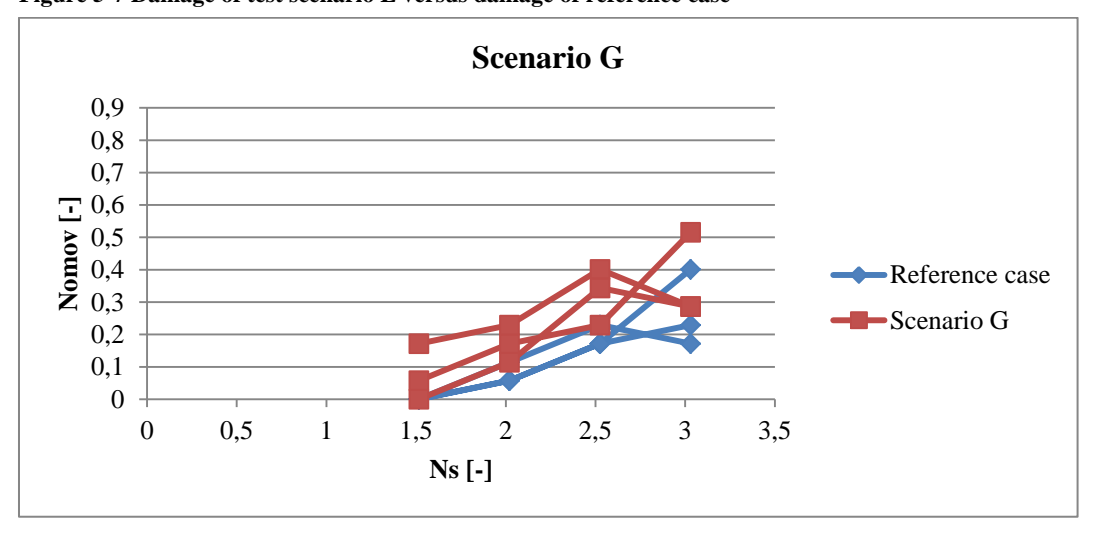


Figure 5-8 Damage of test scenario G versus damage of reference case

From the figures it becomes clear that the damage is larger than in the reference case for all scenarios. The damage number increases with larger tolerances and the scatter in the results is for all scenarios larger than in the reference case.

Deviations over a large length scale

In the figures below the damage number is plotted versus the stability number.

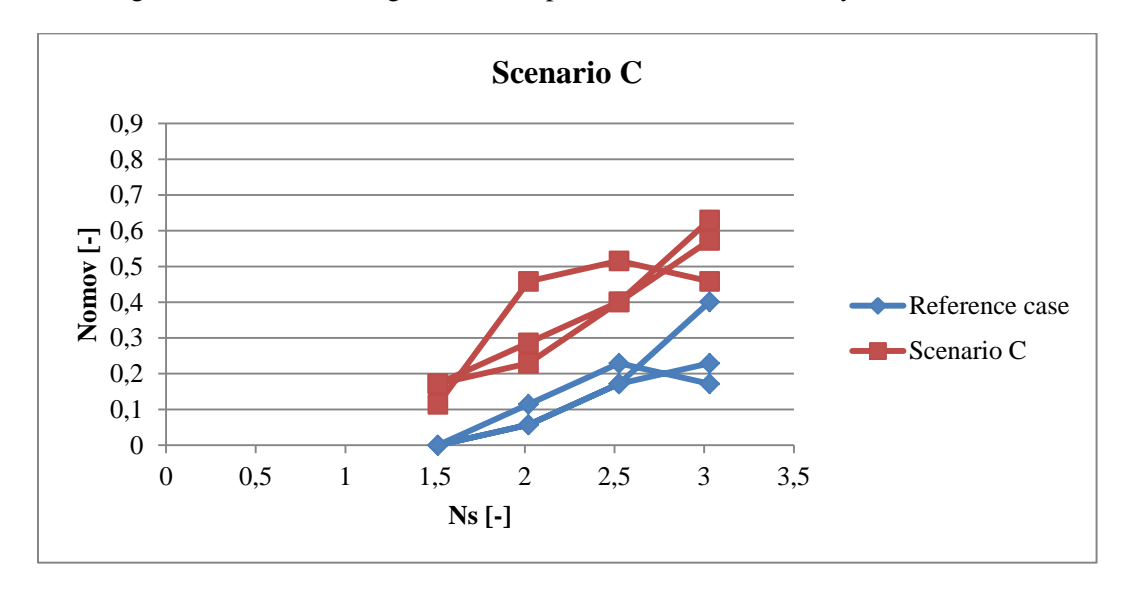


Figure 5-9 Damage of test scenario C versus damage of reference case

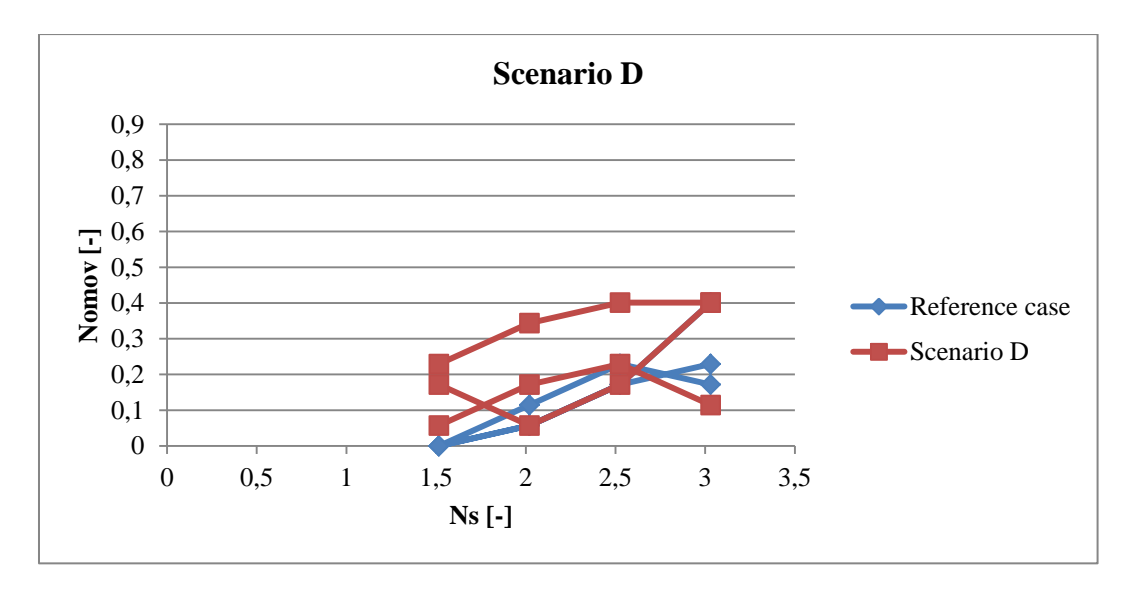


Figure 5-10 Damage of test scenario D versus damage of reference case

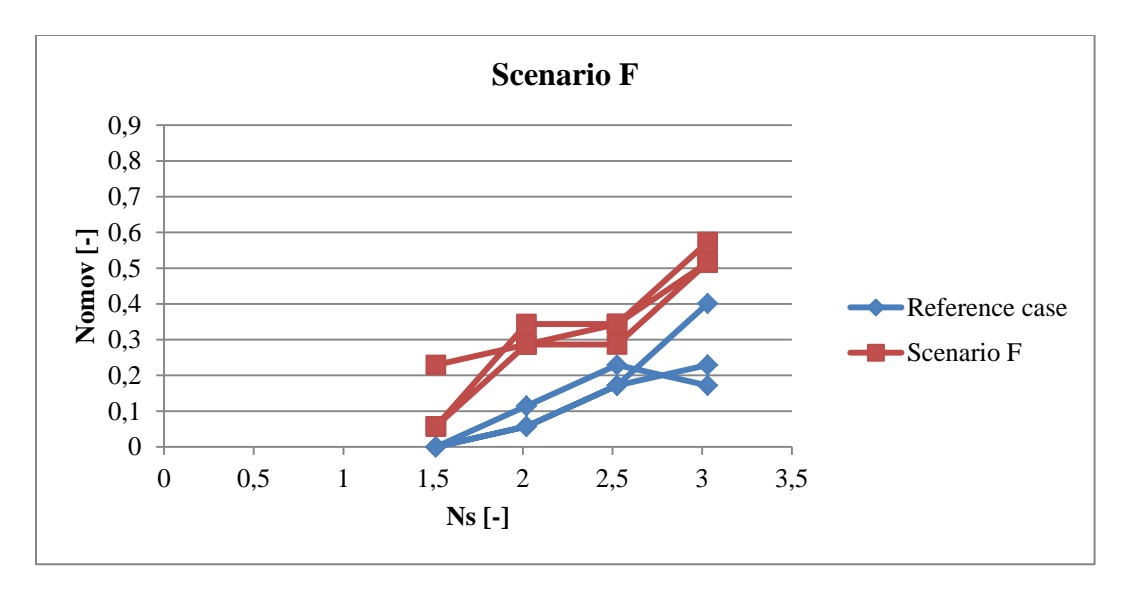


Figure 5-11 Damage of test scenario F versus damage of reference case

From the figures it becomes clear that the damage number increases for larger tolerances, although the length scale is relatively large. The tests with the convex profile showed a small increase in damage number but the scatter in the results is large.

Comparison of damage during design wave height

From the observations which are given in chapter 4 and the damage numbers presented in this section it becomes clear that every test scenario results in a higher degree of damage than the reference case. In Figure 5-12 a boxplot is given of the damage number for the different scenarios during the design conditions (100% condition).

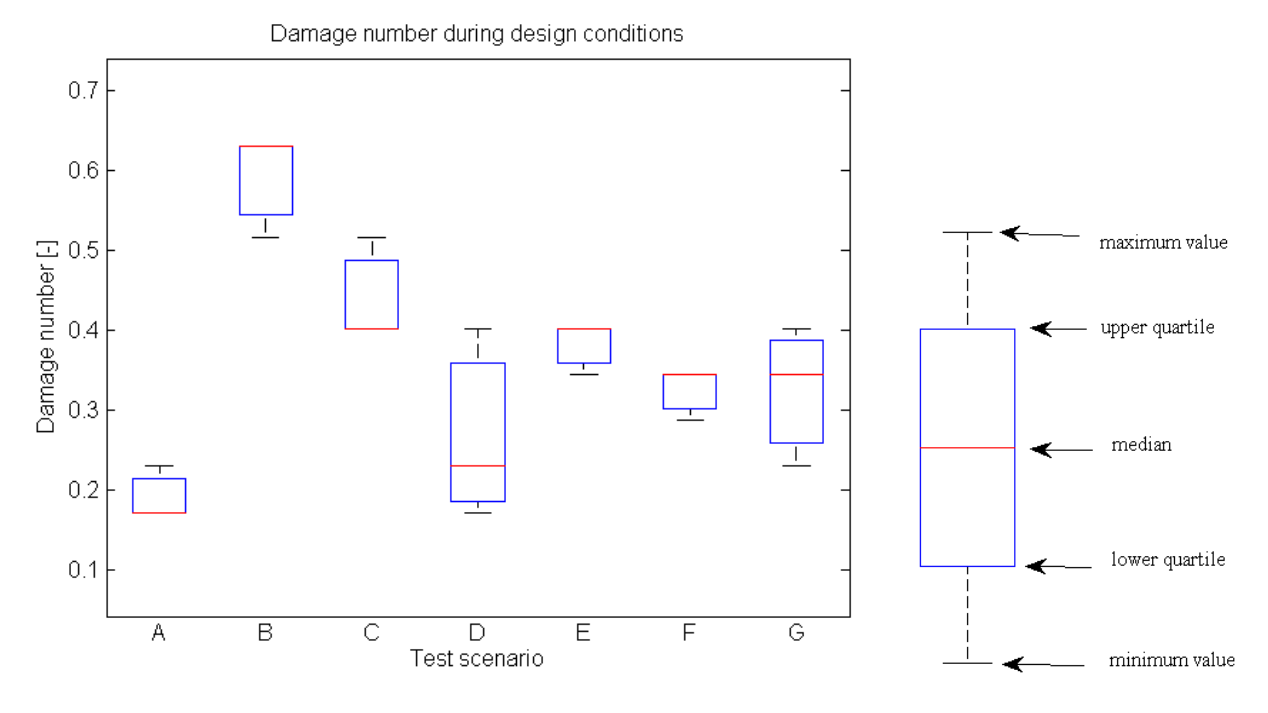


Figure 5-12 Boxplot of damage numbers of the different scenarios during design conditions

On the right side of Figure 5-12 a description of the symbols in the boxplot is given. The lower quartile is the value between the smallest number and the median. The upper quartile is the value between median and highest number. The difference between the upper and lower quartile serves as a robust measure of the amount of variability among the elements of the dataset [DEKKING *et al*, 2005].

From the figure it becomes clear that not only the damage number is larger for every case compared to the reference case (case A), but also the scatter in the results is in general larger.

5.3.2 Relation between damage and tolerances

In the previous section the damage for every scenario is discussed. From section 5.2.4 it becomes clear that every individual test has different tolerances and therefore the view of average tolerances per test scenario is simplistic.

Results

In Figure 5-13 the damage numbers during design conditions are plotted against the tolerances for every test. Because no clear relation was found between the positive and negative tolerance, for every individual test the average is taken of the positive and negative tolerance from Table 5-6.

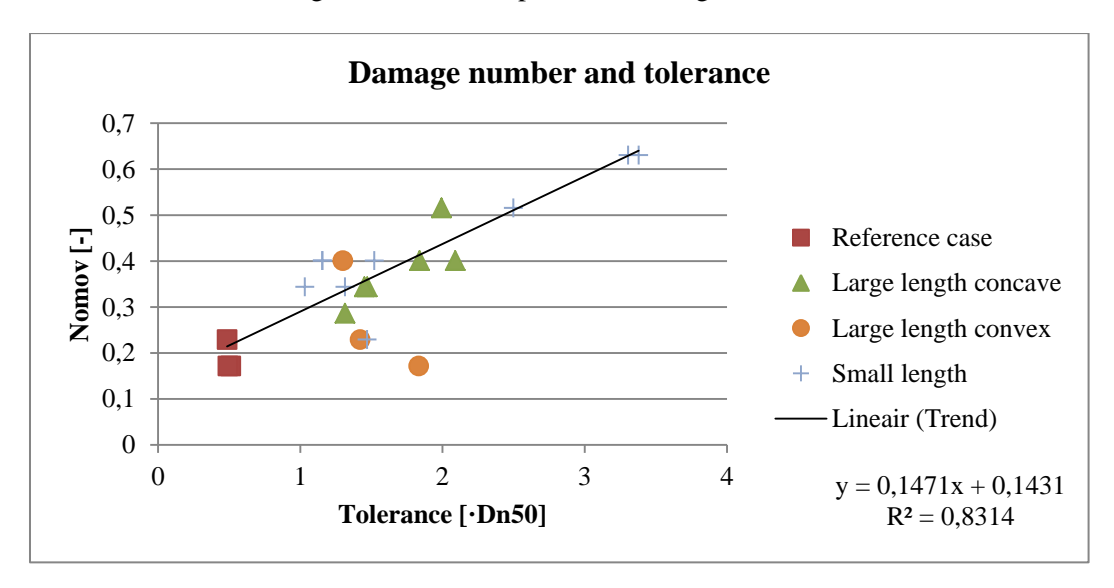


Figure 5-13 Damage numbers during design conditions plotted versus tolerances for individual tests

Figure 5-13 shows that damage numbers increase for larger tolerances. A distinction is made between small and large lengths of deviations. It seems that there is no clear distinction between the small and large lengths of deviations. Apparently the length scale of the deviations has minor influence on the damage number. It can be concluded that the convex profile is more stable than the concave profile, because two of the three data points in the graph are below the trend line. A trend line is plotted based on all data points except the data of the tests with convex profiles, because this type of profile has a different influence on the stability of the armour units. The observed relation between the damage number N_{omov} and tolerance t can be described with the equation below.

$$N_{omov} = 0.1471 \cdot t + 0.1431 \tag{5.6}$$

In which the vertical tolerance t is expressed in terms of the D_{n50} of the under layer material.

Relation with design guidelines

The prescribed tolerances of the under layer are \pm 10.5 D_{n50} in perpendicular direction, which implies \pm 10.6 D_{n50} in vertical direction. Rocking is allowed for a maximum of 2% of the armour units according to DMC. Because there are 190 armour units on the slope, 3.8 rocking units are allowed. In practice this value is rounded off which implies that 4 rocking units are allowed. 3.8 rocking units correspond to a damage value of 0.22. Based on equation 5.6, this damage value corresponds to a

tolerance of $0.52\ D_{n50}$. So strictly speaking the tolerances cannot be further adapted, because it will lead to unacceptable damage levels. The prescribed vertical tolerance of $0.6\ D_{n50}$ corresponds to a damage value of 0.23, which represents 4 rocking armour units. This is the limit of the accepted damage number, if the value of 3.8 is rounded off. The standard deviation of N_{omov} has a value of 0.054 [-], which corresponds to a difference in tolerance of $0.36\ D_{n50}$. This value of the standard deviation indicates that it is not easy to determine the exact limit of stability of the armour layer for different tolerances of the under layer. Because the tolerances which correspond to the stability limit (based on equation 5.6) are fairly close to the prescribed tolerance of $0.6\ D_{n50}$ and because the scatter in the results makes it difficult to determine the exact limit of acceptance, the current prescribed tolerances of the under layer are considered appropriate.

Correction factors for adapted tolerances

An attempt was made to determine correction factors for increased tolerances. It would be convenient to know by how much the weight of an armour unit should be increased if a certain tolerance is not achieved. The determination is done by plotting the tolerances and damage numbers in the same graph for the conditions with lower wave heights. By determining the intersection point of the trend line with the stability limit of the damage number, the tolerance at which the condition is just stable enough is calculated. Unfortunately the scatter in the results is large. In order to indicate the scatter, the mean plus and minus the standard deviation is plotted. This is indicated in Figure 5-14 for the 80% condition and in Figure 5-15 for the 60% condition.

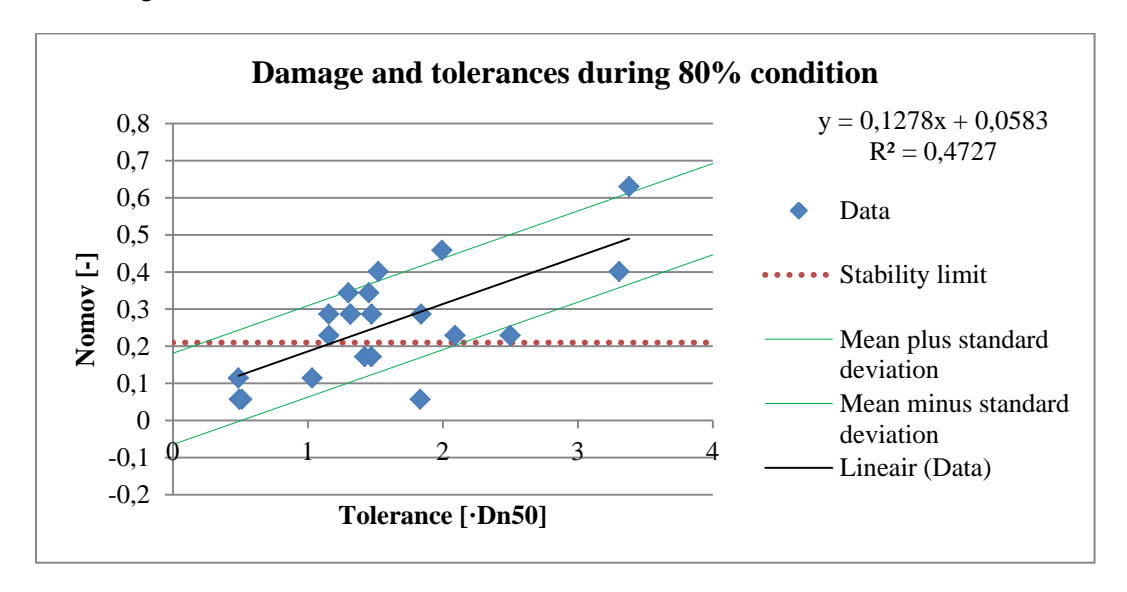


Figure 5-14 Damage number versus tolerance for the 80% condition

From Figure 5-14 and Figure 5-15 it becomes clear that the scatter is large. The coefficient of determination, R^2 , indicates how well the data fit in a line. The values of R^2 are 0.47 for the trend line of the 80% condition and 0.27 for the trend line of the 60% condition.

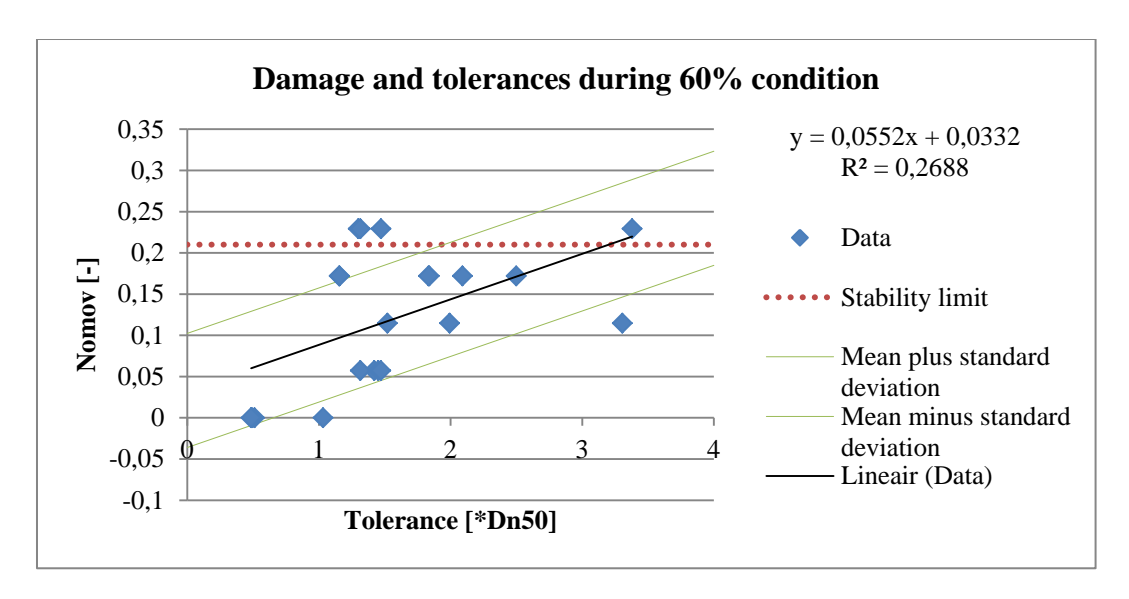


Figure 5-15 Damage number versus tolerance for the 60% condition

It is clear that the scatter is large. It is considered too large to determine the correction factors. The results of the tests show that a larger tolerance of the under layer leads to more damage of the armour layer. Based on this finding and the fact that the correction factors on the weight of the armour unit for increased tolerances cannot be determined accurately, it is recommended to not exceed the prescribed tolerances.

5.3.3 Placement density

The placement densities are determined with the photos taken which are taken before every test. With the help of a Matlab script the position of the centre of gravity of the armour units is determined. This script is given in appendix O.

Method

The Relative Placement Density (RPD) is determined with the help of photographs. Photos are taken before and after every tests and the camera is kept at a fixed position. These photos are loaded in Matlab where the centres of gravity of every armour unit are determined by simply clicking on the location which is visually determined to be the centre of gravity. The result is a matrix with coordinates of the armour units, from which the distances between armour units in lateral and upslope direction are derived. A few photos are taken with an A4 sheet of paper located directly on top of the armour layer in order to calibrate the distance. Equation 2.9 describes how the RPD can be determined. Generally, only the upslope distances are measured to determine the RPD. The RPD then becomes a ratio of the designed length between the lowest and highest armour unit on the slope and the actual upslope length between these armour units. This is made more clear in Figure 5-16. The black arrow indicates the upslope distance L_y , which is determined by calculating the average upslope distance between the armour units on the first and top row. The green arrows indicate the horizontal distance between the upper right and left armour units. For the determination of the RPD only the upslope distance L_y is used.

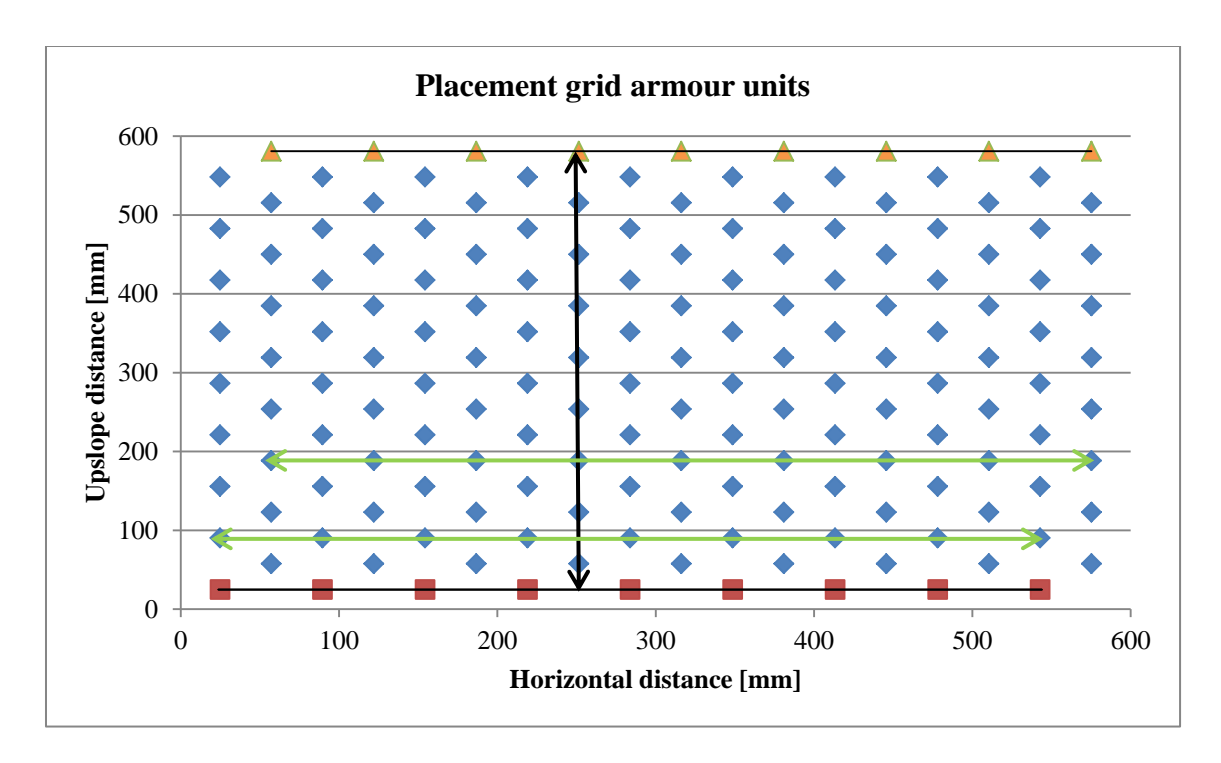


Figure 5-16 Placement grid of armour units

Results

The slope length is larger than in the reference case due to the deviations in under layer profile. This is not visible on the photos and therefore the placement density is multiplied by a correction factor which is equal to:

$$\gamma_{RPD} = \frac{l_{slope,reference}}{l_{slope,actual}}$$
 5.7

In which $l_{slope,reference}$ is the length of the slope in the reference case and $l_{slope,actual}$ is the actual slope length. In Table 5-9 the average RPD's after multiplication of the correction factor are presented. One is referred to section 2.2.6 for details on the RPD.

Table 5-9 Average relative placement densities of the tests

Test	RPD [%]
A-1	101.7
A-2	100.1
A-3	99.0
B-1	101.4
B-2	100.0
B-3	101.5
C-1	100.1
C-2	101.2
C-3	101.6
D-1	100.0
D-2	97.2

Test	RPD [%]
D-3	97.5
E-1	100.7
E-2	98.5
E-3	100.2
F-1	101.1
F-2	103.3
F-3	102.3
G-1	103.2
G-2	101.7
G-3	101.5

The values presented in Table 5-9 are average values of the RPD based only on L_y , which is the common method of DMC to determine the RPD. Because the horizontal distance L_x can also be

determined with the photographs, the RPD based on L_y and L_x is calculated as well. In Figure 5-17 the differences in RPD between the two methods are presented. It becomes clear that in some cases the difference in result of the two methods is very small, while in other cases the differences are more than 2 per cent. The comparison indicates that the value of L_x determined with the photo analysis is not constant between the tests and therefore influences the RPD.

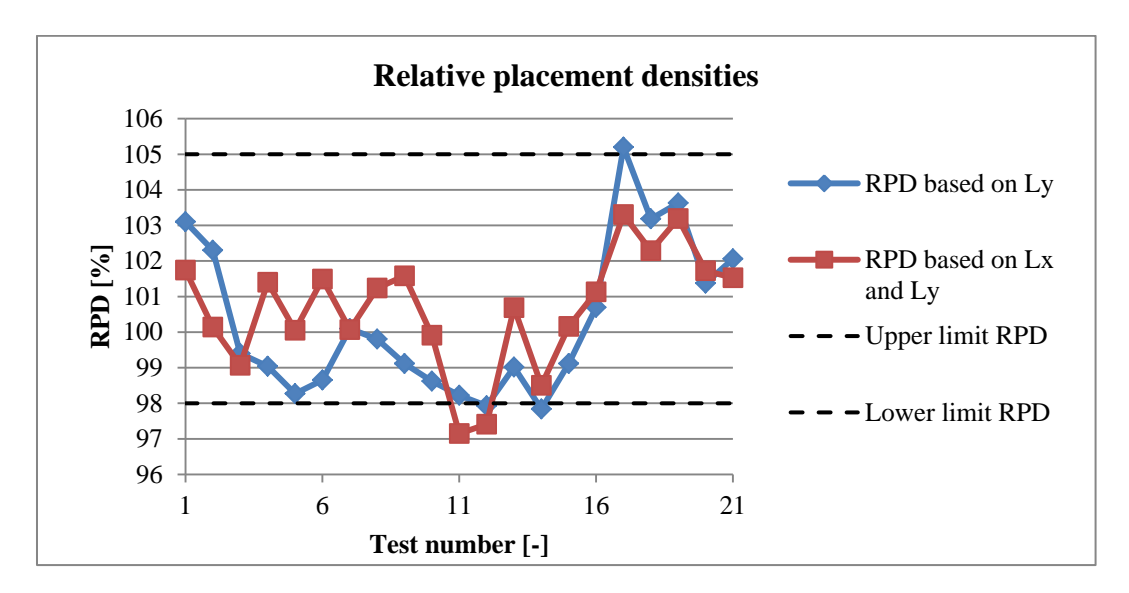


Figure 5-17 RPD's of the individual tests for the two methods

The RPD on the upper and lower half of the slope is also determined. It is found that the RPD is lower at the lower half of the slope than in the upper half of the slope. This trend is found for every individual test. In a few cases this difference is larger than 10%. This large differences can partly be explained by the differences in slope angle along the slope due to the deviated under layer profiles. These differences in slope angle influence the locations of the armour units on the photos.

Accuracy

According to DMC the RPD has to be between 98 and 105%. From Table 5-9 it becomes clear that in case of test D-2 and D-3 this prescribed RPD is not achieved, however these tests do meet the RPD requirement if L_x is also taken into account. For test A-3 and test B-1 the distance from the bottom to the top row is measured for every unit. It appears that the average difference between the distance measured with the ruler and the distance determined with the script is less than 1 cm. Although the differences in measured distance are only a few per cent, it has a major influence on the value of the RPD. The photos before the tests are compared with each other and the same trend is observed in placement density as the values show in Table 5-9. For two tests the method to determine the RPD is done a second time in order to quantify the differences. The mean difference in position of the centre of gravity of an armour unit is less than 1mm with a standard deviation of 2.5mm, which is approximately 5% of the height of the armour unit. Maximum differences of up to 10mm are obtained, which corresponds to approximately 20% of the height of the armour unit. The maximum difference which is found in RPD is 0.5%.

Validity

Earlier research with Xbloc model units showed that it is very difficult to determine the RPD accurately (e.g. VAN ZWICHT, 2009). All these research projects are performed on a well-built under layer profile. It is probably more easy to determine the distance between centres of gravity from a digital photo than with an in-situ measurement with a ruler. However, the introduction of deviations in under layer profile make the method with the digital photo less reliable because the profile is not

always perpendicular to the camera due to a varying slope angle. This can result in small errors in distance which have a large influence on the RPD. Therefore the values of the RPD are considered to give a good impression of the placement density, but the exact numbers should not be used for data processing.

Discussion

The analyses show that the RPD is a sensitive parameter. It is very sensitive for measurement errors and different methods of determining distances (e.g. in situ measurements with a ruler or photo analysis) results in a different value of the RPD. In earlier research (e.g. VERDEGAAL, 2013) the sensitivity of the RPD was mentioned as well. Based on the tests results of this thesis no link between the RPD and stability is found. Research by BAKKER *et al.*, 2005 shows that a more or less constant stability number at the start of damage is found for RPD values between 1.13 and approximately 1.21 [units/D²]. Furthermore the RPD's are in general between the prescribed value of 98 and 105% and therefore it's not a surprise that the RPD does not give an indication of the stability/

5.3.4 Settlements

The settlements of the armour units are determined by comparing the photos which are taken before the test with the ones which are taken after the 100% condition. The Matlab script, which is given in appendix O, is used to determine the magnitude and directions of the settlements. The photos which are taken before and after the test runs are given in appendix Q. For more detailed figures and data of the settlements one is referred to appendix P.

Results

The magnitude of the settlements show a large scatter between the different tests. Both the average and maximum settlements differ greatly. Earlier research (e.g. BAKKER et al., 2005) on Xbloc armour units show that there is a trend between the placement density and the settlements. In general a lower placement density results in larger settlements. Based on the test results there is no clear influence of the placement density on the settlements. No relation is found between settlements and damage. Furthermore no trend is found between the settlements and the difference in profile measurements of both under and armour layer before and after the tests. These measurements are discussed in section 5.3.5. However, a trend is observed between the average settlement of the armour units and the number of units that settle more than 0.5 times the diameter of the armour unit D. In general more units that settle more than 0.5 D correspond to larger average settlements. In Figure 5-18 the settlements during the reference case tests are presented. 'x' represents the lateral direction and 'y' the upslope direction. The red line in the plots indicates the location of the water surface. The settlements are expressed in terms of the diameter of the armour unit. Although the setup of the three tests is the same, it becomes clear that the settlements differ between the three tests. No clear explanation is found for the settlement of the armour units. Further research on this topic is recommended in order to obtain more insight in this process.

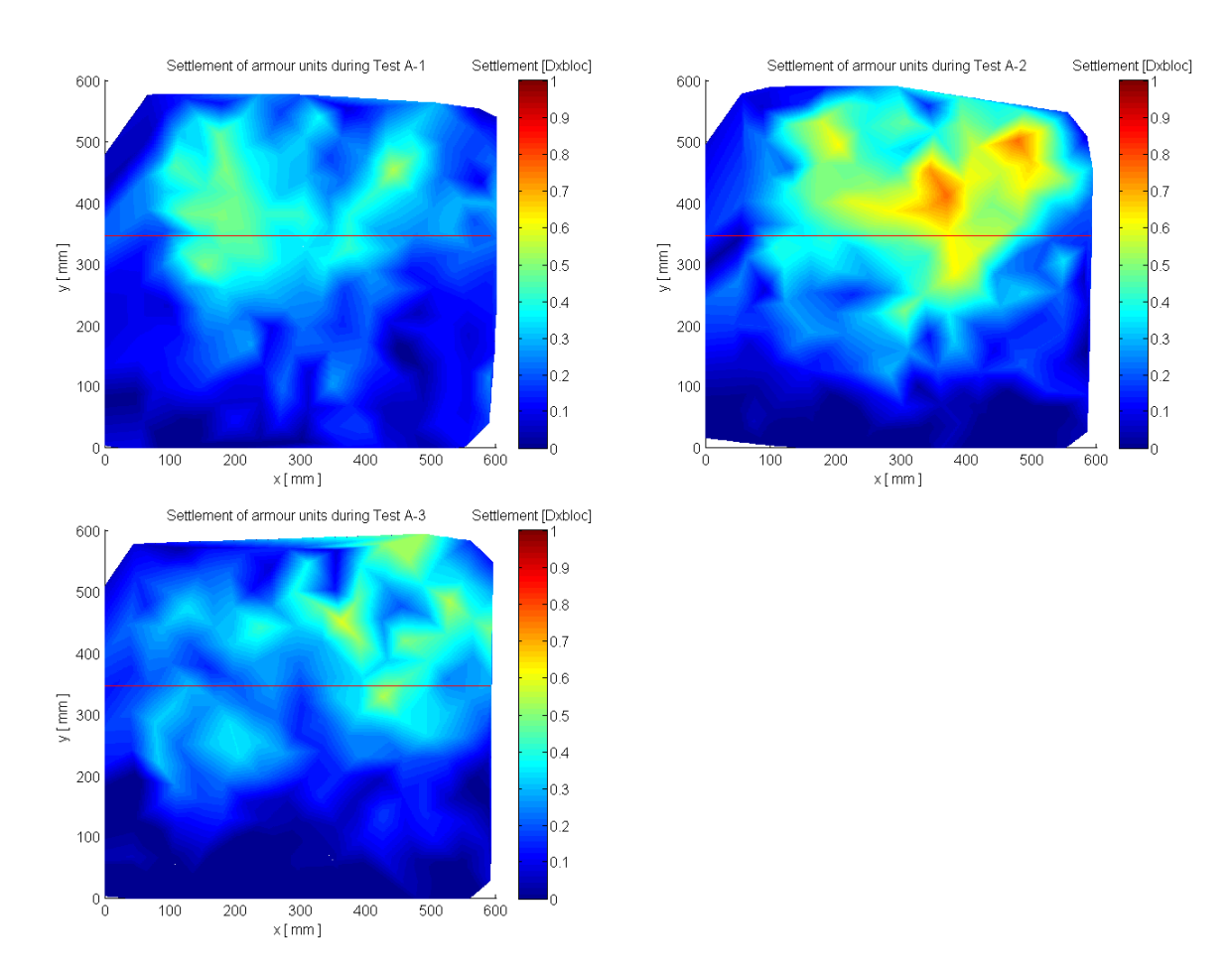


Figure 5-18 Settlements during the reference case tests

It is found that for larger settlements the area in which considerable settlements have been observed is larger. In general the upper half of the slope experiences the most settlements during the reference case tests. Settlements of more than 0.5D occurred in the area above the 10th row, while during tests with the largest settlements this area expands to further down the slope. From the photo analysis it becomes clear that except for scenario C for all test scenarios larger settlements occurred. For under layer tolerances between 1 and 1.5 D_{n50} the largest settlements occurred. This can be explained for the short length scale deviations by the fact that the sections with very mild slopes are smaller than for larger tolerances. A logical consequence is that these mild sloped sections do not hinder the settlements as much as for larger tolerances. For the large length scale deviations the large settlements there is no clear explanation. Due to a lower steepness on the upper half of the slope less settlements are expected, but the opposite occurs. A partial explanation of the settlements can be found in the differences in placement density on the slope. When tests of the same scenario are compared, a general trend is observed between the difference in RPD on the lower and upper part of the slope and the magnitude of the average settlement. One is referred to appendix P for the details. Unfortunately these results are not comparable between different scenarios due to the varying slope angle of the test scenarios.

Development in RPD before and after the test

In the previous section the RPD is discussed. The RPD after the tests are determined and it has been observed that the RPD increases during every tests. This is a logical consequence of the settlements. The differences in the RPD in the lower and upper half of the slope are compared as well. As mentioned, before the test the RPD is larger on the upper half than on the lower half of the slope. For almost every individual test the RPD on the upper half becomes smaller during the test, while the RPD

on the lower half becomes larger. This effect is a logical consequence of the settlements. The armour units which are located in the area of the middle to approximately a few rows below the top row experience the largest settlements. Therefore the distance between units on the lower half of the slope becomes smaller during the tests, while the units on the upper rows do not settle as much as the units in the middle of the slope. This implies that the distance between the armour units on the upper half of the slope becomes larger and thus the RPD decreases. Details on this are given in appendix P.

Accuracy and validity

The same procedure which is used to determine the RPD is applied to determine the settlements. This method is considered accurate on reference case profiles. However for deviated profiles the slope angle is different along the slope and as a result of this the distances on the photo are not accurate anymore. Therefore the magnitude of the settlements is considered to give a good qualitative overview but is not accurate enough to use for data processing.

5.3.5 Interaction between under layer and armour layer

For the majority of the tests both the armour layer and under layer are measured before and after the test. In this section a qualitative overview of the results is given.

Results

In Figure 5-19 the results of the scans before and after a test (G-2) is given. The results of the measurements before the beginning of the test and after the 120% condition are presented. Although only the results of one test are presented in the figure, it gives a qualitative overview of the profiles of the two layers before and after a test. The findings which are discussed below are based on an analysis of all the profiles which are measured.

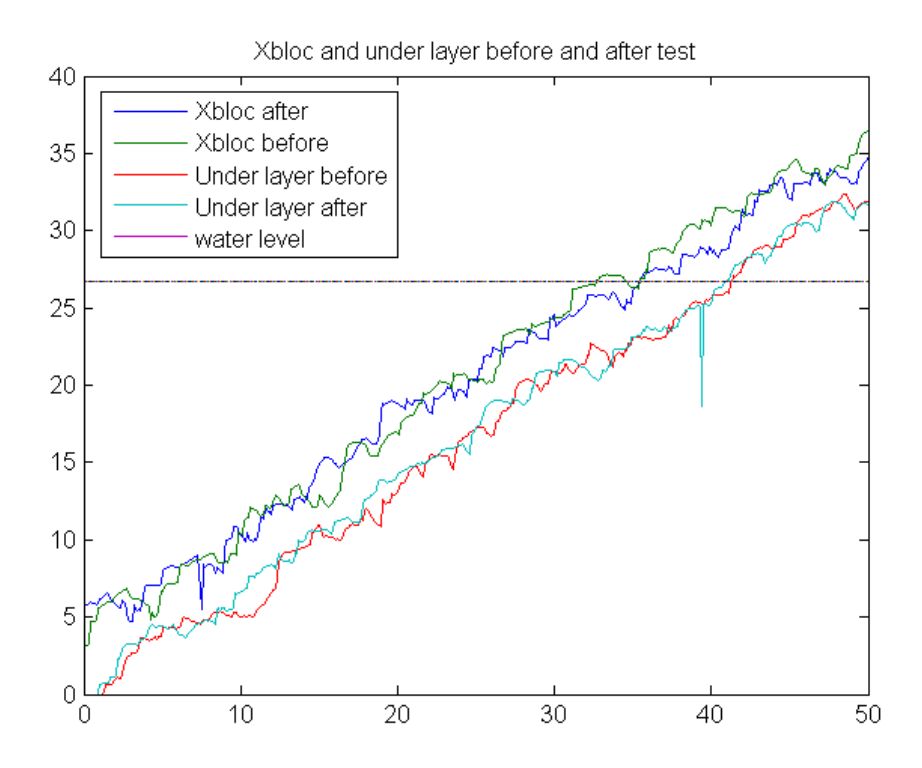


Figure 5-19 Scan of armour and under layer before and after test G-2

Behaviour of armour layer

From Figure 5-19 it becomes clear that the profile height of the armour layer decreases considerable just below the water surface during the test. Further down the slope the armour layer profile is lifted a bit during the test. The difference in profile is comparable to the development of S-curves which occur as a consequence of wave attack at breakwaters with natural rock. However, the mechanism is different because no erosion of armour units occurs. An example of a S-curve is given in Figure 5-20. The under layer develops in a similar way during the test. However, the difference in under layer profile is in general less than the difference in armour layer profile. This can be explained by the behaviour of the Xbloc armour units. During removal of the armour units after the tests it was observed that some units were located between stones of the armour units with one of the legs of the Xbloc. It appears that the Xbloc armour units not only interlock with the neighbouring armour units, but also with the under layer. This seems to be especially true for the units located just below and above the water surface.

Behaviour of the under layer

From Figure 5-19 it can be observed that the under layer settles. Earlier it was mentioned that the under layer profile develops in a similar way as the armour layer profile. It is therefore plausible that settlement of the armour units is (partially) only possible if the under layer rocks can settle. The settlement of the under layer implies that there is transport of under layer material in downslope direction. As a consequence of this transport the average steepness of the slope (in both armour and under layer profile) becomes less during the test. The difference in slope angle before and after the test is rather small, in general less than 1°.

Damage levels of the under layer

For breakwaters which are constructed with natural rock the damage level is generally expressed by means of the damage parameter S, which is based on the erosion area of a breakwater profile. This is made more clear in Figure 5-20, in which the development of the S-curve is visible.

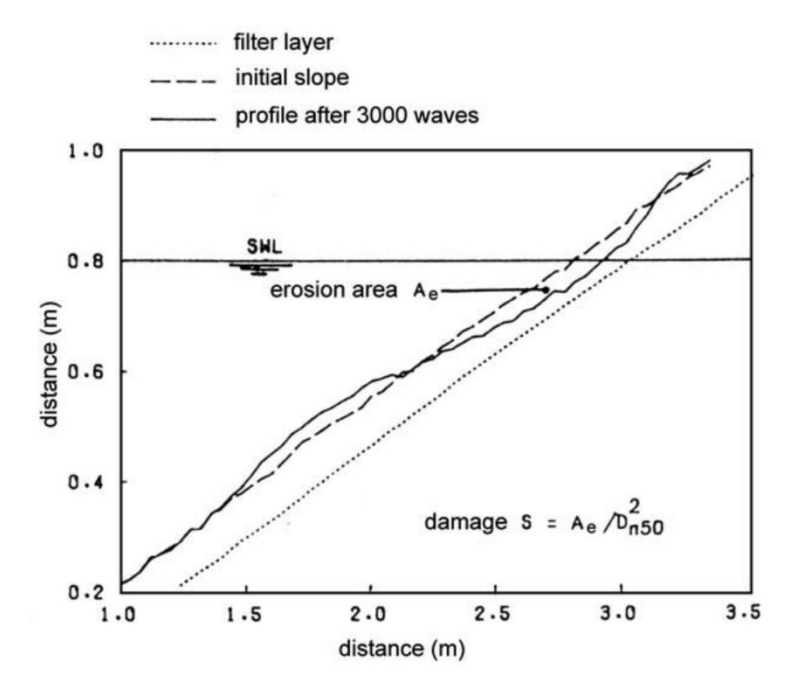


Figure 5-20 Damage level S and the development of an S-curve with erosion area A. Figure from Verhagen $et\ al.$, 2012

The damage levels of the under layer are determined by integrating the difference in profile before and after the test over the horizontal distance x. No trend is found between damage levels of the under

layer and damage number of the armour layer (N_{omov}) . This can be explained by the assumption that the damage of the under layer is predominantly caused by the deformation of the armour layer. The deformation of the armour layer is not dependent on the damage number N_{omov} . Therefore it is logical that no trend can be found between the damage level of the under layer and the damage number of the armour layer N_{omov} .

Deformation of the armour layer

The damage of the armour layer is expressed by N_{omov} which is based on the number of moved units. The erosion areas of the armour layer are determined with the same procedure as for the under layer. Again no trend is found between the magnitude of the erosion area and N_{omov} . This can be explained by the fact that no real erosion of armour units occurs. Therefore the erosion area is not really a consequence of erosion but a consequence of deformation of the armour layer. It is therefore better to speak of a 'deformation area' instead of an erosion area. A proportionality is found between the deformation of the under layer and armour layer; if the deformation of the armour layer is relatively large, then the deformation of the under layer is relatively large as well.

Accuracy

Both the under layer and amour layer is measured before and after the tests. Because the same laser device is used, it is considered that the measurements of the armour layer have the same accuracy. This is different for the under layer measurements after the tests. In this case the armour units have to be removed first, before the layer can be measured. Although the armour units have been removed carefully, it was observed that some stones of the under layer moved during removal. This effect is minimized by averaging over three profiles but does introduce an error. This is not considered a problem because only a qualitative overview is given in this section.

5.3.6 Conclusions

From the test results it becomes clear that larger damage levels have been observed for larger tolerances of the under layer. No clear distinction between short and large length scales is found. The damage levels are larger than in the reference case for all test scenarios and in general the scatter in results is larger as well. It can therefore be concluded that a larger additional roughness results in larger damage levels. The observed relation between tolerances of the under layer and damage level (equation 5.6) makes clear that the tolerances of the under layer cannot be increased because it will lead to unacceptable damage levels. The hypothesis which is defined in section 1.3.2 is therefore partially true. The hypothesis is defined as:

The tolerance levels of the under layer for breakwaters, which are constructed with interlocking armour units, may not exceed $0.5D_{n50}$ in perpendicular direction. The stability of the armour layer decreases for larger tolerance levels and this effect is larger for short length scales of deviations in the under layer profile.

The tolerances cannot be further adapted and the effect of length scales is not found. It should be mentioned that small length scales are in the order of 2 to 4 armour units and large length scales in the order of 8 armour units. The settlements of the armour units are analysed as well. It is found that it is hard to recognise trends or patterns in the settlements.

5.4 Discussion

In this section some issues are discussed. Firstly a comparison is made between earlier research on under layer tolerances with extraction force tests and research on low crested structures. Furthermore an additional test scenario with different under layer material is discussed. This section ends with a discussion on the accuracy of the observed damage numbers and three dimensional effects which have been neglected so far.

5.4.1 Comparison with earlier research

In Figure 5-21 the most important results of earlier research on the influence of the tolerances of the under layer are presented. Extraction force tests are performed for different tolerances.

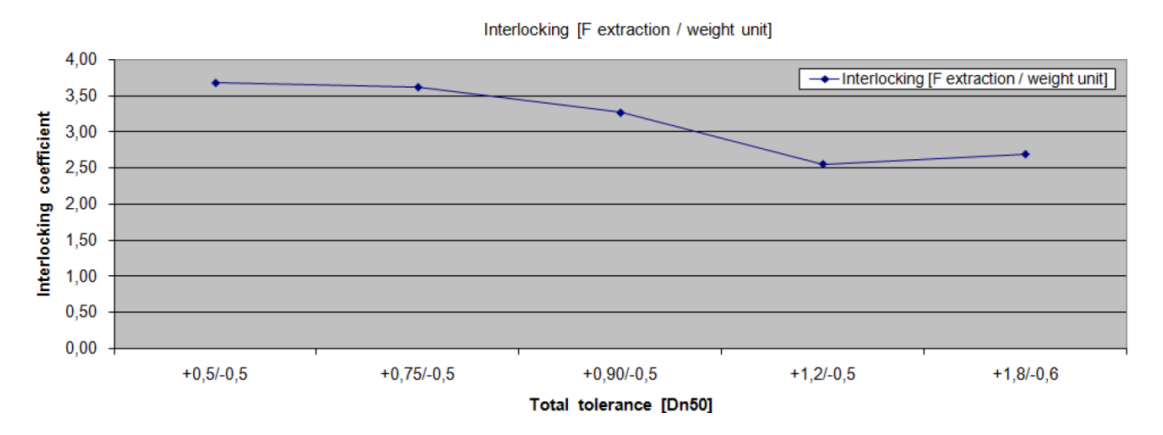


Figure 5-21 Relation between extraction force and tolerance. Figure from Monster and Philipsen, 2010

The interlocking coefficient is defined as the force required to extract an armour unit from the armour layer divided by the weight of the armour unit.

Comparison of results

In Figure 5-22 the results of the extraction force tests are plotted in the same graph as the obtained relation between damage and tolerances during design conditions (equation 5.6). The loss of stability indicates the loss in interlocking coefficient and the decrease in damage number. The tolerances of the tests are translated to average tolerances by adding the positive and negative tolerance and dividing the sum by two.

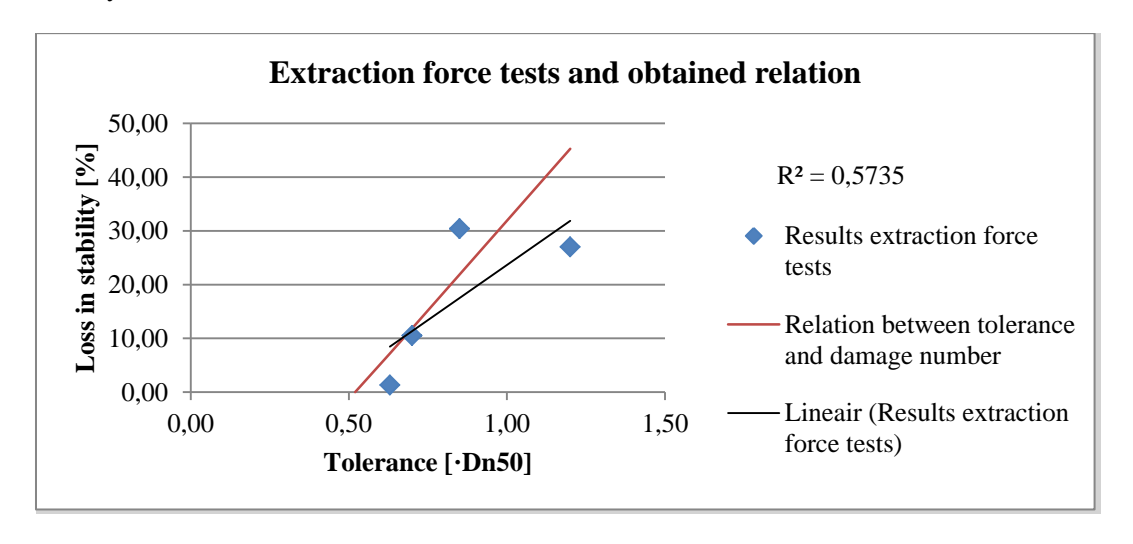


Figure 5-22 Results of the extraction force tests and the found relation between damage and tolerances

The results of the two datasets show the same trend, although there is scatter in the results of the extraction force tests. Based on the results of the extraction force tests the conclusion that larger

tolerances lead to unacceptable damage can be justified. It should be noted that the tests performed by Monster and Philipsen are conducted with tolerances up to $1.2D_{n50}$ while the tests of this thesis are performed with tolerances up to $3.5D_{n50}$. Therefore the range of the dataset is different and this makes the comparison less reliable.

Difference between interlocking coefficient and damage number

Although the results of the hydraulic tests of this thesis and the extraction force tests show approximately the same results, there is a physical difference in the generation and mode of damage. Damage of the hydraulic tests is defined as the relative number of armour units which moved during a test, which is described in section 3.5.1. In general the damage number N_{omov} is predominantly influenced by the number of rocking armour units, because significantly more rocking than extraction has been observed. The interlocking coefficient, which is used to indicate the stability of the armour layer during the extraction force tests, is solely based on extraction of an armour unit. Therefore the modes of damage which occur during hydraulic and extraction force tests are different.

Physical differences in extraction

For both physical tests and extraction force tests extraction is considered damage. However, there is a physical difference in the generation of the extraction between the two test methods. During hydraulic tests the water motion can induce extraction of armour units. During extraction force tests a sling is connected to an armour unit, in perpendicular direction of the slope, and by pulling this sling the unit is extracted. The major difference is that the interlocking of the armour unit which is extracted is different in hydraulic and extraction force tests. For hydraulic tests the interlocking of the armour unit is significantly less during extraction of the unit than right after placement of the armour layer, as a result of settlements of armour units which occur due to wave loading. For extraction force tests the interlocking is not reduced, because there is simply no wave attack. In general during hydraulic tests an armour unit cannot be extracted in case it is properly interlocked, while during extraction force tests In Figure 5-23 the difference in forces on the armour unit is made more clear. The left part of the figure represents the situation of hydraulic tests and the right part the situation during extraction force tests.

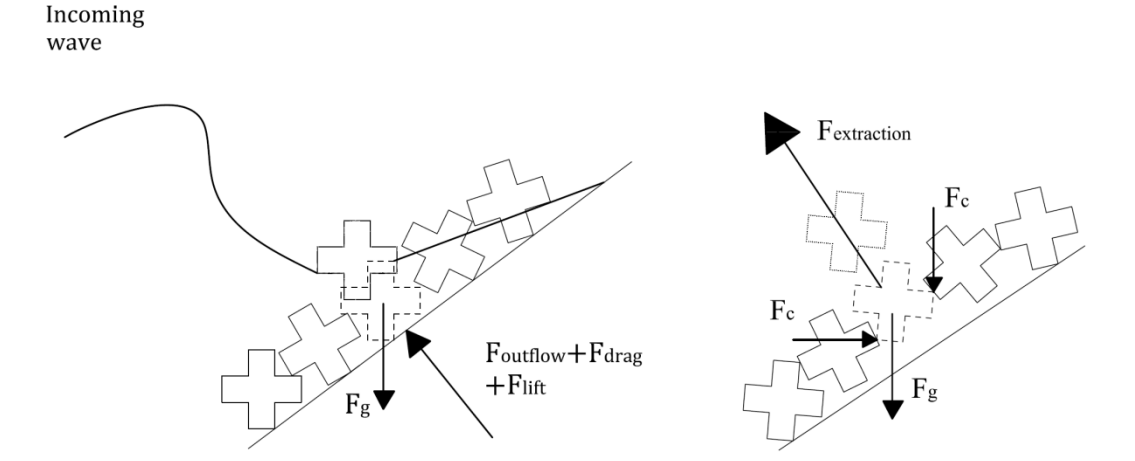


Figure 5-23 Forces on armour unit during hydraulic and extraction force tests

During hydraulic tests the interlocking is less due to settlements. Furthermore the sum of outflow of water from the core, lift and drag reduces the interlocking from the unit above as well. If the sum of these forces in perpendicular direction of the slope is larger than the weight of the armour unit decomposed in perpendicular direction, the unit is extracted from the armour layer. During extraction force tests not only the weight of the unit acts as a stabilizing force, but also the contact forces

(denoted with F_c in Figure 5-23) from interlocking neighbouring units act as stabilizing forces. From the analysis of the two test methods it becomes clear that the generation of extraction is different and therefore it's not easy to compare the results of the two test methods with each other. Although the extraction force tests give a good impression of the interlocking after placement, it does not give any information about the actual stability during and/or after wave attack. Furthermore the damage in hydraulic tests is predominantly generated by rocking and not by extraction. This makes the comparison between the damage number N_{omov} and the interlocking coefficient less reliable.

Validity of the comparison

As mentioned there is a significant difference in the definition and generation of damage of the two test methods. Settlements during hydraulic tests result in differences in RPD and this enables rocking and extraction. The analysis of the settlements during hydraulic tests (section 5.3.4) shows that settlements are unpredictable. Because of these reasons the difference in tests methods is considered too large to make a quantitative comparison between the results. Although a quantitative comparison is considered not possible, the results of the extraction force tests do give a small degree of support to the conclusion because qualitatively the same effect was observed.

5.4.2 Relation with low crested structures

Research has been performed on the stability of interlocking armour units on low crested structures. Because the profiles with deviations consists of locally horizontal slopes, comparable results are expected. This is because the (nearly) horizontal slope can be interpreted as a local crest. In this section a distinction is made between the damage on the slope and on the crest of the breakwater. Only the scenarios with short length scales of the deviations are considered in this section, because only in these scenarios locally horizontal slopes are present. An important parameter is the **crest freeboard**, which is defined as the height of the crest divided by the design wave height. The crest freeboard of the tests which are conducted for this thesis refers to the height of the profile of the armour layer on the horizontal section. Because there are a few of these sections present in the profiles, the horizontal section which is located the closest to the water surface is considered.

General findings

The crest freeboard in scenario B and G is 0, while scenario E has a freeboard of -0.3. The largest damage occurs at a crest freeboard of 0 [VAN DEN BOSCH *et al.*, 2012]. In Figure 5-24 the stability number at start of damage is plotted against the crest freeboard.

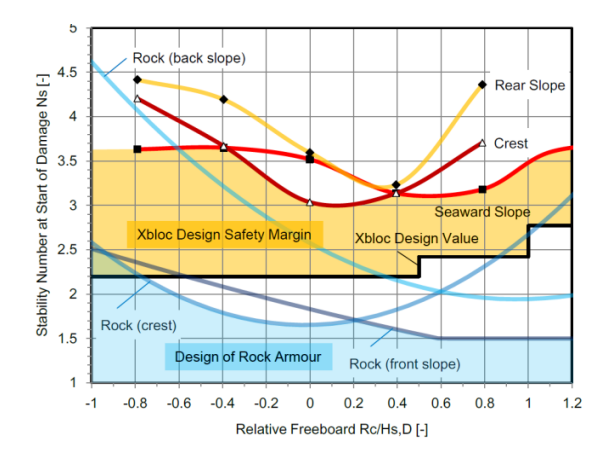


Figure 5-24 Stability of different parts of a breakwater as a function of the relative freeboard. Figure from VAN DEN BOSCH et al., 2012

According to the figure the freeboards of scenario B, E and G are unfavourable when it comes to damage of the armour layer. For these magnitudes of the freeboard more damage is expected to occur at the crest than at the slope. The rear slope is not part of the scope and therefore not discussed here.

Observed damage

The results of physical model tests with low crested structures make clear that more rocking occurs at the crest with a lower crest freeboard, in case the freeboard is less than -0.1 [VAN DEN BOSCH *et al.*, 2012]. For a larger freeboard more rocking on the slope is expected. This is made more clear in Figure 5-25.

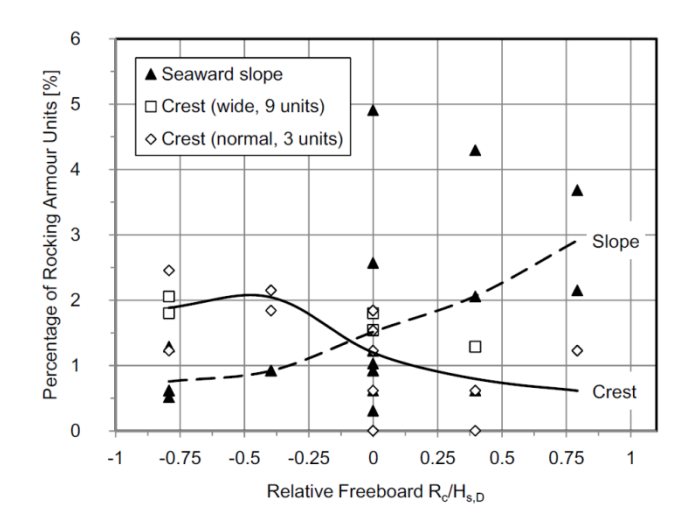


Figure 5-25 Occurrence of rocking on crest and slope. Figure from VAN DEN BOSCH et al., 2012

The location of rocking units of scenario B, E and G are analysed. During design conditions of scenario B 9 rocking units on the crest and 21 on the slope have been observed. The results of scenario E are 10 units on the slope and 4 on the crest. For scenario G 8 rocking units on the crest and 1 on the slope have been observed. The trend in results is different than expected based on Figure 5-25. Furthermore the difference between number of rocking units on the slope and on the crest is significantly larger than the lines in the figure. It has to be mentioned that apparently the scatter in rocking armour units for a freeboard of zero is large. This is also observed during the tests for this thesis.

Comparison of the two test series

In section 4.2.4 the influence of the transition from slope to crest is compared to the region around the step. This area which is a transition of a relatively steep to a mild slope is vulnerable to damage. This is observed in the tests with low crested structures and during the tests of this thesis. In both test series the most damage occurred in this area. However, the results are different in trend and magnitude. This can be explained by the fact that the tests for this thesis are conducted with profiles which consists of two or three horizontal sections. As a result two or three horizontal sections are present. The step at these sections is vulnerable to damage and this can partially explain that no comparison can be made with low crested structures. Another (probably more important) aspect which is different between the test with low crested structures and the tests of this thesis are the actual crest heights. In Figure 5-26 this is made more clear.

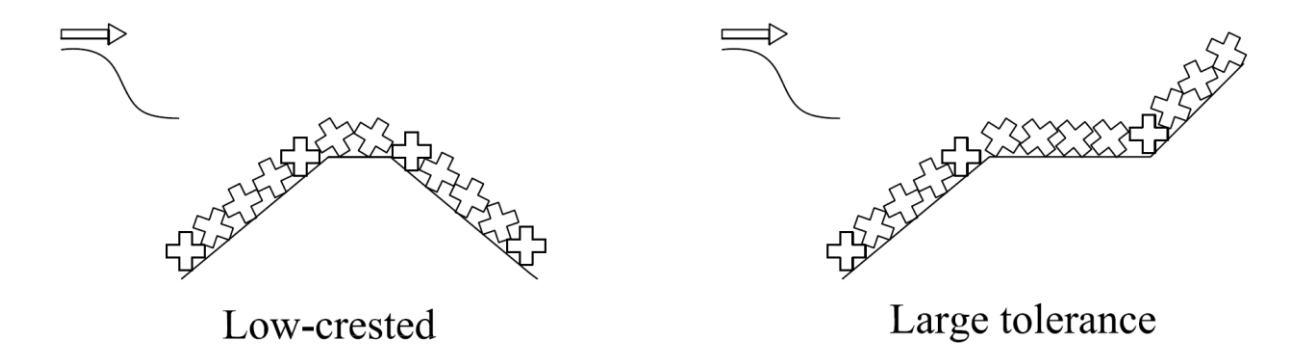


Figure 5-26 Physical difference between low-crested breakwaters and breakwaters with a large tolerance

For the tests with low crested structures the transition from steep to horizontal slopes is the highest point of the structure. This difference has a large influence on the water movement in and in front of the structure. The difference in water movement results in different forces on the armour units. The difference in forces on the armour units explains why no clear relation with low crested structures can be found.

5.4.3 Influence natural roughness

Although the focus of this thesis is on the influence of the additional roughness of the under layer on the stability of the armour layer, also tests with a larger natural roughness have been conducted. In this case the D_{n50} is larger and the grading is narrower, which means that the diameter of the stones is closer to the mean diameter than in the other test scenarios. This implies that this grading has a larger natural roughness than the grading applied in the other test scenarios.

Characteristics of the grading

As mentioned the grading of the under layer of this test scenario is larger and narrower compared to the grading applied in the other scenarios. The D_{n50} is in this case 16.5mm and for the other scenarios the D_{n50} is 14.5mm. Furthermore the ratio W_{85}/W_{15} is 2.4 in this case and 3.2 for the other test scenarios, which implies that the grading is narrower. The sieve curve is given in appendix C.

Tolerances

The tolerances are determined with the same procedure as described in section 5.2. In Table 5-10 the tolerances of the two tests are presented, in terms of the $D_{n50,original}$ of test scenario A to G, which is 14.5mm. In the most right column the tolerance is expressed in terms of the actual D_{n50} of this scenario, which is 16.5mm. The plots of the under layer profile are given in appendix J.

Table 5-10 Tolerances of tests with different under layer grading

Test	Positive tolerance $[\cdot D_{n50,original}]$	Negative tolerance $[\cdot D_{n50,original}]$	Average tolerance $[\cdot D_{n50,original}]$	Average tolerance $[\cdot D_{n50,actual}]$
Extra-1	0.86	0.80	0.83	0.73
Extra-2	0.79	0.67	0.73	0.64

From Table 5-10 it becomes clear that the tolerances are larger although the profile is constructed in the same way as the reference case, which has an average tolerance of approximately $0.5\,D_{n50}$. This is a logical consequence of the larger D_{n50} . Remarkable is that the increase in tolerance between the reference scenario with the standard grading and this scenario is larger than the increase in D_{n50} between the two scenarios. It can therefore be concluded that a narrower grading results in larger tolerances. This can be explained by the absence of smaller stones in the grading, which are able to fill up holes between larger stones and hereby reducing deviations in the profile and thus reduce the tolerances.

Damage

The damage numbers are larger than in the reference case. This is shown in Figure 5-27. The RPD for these tests is 101.9 and 102.6% and is thus according to the design.

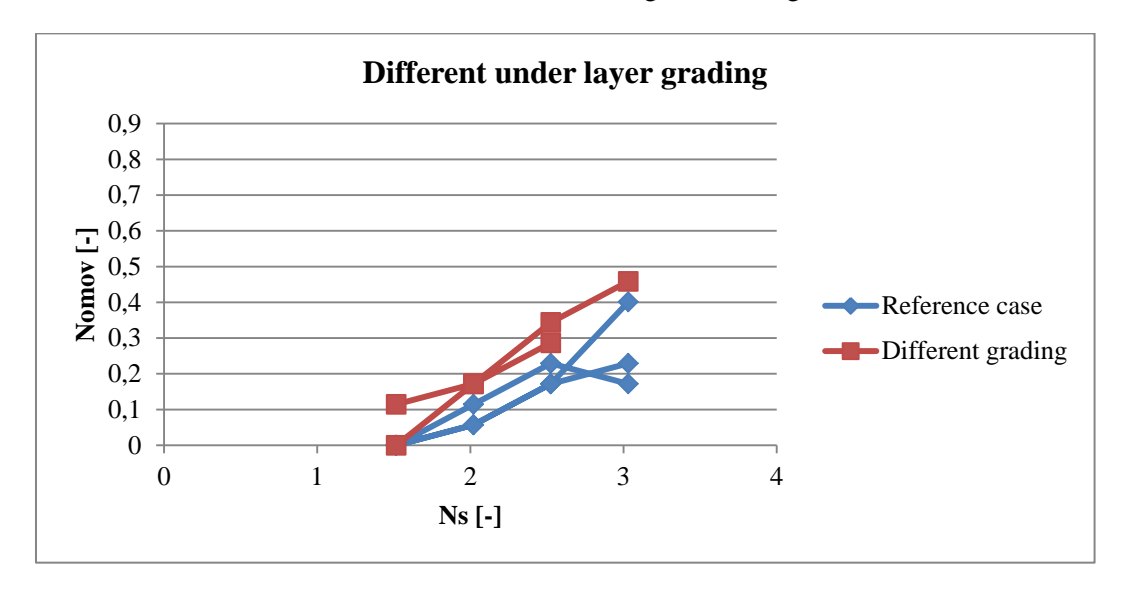


Figure 5-27 Damage of test scenario with different under layer grading versus damage of reference case

From Figure 5-27 it becomes clear that the observed damage is larger than in the reference case. Based on the characteristics of the grading, it seems plausible that larger under layer stones and/or a narrower grading of the under layer leads to more damage of the armour layer. The damage numbers during design conditions are larger than expected, based on the found relation between tolerances and damage numbers (equation 5.6). Based on this relation values of N_{omov} of approximately 0.25 are expected, but the observed damage corresponds to values of 0.29 or larger. The increased damage can be explained by the fact that a larger natural roughness hinders settlement of the armour units (the settlements are discussed in section 5.3.4). Average settlements of 8 mm occurred for this scenario, while in the reference case average settlements of 11mm occurred. Due to the hindered settlement differences in packing density occur and the interlocking decreases. This mechanism enables rocking.

Ratio in diameter of armour and under layer

As mentioned in section 2.3.1 the ratio in diameter of the armour unit and under layer stones is not constant for different sizes of Xbloc. When one calculates the ratio of prescribed diameter of the

armour unit D_{Xbloc} and nominal diameter of the under layer $D_{n50,under\,layer}$, a value between 2.7 and 3.9 is obtained. This ratio can be determined based on the design guidelines for Xbloc [Delta Marine Consultants, 2011]. This ratio is 3.4 for the tests of scenario A to G of this thesis and 3.0 for the extra scenario which is described in this section. It can therefore be concluded that the nominal diameter of the under layer of this extra scenario is in the prescribed range, however the grading of the under layer material is narrower.

Porosity and permeability

Due to the larger stone size and narrower grading, the porosity and permeability of the under layer are expected to be different for this scenario. In general a wider grading leads to a lower porosity, because finer material can fill the pores which exist between larger stones. Furthermore the shape of the stones influences the porosity and permeability. Because the grading is narrower than the grading used in the other test scenarios, a higher porosity is expected. Because the pores are larger in this grading, it is expected that friction has less effect on the flow and therefore the permeability is higher. Earlier research performed by BURCHARTH et al., 1998 and VERDEGAAL, 2013 show different influences of the core permeability on the stability of the armour layer. Burcharth performed tests with Accropode armour units and Verdegaal with Xbloc. Burcharth found a decrease in stability for decreasing permeability of the core for different wave steepness's. Verdegaal found a decrease in stability for an impermeable core for swell waves, while for sea waves no influence on the stability was found. For an open core Verdegaal found a decrease in stability for sea waves while for swell waves no effect was found. It should be mentioned that these reports only discuss the influence of the permeability of the core and not the permeability of the under layer. Furthermore the conclusions of the two reports are not in line with each other. Therefore it's not possible to draw conclusions about the effect of a higher permeability of the under layer on the stability of the armour layer.

Recommendation for further research

As mentioned in section 2.3.1 DMC prescribes standard gradings of natural rock to be used in under layers for different Xbloc sizes. This implies that the ratio of nominal diameter of the under layer and diameter of the Xbloc unit is not constant. The damage numbers of this test scenario could indicate that the stability of the armour layer is dependent on this ratio. However, this ratio is in the same range as prescribed by DMC for this scenario. Another aspect is the width of the grading. In this case the grading was narrower than the scaled standard 300-1000kg grading. The damage numbers of this test could indicate that the width of the grading of under layer material has influence on the stability of the armour layer. It is therefore recommended to do further research into different under layer gradings to investigate the influence of the diameter and width of the under layer grading on the stability of the armour layer with interlocking armour units. Furthermore it is recommended to DMC to pay attention to the grading of under layer material during the construction phase, because these tests shows that the grading of the under layer has an influence on the stability of the armour layer.

5.4.4 3D effects

The tests which are performed for this thesis are two dimensional tests. This implies that effects in lateral direction are not considered. Furthermore the waves approach the structure in normal direction. In reality the problem which is considered in this thesis is therefore a three dimensional problem. In this section the neglected aspects of the three dimensionality are given and, if possible an indication of the effects of these neglected aspects is given.

Influence of the angle of wave incidence

Research on the angle of wave incidence has been performed with Xbloc armour units. The results are given in Figure 5-28.

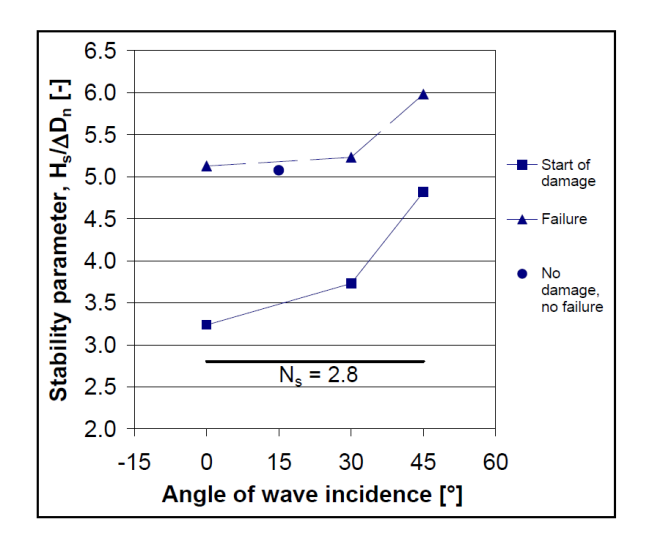


Figure 5-28 Influence angle of wave incidence on stability of the armour layer. Figure from BAKKER et al., 2005.

From Figure 5-28 it can be seen that damage and failure occurs at larger wave heights for increasing angles of wave incidence. For a reference case profile it is therefore expected that more oblique waves lead to a more stable situation. For tests with deviated under layer profiles it is hard to estimate what the effect will be. Deviations in the profile are likely to occur in lateral direction as well. As a result the interlocking will not only be less in vertical direction but also in lateral direction. In order to assess these effects further research with three dimensional scale models is required.

Influence of curved sections

DMC prescribes larger Xbloc units on curved sections and breakwater heads. This is because on curved section and breakwater roundheads the interlocking is less [TEN OEVER, 2006]. In these sections the interlocking in lateral direction is less, due to the shape of the profile. It is likely that in prototype the deviations in under layer profile are also present in lateral direction. This implies that due to the deviations in under layer profile the interlocking decreases in alongslope and lateral direction. In this thesis the lateral direction is not considered because the tests are two dimensional. It is therefore expected that in prototype situation the stability is less for deviated under layer profiles, because interlocking decreases in both alongslope and lateral direction.

5.4.5 Accuracy of the observed damage

The damage numbers which are presented in section 5.3.1 originate from visual observations of rocking and extraction during the tests. According to the definition of DMC, an armour unit is rocking when it is visibly moving during more than 2% of the waves. Although this definition is clear, it is hard to observe the rocking. Extraction on the other hand, is not hard to observe because one can easily see when the unit is removed from the armour layer. Complicating factors for observing rocking are the rapidly varying water level and the breaking of waves on the slope, especially because the area in which the waves break is in general the most vulnerable to rocking. The complexity increases if more units are moving. If units are moving both below and above the water level the observer has to observe carefully which units are moving and at the same time count during how many waves an armour unit has moved order to determine which units are actually rocking. It is therefore expected

that the accuracy goes down with larger damage numbers. Unfortunately the magnitude of the possible error in damage number cannot be determined because there is no other method available which is more accurate Although the tests are recorded on video, observing rocking is even harder from the video than observing it live in the flume.

It would be convenient if a more reliable indicator of rocking would be available. An option could be to equip all the armour units with wireless accelerometers. Because the majority of the armour units does not move during wave attack the difference in acceleration with rotating units is large. Based on the measurements of the acceleration it would be possible to determine which units are moving during more than 2% of the waves and are (thus) rocking.

6 Conclusions and recommendations

In this thesis the influence of the under layer profile on the stability of the armour layer is investigated. The research objective, which is defined in section 1.3.1, reads:

The primary goal of this thesis is to investigate and quantify the influence of deviations in the under layer profile on the stability of the armour layer, including a comparison between different measurement methods of the under layer profile. Then recommendations can be made to parties involved in the construction process.

In this chapter the final conclusions are drawn and recommendations are given.

6.1 Conclusions

6.1.1 Main conclusions

The following general conclusions are drawn during the process of this thesis. The section in which the conclusion is elaborated is indicated between brackets.

- Larger damage numbers have been observed for larger tolerances. This implies that there is a positive trend between additional roughness and damage of the armour layer. (4.2)
- During tests with deviated under layer profiles most damage has been observed in the area around the step. This area has a lower packing density and/or lower degree of interlocking. (4.2.4)
- Most damage has been observed at the step which is located just below the water surface, in case of multiple steps present in the slope. (4.2.2)
- Convex shaped profiles are more stable than concave shaped profiles, due to the absence of a step which is vulnerable to damage. (4.2.3)
- There is a difference in measured under layer profile between the laser device and simulated spherical foot staff. The measured profile of the simulated sphere is higher than the laser device. The difference in results between the two methods is in line with earlier research. (5.2.3)
- In general a larger positive tolerance is found with the simulated spherical foot staff than a negative tolerance. Unfortunately the measurement method is sensitive to measurement errors and therefore the average tolerance is used for further processing. (5.2.4)
- The lower bound of the tolerance is $0.5 \ D_{n50}$. This value is found for all the reference case profiles. It can therefore be concluded that it is not possible to construct under layer profiles with tolerances smaller than $0.5 \ D_{n50}$. (5.2.6)
- The settlements are determined by means of analysis of photos of the armour layer. It is hard to determine the settlements accurately due to the varying slope angle for the different test scenarios. A trend is found between the average settlement and the number of units that settle more than 0.5 D. Furthermore a qualitative trend is observed between difference in RPD and magnitude of the average settlement. (5.3.4)
- The results of this thesis are compared with earlier research which was performed with extraction force tests. Although this research method is significantly different, comparable results are obtained. (5.4.1)
- An extra scenario which consists of under layer rocks with a larger diameter and narrower grading is tested. Not considering possible differences in permeability, it is found that a larger natural roughness of the under layer results in smaller settlement and more damage of the armour layer. (5.4.3)

6.1.2 Testing of the hypothesis

The hypothesis, which is defined in section 1.3.2, reads as follows:

The tolerance levels of the under layer for breakwaters, which are constructed with interlocking armour units, may not exceed $0.5D_{n50}$ in perpendicular direction. The stability of the armour layer decreases for larger tolerance levels and this effect is larger for short length scales of deviations in the under layer profile.

The results of the physical model tests prove that the tolerances cannot be increased to a value larger than 0.5 times the nominal diameter D_{n50} in perpendicular direction. The observed relation between the magnitude of the tolerance and the damage number during design conditions is quantified as follows:

$$N_{omov} = 0.1471 \cdot t + 0.1431 \tag{6.1}$$

The relation is based on all test results except the tests with convex shaped profiles. This relation is made more clear in Figure 6-1.

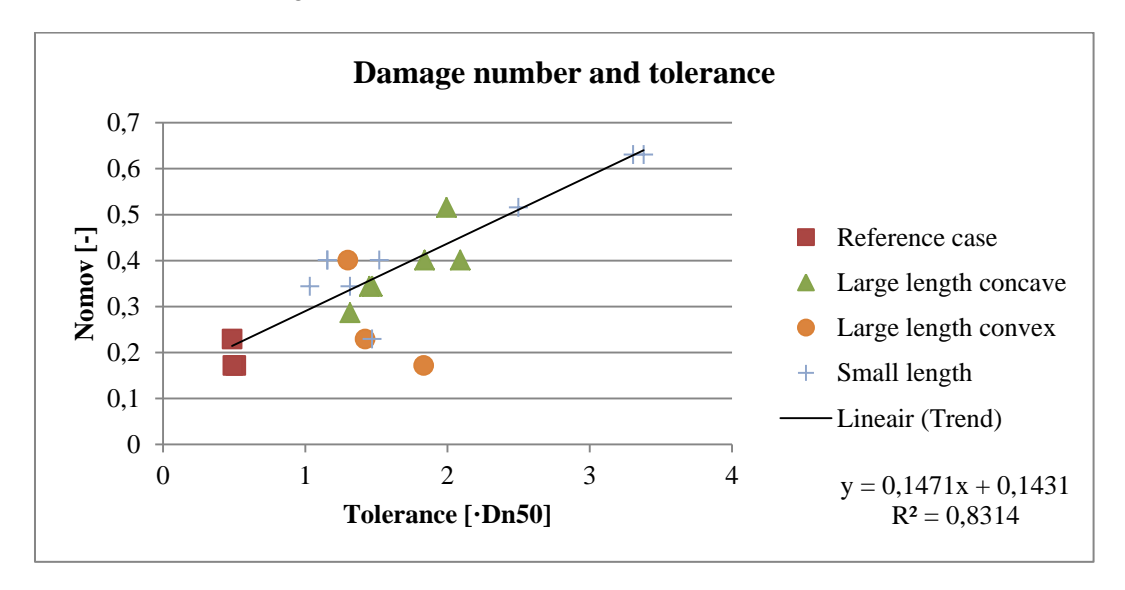


Figure 6-1 Damage numbers during design conditions plotted versus vertical tolerances for individual tests

Based on the tests results it can be concluded that a larger tolerance than prescribed leads to unacceptable damage numbers. No clear influence of the magnitude of the length scales of the tolerances on the damage numbers is found. Therefore this part of the hypothesis is falsified.

6.2 Recommendations

6.2.1 Recommendations for stakeholders

Based on the findings of this thesis some recommendations for stakeholders such as consultants, clients or contractors are drawn. They are indicated below. The section in which the recommendation is elaborated is indicated between brackets.

• The tolerances for under layers should not be increased to a value above $0.5\ D_{n50}$ in perpendicular direction. Tolerances in the reference tests are close to this value. Therefore the quality of placement of the under layer is of major importance and needs full attention. (5.3.2 and 5.2.6)

- It is important to perform measurements of the under layer profile making use of the spherical foot staff method with recommended sphere diameter and fixed interval between measurement points. If other methods are used attention should be paid to this as well, because the difference in measurement method can have a large influence on the measured profile. (5.2.3 and 2.3.5)
- The grading of the under layer in prototype should be checked carefully. The results of the additional test scenario show that the grading of the under layer influences the stability of the armour layer (5.4.3)

6.2.2 Suggestions for further research

Based on the findings of this thesis some suggestions for further research are given, they are indicated below. The section in which the suggestion is elaborated is indicated between brackets.

General aspects

• It is found that rocking is not easy to observe. When more units move during model tests this difficulty increases and it is expected that, as a consequence, the accuracy in the observed damage decreases. It is therefore recommended to do research into the accuracy of the observed number of rocking units with e.g. an accelerometer. (5.4.5)

Under layer aspects

- The exact values of the tolerances of the tests could not be determined accurately. In general a larger positive tolerance is found than a negative one. Further research on the exact magnitude of tolerances should prove this. A research on with a larger scale model is recommended. (5.2.4)
- In prototype the deviations are likely to occur in all (three) directions. This could result in a loss of interlocking in lateral directions, which is not considered in this thesis. Therefore it's recommended to do further research with three dimensional models. With these models the angle of wave incidence and deviations of the under layer profile in lateral direction can be varied. (5.4.4)
- Based on results of tests with a different under layer grading, it's plausible that the diameter and/or width of the grading of the under layer influences the stability of the armour layer. Therefore it's recommended to do further research with different gradings of the under layer by varying diameter and width of these gradings to investigate the influence of these parameters on the stability of the armour layer. Important aspect is the change in permeability of the under layer, which can influence the stability of the armour layer. (5.4.3)

References

ARCHETTI, R. AND LAMBERTI, A. (1996). Reshaping breakwater: profile parametrisation. *Berm breakwater workshop*. *Trondheim*.

BAKKER, P., KLABBERS, M., MUTTRAY, M. AND VAN DEN BERGE, A. (2005). Hydraulic performance of Xbloc armour units. *Proceedings on coastal zone management and engineering in the Middle East.*

BAKKER, P., VAN DEN BERGE, A., HAKENBERG, R., KLABBERS, M., MUTTRAY, M., REEDIJK, B. AND ROVERS, I. (2003) Development of concrete breakwater armour units. *Proceedings 1st Coastal, Estuary and Offshore Engineering, Moncton.*

BOSMA, C. (2001). Porositeit in breuksteenconstructies. *Master Thesis Delft University of Technology*.

BURCHARTH, H.F. (1993). Structural Integrity and Hydraulic Stability of Dolos Armour Layers. *Hydraulics & Coastal Engineering Laboratory. Department of Civil Engineering. Aalborg University.*

BURCHARTH, H.F., LIU, Z. AND TROCH, P. (1999). Scaling of core material in rubble mound breakwater model tests. *Proceedings of the COPEDEC V, Cape Town*.

BURCHARTH, H. F., CHRISTENSEN, M., JENSEN, T., & FRIGAARD, P. (1998). Influence of core permeability on accropode armour layer stability. *Proceedings coastlines, structures and breakwater, Institution of Civil Engineers*.

CIRIA (2007). Rock Manual. The use of rock in hydraulic engineering (2nd edition). *C683*, *CIRIA*, *London*.

DE LANGE, M. (2010). Extraction force Xbloc: model tests. *Additional Master Thesis Delft University of Technology*.

DEKKING, M., KRAAIKAMP, C., LOPUHAÄ, H. AND MEESTER, L. (2005). A modern introduction to probability and statistics. *Springer-Verlag, London*.

DELTA MARINE CONSULTANTS (2011). Guidelines for Xbloc concept designs.

FROEHLICH, D.C. (2011). Mass Angle of Repose of Open-Graded Rock Riprap. *Journal of irrigation and drainage engineering, ASCE*.

HAUER, M. (2000). Maak- en meetnauwkeurigheden bij de uitvoering van baggerwerken en steenbestortingen. VBKO, Leidschendam.

HOLTHUISEN, L.H. (2007). Waves in oceanic and coastal waters. Cambridge University Press, Cambridge.

HUGHES, S.A. (1993). Physical models and laboratory techniques in Coastal Engineering. *World Scientific Publishing, Singapore*.

MANSARD, E.P.D. AND FUNKE, E.R. (1980). The measurement of incident and reflected wave spectra using a least squares method. *Proceedings Coastal Engineering 1980*.

MEULEPAS, G., VAN REENEN, J. AND VAN DER BURG, P. (1999). Uitvoeringsrapport. Een onderzoek naar hoogteligging breuksteen met multi- en singlebeam echosounders.

MONSTER, H. AND PHILIPSEN, K. (2010). Underlayer tolerances Xbloc breakwater units. *Bachelor thesis Hogeschool van Arnhem en Nijmegen*.

MUTTRAY, M. (2000). Wellenbewegung an und in einem geschütteten Wellenbrecher. *PhD thesis Technischen Universität Braunschweig*.

MUTTRAY, M., REEDIJK, B., VOS-ROVERS, I. AND BAKKER, P. (2005). Placement and structural strength of Xbloc and other single layer armour units. *Proceedings Coastlines. Structures and Breakwaters*.

RAO, A. (2000). Basic and applied Soil Mechanics. New age international publishers, New Delhi.

REEDIJK, B., BAKKER, P., VAN DER VORM-HOEK, C. AND VOS-ROVERS, I. (2005). Development and application of an innovative breakwater armour unit. *Proceedings on coastal zone management and engineering in the Middle East*.

SCHIERECK, G.J. (2001). Introduction to bed. Bank and shoreline protection. VSSD, Delft.

TEN OEVER, E. (2006). Theoretical and experimental study on the placement of Xbloc. *Master Thesis Delft University of Technology*.

TIRINDELLI, M. AND LAMBERTI, A. (2004). Wave Action on Rubble Mound Breakwaters: the Problem of Scale Effects. *University of Bologna, Bologna*.

VAN DEN BOSCH, I., TEN OEVER, E. AND MUTTRAY, M. (2012). Stability of interlocking armour units on a breakwater crest. *Proceedings coastal engineering 2012*.

VAN ZWICHT, B.N.M. (2009). Effect of concrete density on the stability of Xbloc armour units. *Master thesis Delft University of Technology*.

VERDEGAAL, I. (2013). The influence of core permeability on the stability of interlocking, single layer armour units. *Master thesis Delft University of Technology*.

VERHAGEN, H.J., D'ANGREMOND, K. AND VAN ROODE, F. (2012). Breakwaters and closure dams. *VSSD*, *Delft*.

ZWANENBURG, S.A.A. (2012). The influence of the wave height distribution on the stability of single layer concrete armour units. *Master Thesis Delft University of Technology*.

Appendices

Appendices

Appendix A: Scaling of core material	81
Appendix B: Mass distribution of Xblocs	83
Appendix C: Under layer details	84
Appendix D: Toe design	86
Appendix E: Rock material on the crest	87
Appendix F: Placement grid of the armour units	88
Appendix G: Wave calibration	89
Appendix H: Wave data	91
Appendix I: Correction factors on the weight of the armour units	97
Appendix J: Profiles measured with the laser device	98
Appendix K: Results of the spherical foot staff measurements	110
Appendix L: Difference between simulated spherical foot staff and laser measurements	114
Appendix M: Sensitivity analysis of the simulated spherical foot staff	115
Appendix N: Specifications of the laser scanning device	117
Appendix O: Matlab scripts	119
Appendix P: Settlements	125
Appendix O: Photos taken before and after the tests	128

Appendix A: Scaling of core material

The core is scaled according to a method described by BURCHARTH *et al.*, 1999. The principle is that the hydraulic gradient is the same in model and prototype:

$$I_{model} = I_{prototype}$$
 A.1

The pore pressure in the core is dependent on time and space:

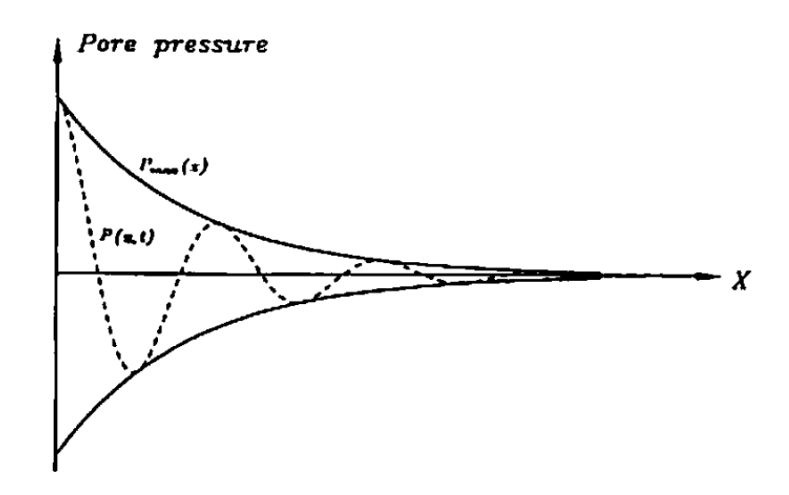


Figure A-1 Pore pressure in the core of a breakwater. Figure from BURCHARTH et al.. 1999

The pore pressure gradient is:

$$I_x = \frac{-\pi H_s}{L'} e^{\frac{-\delta 2\pi x}{L'}} \left[\delta \cos(\frac{2\pi x}{L'} + \frac{2\pi t}{T_p}) + \sin(\frac{2\pi}{L'} + \frac{2\pi t}{T_p}) \right]$$
 A.2

With the pressure gradient known. The characteristic pore velocity can be calculated with the Forchheimer equation:

$$I_{x} = \alpha \left(\frac{1-n}{n}\right)^{2} \frac{\nu}{g d_{50}^{2}} \frac{U}{n} + \beta \frac{1-n}{n} \frac{1}{g d_{50}^{2}} \left(\frac{U}{n}\right)^{2}$$
A.3

In which:

 α . β Coefficients depending on Reynolds number n Porosity of the core x Horizontal distance T_p Wave period ν Kinematic viscosity of water U Characteristic pore velocity

With damping coefficient δ :

$$\delta = 0.014 \cdot \frac{n^{\frac{1}{2}}L_p^2}{H_s b} \tag{A.4}$$

In which b is the core width. For the wave length in the core L' holds:

$$L' = \frac{L}{D}$$
 A.5

Now the characteristic pore velocity is known. This velocity can be scaled according to the Froude criterion. Limiting factor is the availability of rock gradings in the laboratory. It is chosen to apply a nominal diameter of 9.6mm for the core material. Froude scaling yields a required characteristic pore velocity in model situation of $1.5 \cdot 10^{-2}$ m/s. In this case this velocity is $1.3 \cdot 10^{-2}$ m/s. Although these values do not match entirely, it is expected that this rather small difference will not introduce significant viscous scale effects and is therefore to be neglected.

Appendix B: Mass distribution of Xblocs

In the figure below the mass distribution of the armour units which were used in the model tests is presented. The mean mass is 95.115 gram and the standard deviation is 0.521 gram.

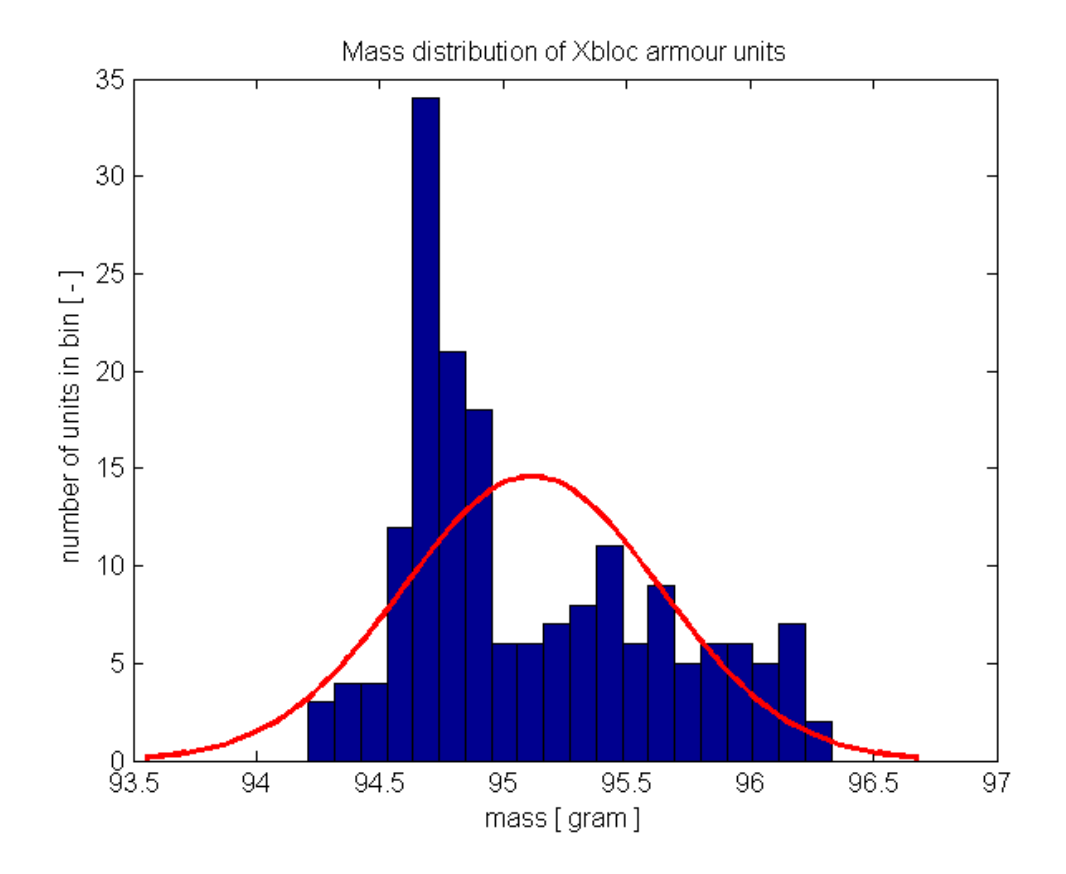


Figure B-1 Mass distribution of the Xbloc units which were used in the physical model tests.

Appendix C: Under layer details

The under layer in prototype consists of natural rock in the standard grading of 300 to 1000 kg. In the figure below the standard grading of 300-1000kg is plotted versus the grading used in the model. The model dimensions are up scaled to prototype values.

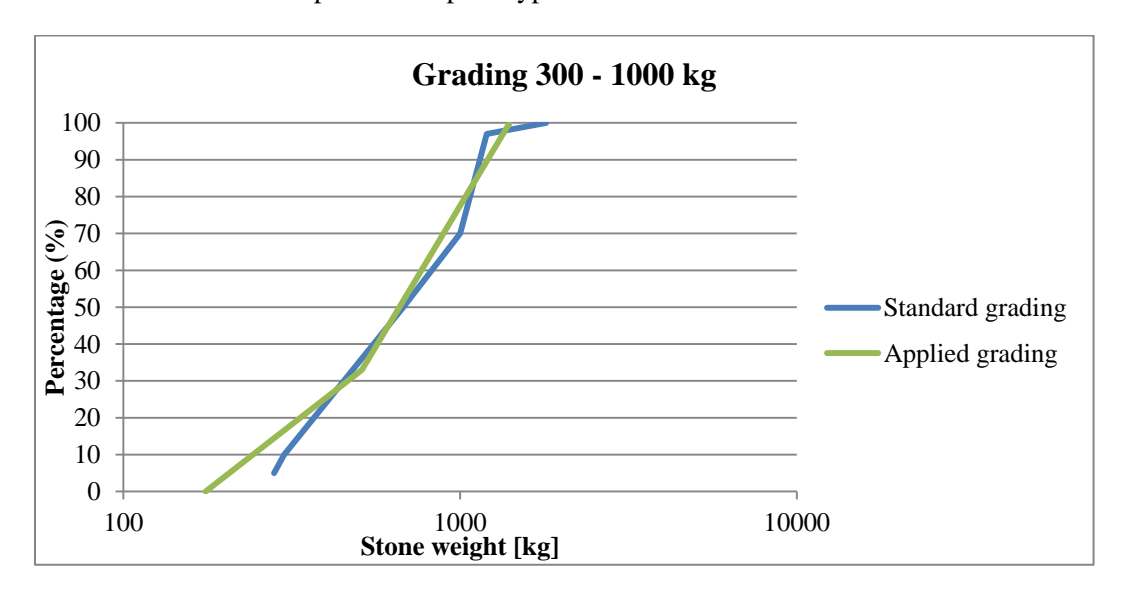


Figure C-1 Standard rock grading (300-1000kg) and grading applied in the model

In the figure below a picture is presented of the stones in the under layer, in order to give an impression of the size and angularity of the material.



Figure C-2 Stones in the under layer of the model

In Figure C-3 the grading which is used in the test scenario with a larger and narrower grading is presented. The model dimensions are up scaled to prototype values.

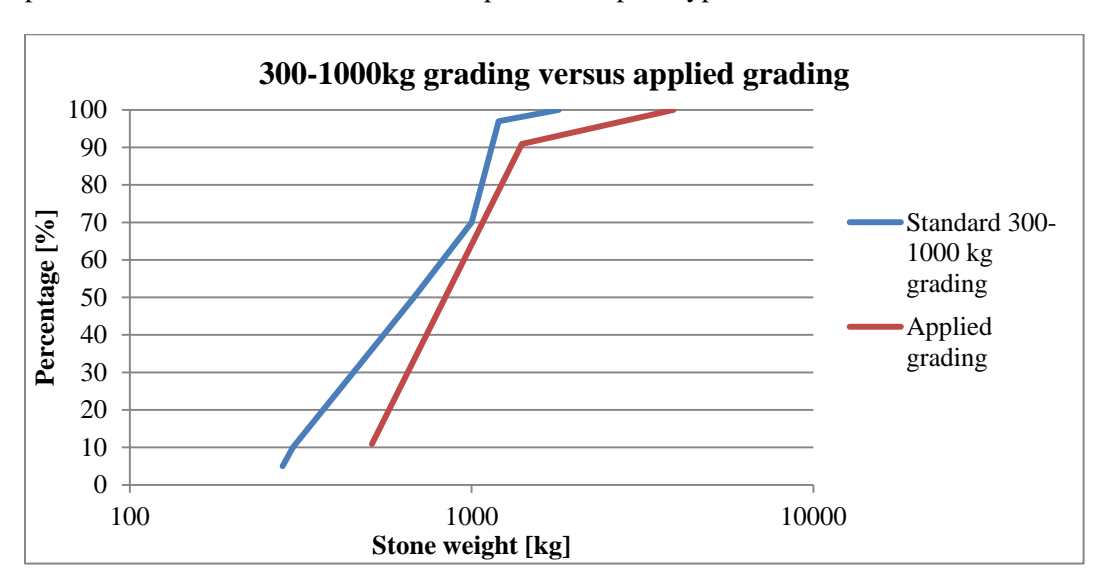


Figure C-3 Larger and narrower grading versus the standard 300-1000 kg grading

Appendix D: Toe design

The required diameter of the toe is calculated with:

$$D_{n50} = \frac{H_s}{(2 + 6.2 \left(\frac{h_t}{h}\right)^{2.7} \cdot N_{od}^{0.15} \cdot \Delta}$$
 D.1

In which:

h_t	water depth above toe	[m]
h	water depth in front of toe	[m]
N_{od}	damage value. Relative number of displaced units	[-]

A damage value of 0.5 is used. Which yields a toe with a mass of 980 kg in prototype. A damage value of 0.5 represents 'start of damage'. In this case a grading is applied which is fairly close to the 1 to 3 ton grading in prototype. So the toe is stable. In the figure below the standard grading of 1-3 ton is plotted versus the grading applied in the model. The mass of the stones in the model are up scaled to values in prototype.

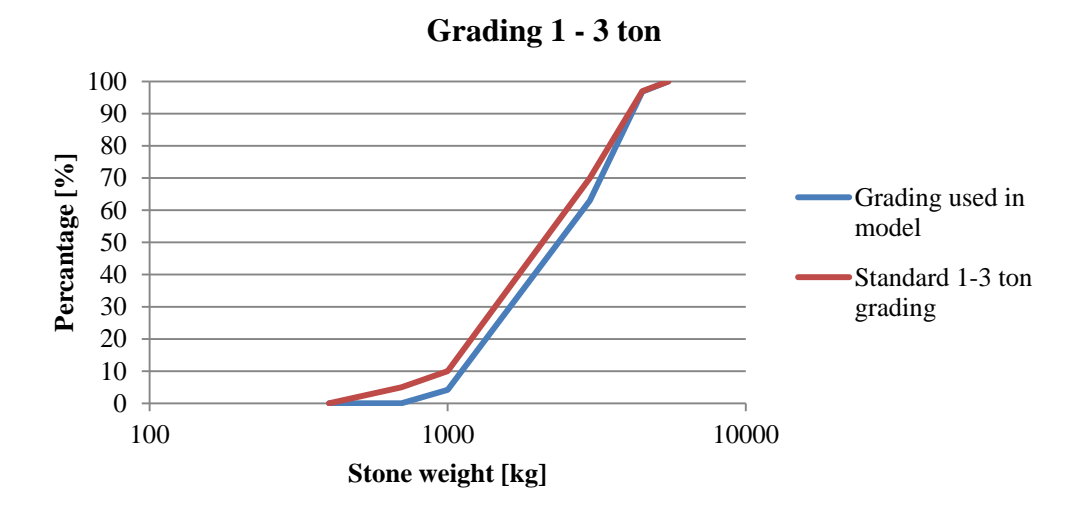


Figure D-1 Standard 1-3 ton grading and the grading applied in the toe of the scale model.

This curve was constructed after weighing the stones individually. In the table below the mass distribution in model and prototype is presented:

Mass in prototype [kg]	Mass in model [gram]	Cumulative percentage in standard grading [%]	Cumulative percentage in applied grading [%]
400	5.0	0	0
700	8.8	5	0
1000	12.6	10	4.2
3000	37.8	70	62.9
4500	56.6	97	96.8
5500	69.2	100	100

Appendix E: Rock material on the crest

In the figure below the grading of the rocks which are located on the crest of the breakwater is presented. For indicative purposes the standard grading of 1-3 ton and 3-6 ton is presented in the figure as well. The mass of the stones is scaled to the prototype values. In the model the mean mass is 54 gram and the nominal diameter is 27.3mm.

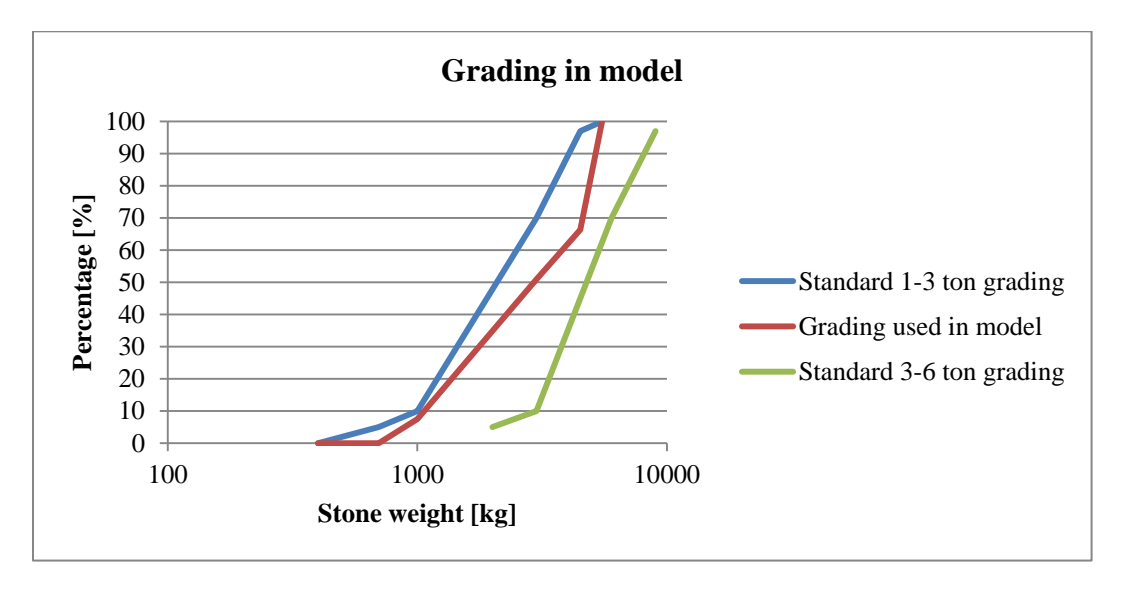


Figure E-1 Grading of material used on the crest of the breakwater

Appendix F: Placement grid of the armour units

Xbloc armour units are placed on a prescribed grid. As a general rule the horizontal distance between the centre of gravity of two neighbouring armour units should be $D_x = 1.32 \, \mathrm{D}$. The upslope distance should be $D_y = 0.63 \, \mathrm{D}$. Because the width of the flume is fixed, it is in general not possible to place the armour units on the prescribed horizontal distance. In this case the horizontal distance has been decreased a bit and the upslope distance has been increased a bit. This can be done only if the number $\sqrt{D_y^2 + D_x^2}$ remains the same. For the physical model tests done in this thesis D_x has been increased to a value of 0.66D and D_y has been decreased to a value of 1.306D. In the figure below the prescribed placement grid for the model tests is presented:

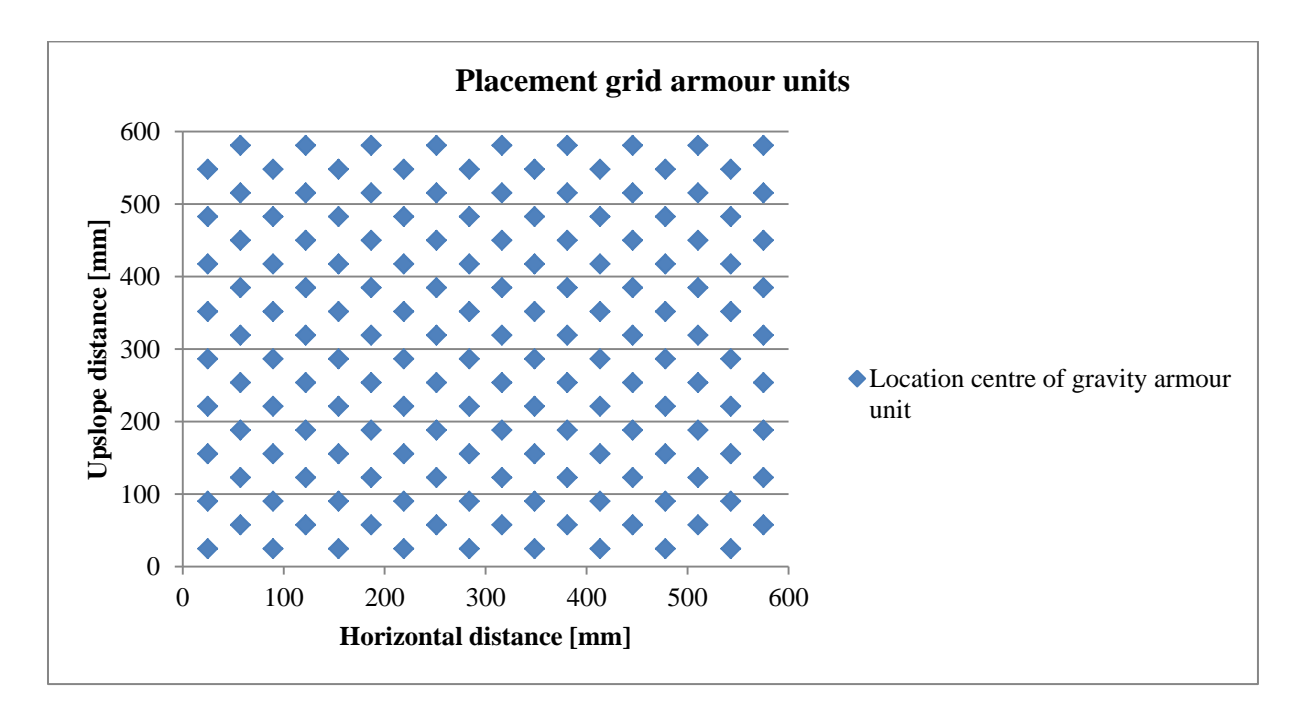


Figure F-1 Prescribed placement grid of the armour units

Appendix G: Wave calibration

The waves which are generated by the wave maker are checked and calibrated before the scale model is constructed. The series of wave gauges near the breakwater are located at a distance of 1m from the structure. Due to the presence of the wooden frame for the laser scanner. Therefore the waves are calibrated with the gauges at the location of the breakwater. In order to determine the magnitudes of the wave parameters at the location of the structure. After this the gauges are moved to the location which they have during the model tests. The location of the gauges during the tests is presented in the figure below:

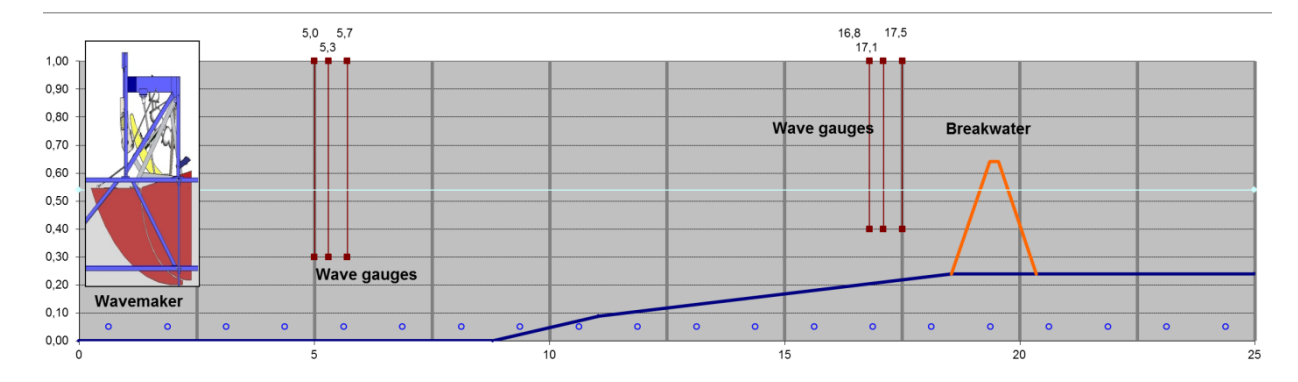


Figure G-1 Location of the wave gauges during the model tests

In order to check the waves on the structure. The middle gauge is moved to the location of the toe of the breakwater. In the table below the imposed wave conditions are presented:

Table G-1 Imposed wave conditions

	H_s [mm]	$T_p[s]$
60%	70.98	1.276
80%	94.64	1.389
100%	118.3	1.554
120%	141.9	1.702

Although there is no maximum wave height specified, it's important to know the magnitude of the larger waves. Research performed by ZWANENBURG, 2012 shows that the magnitude of the larger waves in the spectrum can have a considerable influence on the stability of the armour layer. In the tables below the wave conditions at the location of the structure and at the location at which the wave gauges will be located during the model tests.

Table G-2 Wave conditions during calibration at the location of the breakwater

	H_{m0} [mm]	H_s [mm]	H_{max} [mm]	T_p [s]
60%	70.16	68.4	131.3	1.231
80%	92.79	92.72	143.8	1.422
100%	118	116.8	160.4	1.561
120%	139.3	135.6	172	1.73

Table G-3 Wave conditions during calibration at the location of wave gauges during test

	H_{m0} [mm]	H_s [mm]	H_{max} [mm]	$T_p[s]$
60%	72.64	69.74	134.2	1.231
80%	92.83	91.19	150.7	1.422
100%	115.1	114.6	166.9	1.561
120%	136	131.9	183.9	1.73

From the values in the tables it can be concluded that the difference in wave conditions between the two locations of the wave gauges is only a few per cent. Especially the 100% and 120% condition show lower wave heights than imposed. It turns out that during the model tests this is not the case and therefore this is not considered to be a problem.

Appendix H: Wave data

In this appendix the detailed wave data for every individual test is given.

Table H-1 Wave data test A-1

	H _s [mm]	H _{m0} [mm]	Imposed H _s [mm]	Difference H_{m0} and imposed H_s [%]	Difference H_s and imposed H_s [%]	<i>T_p</i> [s]	Imposed T_p [s]	Difference T_p and imposed T_p [%]
60%	70.42	72.02	70.98	1.46	-0.78	1.306	1.28	2.03
80%	94.69	96.85	94.64	2.33	0.05	1.455	1.39	4.67
100%	116.7	119.8	118.3	1.26	-1.35	1.561	1.55	0.70
120%	138.1	142.7	141.96	0.52	-2.71	1.73	1.7	1.76

Table H-2 Wave data test A-2

	H _s	<i>H</i> _{m0} [mm]	Imposed H _s [mm]	Difference H_{m0} and imposed H_s [%]	Difference H_s and imposed H_s [%]	T_p [s]	Imposed $T_p[s]$	Difference T_p and imposed T_p [%]
60%	69.85	71.43	70.98	0.63	-1.59	1.306	1.28	2.03
80%	93.45	95.54	94.64	0.95	-1.25	1.455	1.39	4.67
100%	115.4	118	118.3	-0.25	-2.45	1.561	1.55	0.70
120%	137.7	142.1	141.96	0.09	-3.00	1.73	1.7	1.76

Table H-3 Wave data test A-3

	H _s [mm]	H _{m0} [mm]	Imposed H _s [mm]	Difference H_{m0} and imposed H_s [%]	Difference H_s and imposed H_s [%]	<i>T_p</i> [s]	Imposed T_p [s]	Difference T_p and imposed T_p [%]
60%	69.69	71.14	70.98	0.22	-1.81	1.306	1.28	2.03
80%	93.5	96.15	94.64	1.59	-1.20	1.455	1.39	4.67
100%	116.3	118.8	118.3	0.42	-1.69	1.561	1.55	0.70
120%	139.4	144	141.96	1.43	-1.80	1.73	1.7	1.76

Table H-4 Wave data test B-1

	H _s [mm]	<i>H</i> _{m0} [mm]	Imposed H _s [mm]	Difference H_{m0} and imposed H_s [%]	Difference H_s and imposed H_s [%]	<i>T_p</i> [s]	Imposed T_p [s]	Difference T_p and imposed T_p [%]
60%	69.25	70.91	70.98	-0.09	-2.43	1.306	1.28	2.03
80%	93.08	95.17	94.64	0.56	-1.64	1.455	1.39	4.67
100%	116	118.3	118.3	0	-1.94	1.561	1.55	0.70
120%	136.9	141.4	141.96	-0.39	-3.56	1.73	1.7	1.76

Table H-5 Wave data test B-2

	H _s [mm]	<i>H</i> _{m0} [mm]	Imposed H _s [mm]	Difference H_{m0} and imposed H_s [%]	Difference H_s and imposed H_s [%]	<i>T_p</i> [s]	Imposed $T_p[s]$	Difference T_p and imposed T_p [%]
60%	69.51	70.86	70.98	-0.16	-2.07	1.306	1.28	2.03
80%	93.34	95.44	94.64	0.84	-1.37	1.455	1.39	4.67
100%	115.7	118	118.3	-0.25	-2.19	1.561	1.55	0.70
120%	138.1	142.8	141.96	0.59	-2.71	1.73	1.7	1.76

Table H-6 Wave data test B-3

	H _s	<i>H_{m0}</i> [mm]	Imposed H _s [mm]	Difference H_{m0} and imposed H_s [%]	Difference H_s and imposed H_s [%]	<i>T_p</i> [s]	Imposed $T_p[s]$	Difference T_p and imposed T_p [%]
60%	69.59	71.63	70.98	0.91	-1.95	1.306	1.28	2.03
80%	93.13	95.27	94.64	0.66	-1.59	1.455	1.39	4.67
100%	115	117.7	118.3	-0.50	-2.78	1.561	1.55	0.70
120%	137.5	141.8	141.96	-0.11	-3.14	1.73	1.7	1.76

Table H-7 Wave data test C-1

	H _s [mm]	H _{m0} [mm]	Imposed H _s [mm]	Difference H_{m0} and imposed H_s [%]	Difference H_s and imposed H_s [%]	<i>T_p</i> [s]	Imposed T_p [s]	Difference T_p and imposed T_p [%]
60%	68.98	70.91	70.98	-0.09	-2.81	1.306	1.28	2.03
80%	92.7	94.82	94.64	0.19	-2.04	1.455	1.39	4.67
100%	114.9	117.7	118.3	-0.50	-2.87	1.561	1.55	0.70
120%	137.8	142.2	141.96	0.16	-2.93	1.73	1.7	1.76

Table H-8 Wave data test C-2

	H _s	H _{m0} [mm]	Imposed H _s [mm]	Difference H_{m0} and imposed H_s [%]	Difference H_s and imposed H_s [%]	<i>T_p</i> [s]	Imposed $T_p[s]$	Difference T_p and imposed T_p [%]
60%	69.57	71.29	70.98	0.43	-1.98	1.306	1.28	2.03
80%	93.49	95.36	94.64	0.76	-1.21	1.455	1.39	4.67
100%	116.1	118	118.3	-0.25	-1.85	1.561	1.55	0.70
120%	137.8	142.2	141.96	0.16	-2.93	1.73	1.7	1.76

Table H-9 Wave data test C-3

	H _s [mm]	H _{m0} [mm]	Imposed H _s [mm]	Difference H_{m0} and imposed H_s [%]	Difference H_s and imposed H_s [%]	<i>T_p</i> [s]	Imposed $T_p[s]$	Difference T_p and imposed T_p [%]
60%	69.7	71.5	70.98	0.73	-1.80	1.306	1.28	2.03
80%	93.71	95.92	94.64	1.35	-0.98	1.455	1.39	4.67
100%	115.4	118	118.3	-0.25	-2.45	1.561	1.55	0.70
120%	136.7	141	141.96	-0.67	-3.70	1.73	1.7	1.76

Table H-10 Wave data test D-1

	H _s [mm]	<i>H</i> _{m0} [mm]	Imposed H _s [mm]	Difference H_{m0} and imposed H_s [%]	Difference H _s and imposed H _s [%]	<i>T_p</i> [s]	Imposed $T_p[s]$	Difference T_p and imposed T_p [%]
60%	69.84	71.54	70.98	0.78	-1.60	1.306	1.28	2.03
80%	93.71	96.06	94.64	1.50	-0.98	1.455	1.39	4.67
100%	115.3	118	118.3	-0.25	-2.53	1.561	1.55	0.70
120%	137.7	142.4	141.96	0.30	-3.00	1.73	1.7	1.76

Table H-11 Wave data test D-2

	<i>H_s</i> [mm]	H _{m0} [mm]	Imposed H _s [mm]	Difference H_{m0} and imposed H_s [%]	Difference H_s and imposed H_s [%]	<i>T_p</i> [s]	Imposed $T_p[s]$	Difference T_p and imposed T_p [%]
60%	69.9	71.55	70.98	0.80	-1.52	1.306	1.28	2.03
80%	93.45	96.13	94.64	1.57	-1.25	1.455	1.39	4.67
100%	115.6	118.1	118.3	-0.16	-2.28	1.561	1.55	0.70
120%	136.3	141.8	141.96	-0.11	-3.98	1.73	1.7	1.76

Table H-12 Wave data test D-3

	H _s	H _{m0} [mm]	Imposed H _s [mm]	Difference H_{m0} and imposed H_s [%]	Difference H_s and imposed H_s [%]	<i>T_p</i> [s]	Imposed $T_p[s]$	Difference T_p and imposed T_p [%]
60%	69.81	71.77	70.98	1.11	-1.64	1.306	1.28	2.03
80%	93.41	95.75	94.64	1.17	-1.29	1.455	1.39	4.67
100%	117.5	120.4	118.3	1.77	-0.67	1.561	1.55	0.70
120%	136	140.8	141.96	-0.81	-4.19	1.73	1.7	1.76

Table H-13 Wave data test E-1

	H _s	<i>H</i> _{m0} [mm]	Imposed H _s [mm]	Difference H_{m0} and imposed H_s [%]	Difference H_s and imposed H_s [%]	<i>T_p</i> [s]	Imposed $T_p[s]$	Difference T_p and imposed T_p [%]
60%	69.46	71.36	70.98	0.53	-2.14	1.306	1.28	2.03
80%	93.6	95.24	94.64	0.63	-1.09	1.455	1.39	4.67
100%	116	118	118.3	-0.25	-1.99	1.561	1.55	0.70
120%	138	142.2	141.96	0.16	-2.78	1.73	1.7	1.76

Table H-14 Wave data test E-2

	H _s	<i>H</i> _{m0} [mm]	Imposed H_s [mm]	Difference H_{m0} and imposed H_s [%]	Difference H_s and imposed H_s [%]	T_p [s]	Imposed $T_p[s]$	Difference T_p and imposed T_p [%]
60%	70.02	71.44	70.98	0.64	-1.35	1.306	1.28	2.03
80%	93.48	95.24	94.64	0.63	-1.22	1.455	1.39	4.67
100%	114.5	117.5	118.3	-0.67	-3.21	1.561	1.55	0.70
120%	138.1	141.9	141.96	-0.04	-2.71	1.73	1.7	1.76

Table H-15 Wave data test E-3

	<i>H_s</i> [mm]	<i>H</i> _{m0} [mm]	Imposed H _s [mm]	Difference H_{m0} and imposed H_s [%]	Difference H_s and imposed H_s [%]	<i>T_p</i> [s]	Imposed $T_p[s]$	Difference T_p and imposed T_p [%]
60%	69.81	71.52	70.98	0.760	-1.64	1.306	1.28	2.03
80%	93.94	96.28	94.64	1.73	-0.73	1.455	1.39	4.67
100%	115.7	118.3	118.3	0	-2.19	1.561	1.55	0.70
120%	138.2	142.6	141.96	0.41	-2.64	1.73	1.7	1.76

Table H-16 Wave data test F-1

	H _s [mm]	H _{m0} [mm]	Imposed H _s [mm]	Difference H_{m0} and imposed H_s [%]	Difference H_s and imposed H_s [%]	<i>T_p</i> [s]	Imposed $T_p[s]$	Difference T_p and imposed T_p [%]
60%	69.79	71.86	70.98	1.23	-1.67	1.306	1.28	2.03
80%	93.98	95.96	94.64	1.39	-0.69	1.455	1.39	4.67
100%	116.2	118.5	118.3	0.16	-1.77	1.561	1.55	0.70
120%	138.9	142.3	141.96	0.23	-2.15	1.73	1.7	1.76

Table H-17 Wave data test F-2

	H _s	H _{m0} [mm]	Imposed H_s [mm]	Difference H_{m0} and imposed H_s [%]	Difference H_s and imposed H_s [%]	<i>T_p</i> [s]	Imposed $T_p[s]$	Difference T_p and imposed T_p [%]
60%	70.37	72.49	70.98	2.12	-0.85	1.306	1.28	2.03
80%	95.54	97.66	94.64	3.19	0.95	1.455	1.39	4.67
100%	115.6	118	118.3	-0.25	-2.28	1.561	1.55	0.70
120%	136.1	140.5	141.96	-1.02	-4.12	1.73	1.7	1.76

Table H-18 Wave data test F-3

	H _s	<i>H_{m0}</i> [mm]	Imposed H_s [mm]	Difference H_{m0} and imposed H_s [%]	Difference H_s and imposed H_s [%]	<i>T_p</i> [s]	Imposed $T_p[s]$	Difference T_p and imposed T_p [%]
60%	69.66	71.49	70.98	0.71	-1.85	1.306	1.28	2.03
80%	94.47	95.81	94.64	1.23	-0.17	1.455	1.39	4.67
100%	116.1	118.4	118.3	0.08	-1.85	1.561	1.55	0.70
120%	138	142.5	141.96	0.38	-2.78	1.73	1.7	1.76

Table H-19 Wave data test G-1

	H _s [mm]	H _{m0} [mm]	Imposed H _s [mm]	Difference H_{m0} and imposed H_s [%]	Difference H_s and imposed H_s [%]	<i>T_p</i> [s]	Imposed $T_p[s]$	Difference T_p and imposed T_p [%]
60%	70.1	71.95	70.98	1.36	-1.23	1.306	1.28	2.03
80%	94.62	95.54	94.64	0.95	-0.02	1.455	1.39	4.67
100%	115.4	118.1	118.3	-0.16	-2.45	1.561	1.55	0.70
120%	137.3	142.1	141.96	0.09	-3.28	1.73	1.7	1.76

Table H-20 Wave data test G-2

	H _s	H _{m0} [mm]	Imposed H _s [mm]	Difference H_{m0} and imposed H_s [%]	Difference H_s and imposed H_s [%]	<i>T_p</i> [s]	Imposed $T_p[s]$	Difference T_p and imposed T_p [%]
60%	69.47	71.37	70.98	0.54	-2.12	1.306	1.28	2.03
80%	93.54	95.79	94.64	1.21	-1.16	1.455	1.39	4.67
100%	115.6	117.9	118.3	-0.33	-2.28	1.561	1.55	0.70
120%	137.8	141.9	141.96	-0.04	-2.93	1.73	1.7	1.76

Table H-21 Wave data test G-3

	H _s	H _{m0} [mm]	Imposed H_s [mm]	Difference H_{m0} and imposed H_s [%]	Difference H_s and imposed H_s [%]	T_p [s]	Imposed $T_p[s]$	Difference T_p and imposed T_p [%]
60%	69.59	71.61	70.98	0.88	-1.95	1.306	1.28	2.03
80%	93.93	95.65	94.64	1.06	-0.75	1.455	1.39	4.67
100%	114.9	117.2	118.3	-0.92	-2.87	1.561	1.55	0.70
120%	139	143.6	141.96	1.15	-2.08	1.73	1.7	1.76

Appendix I: Correction factors on the weight of the armour units

The design formula (equation 2.7) is applicable for typical cross sections of breakwaters and shore protections. There is however a number of phenomena which require to increase the Xbloc size. The phenomena and the proposed correction factor on the unit weight are described below:

Table I-1 Correction factors on armour unit weight [DMC, 2011]

Phenomenon	Effect on Armour Stability	Correction factor on unit weight
Units are placed on a breakwater head or on curved sections	Accurate placement in a staggered grid is complicated by the breakwater geometry and wave impact is affected by the geometry, therefore the stability is reduced.	1.25
Frequent occurrence of near- design wave height during the lifetime of the structure	Rocking of units, which can occur for a small percentage of the armour units during the design event of a breakwater, can occur frequently during the lifetime of the structure. Therefore rocking should be carefully assessed during the physical model tests.	1.25
The foreshore in front of the structure is steep	A steep foreshore can lead to adverse wave impact against the armour layer.	 1.1 for a steepness between 1:30 and 1:20 1.25 for a steepness between 1:20 and 1:15 1.5 for a steepness between 1:15 and 1:10 2 for a steepness greater than 1:10
The structure is low crested		2 for a relative freeboard < 0.5 1.5 for a relative freeboard < 1
The water depth is large	For typical nearshore breakwater cross sections, the ratio between the highest wave heights in the spectrum and the significant wave height is in the order of 1.2 - 1.4. For breakwaters in deep water, this ratio can be up to 1.8 - 2. As the largest waves in the spectrum cause the largest loads on the armour layer, the stability of the armour layer is reduced compared to breakwaters in lower water depths. Furthermore a breakwater cross section in deep water typically contains a high rock toe which can affect the wave impacts on the armour slope. Therefore rocking should be carefully assessed during the physical model tests.	2 for a water depth > 3.5 x H _s
The core permeability is low	A low core permeability can lead to large pressures in the armour layer and reduce the stability of the armour layer. The permeability of the core depends on the materials used and the distance at the water line between the armour layer and the impermeable layer.	1.5 for a low core permeability 2 for an impermeable core

Appendix J: Profiles measured with the laser device

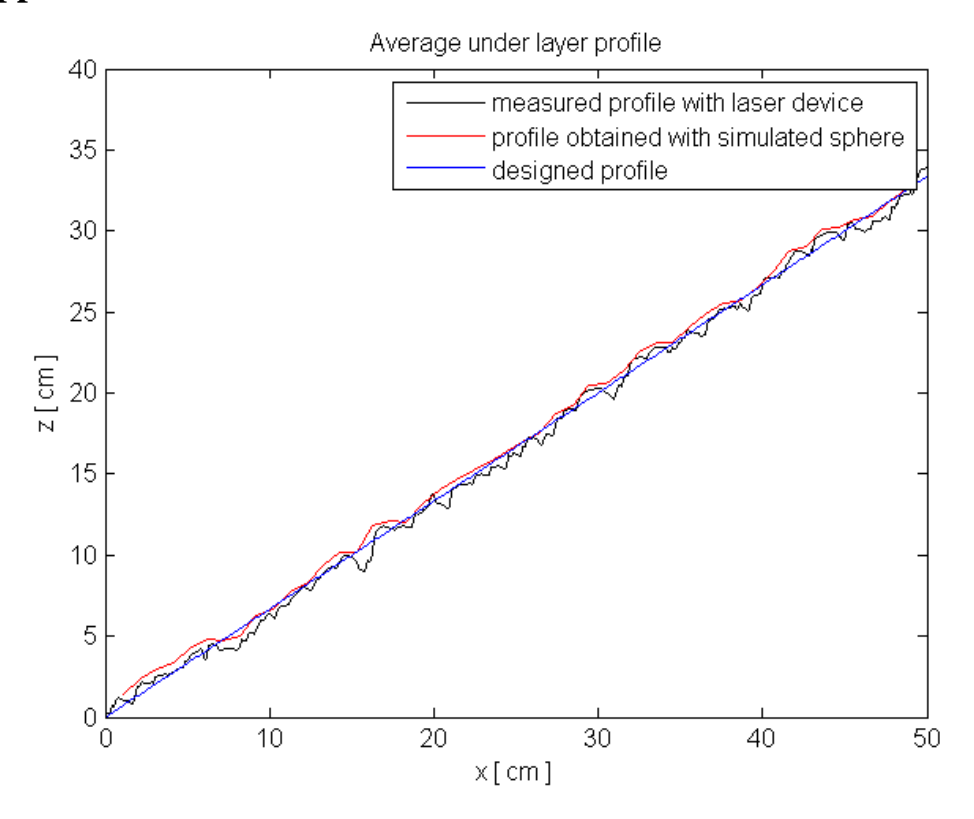


Figure J-1 Profile of test A-1 measured with laser device and simulated sphere

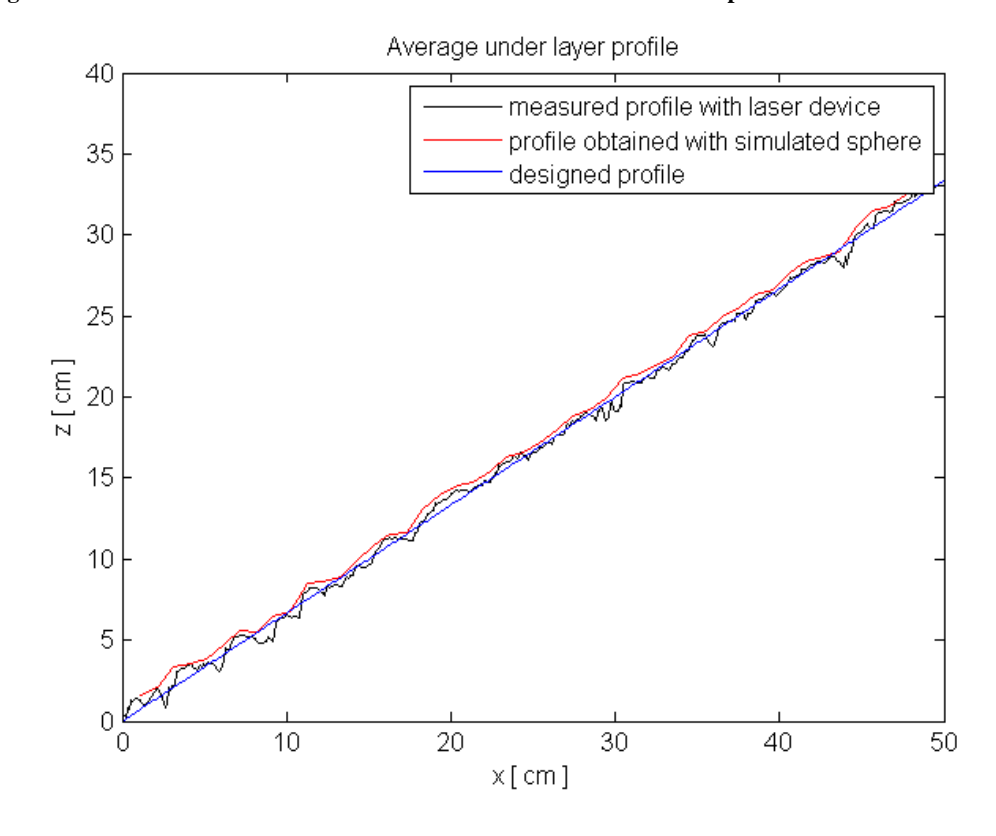


Figure J-2 Profile of test A-2 measured with laser device and simulated sphere

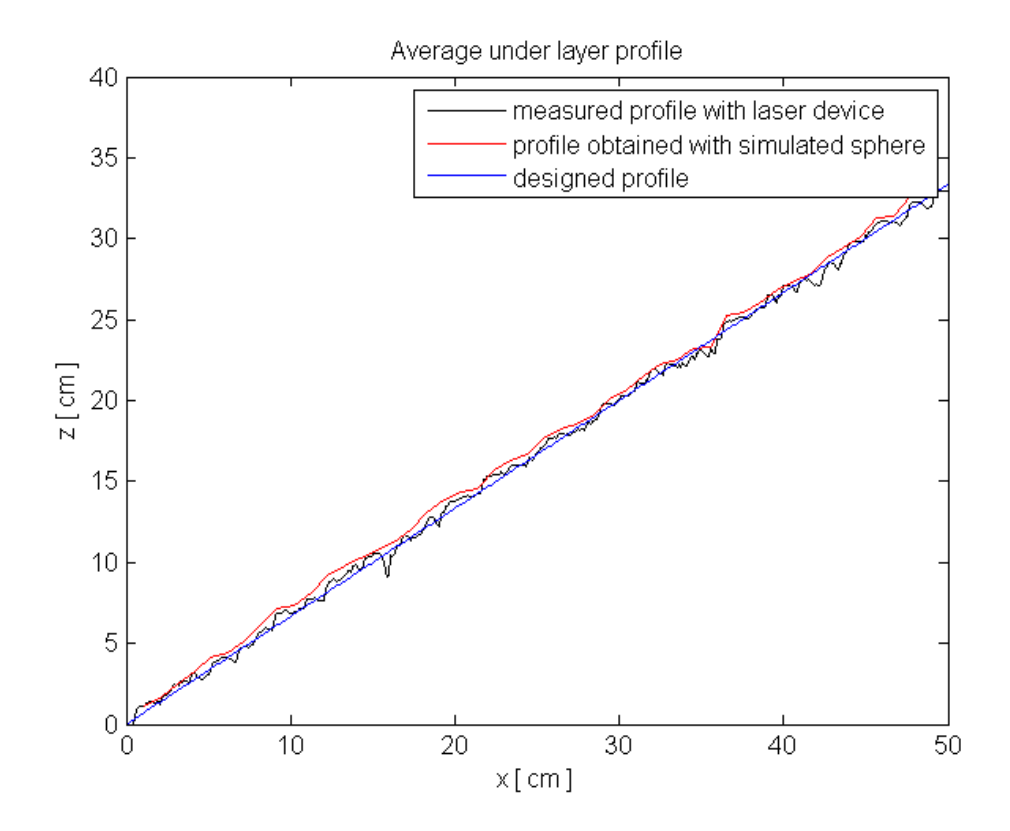


Figure J-3 Profile of test A-3 measured with laser device and simulated sphere

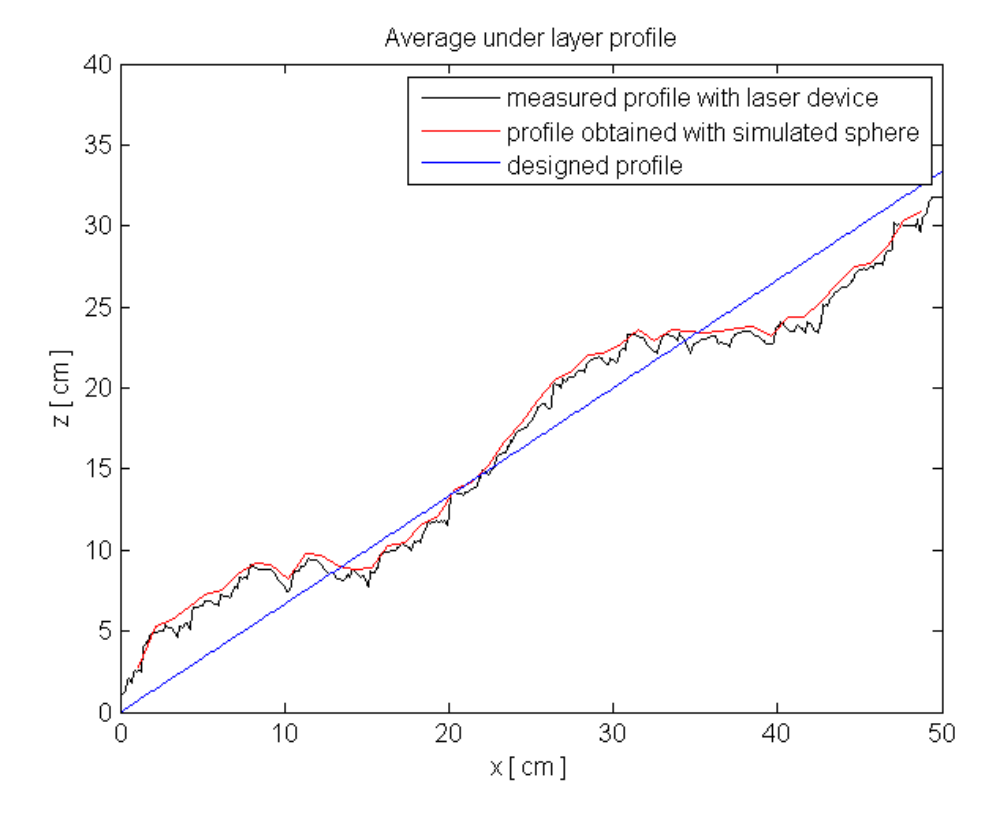


Figure J-4 Profile of test B-1 measured with laser device and simulated sphere

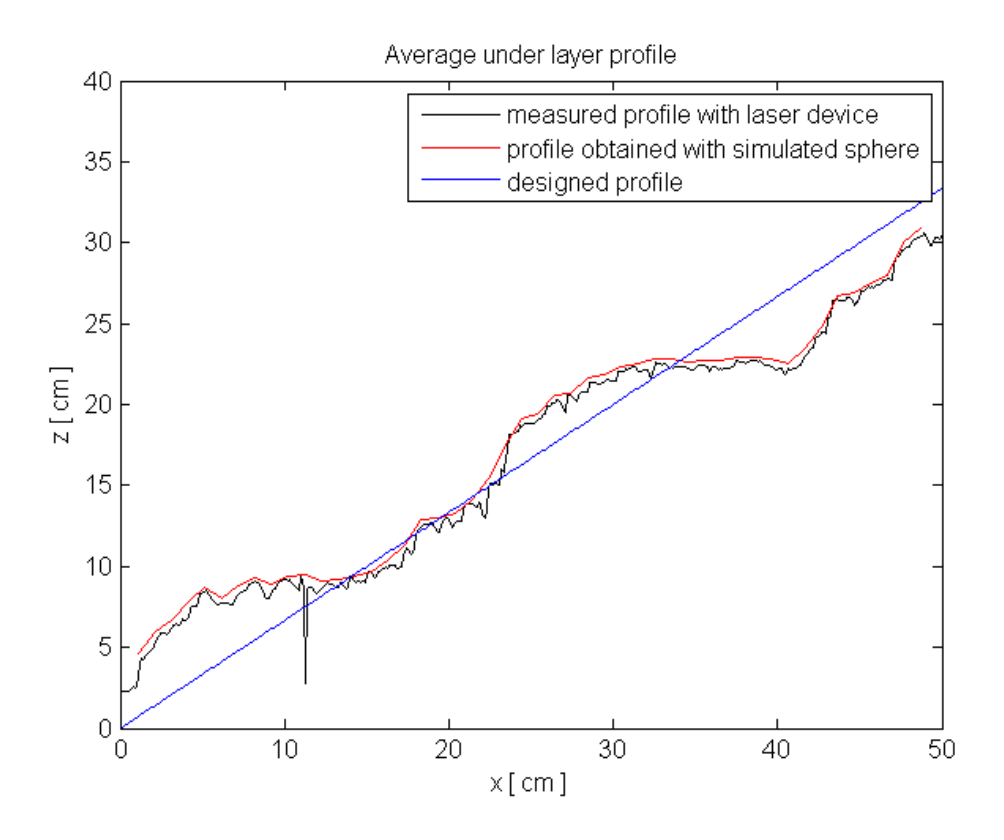


Figure J-5 Profile of test B-2 measured with laser device and simulated sphere

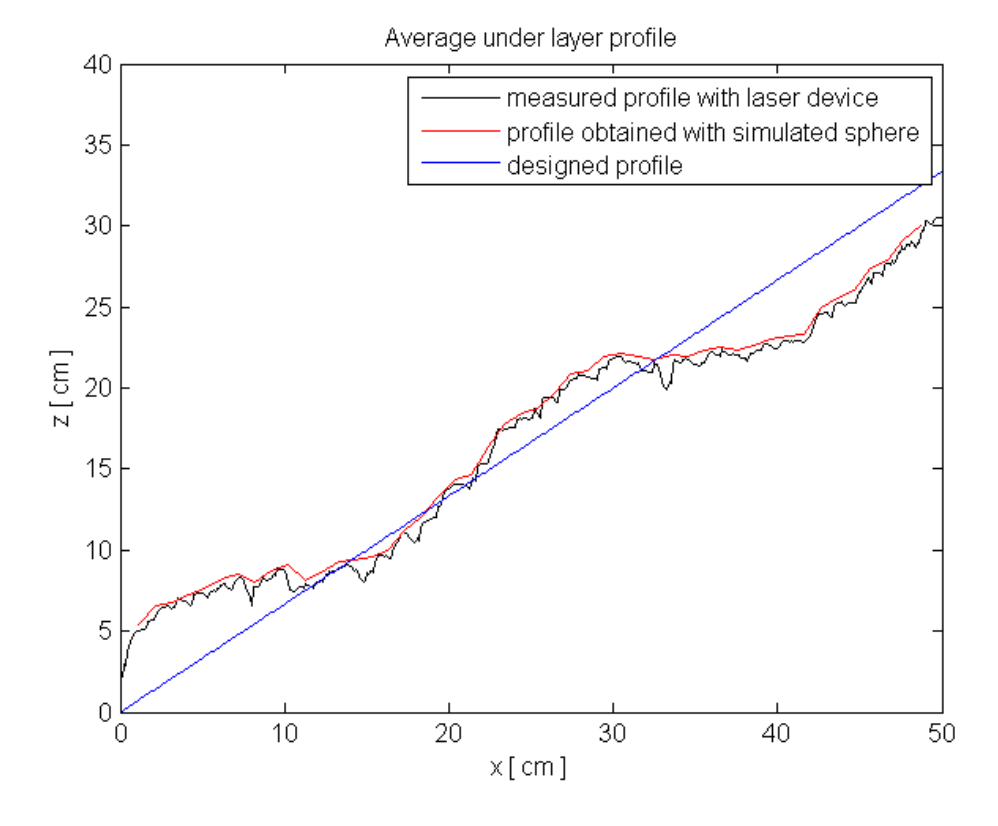


Figure J-6 Profile of test B-3 measured with laser device and simulated sphere

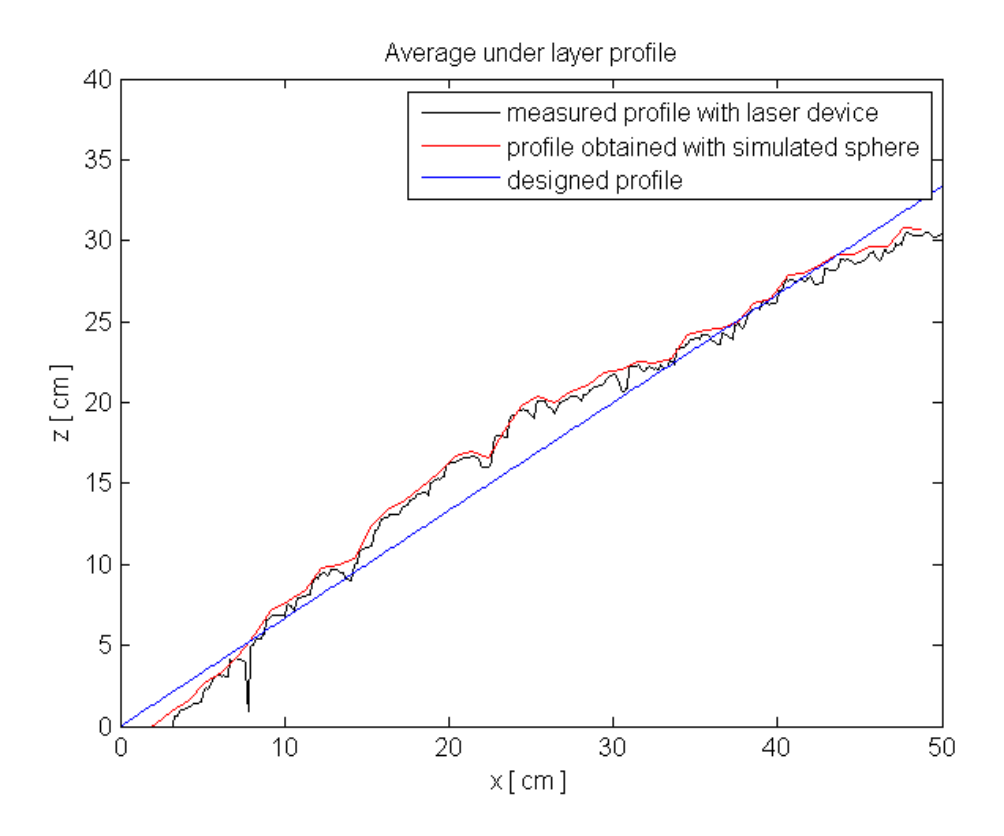


Figure J-7 Profile of test C-1 measured with laser device and simulated sphere

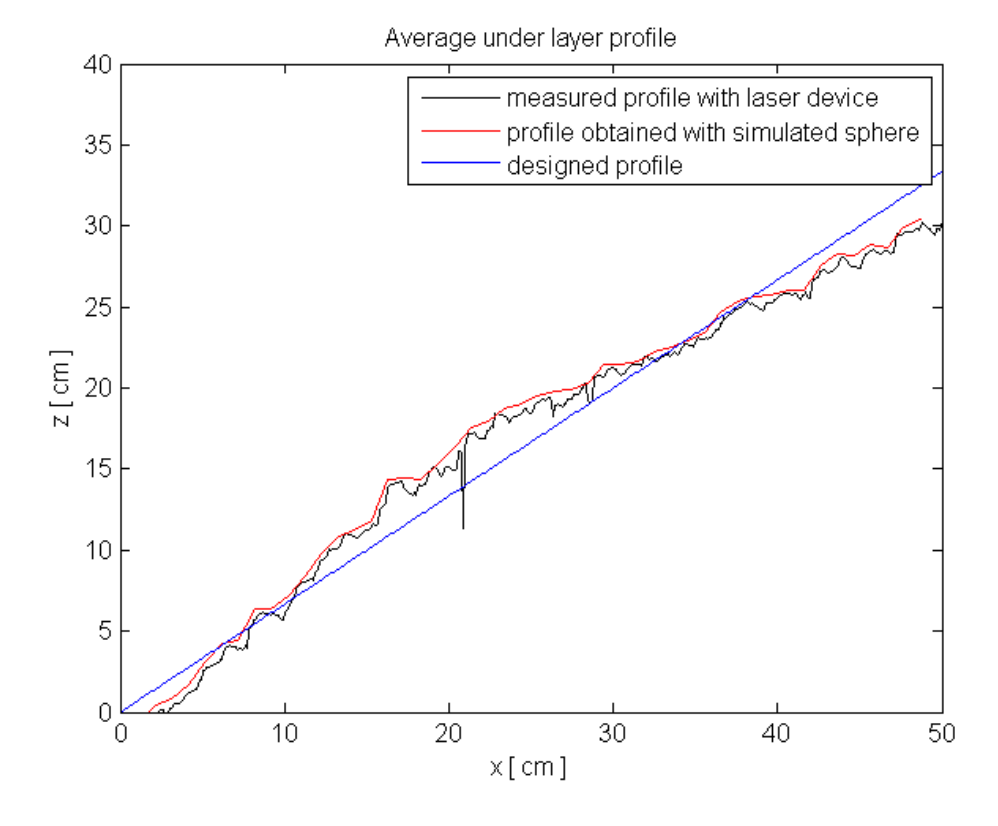


Figure J-8 Profile of test C-2 measured with laser device and simulated sphere

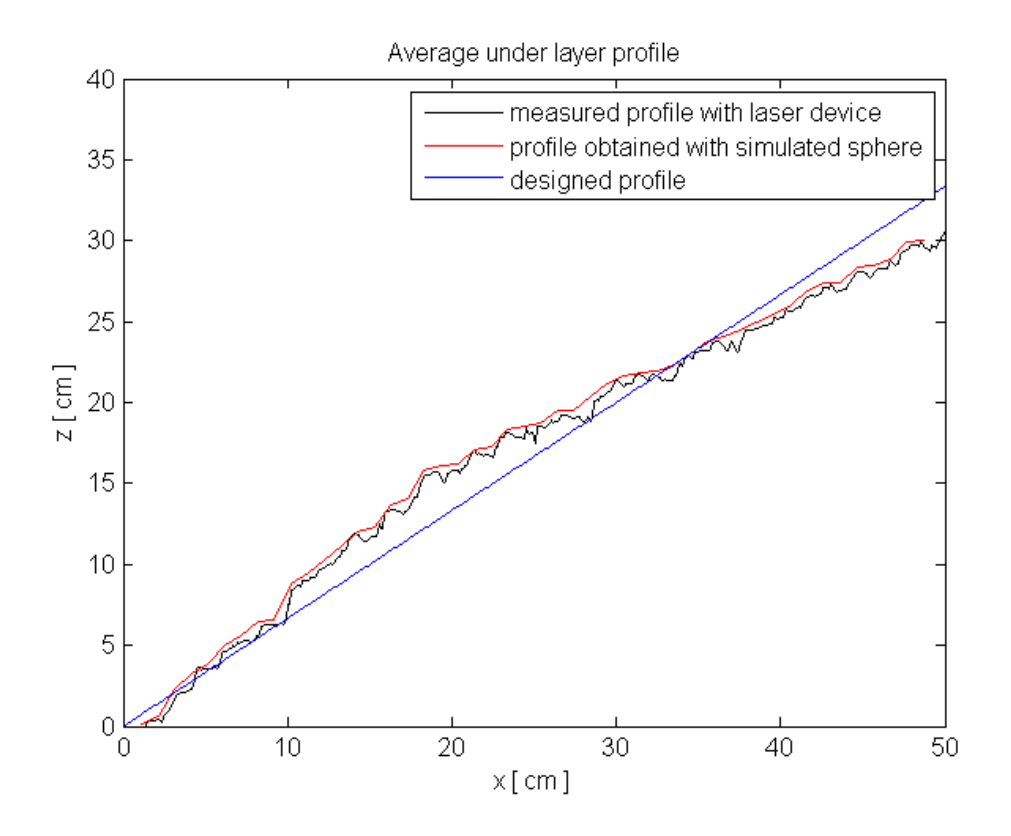


Figure J-9 Profile of test C-3 measured with laser device and simulated sphere

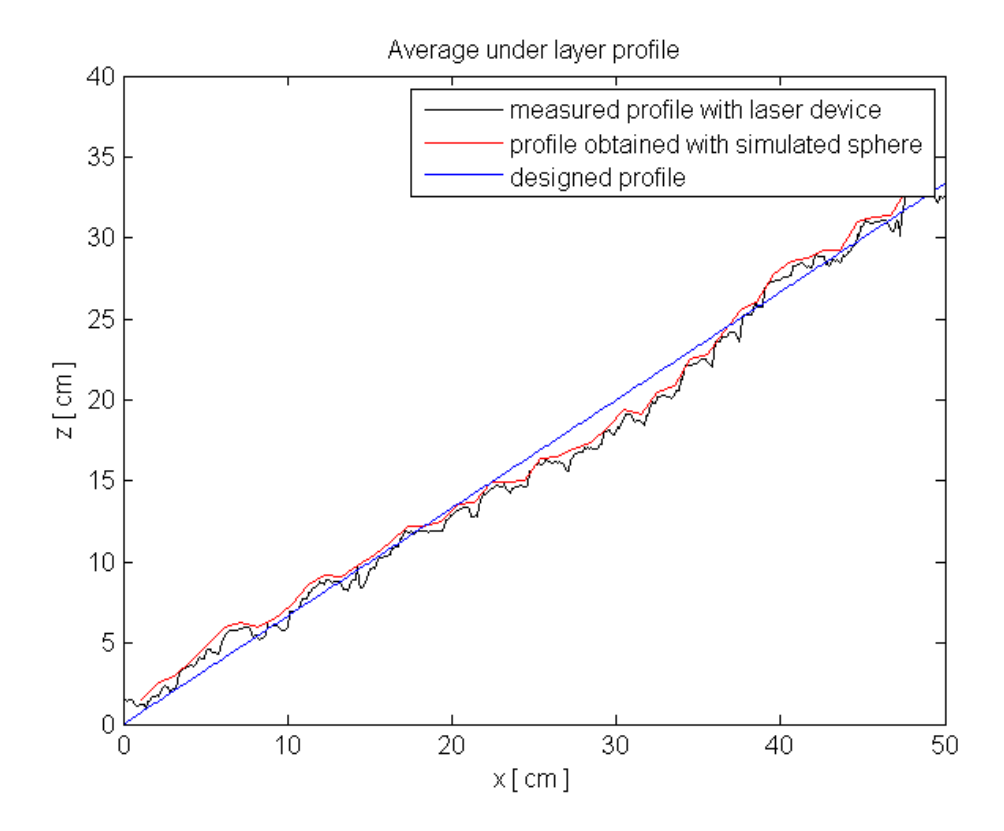


Figure J-10 Profile of test D-1 measured with laser device and simulated sphere

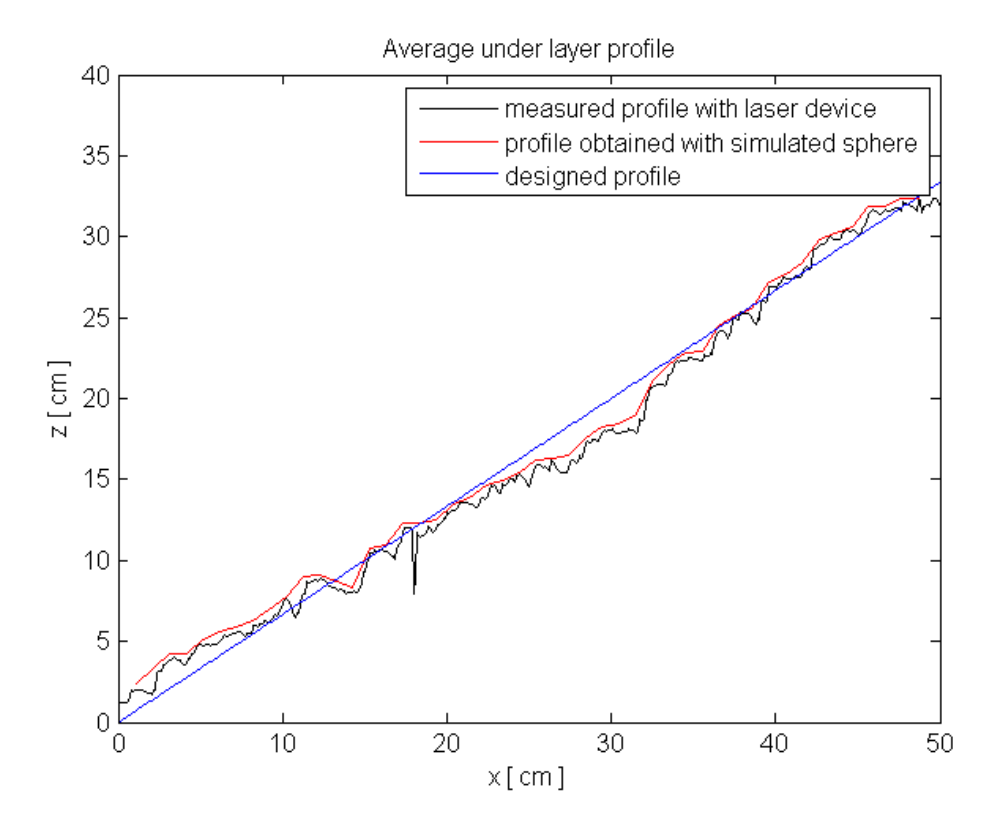


Figure J-11 Profile of test D-2 measured with laser device and simulated sphere

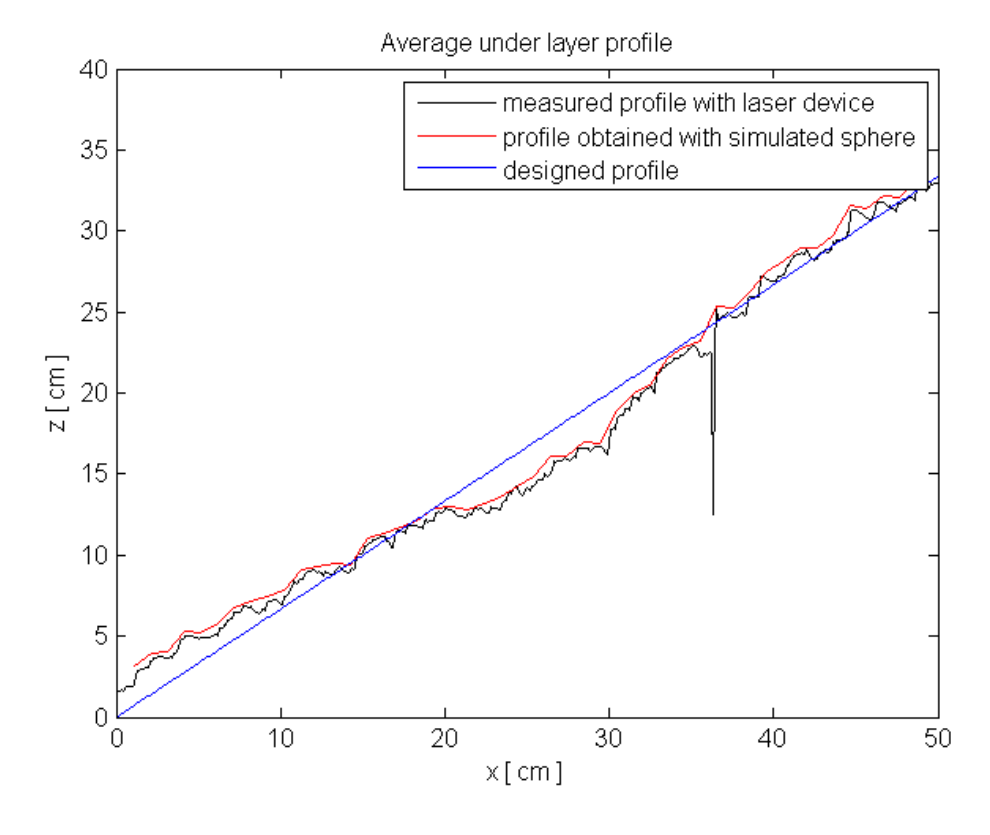


Figure J-12 Profile of test D-3 measured with laser device and simulated sphere

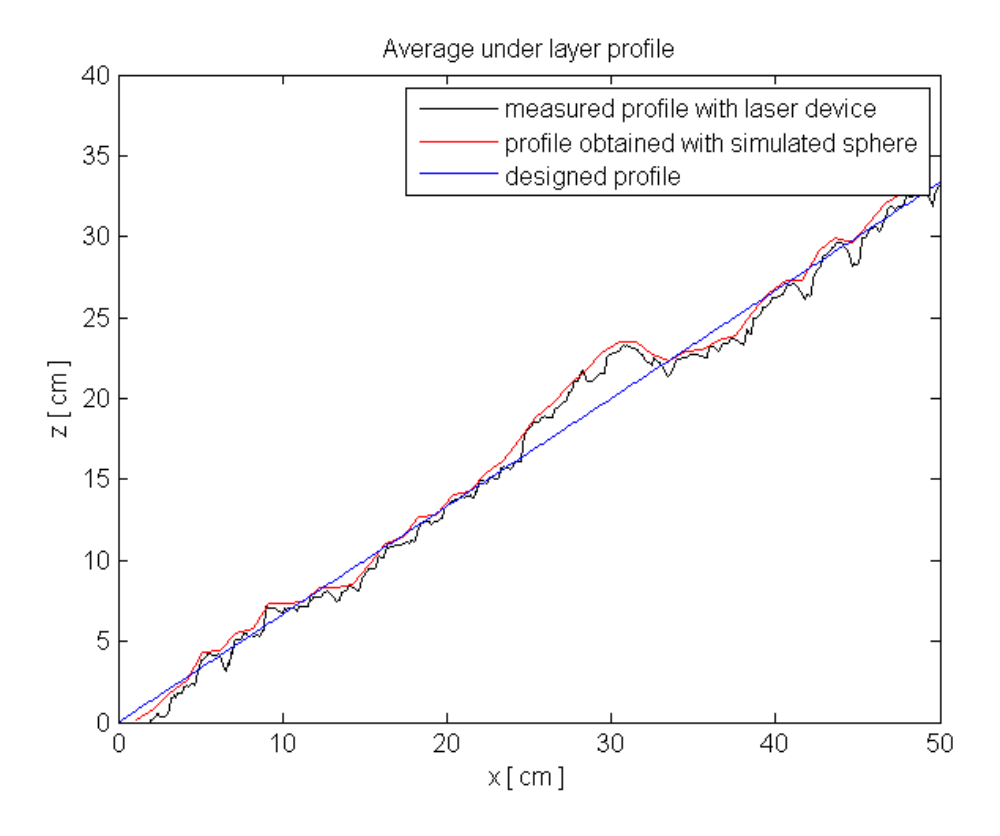


Figure J-13 Profile of test E-1 measured with laser device and simulated sphere

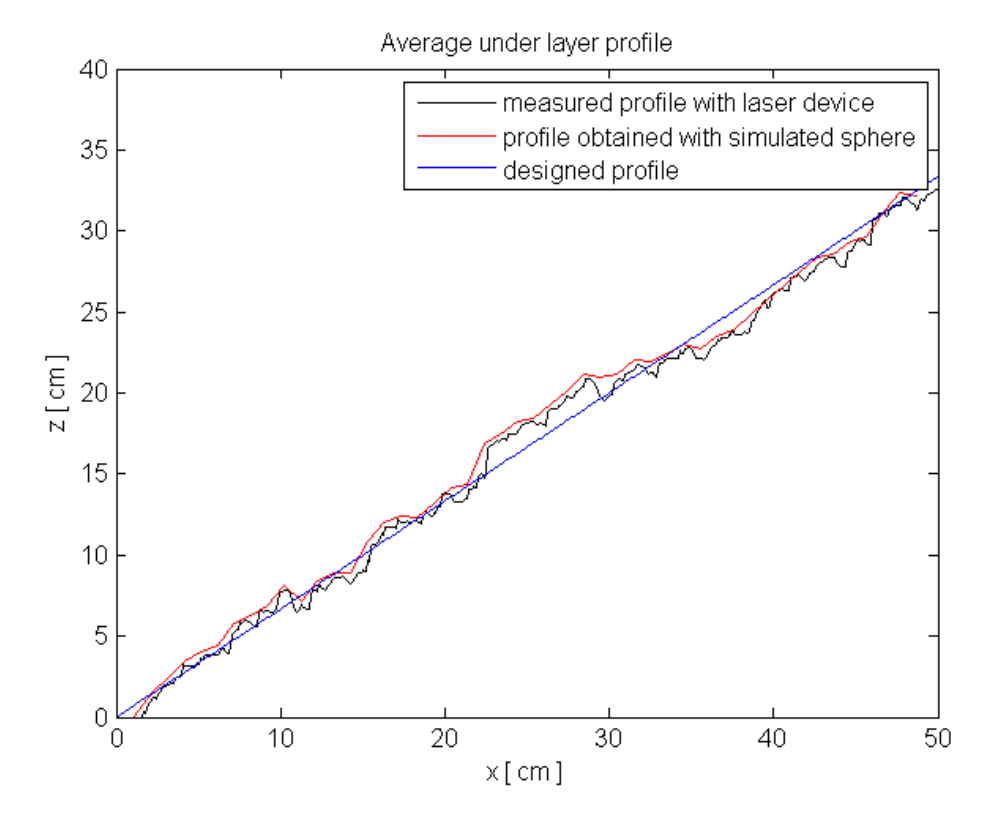


Figure J-14 Profile of test E-2 measured with laser device and simulated sphere

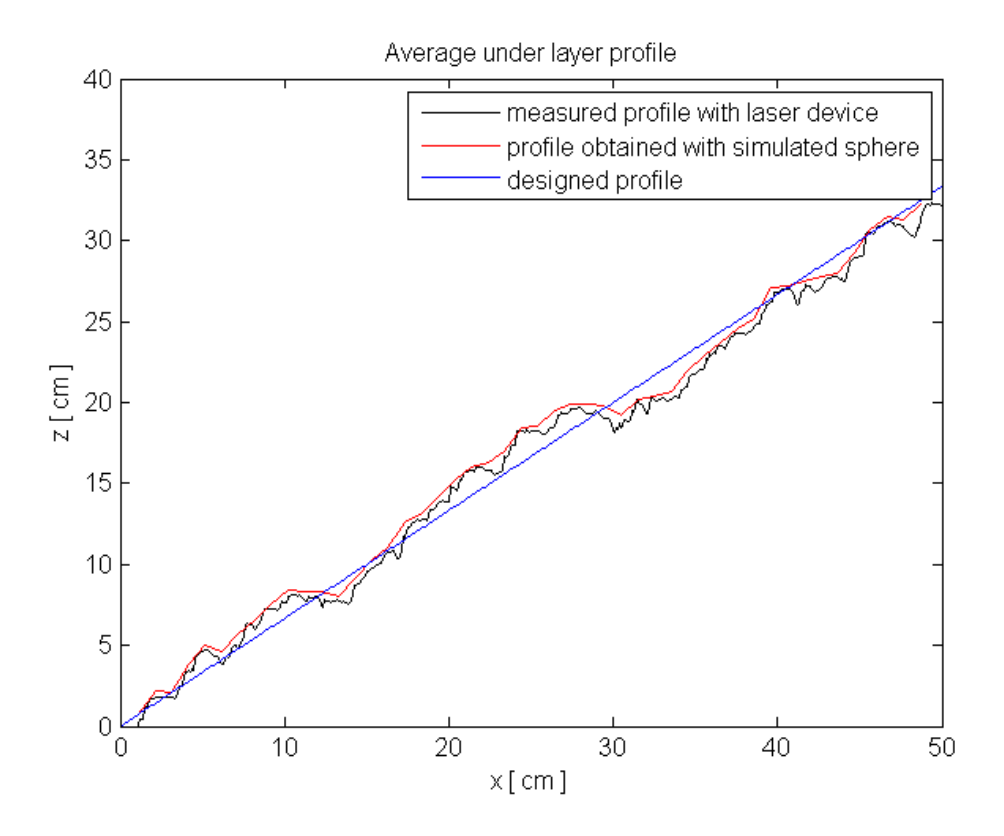


Figure J-15 Profile of test E-3 measured with laser device and simulated sphere

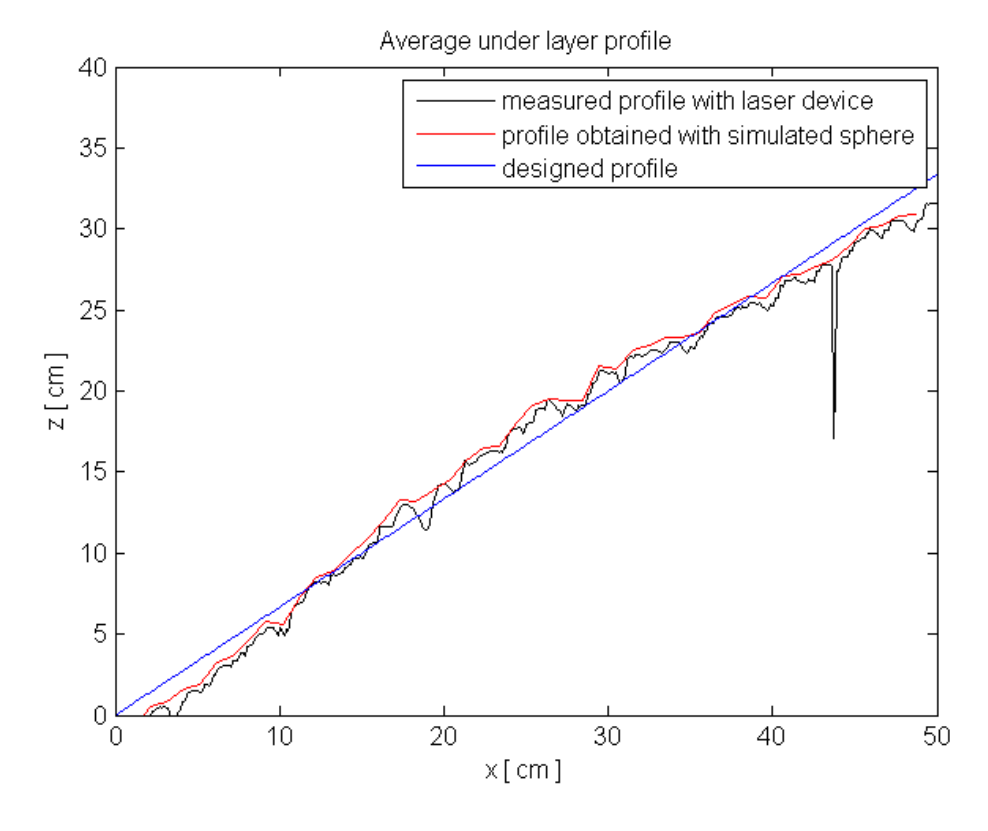


Figure J-16 Profile of test F-1 measured with laser device and simulated sphere

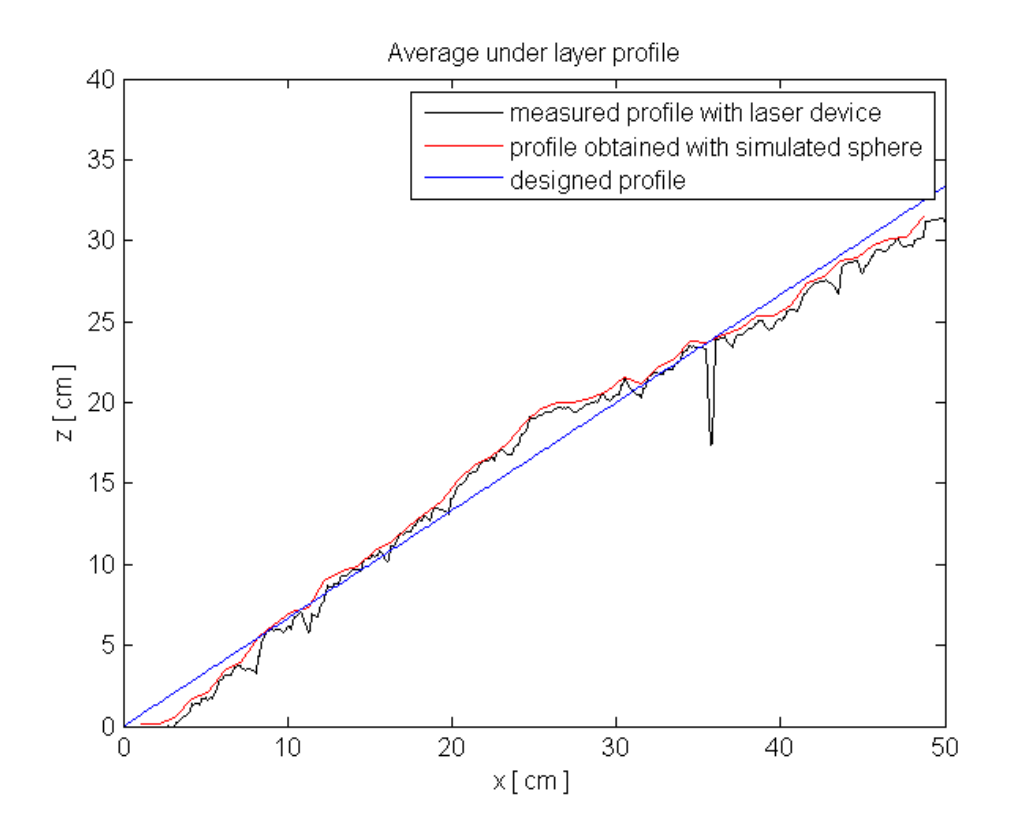


Figure J-17 Profile of test F-2 measured with laser device and simulated sphere

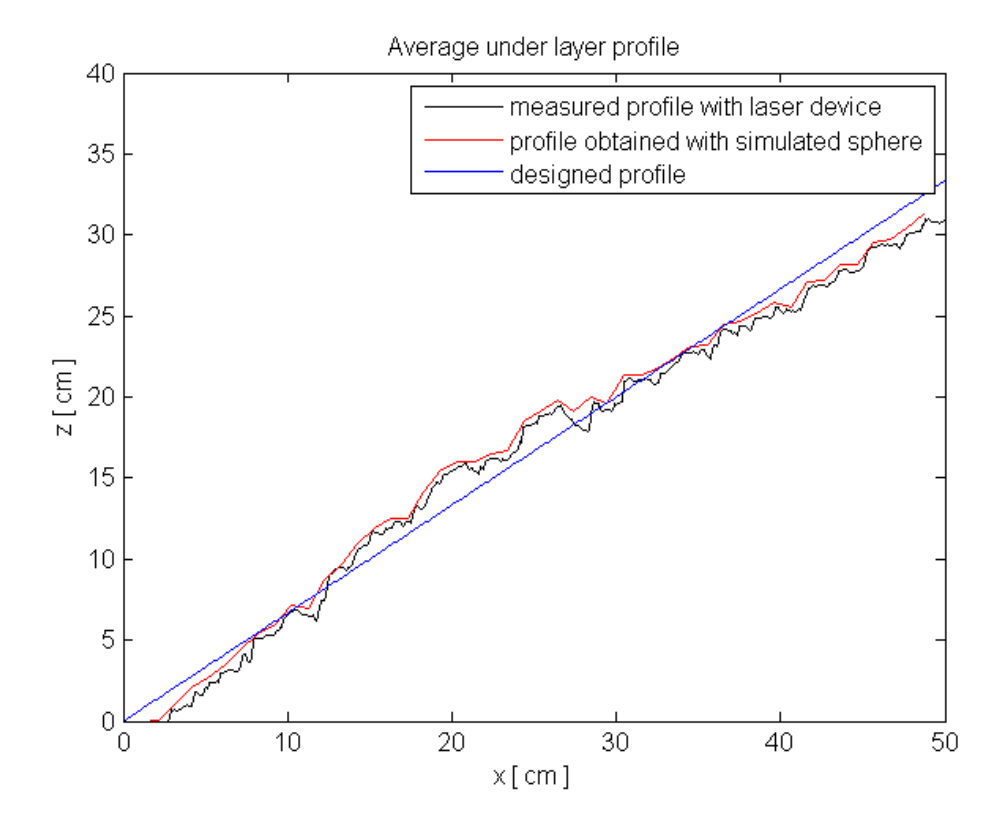


Figure J-18 Profile of test F-3 measured with laser device and simulated sphere

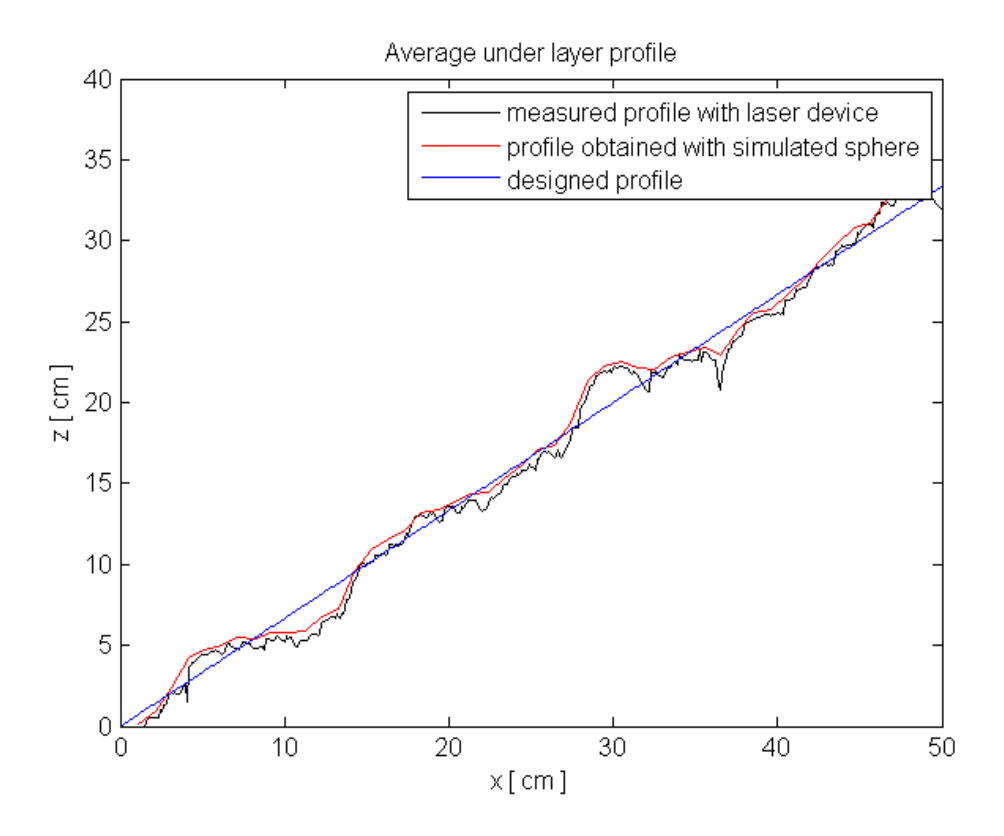


Figure J-19 Profile of test G-1 measured with laser device and simulated sphere

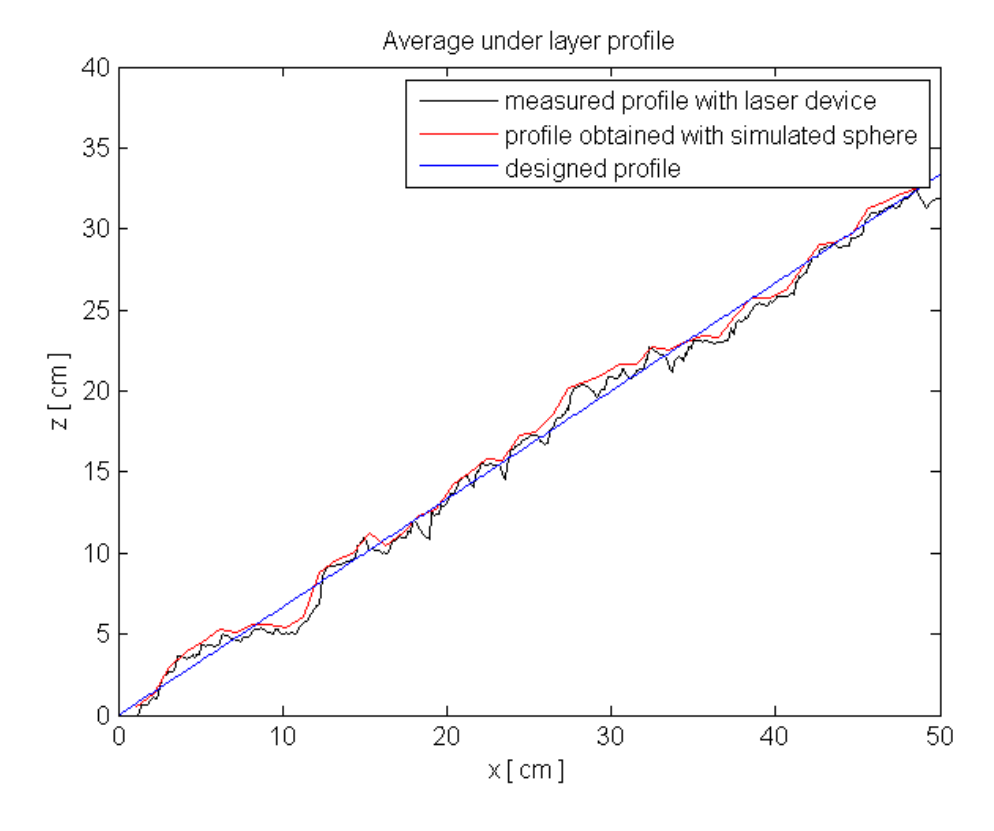


Figure J-20 Profile of test G-2 measured with laser device and simulated sphere

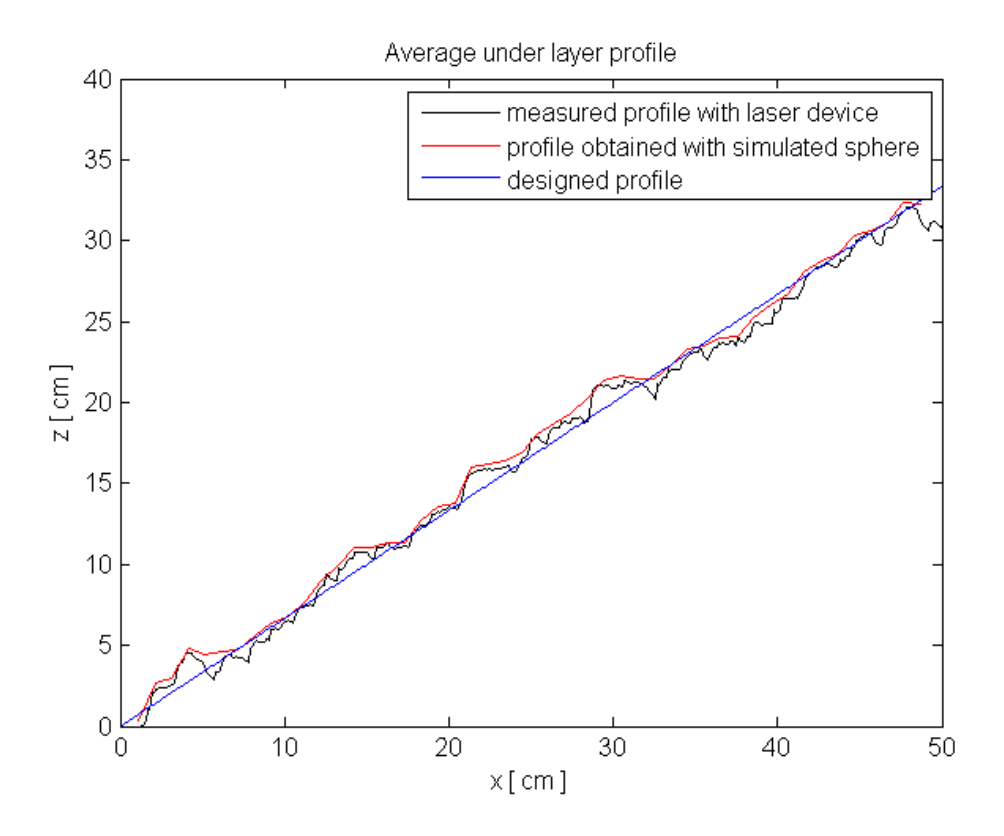


Figure J-21 Profile of test G-3 measured with laser device and simulated sphere

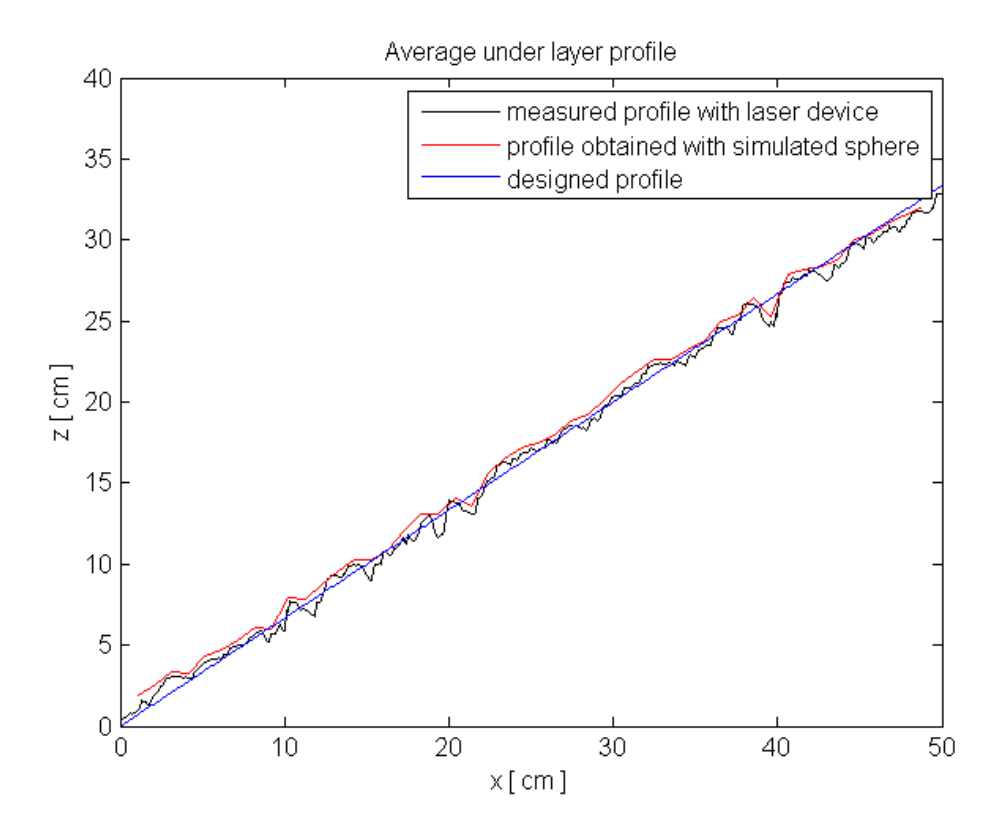


Figure J-22 Profile of test Extra-1 measured with laser device and simulated sphere

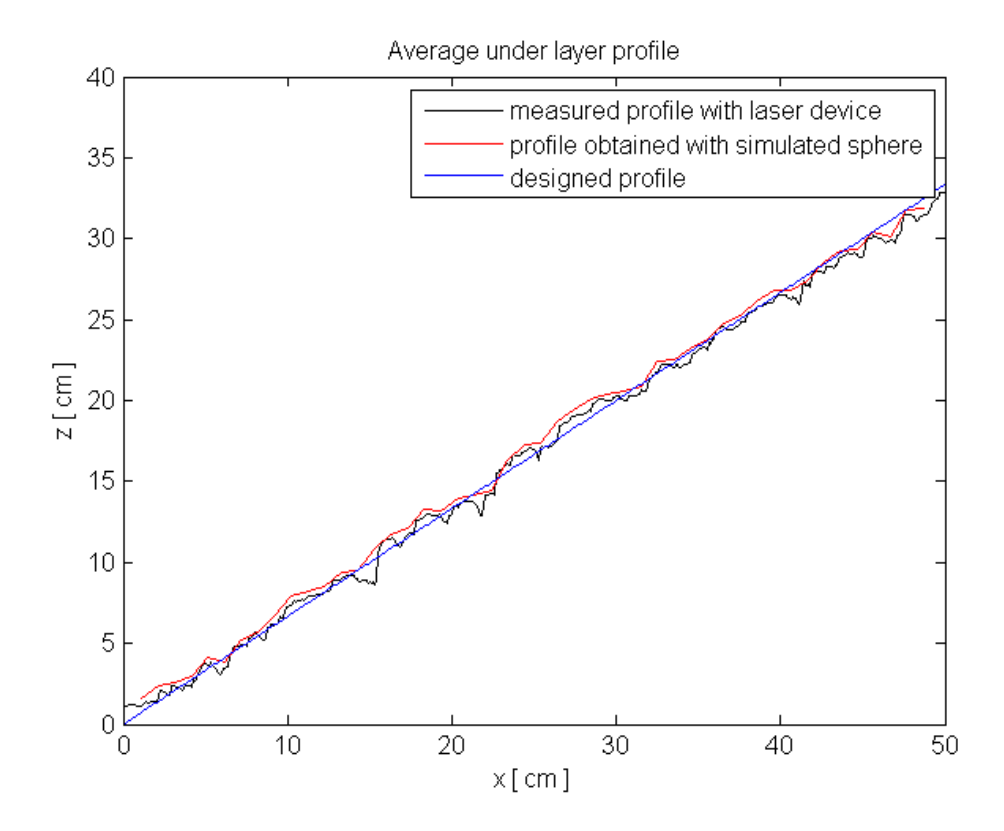


Figure J-23 Profile of test Extra-2 measured with laser device and simulated sphere

Appendix K: Results of the spherical foot staff measurements

Spherical foot staff measurements have been carried out two times on a test case which is also measured with the laser device. In the figures in this appendix the results are given.

Results of the measurements of a reference test case

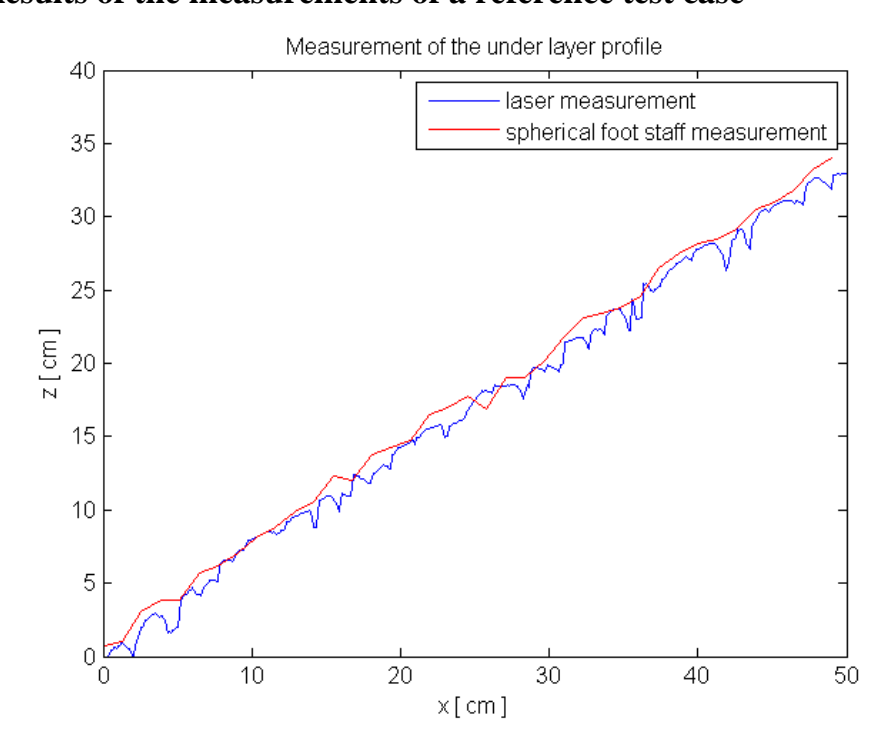


Figure K-1 Measurement from the left side

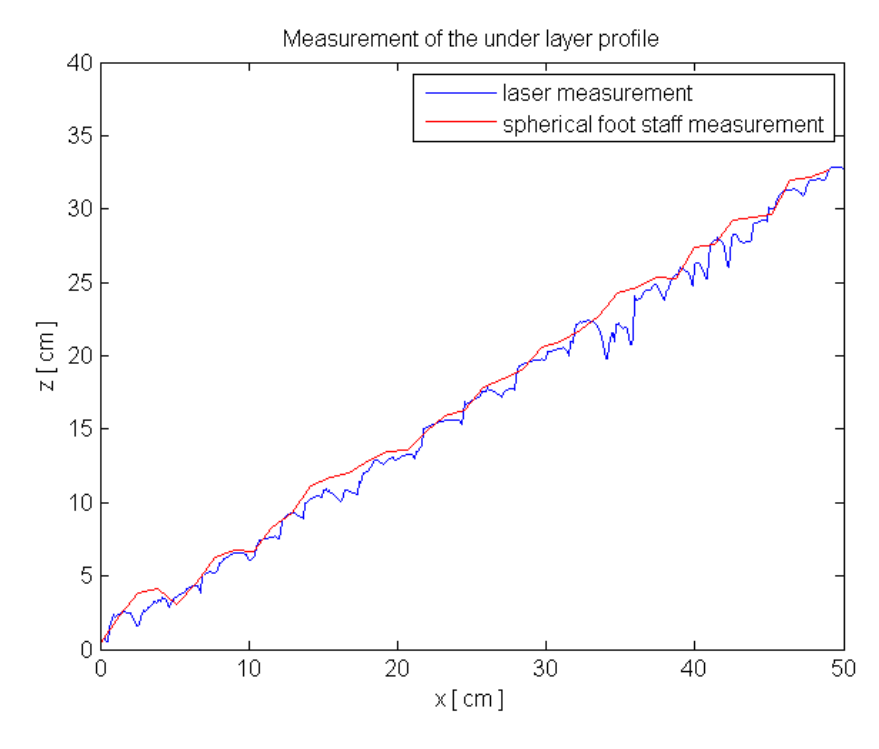


Figure K-2 Measurement from the middle location

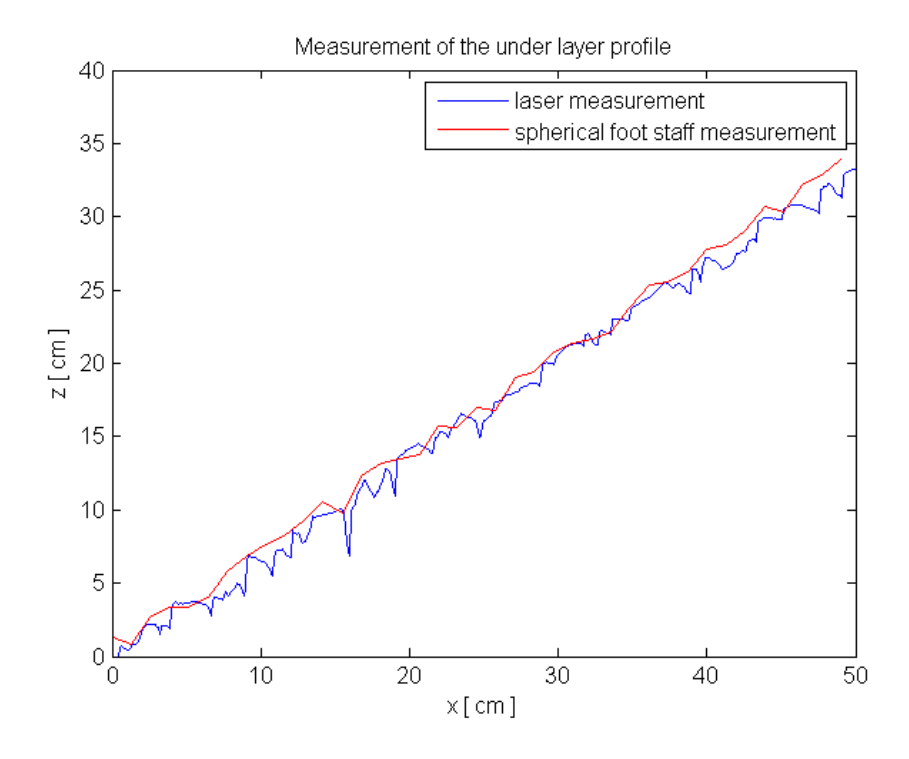


Figure K-3 Measurement from the right side

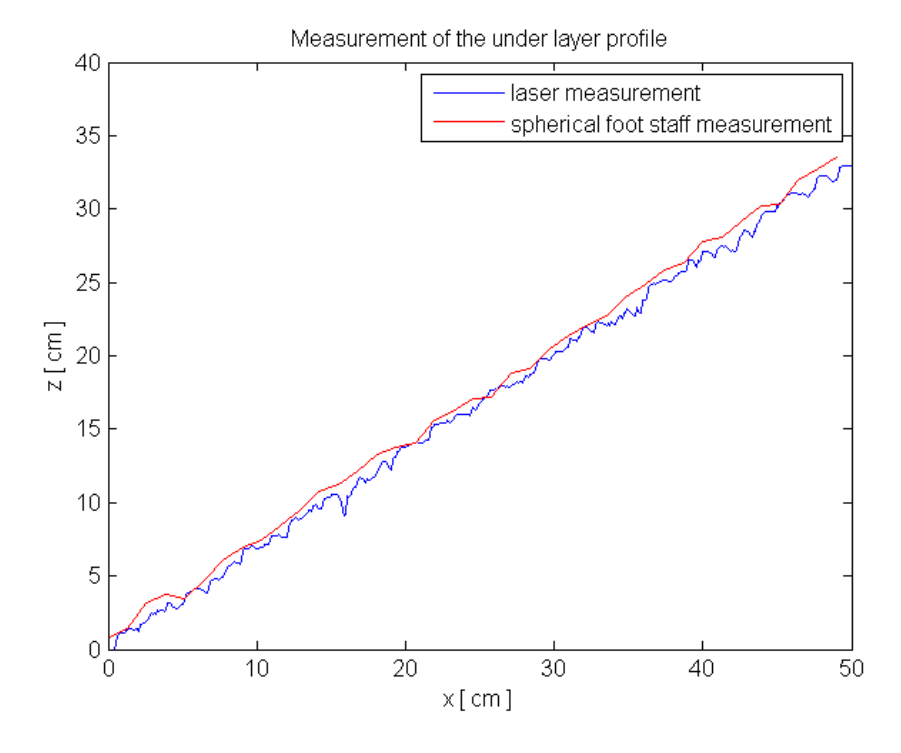


Figure K-4 Average measurement

Results of the measurements of a deviated profile

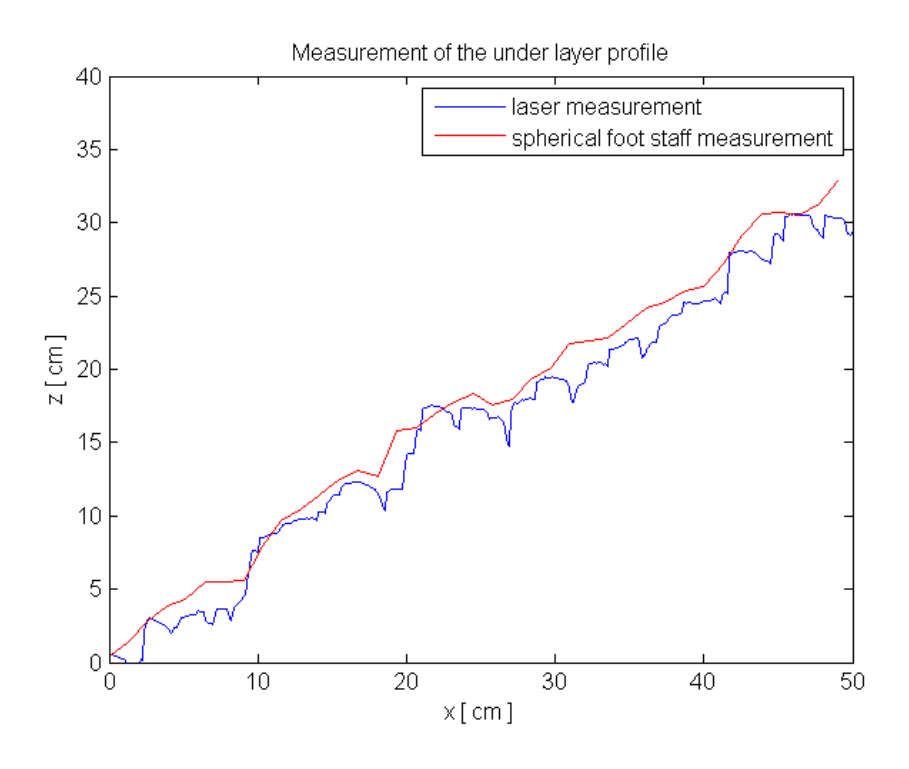


Figure K-5 Measurement from the left side

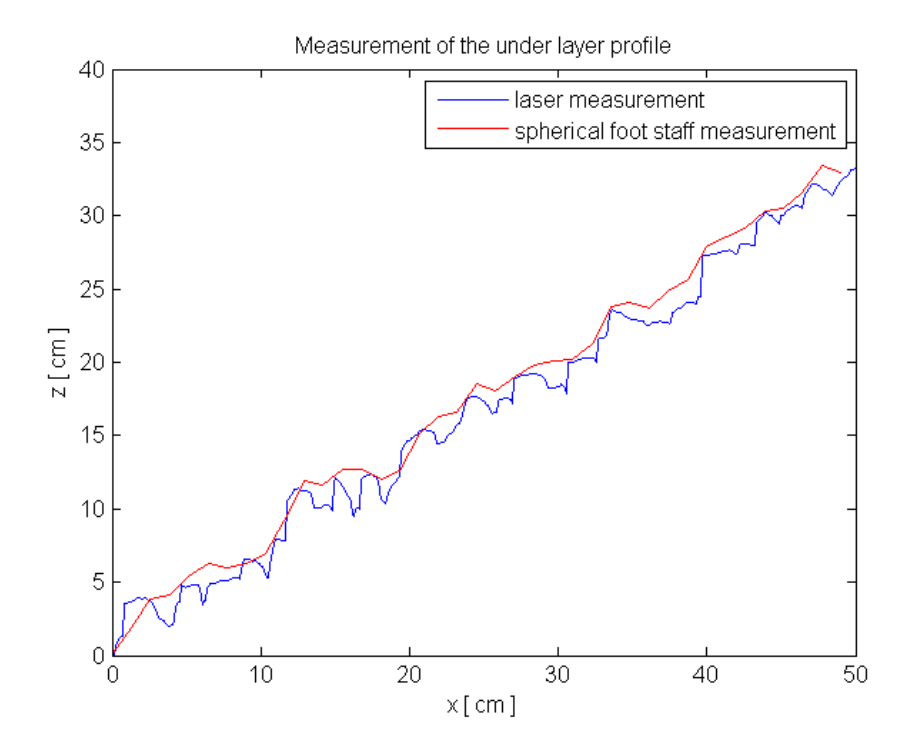


Figure K-6 Measurement from the middle location

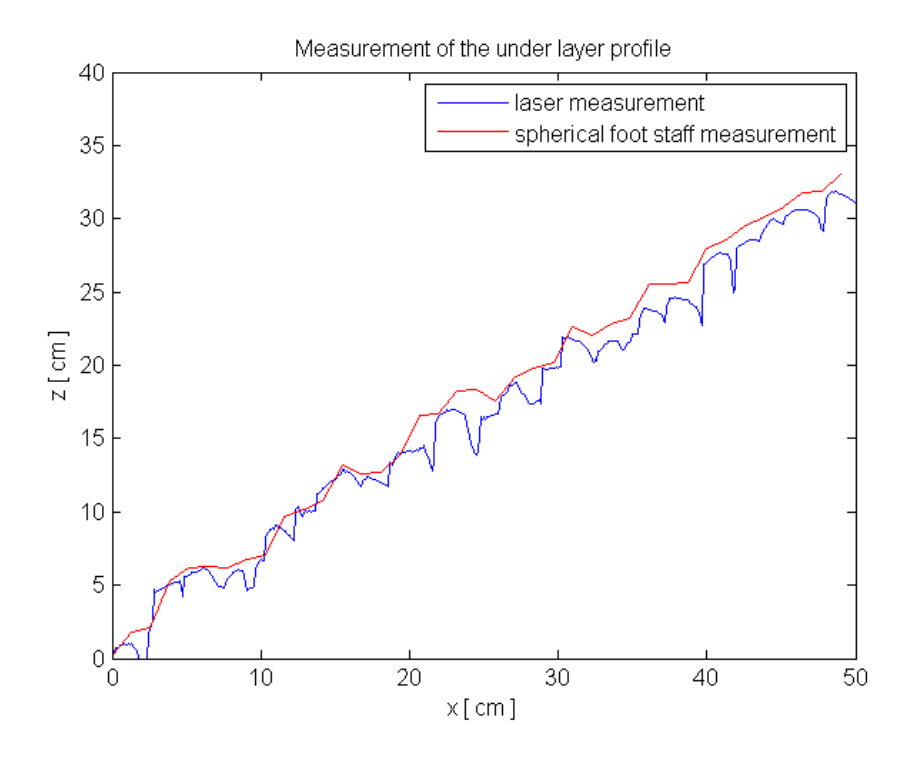


Figure K-7 Measurement from right side

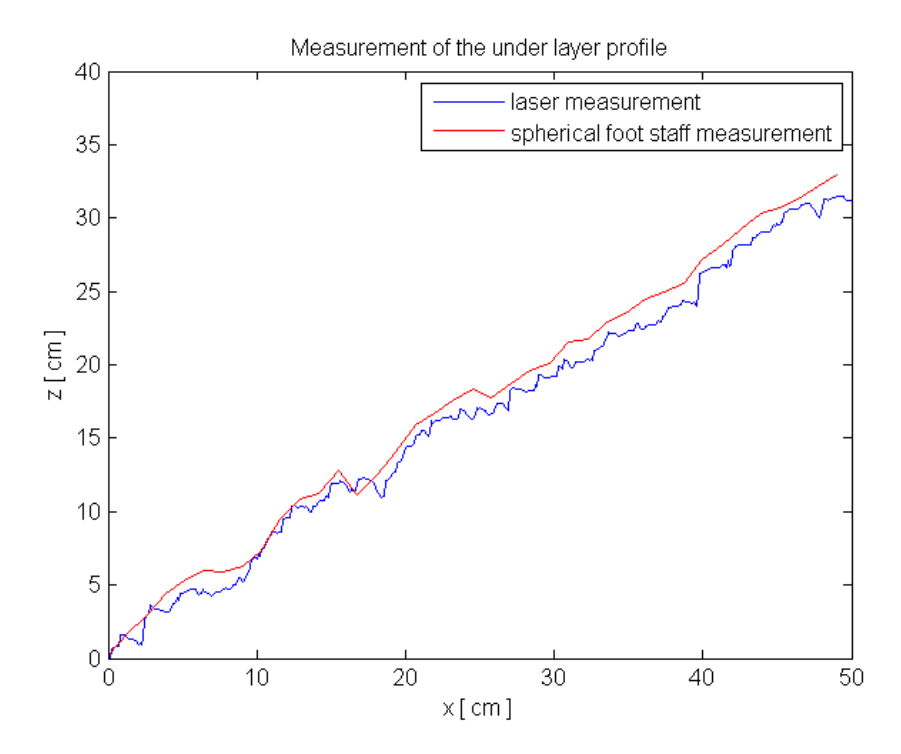


Figure K-8 Average measurement

Appendix L: Difference between simulated spherical foot staff and laser measurements

The differences between the two measurement methods are calculated. In the table below the mean difference per test is given.

Table L-1 Difference between simulated sphere and laser measurements

Test	Difference in profile height [mm]	Difference in profile height $[\cdot D_{n50}]$
A-1	5.11	0.35
A-2	4.79	0.33
A-3	4.39	0.30
B-1	4.52	0.31
B-2	5.18	0.36
B-3	4.93	0.34
C-1	4.37	0.30
C-2	5.18	0.36
C-3	5.03	0.35
D-1	4.83	0.33
D-2	5.39	0.37
D-3	5.29	0.36
E-1	5.47	0.38
E-2	4.79	0.33
E-3	5.08	0.35
F-1	4.69	0.32
F-2	4.86	0.33
F-3	5.17	0.36
G-1	5.45	0.38
G-2	4.66	0.32
G-3	4.84	0.33

The mean difference in profile height is 34% of D_{n50} . Which is approximately 5mm. The standard deviation is 6.4% of the mean. Which is 0.3mm.

Appendix M: Sensitivity analysis of the simulated spherical foot staff

In the table below the results of the sensitivity analysis of the simulated spherical foot staff method is given. A number of parameters is varied in order to get an impression of the sensitivity of the parameters.

Table M-1 Sensitivity of the diameter and interval of the sphere of test A-3

Test A-3

	max	min	Average	Absolute	Absolute	Relative
Diameter	tolerance	tolerance	tolerance	difference	difference	difference
[mm]	[cm]	[cm]	[cm]	[cm]	$[\cdot D_{n50}]$	[%]
3	0.83	-0.30	0.56	-0.13	-0.09	-19.6
5	0.89	-0.37	0.63	-0.06	-0.04	-9.2
7	1.01	-0.38	0.70	0	0	0
9	1.21	-0.22	0.72	0.01	0.01	2.8
11	1.45	0.07	0.68	-0.01	-0.01	-2.1
13	1.57	0.02	0.77	0.07	0.05	10.8
15	1.74	0.03	0.85	0.14	0.10	21.1
Interval						
[mm]						
6	1.02	-0.34	0.68	-0.02	-0.01	-3.1
8	1.2	-0.07	0.62	-0.08	-0.06	-11.8
10	1.01	-0.38	0.70	0	0	0
12	1.02	0.03	0.49	-0.20	-0.14	-29.5
14	0.90	-0.38	0.64	-0.05	-0.04	-7.8

Table M-2 Sensitivity of the diameter and interval of the sphere of test B-2

Test B-2

Diameter	max tolerance	min tolerance	Average tolerance	Absolute difference	Absolute difference	Relative difference
[mm]	[cm]	[cm]	[cm]	[cm]	$[\cdot D_{n50}]$	[%]
3	4.65	-4.74	4.69	-0.09	-0.06	-1.9
5	4.99	-4.61	4.80	0.01	0.01	0.2
7	5.17	-4.41	4.79	0	0	0
9	5.377	-4.21	4.79	0.01	0	0.1
11	5.5268	-3.95	4.74	-0.05	-0.03	-1.1
13	5.6293	-3.65	4.64	-0.15	-0.10	-3.2
15	5.7692	-3.45	4.60	-0.18	-0.13	-3.8
Interval						
[mm]						
6	5.09	-4.42	4.75	-0.03	-0.02	-0.7
8	5.09	-4.42	4.75	-0.03	-0.02	-0.7
10	5.17	-4.41	4.79	0	0	0
12	5.09	-4.42	4.75	-0.03	-0.02	-0.7
14	4.92	-4.43	4.59	-0.19	-0.13	-4.0

Appendix N: Specifications of the laser scanning device

The ILD-1700-750 device is used in the model tests. The specifications are given on this page and the next page:

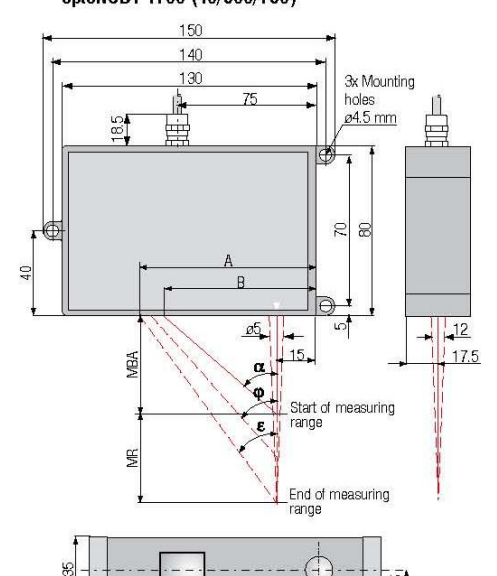
Model		ILD 1700- 2	ILD 1700- 10	ILD 1700- 20	ILD 1700- 40	ILD 1700- 50	ILD 1700- 100	ILD 1700- 200	ILD 1700- 250 V T	ILD 1700- 500	ILD 1700- 750	
Measuring range		2mm	10mm	20mm	40mm	50m m	100mm	200mm	250mm	500mm	750mm	
Start of measuring range	SMR	24mm	30mm	40mm	175mm	45mm	70mm	70mm	70mm	200mm	200mm	
Midrange	MMR	25mm	35mm	50mm	195mm	70mm	120mm	170mm	195mm	450mm	575mm	
End of measuring range	EMR	26m m	40mm	60mm	215mm	95mm	170mm	270mm	320mm	700mm	950mm	
T the constant		2µm	8µm	16μm	32µm	40μm	80µm	200μm	630µm	400μm	750μm	
Linearity -	FSO	≤0.1%			≤0.08%		00-	≤0.1%	≤0.25%	≤0.08%	≤0.1%	
Resolution (at 2.5kHz without averagin	ng)	0.1 <i>µ</i> m	0.5µm	1.5µm	4μm	Зμт	6µm	12µm	50µm	30µm	50μm	
Measuring rate				2.	5kHz / 1.25	kHz / 625h	tz / 312.5H	łz (adjustal	ole)			
Light source					semicono	luctor lase	1 < 1mW, 6	70nm (red)				
Permissable at 2.5kHz ambient light					10,000lx				15,000lx	10,0	10,000lx	
Laser safety class					class 2 a	acc. DIN El	N 60825-1	: 2001-11				
Control of the Contro	SMR	80µm	110µm	320µm	230µm	570μm	740µm	1300µm	1500µm	1500µm	1500µm	
Spot diameter	MMR	35µm	50μm	45μm	210µm	55µm	60µm	1300µm	1500µm	1500µm	1500µm	
	EMR	80µm	110µm	320µm	230µm	570μm	700µm	1300µm	1500µm	1500µm	1500µm	
Temperature stability*		0.025% 0.01 % FSO/°C 0.025% 0.01 % FSO/°C FSO/°C FSO/°C FSO/°C										
Operation temperature		0+50°C										
Storage temperature		-20 +70°C										
Output	m easure- m ents	selectable: 4 20mA / 0 10V / RS 422 / USB (optional with cable PC1700-3/USB)										
Output -	switching outputs	1 x error or 2 x limit (each pogrammable)										
Switch Input		laser ON-OFF / zero										
Operation		via touch screen on sensor or via PC with ILD 1700 tool										
Power supply					24VDC	(11 30\	/DC), max.	150mA				
Electromagnetic compatib	ility (EMC)				EN	61000-6-3	EN 61000	0-6-2				
Sensor cable length (with o	0.25m (integrated cable with connector) option: 3m or 10m											
Synchronisation				possi	ble for sim	ultaneous	or alternatir	ng measure	ements			
Protection class					IP	65						
Vibration		2g / 20 500Hz										
Shock					15g	/6ms						
Weight (with 0.25m cable)			~ 550g		~ 600g		~ ;	550g		~ 6	i00g	

FSO = Full Scale Output All specifications apply for a diffusely reflecting white ceramic target based on digital output SMR = Start of measuring range MMR = Midrange EMR = End of measuring range

Figure N-1 Specifications of the laser device used in the model tests (1/2)

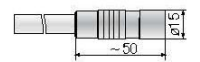
optoNCDT 1700 (2/10/20/50/100/200/250VT)

optoNCDT 1700 (40/500/750)



Connector (sensor side)

Article Number: 0323243



Connector (sensor cable)

Article Number: 0323272



MR

2 10

20

50

100

200

250VT

40

500

750

SMR

24

30

40

45

70

70

70

175

200

200

35°

28.8°

26.5°

19.0°

19.0°

19.0°

22.1°

19.3°

19.3°

Α

25.8

28.7

30.1

31.5

32.6

33.1

33.5

101

101

101

φ

40°

35.2°

27.5°

23.0°

15.4°

9.78°

8.4°

21.9°

9.8

44.8°

35.6°

26.7°

18.3°

10.9

6.97°

6.0°

21.8°

7.09

5.0°

В

16.8

20.5

22.0

22.5

24.1

24.1

24.1

86

85

85

Accessories optoNCDT 1700

Supply and output cable

PC 1700-3 (3 m)

PC 1700-10 (10 m)

PC 1700-10/3/IF2004 (10 $\mbox{m}_{\mbox{\tiny T}}$ for use with

interface-card IF2004)

PC 1700-10/D-Sub/9-pol.

PC 1700-3/3/USB/BNC/US (power supply converter)

PC 1700-3/USB (3 m, with USB-RS422-converter,

supply 90 ... 230 VAC)

PC1700-3/3/USB/OE/US (3 m, with

USB-RS422-converter, supply 90 ... 230 VAC)

Interface-card

IF2004 (RS422 PCI-interface-card for PC for 1-4 sensors optoNCDT or 3 sensors and 1 encoder)

External Trigger

Triggerbox 1700 (Electronics for triggering optoNCDT 1700 sensors. Acceptable trigger levels are from +2.4 VDC to +24 VDC, L/W/H 98x64x34 mm)

Display

CSP301 (digital processing and readout unit, programmable for two analog outputs)

Power supply

PS 2010 (for top-hat rail mounting; L/W/H 120x120x40 mm Input 115 / 230 VAC selectable; output 24 VDC / 2.5 A)

Protective housing

SGx 1800 (for models ILD 1700-2/10/20/50/100/200/250VT)
SGx 2200-200 (for models ILD 1700-40/500/750)
SGxF 1800 (option with compressed air clean setup)
SGxF 2200-200 (option with compressed air clean setup)

Figure N-2 Specifications of the laser device used in the model tests (2/2)

Appendix O: Matlab scripts

A few Matlab scripts are used. In this appendix they are presented.

Script used to determine the position of armour units

```
clc;
clear all;
close all;
data = imread('A4.jpg'); %adjust filename
figure(100);
%%%turn this part on in order to determine the scale!
% clf;
% h = imagesc(data);
% axis ([700 2500 0 1200]);
% schaal = ginput;
% save schaal.txt schaal -ASCII;
  scale = (abs(schaal(2))-abs(schaal(1)))/297; %schaalfactor voor
afstanden tot millimeters
% close all;
% data = imread('Test001b.jpg');
% figure(89);
% clf;
% g = imagesc(data);
% axis image
% na = ginput;
% save na.txt na -ASCII;
% verschil = voor - na;
% % plot(voor. Na);
응응응
load scale.txt;
data2 = imread('Test014a.jpg');
                                %adjust filename
figure(101);
clf;
h = imagesc(data2);
axis ([700 2500 0 1200]);
                                       %adjust axis in order to have a good view
Test0014a_px = ginput;
                                          %adjust filename. Click centre of gravity
points
save Test014a px.txt Test0014a px -ASCII; %adjust filename
%optioneel
x = Test0014a_px(:.1)/scale;
                                        %aadjust filename
y = -Test0014a px(:.2)/scale;
                                      %adjust filename
Test014a=[x.y];
                              %adjust filename
save Test014 voor mm.txt Test014a -ASCII; %adjust filename
plot(x.y)
```

Script used to plot the position of armour units

```
clear all; close all;
load Test004_na_mm.txt; load Test004_voor_mm.txt;
x voor=Test004 voor mm(:,1);
                                                                                                                                   %adjust filename
                                                                                                                                   %adjust filename
y voor=Test004 voor mm(:,2);
x_na=Test004_na_mm(:,1);
                                                                                                                                  %adjust filename
y na=Test004 na mm(:,2);
                                                                                                                                   %adjust filename
bewegingx=x na(1)-x voor(1);
bewegingy=y na(1)-y voor(1);
x na2=x na-bewegingx-980;
y_na2=y_na-bewegingy+895;
x_voor2=x_voor-980;
% plot(x_voor2, y_voor2, '+');
% hold on;
% plot(x_na2,y_na2, 'r+');
% hold on
wl=[0.58, 0.58];
xwl = [0.13, 0.77];
title('Settlement of armour units during Test A-1');
h = legend('position before', 'position after');
xlabel('x [ mm ]');
ylabel('y [ mm ]');
Nx=9;
Ny=19;
%determine average distance in x and y direction
Lx=(1/19)*(abs((x_voor(10)-x_voor(2)))+abs((x_voor(19)-x_voor(2))))
x_voor(11)))+abs((x_voor(28)-x_voor(20)))+abs((x_voor(37)-
x voor(29)))+abs((x voor(46)-x voor(38)))+abs((x voor(55)-
x_voor(47)))+abs((x_voor(64)-x_voor(56)))+abs((x_voor(73)-
x_voor(65)))+abs((x_voor(82)-x_voor(74)))+abs((x_voor(91)-
x voor(83)))+abs((x voor(100)-x voor(92)))+abs((x voor(109)-
\bar{x} voor(101)))+abs((\bar{x} voor(118)-\bar{x} voor(110)))+abs((\bar{x} voor(127)-
x voor(119)))+abs((x voor(136)-x voor(128)))+abs((x voor(145)-
x_voor(137)))+abs((x_voor(154)-x_voor(146)))+abs((x_voor(163)-
x_{voor}(155))+abs((x_{voor}(172)-x_{voor}(164))));
Ly=-(1/9)*((y_voor(2)-y_voor(164))+(y_voor(3)-y_voor(165))+(y_voor(4)-y_voor(4))+(y_voor(4)-y_voor(4))+(y_voor(4)-y_voor(4))+(y_voor(4)-y_voor(4))+(y_voor(4)-y_voor(4))+(y_voor(4)-y_voor(4))+(y_voor(4)-y_voor(4))+(y_voor(4)-y_voor(4))+(y_voor(4)-y_voor(4))+(y_voor(4)-y_voor(4))+(y_voor(4)-y_voor(4))+(y_voor(4)-y_voor(4))+(y_voor(4)-y_voor(4))+(y_voor(4)-y_voor(4))+(y_voor(4)-y_voor(4))+(y_voor(4)-y_voor(4))+(y_voor(4)-y_voor(4))+(y_voor(4)-y_voor(4))+(y_voor(4)-y_voor(4))+(y_voor(4)-y_voor(4))+(y_voor(4)-y_voor(4))+(y_voor(4)-y_voor(4))+(y_voor(4)-y_voor(4))+(y_voor(4)-y_voor(4))+(y_voor(4)-y_voor(4))+(y_voor(4)-y_voor(4))+(y_voor(4)-y_voor(4))+(y_voor(4)-y_voor(4))+(y_voor(4)-y_voor(4))+(y_voor(4)-y_voor(4))+(y_voor(4)-y_voor(4))+(y_voor(4)-y_voor(4))+(y_voor(4)-y_voor(4))+(y_voor(4)-y_voor(4))+(y_voor(4)-y_voor(4))+(y_voor(4)-y_voor(4))+(y_voor(4)-y_voor(4))+(y_voor(4)-y_voor(4))+(y_voor(4)-y_voor(4))+(y_voor(4)-y_voor(4))+(y_voor(4)-y_voor(4))+(y_voor(4)-y_voor(4))+(y_voor(4)-y_voor(4)-y_voor(4))+(y_voor(4)-y_voor(4)-y_voor(4))+(y_voor(4)-y_voor(4)-y_voor(4)-y_voor(4))+(y_voor(4)-y_voor(4)-y_voor(4)-y_voor(4)-(y_voor(4)-y_voor(4)-y_voor(4)-(y_voor(4)-y_voor(4)-y_voor(4)-(y_voor(4)-y_voor(4)-y_voor(4)-(y_voor(4)-y_voor(4)-y_voor(4)-(y_voor(4)-y_voor(4)-(y_voor(4)-y_voor(4)-(y_voor(4)-y_voor(4)-(y_voor(4)-y_voor(4)-(y_voor(4)-y_voor(4)-(y_voor(4)-y_voor(4)-(y_voor(4)-y_voor(4)-(y_voor(4)-y_voor(4)-(y_voor(4)-y_voor(4)-(y_voor(4)-y_voor(4)-(y_voor(4)-y_voor(4)-(y_voor(4)-y_voor(4)-(y_voor(4)-y_voor(4)-(y_voor(4)-y_voor(4)-(y_voor(4)-y_voor(4)-(y_voor(4)-y_voor(4)-(y_voor(4)-y_voor(4)-(y_voor(4)-y_voor(4)-(y_voor(4)-y_voor(4)-(y_voor(4)-y_voor(4)-(y_voor(4)-y_voor(4)-(y_voor(4)-y_voor(4)-(y_voor(4)-y_voor(4)-(y_voor(4)-y_voor(4)-(y_voor(4)-y_voor(4)-(y_voor(4)-y_voor(4)-(y_voor(4)-y_voor(4)-(y_voor(4)-y_voor(4)-(y_voor(4)-y_voor(4)-(y_voor(4)-(y_voor(4)-y_voor(4)-(y_voor(4)-(y_voor(4)-(y_voor(4)-(y_voor(4)-(y_voor(4)-(y_voor(4)-(y_voor(4)-(y_voor(4)-(y_voor(4)-(y_voor(4)-(y_voor(4)-(y_voor(4)-(y_voor(4)-(y_voo
y_{voor}(166) + (y_{voor}(5) - y_{voor}(167)) + (y_{voor}(6) - y_{voor}(168)) + (y_{voor}(7) - y_{voor}(166)) + (y_{voor}(168)) + (y_{vo
y_voor(169))+(y_voor(8)-y_voor(170))+(y_voor(9)-y_voor(171))+(y_voor(10)-
y voor(172)));
%determine PD and RPD
PD placed=(Nx-1)*(Ny-1)/(Lx*Ly);
 % PD design=(8*18)/(587*518);
PD design=1.2/(49.6*49.6);
RPD=(PD placed/PD design) *100
x_voor;
%determine settlements
xdiff=x na2-x voor2;
ydiff=(y na2-y voor2)/-49.6;
% save ydiff20.txt ydiff -ASCII;
% plot(x_voor, y_voor, '+')
```

```
hold on;
hold on;
annotation('line', xwl,wl,'Color', 'r');
hold on;
refline(0,345);
Z=[x_voor2,y_voor2];
F=[xdiff,ydiff];
% contour(Z,ydiff);
% colormap(jet);
% plot(xwl,wl,'r');
% quiver(x_voor2,y_voor2,xdiff,ydiff);
A=[x_voor2,y_voor2,ydiff];
data = A;
x=data(:,1);
y=data(:,2);
z=data(:,3);
a=size(data);
b=a(:,1);
xlin=linspace(min(x), max(x), 1000);
ylin=linspace(min(y), max(y), 1000);
[X,Y] = meshgrid(xlin,ylin);
Z=griddata(x,y,z,X,Y);
mesh(X,Y,Z);
colorbar;
caxis([0 1]);
title(colorbar, 'Settlement [Dxbloc]');
hold on;
% plot(xwl,wl,'+');
hold on;
% refline(0,345);
% image(x_voor,y_voor,A);
colormap(jet);
axis([0 600 0 600]);
% axis([-1000 1000 0 800]);
%determine settlements >0.5D
n=sum(ydiff<-25);
% n=sum(ydiff<-20 & ydiff>-30);
```

Simulation of the spherical foot staff method

This function can be loaded from the script which is used to generate plots of the under layer profile.

```
function datasetnew = halvebol(datasetold.interval.diameter)
radius = floor(diameter/2);
                                                         %determine radius
datasetnew = datasetold(1:interval:end-interval.:);
                                                              %generate new dataset
dimensions
datasetnew= datasetnew(2:end.:);
z = [datasetold(:.1) zeros(size(datasetold.1).1)];
                                                        %determine z
for ii = 1:size(datasetnew.1)
    difference = zeros(diameter+1.1);
                                                         %generate difference vector
    zbolmidden = datasetnew(ii.2) - radius/10;
                                                          %determine middle point of
sphere. Convert mm to cm
    for jj = -radius:radius
                                              +
        z(ii*interval+jj.2)
                                                     (\operatorname{sqrt}(\operatorname{radius}^2 - jj^2)/10);
                                  zbolmidden
%determine virtual height of sphere in diameter range
       difference(jj+radius+1) = datasetold(ii*interval+jj.2)-z(ii*interval+jj.2);
%determine difference virtual height with measured profile height
    datasetnew(ii.2) =
                                    datasetnew(ii.2)
                                                           +
                                                                   max(difference);
%add maximum difference to profile height on the location of measurement
```

Script used to plot the profiles

This script is used to load the data produced by the laser device and plot the profile height.

```
Close all; clear all;
%inlezen Dasylab ascii-file 1:
filenaam1='T006LINKS.ASC';
data1 = textread(filenaam1.''.'delimiter'.';'.'headerlines'.7);
nrows1=size(data1.1);
ncolumns1=size(data1.2);
data 1=data1(:.1:ncolumns1-1);
data_1(data_1 == 10.0) = NaN;
datal=inpaint_nans(data_1);
%inlezen Dasylab ascii-file 2:
filenaam2='T006MIDDEN.ASC';
data2 = textread(filenaam2.''.'delimiter'.';'.'headerlines'.7);
nrows2=size(data2.1);
ncolumns2=size(data2.2);
data_2=data2(:.1:ncolumns2-1);
data^{2}(data 2 == 10.0) = NaN;
data2=inpaint_nans(data_2);
%inlezen Dasylab ascii-file 3:
filenaam3='T006RECHTS.ASC';
data3 = textread(filenaam3.''.'delimiter'.';'.'headerlines'.7);
nrows3=size(data3.1);
ncolumns3=size(data3.2);
data 3=data3(:.1:ncolumns3-1);
data 3 (data 3 == 10.0) = NaN;
data3=inpaint_nans(data_3);
data=(data1+data2+data3)/3; %determine average of datasets
lengte = length(data);
x = 0.1012383901*(1:lengte); %horizontale afstand in cm
z = -7.47741136634865 * data(1:lengte.2) -20.0;
f= 0.667*x - 83.5; %functionele beschrijving ontwerplijn onderlaag g= 0.667*x - 83.5-0.5*1.44;
h = 0.667*x - 83.5+0.5*1.44;
H = [x; z'];
datasetnew = halvebol(F.10.7); %load spherical foot simulated data
zhb=datasetnew(:.2);
xhb=datasetnew(:.1);
                                 %x-sphere
d=z-f';
max laser=max(d);
                                 %max deviation laser
min laser=min(d);
                                 %min deviation laser
M=mean(d);
s=std(d);
u=f';
p=u(11:10:end-10);
q=zhb-p;
max halvebol=max(q);
                                         %positive tolerance
min halvebol=min(q);
                                         %negative tolerance
plot(x.z.'b'.xhb.zhb.'g'.x.f);
% plot(x.z.x.f.x.g.x.h.'k');
hold on;
```

Appendix P: Settlements

In this appendix more details on the settlement of the armour units is given.

Influence of the tolerance on the settlements

As mentioned in section 5.3.4 no relation between tolerances of the under layer and the settlement is found. This is made more clear in the figure below:

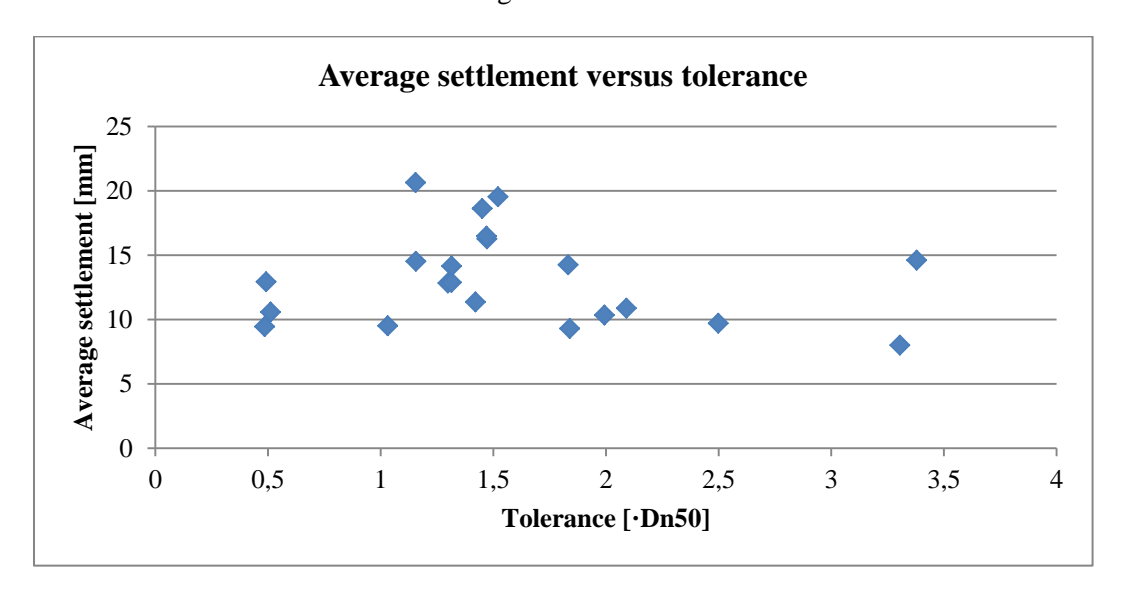


Figure P-1 Average settlement and tolerances of the under layer

Influence of the local difference in RPD on the settlements

As mentioned in section 5.3.4 a relation between difference in RPD on the upper and lower half of the slope and the settlements can be found, when one compares individual tests of the same scenario. This is made more clear in the figure below:

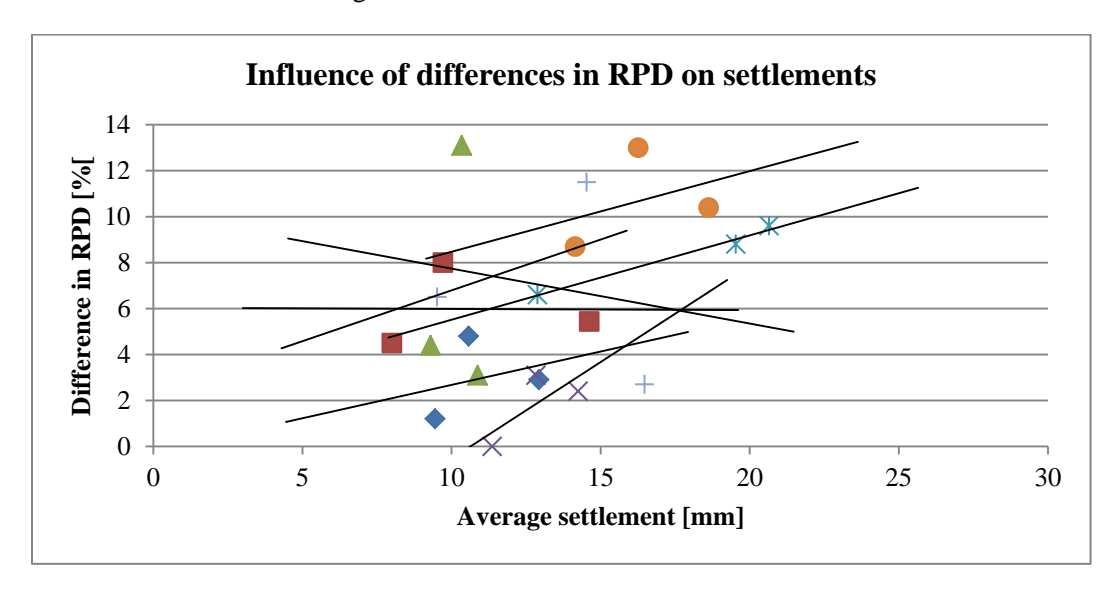


Figure P-2 Influence of differences in RPD on the slope on average settlement

In the figure above the settlements of test scenarios are plotted versus the difference in RPD on the lower and upper half of the slope. The trend lines are plotted as well. Because 5 out of 7 trend lines are increasing it can be concluded that in general differences in RPD lead to larger settlements of the

armour units. It should be noted that the RPD calculation is very sensitive to small errors and therefore these results are rather indicative.

Detailed data of the settlements

In the table on the next page the important magnitudes of the settlements is given. Info on the RPD before and after the tests is given as well. In the table below the average settlements per test scenario are given:

Table P-1 Magnitudes of the average settlement for the different scenarios

Test scenario	Average settlement [mm]								
	mean	standard deviation							
A	10.9	1.45							
В	10.7	2.80							
С	10.1	0.65							
D	12.8	1.17							
Е	17.6	3.42							
F	16.3	1.82							
G	13.5	2.93							

Table P-2 Details on settlements and RPD

	Average RPD before	Average RPD after	RPD lower half	RPD upper half	RPD lower half	RPD upper half	# units which settle	Difference average before	Average	Difference upper/low er before	Difference upper/low er after	Difference upper before/after	Difference lower before after
Test	[%]	[%]	before	before	after	after	>0.5D	after [%]	settlement	[%]	[%]	[%]	[%]
			[%]	[%]	[%]	[%]							
A-1	103.1	103.96	100.3	105.1	103.6	102.4	1	0.86	10.6	4.8	-1.2	-2.7	3.3
A-2	102.3	104.7	101.1	104	106.8	102.2	22	2.4	12.9	2.9	-4.6	-1.8	5.7
A-3	99.3	101.7	98.2	99.4	104	98	7	2.4	9.4	1.2	-6	-1.4	5.8
B-1	97.4	99.8	94.2	101.9	99.8	99.7	5	2.3	9.7	7.7	-0.1	-2.2	5.6
B-2	96.7	98.8	94.5	99.7	101.3	76.9	18	2.0	14.6	5.2	-24.4	-22.8	6.9
B-3	97.2	98.8	96.3	100.6	99.9	99.6	4	1.6	8.0	4.3	-0.3	-1.0	3.7
C-1	100.1	100.4	99.0	103.3	104.3	97.0	6	0.3	9.3	4.3	-7.3	-6.3	5.3
C-2	99.8	102.1	94.4	107.3	101.7	103.0	3	2.3	10.3	12.9	1.3	-4.3	7.3
C-3	99.1	100.9	97.9	101.0	103.5	97.3	3	1.8	10.9	3.1	-6.2	-3.6	5.6
D-1	98.6	100.3	96.9	100	101.9	97.3	15	1.7	12.8	3.1	-4.5	-2.7	4.9
D-2	96.1	99.6	96.4	96.4	100	98.6	22	3.6	11.4	0	-1.4	2.3	3.6
D-3	96.9	100.2	95.5	97.8	99.8	98.9	30	3.3	14.2	2.4	-0.9	1.1	4.3
E-1	99.0	102.1	95.5	104.1	104.0	100.1	56	3.0	19.5	8.6	-3.9	-4.0	8.5
E-2	97.8	99.6	94.0	103.4	103.0	96.0	66	1.8	20.6	9.4	-7.0	-7.5	8.9
E-3	99.1	100.6	97.1	103.5	101.2	100.6	13	1.5	12.9	6.5	-0.6	-2.9	4.1
F-1	100.7	102.2	97.1	105.8	106.0	99.1	27	1.5	14.1	8.6	-6.9	-6.7	8.8
F-2	105.6	105.9	99.5	112.4	109.1	100.4	36	0.3	16.3	12.9	-8.7	-12.0	9.6
F-3	103.2	105.7	98.6	108.9	110.5	101.5	49	2.7	18.6	10.3	-9.0	-7.4	11.9
G-1	103.6	106.0	102.6	105.2	110	101.2	33	2.4	16.5	2.6	-8.8	-4.0	7.5
G-2	101.3	103.4	95.5	106.8	105.6	100.8	19	2.2	14.5	11.3	-4.8	-6.0	10.1
G-3	102.1	104.0	99.2	105.6	105.6	102.7	6	1.9	9.5	6.4	-2.8	-2.8	6.4

Please note that the values in the table above are calculated with both L_x and L_y (see section 5.3.3)

Appendix Q: Photos taken before and after the tests

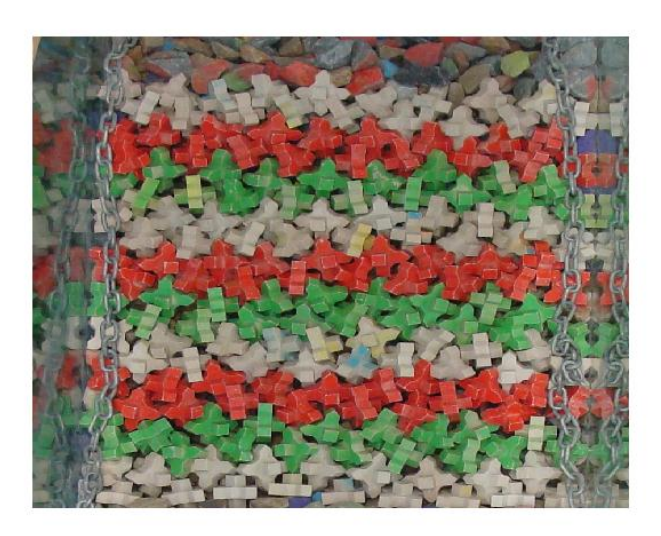
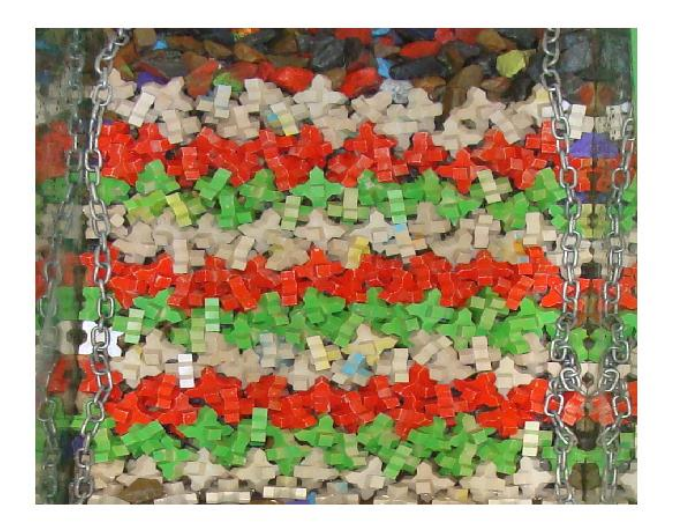


Figure Q-1 Photos before (left) and after (right) test A-1



Figure Q-2 Photos before (left) and after (right) test A-2





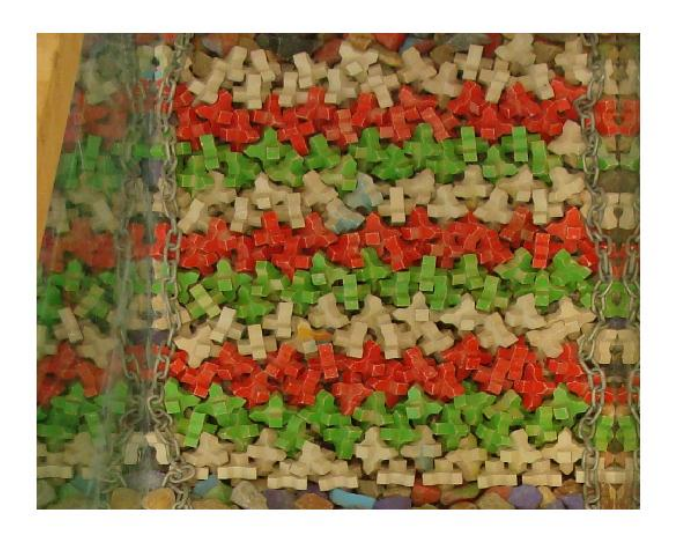


Figure Q-3 Photos before (left) and after (right) test A-3



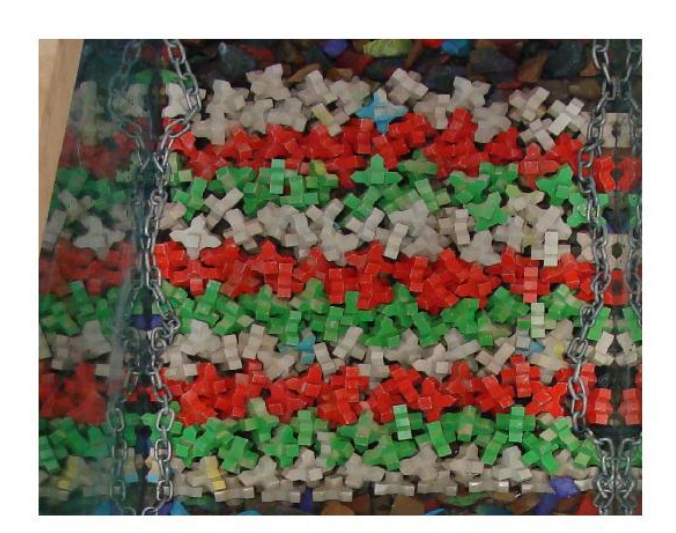


Figure Q-4 Photos before (left) and after (right) test B-1

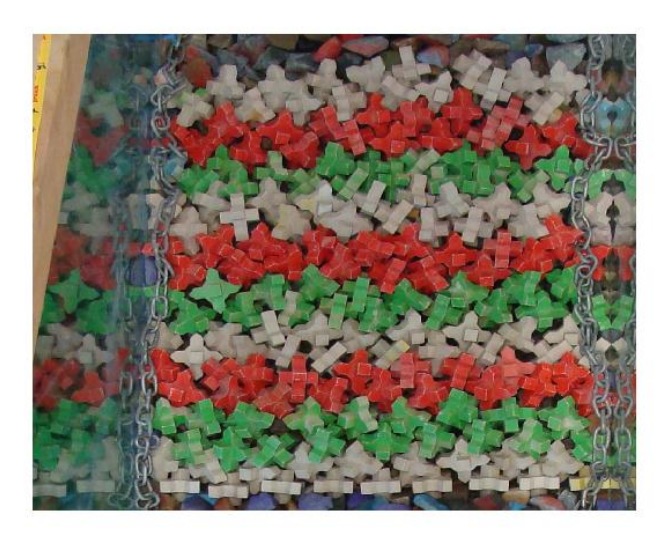
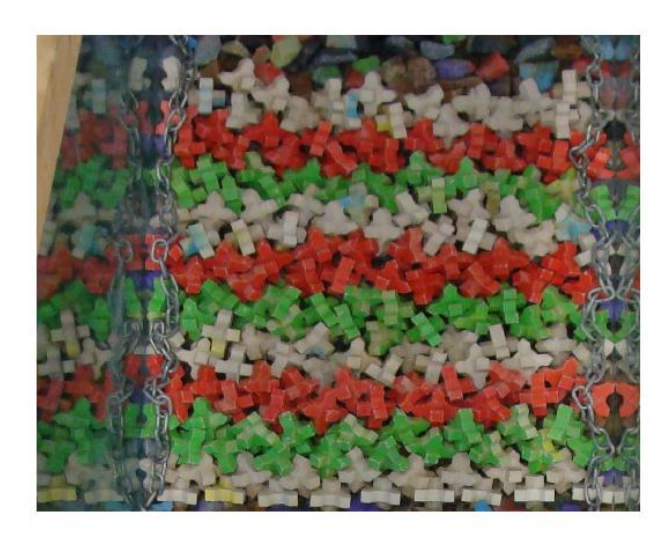


Figure Q-5 Photos before (left) and after (right) test B-2



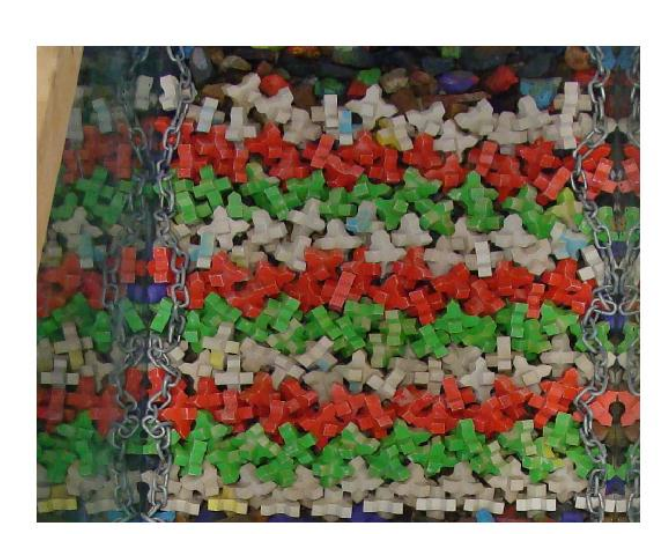


Figure Q-6 Photos before (left) and after (right) test B-3



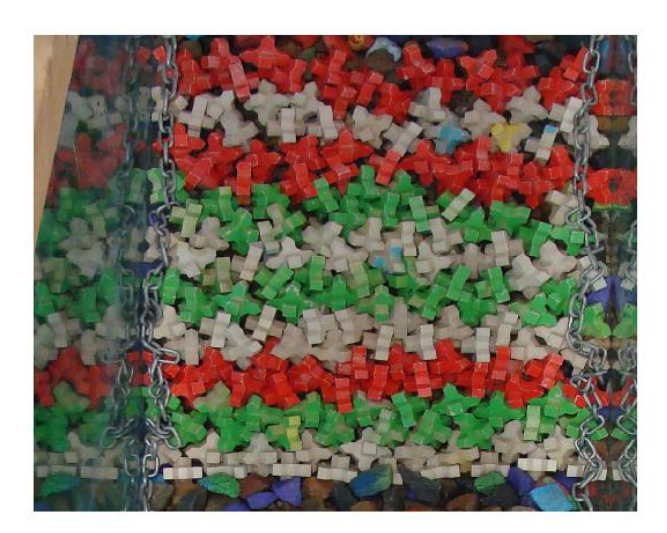
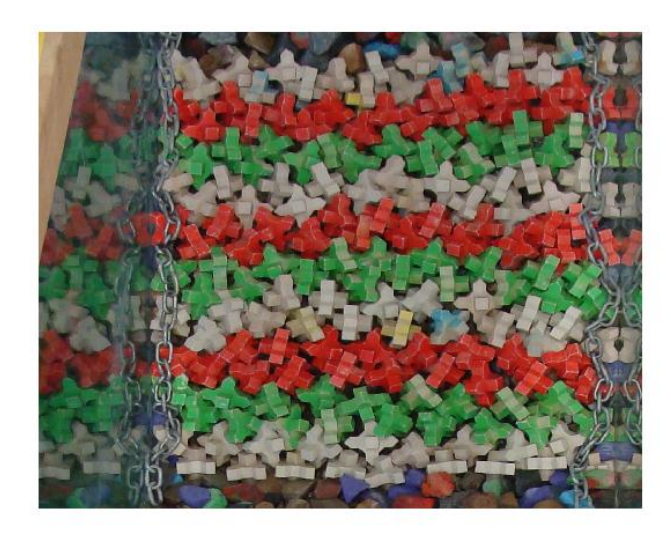


Figure Q-7 Photos before (left) and after (right) test C-1



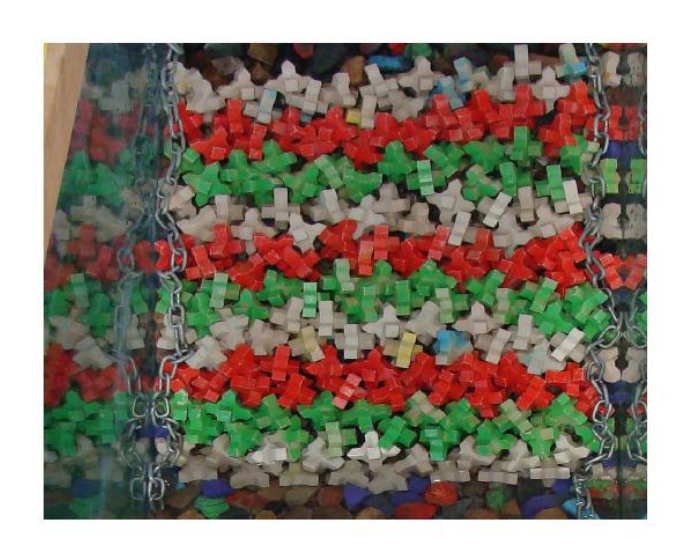
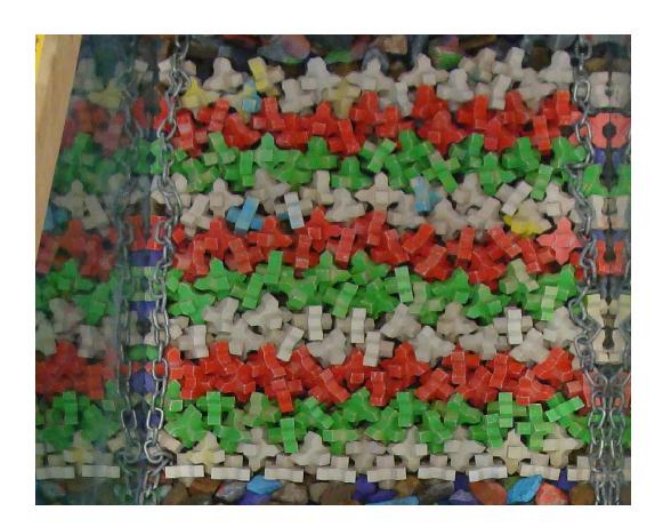


Figure Q-8 Photos before (left) and after (right) test C-2



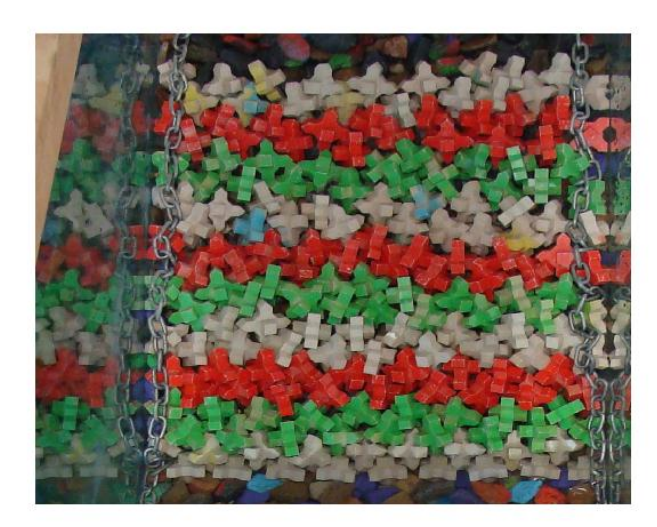
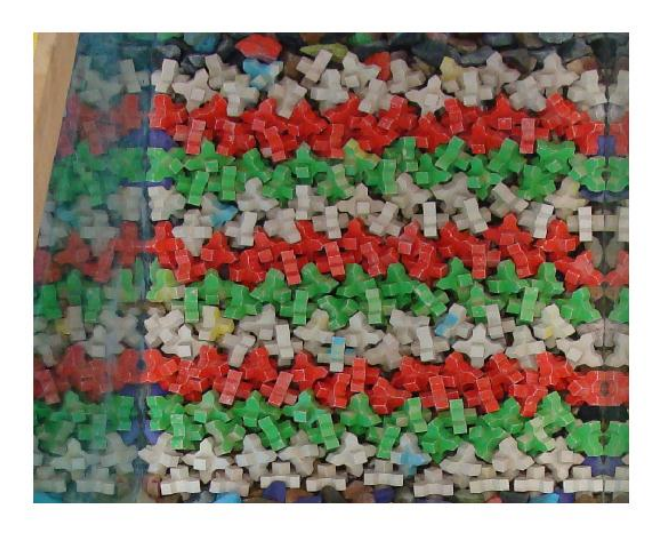


Figure Q-9 Photos before (left) and after (right) test C-3



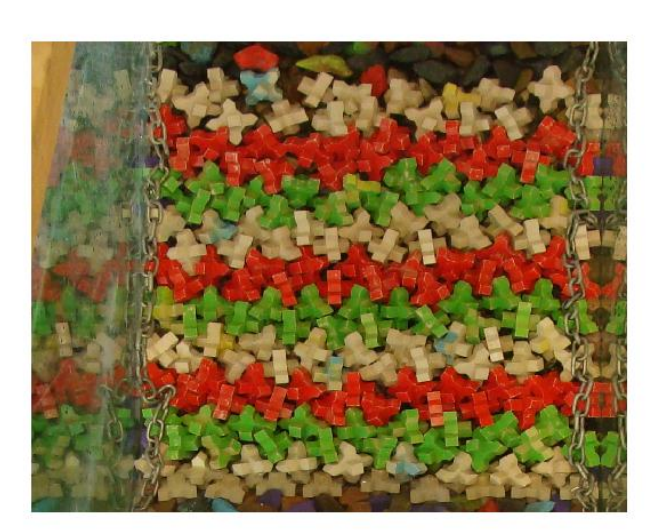
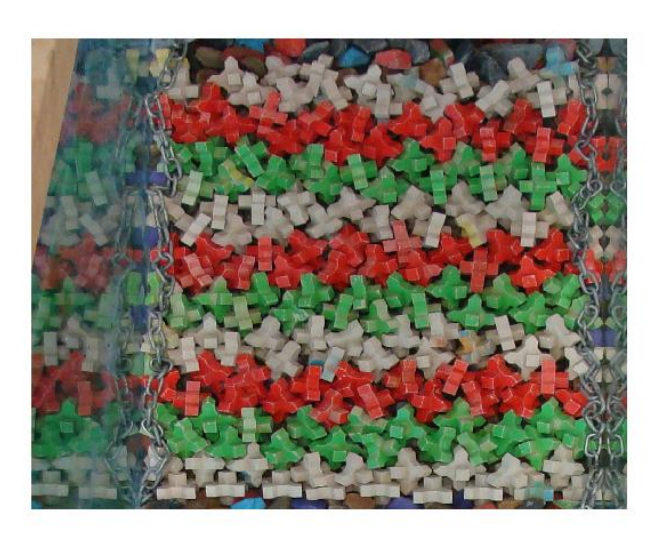


Figure Q-10 Photos before (left) and after (right) test D-1



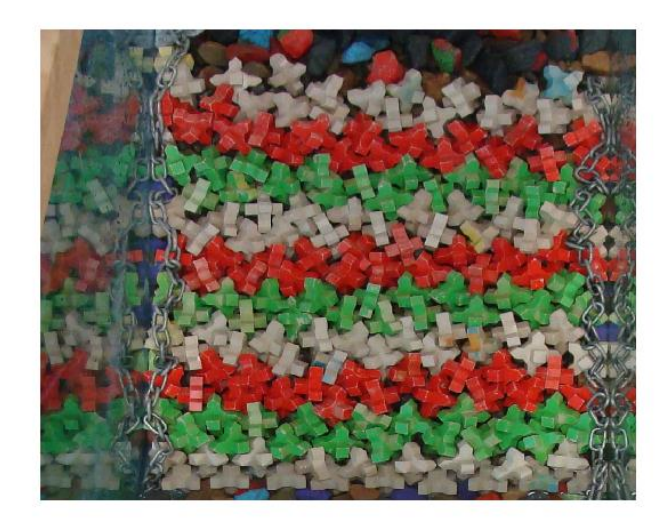
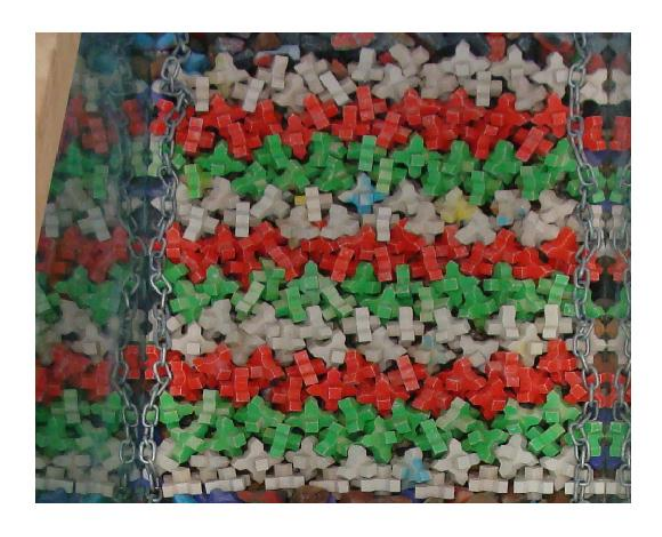


Figure Q-11 Photos before (left) and after (right) test D-2



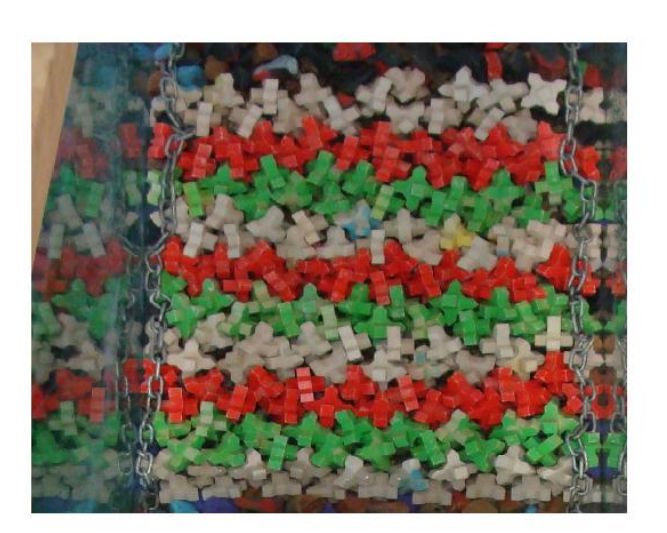
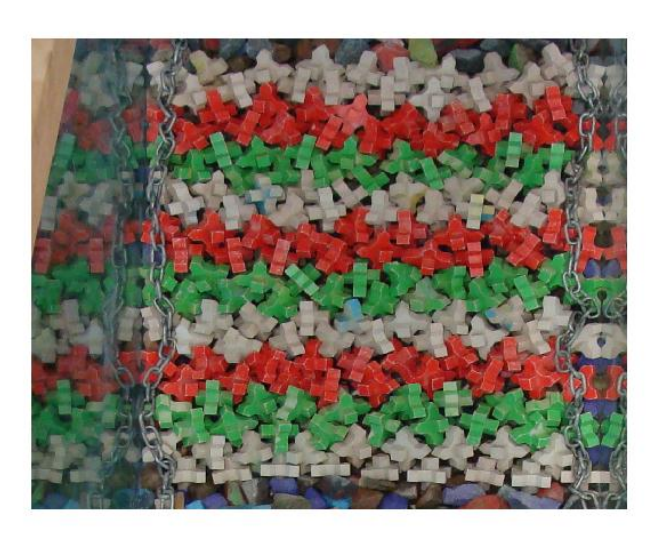


Figure Q-12 Photos before (left) and after (right) test D-3



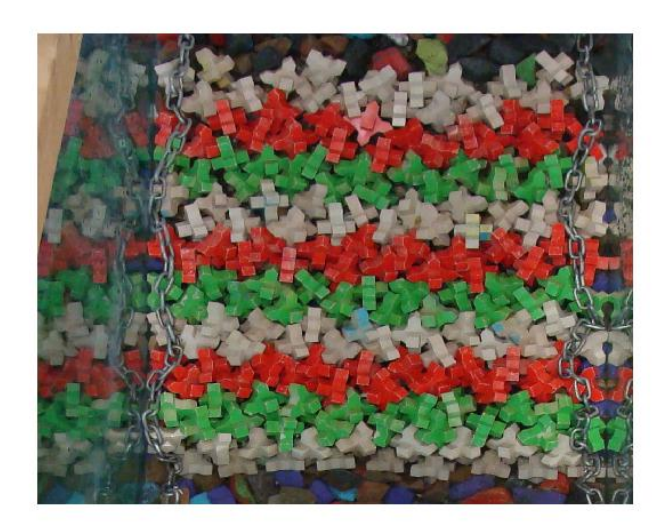


Figure Q-13 Photos before (left) and after (right) test E-1

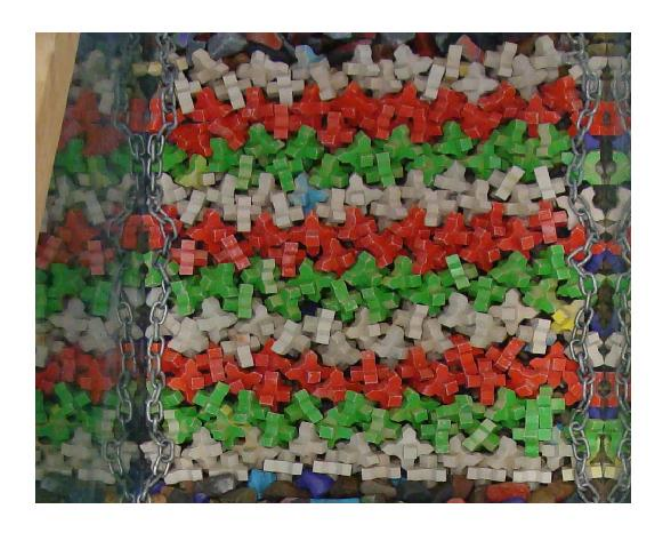




Figure Q-14 Photos before (left) and after (right) test E-2

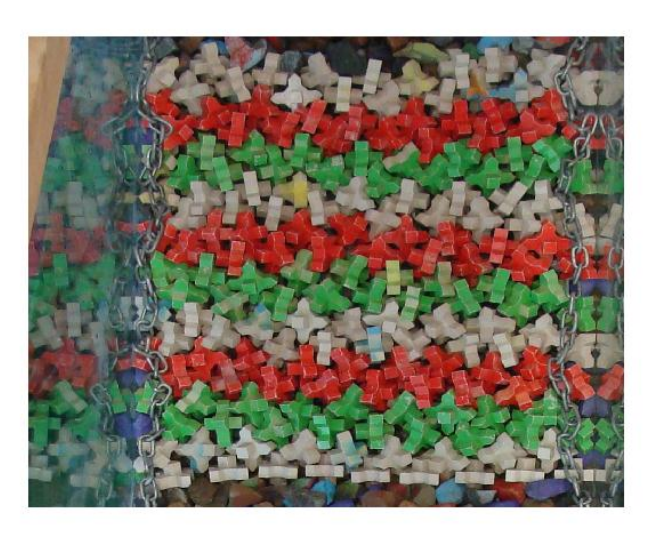




Figure Q-15 Photos before (left) and after (right) test E-3

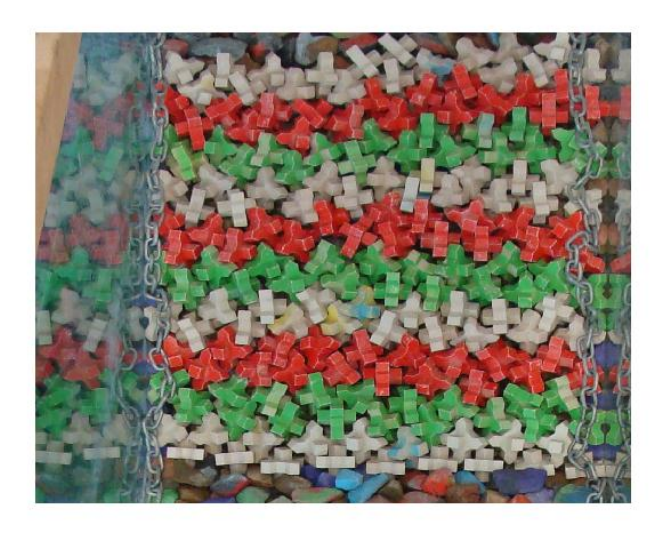


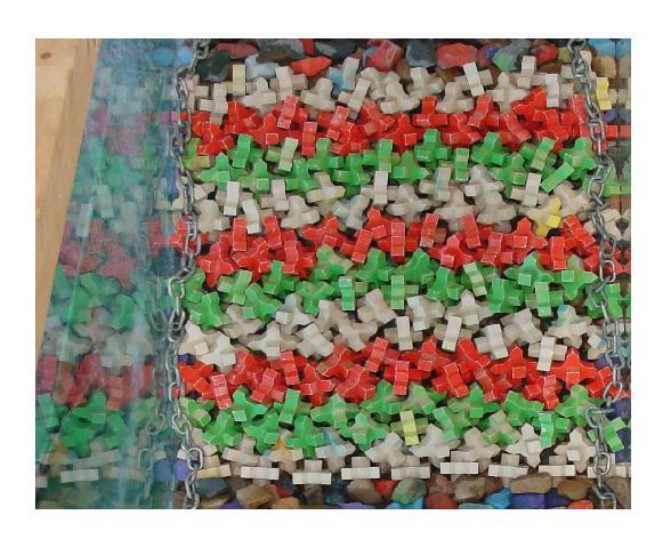


Figure Q-16 Photos before (left) and after (right) test F-1





Figure Q-17 Photos before (left) and after (right) test F-2



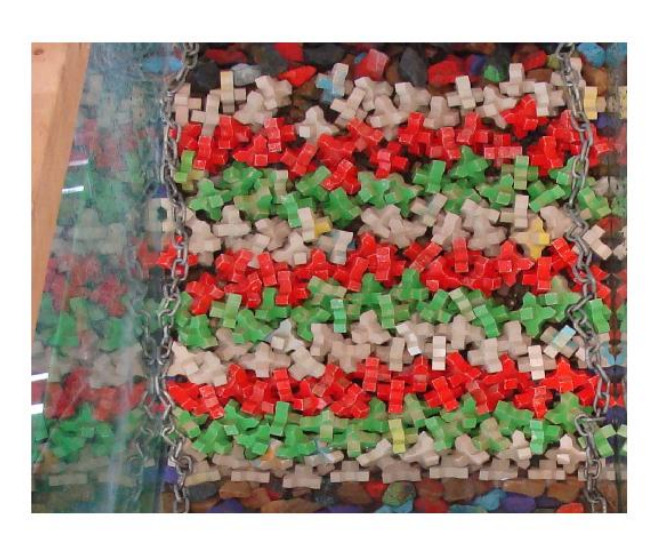
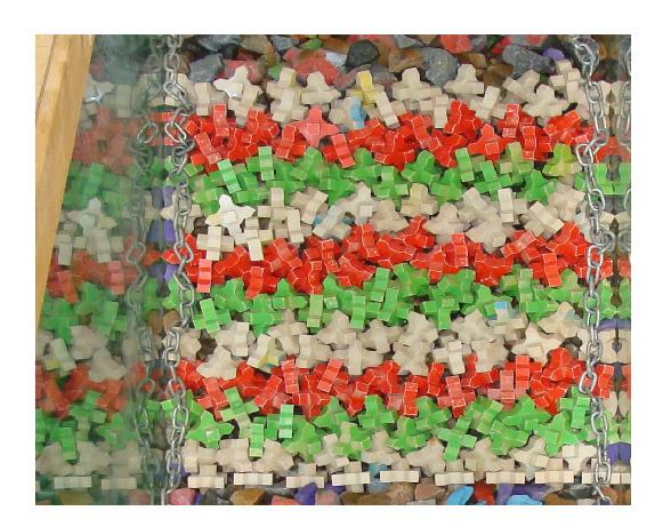


Figure Q-18 Photos before (left) and after (right) test F-3



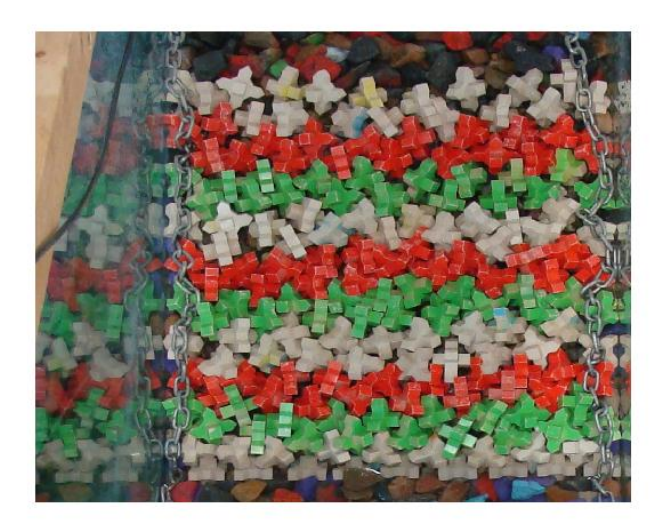
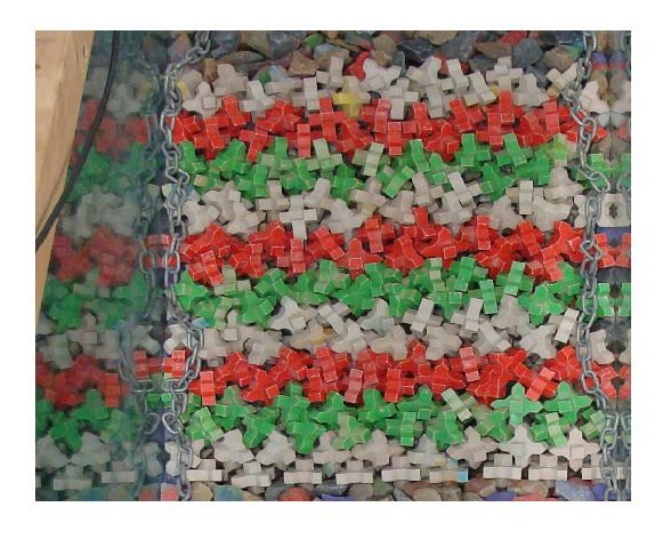


Figure Q-19 Photos before (left) and after (right) test G-1



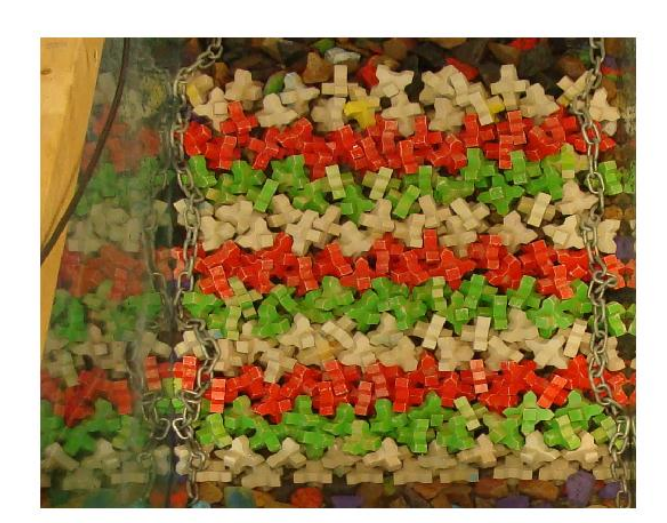
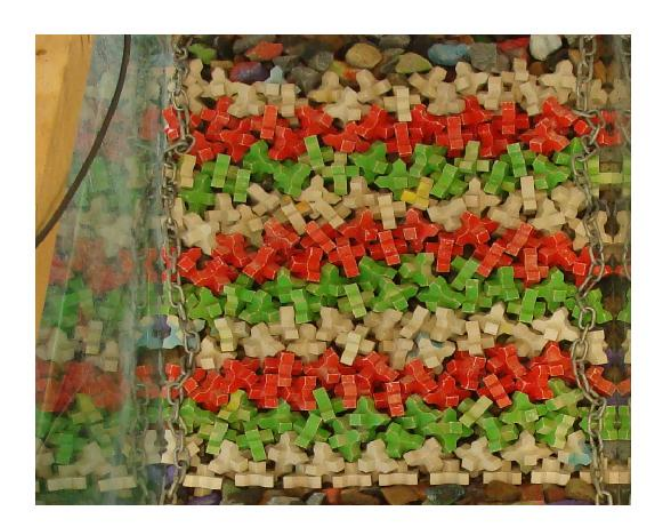


Figure Q-20 Photos before (left) and after (right) test G-2



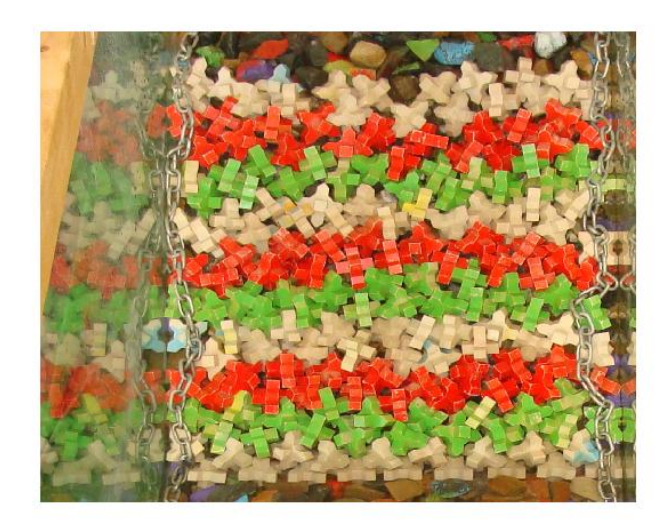


Figure Q-21 Photos before (left) and after (right) test G-3





Figure Q-22 Photos before (left) and after (right) test Extra-1



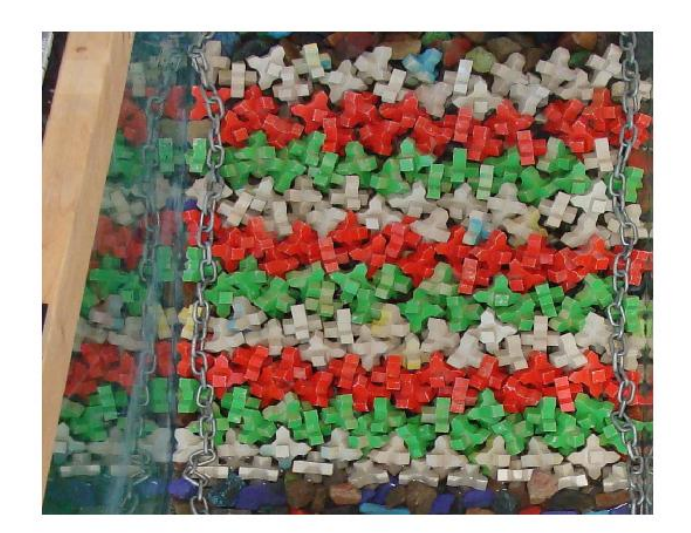


Figure Q-23 Photos before (left) and after (right) test Extra-2